Physiological and genomic characterization of thermophilic methanotrophic archaea and their partner-bacteria

Dissertation
zur Erlangung des Doktorgrades
der Naturwissenschaften
- Dr. rer. nat. -

dem Fachbereich Biologie/Chemie
der Universität Bremen
vorgelegt von

Viola Krukenberg

Bremen, November 2015

Die vorliegende Arbeit wurde in der Zeit von Januar 2012 bis November 2015 am Max-Planck-Institut für Marine Mikrobiologie angefertigt.

1. Gutachterin: Prof. Dr. Antje Boetius
2. Gutachter: Prof. Dr. Ulrich Fischer

1. Prüfer: Prof. Dr. Jens Harder
2. Prüfer: Dr. Gunter Wegener

Tag des Promotionskolloquiums: 11.12.2015

Table of contents

Summary

Methane is a potent greenhouse gas and its atmospheric concentration is strongly influenced by microbial processes. In anoxic marine environments 80% of the methane is oxidized by anaerobic microorganisms leading to reduced oceanic methane emissions. This anaerobic oxidation of methane (AOM) is coupled to sulfate reduction and is mediated by microbial consortia of anaerobic methane-oxidizing archaea and partner bacteria. The physiology of the consortia is incompletely understood but is thought to base on a metabolic interdependency of the partners, a syntrophy. The research presented in this PhD thesis focused on the physiology and genomic profile of AOM consortia, in particular on the microorganisms that are active at elevated temperatures (thermophiles). The thermophilic AOM is performed by a unique consortium of ANME-1 archaea and HotSeep-1 bacteria. In **Chapter II** we describe physiological studies and gene expression experiments with thermophilic AOM consortia and propose a syntrophy of AOM via direct exchange of reducing equivalents. In support of this hypothesis we visualized cell-to-cell connections in these consortia that we suggest to function as conductive nanowires in interspecies electron transfer. For the thermophilic bacterial partner, HotSeep-1 we obtained an ANME-1-free enrichment culture using hydrogen as alternative energy source, and by physiological and genomic investigation we show in **Chapter III** that this bacterial partner grows as chemolithoautotrophic sulfate reducer. Based on phylogenetic analysis we propose that HotSeep-1 presents a novel species, *Candidatus* Desulfofervidus auxilii. ANME-1, the archaeon participating in thermophilic AOM, belongs to a large group of uncultured organisms, which are known to have reversed the methanogenesis pathway to metabolize methane. The metabolic diversity among members of the ANME-1 group is still widely unexplored. In a comparative genome analysis of different ANME-1 in **Chapter IV** we show central aspects of their metabolism including a modified reverse methanogenesis pathway and abundant cytochromes possibly relevant for electron transfer. Environments of AOM activity and *in vitro* AOM enrichments are dominated by AOM consortia, but other microorganisms sustain as low abundant community whose function is not well understood. In **Chapter V** we show the cultivation of methanogens and sulfur-disproportionating bacteria from AOM enrichments. In conclusion the work of this PhD thesis has advanced our understanding of the functioning of thermophilic AOM, while further detailed comparative approaches are necessary to comprehend AOM syntrophy in all its detail and diversity.

Zusammenfassung

Methan ist ein wichtiges Klimagas, dessen atmosphärische Konzentration stark von mikrobiellen Prozessen beeinflusst ist. In sauerstofffreien marinen Sedimenten wird 80% des Methans durch Mikroorganismen verbraucht, was zu verminderter Methanemission der Ozeane beiträgt. Diese anaerobe Oxidation von Methan (AOM) ist gekoppelt mit Sulfatreduktion und findet in Konsortien aus anaerob methan-oxidierenden Archaeen (ANME) und Partnerbakterien statt. Die Physiologie dieser Konsortien ist unvollständig verstanden, aber basiert vermutlich auf metabolischer Abhängigkeit der Partner, einer Syntrophie. Diese Doktorarbeit behandelt die Physiologie und die genomischen Eigenschaften von AOM Konsortien, speziell solcher die bei erhöhter Temperatur leben (thermophile). Thermophile AOM wird von einem einzigartigen Konsortium aus ANME-1 Archaeen und HotSeep-1 Bakterien durchgeführt. In **Kapitel II** beschreiben wir physiologische Studien und Genexpressions-Experimente und schlagen vor, dass die Syntrophie von ANME-1 und HotSeep-1 auf dem direkten Austausch von Elektronen beruht. Diese Hypothese unterstützend weisen wir Zell-zu-Zell Verbindungen nach, die wir als mikrobielle Drähte (‚nanowires') beschreiben und für den Austausch von Elektronen vorschlagen. Den bakteriellen Partner HotSeep-1 konnten wir ohne ANME, mit Wasserstoff als alternativem Wachstumssubstrat, anreichern und zeigen in **Kapitel III** in physiologischen und genomischen Untersuchung, dass HotSeep-1 chemolithoautotroph als Sulfatreduzierer wächst. Zusammen mit phylogenetischen Analysen schlagen wir vor, dass HotSeep-1 eine neue Art darstellt: *Candidatus* Desulfofervidus auxilii. Das Archaeum, beteiligt an thermophiler AOM, gehört zu einer großen Gruppe unkultivierter Organismen, von denen bekannt ist, dass sie den methanogenen Stoffwechselweg umkehren um Methan zu oxidieren. Die metabolische Diversität innerhalb der ANME-1 Gruppe ist noch weitgehend unerforscht. In **Kapitel IV** zeigen wir mithilfe von vergleichender Genomanalyse zentrale metabolische Aspekte von ANME-1, u.a. eine modifizierte reverse Methanogenese und häufige Cytochrome, welche vermutlich relevant für den Elektronentransfer sind. Standorte natürlicher AOM Aktivität und *in vitro* AOM Anreicherungen sind dominiert von AOM Konsortien, dennoch überleben auch andere Mikroorganismen langfristig, deren Funktion kaum verstanden ist. In **Kapitel V** zeigen wir, dass aus AOM Anreicherungen Methanogene und Schwefeldisproportionierer kultivert werden können. Zusammenfassend hat diese Doktorarbeit unser Verständnis der Physiologie der thermophilen AOM vorangebracht, während weitere vergleichende Analysen nötig sind, um die AOM Syntrophie im Detail und in aller Diversität zu verstehen.

Abbreviations

AFM	Atomic Force Microscopy
ANME	ANaerobe MEthane-oxidizing archaea
AOM	Anaerobic Oxidation of Methane
AQDS	AnthraQuinone-2,6-DiSulfonate
APS	Adenosine-5'-PhosphoSulfate
ATP	Adenosine TriPhosphate
CARD-FISH	CAtalyzed Reporter Deposition Fluorescence *In Situ* Hybridization
CFE	Carbon Fixation Efficiencies
DAPI	4,6-DiAmidino-2-PhenylIndole
COG	Cluster of Orthologous Groups
DBB	*Desulfobulbus*
DIC	Dissolved Inorganic Carbon
DIET	Direct Interspecies Electron Transfer
DNA	DeoxyriboNucleic Acid
DSS	*Desulfococcus/Desulfosarcina*
GC	Guanine Cytosine
HRP	HorseRadish Peroxidase
IPL	Intact Polar Lipids
ORF	Open Reading Frame
OTU	Operational Taxonomic Unit
PCR	Polymerase Chain Reaction
POC	Particulate Organic Carbon
RNA	RiboNucleic Acid
RT	Room Temperature
SEM	Scanning Electron Microscopy
SMTZ	Sulfate Methane Transition Zone
SRB	Sulfate-Reducing Bacteria
TAOM	Thermophilic Anaerobic Oxidation of Methane
TEM	Transmission Electron Microscopy
TLE	Total Lipid Extracts
TPM	Transcripts Per Million
T4P	Type IV Pili

Chapter I

Introduction

The anaerobic, microbially-mediated oxidation of methane coupled to the reduction of sulfate is a vitally important process in the global carbon cycle. In the marine realm, this process, alongside the production of methane by microbial communities, controls oceanic methane emissions and thus the impact of this ecosystem on the global methane budget. The metabolic processes involved in transformation of complex organic matter into methane and microbial methane oxidation under anaerobic conditions are closely tied to interspecies microbial cooperation. This cooperation is based on mechanisms of microbial syntrophy, or "feeding together", which require specific physiology and interaction strategies.

This introduction section emphasizes the relevance of microbial methane formation and consumption in context of the global methane budget and outlines the microbial processes involved in anaerobic transformation of complex organic matter to methane. The importance of microbial cooperation in anaerobic metabolism is highlighted and the concept of microbial syntrophy is introduced including an overview to different mechanisms of interspecies interaction. The main focus of this introduction is on the process of anaerobic oxidation of methane coupled to sulfate reduction. The involved organisms, aspects of their physiology and possible strategies of their interaction are covered in detail. Following this presentation of the state of research on anaerobic oxidation of methane, the main objectives of this thesis are summarized. In a subsequent material and methods section the microorganisms specifically studied are introduced and the main methods employed are described. Finally, an overview of the enclosed manuscripts and the contribution from this thesis is provided.

1.1. Relevance of microbial processes in the global methane budget

Methane is the simplest and most reduced organic compound and the most abundant hydrocarbon on Earth. The atmospheric methane content is critical to Earth's climate as methane presents the second most important anthropogenic greenhouse gas, with a per mol 25 times stronger global warming effect than carbon dioxide (Lelieveld *et al.*, 1998). Microbial activity is central in the understanding of the global methane budget: microbial communities able to produce and consume methane constitute both a major source and sink of the molecule.

The major sources of atmospheric methane are emissions from natural wetlands and from anthropogenic activity such as agriculture (livestock and rice paddy emissions), fossil fuel production (fossil methane) or biomass burning. Anthropogenic activity has resulted in an increase in the concentration of atmospheric methane from 715 ppbv to 1770 ppbv since preindustrial times (Conrad, 2009). The total present day methane emissions are estimated to be between 500 to 600 Tg yr^{-1} (IPCC, 2007). Microbial methane production in both natural and man-made environments accounts for 70% of total methane emissions (Conrad, 2009). Indeed, most methane on Earth is biogenic, produced in anoxic environments such as terrestrial wetlands or marine subsurface sediments. In these environments methanogenic archaea produce methane (microbial methane) as the final product in the degradation of organic matter through a process termed methanogenesis (Whiticar *et al.*, 1986; Reeburgh, 2007). Methane furthermore derives from the thermal alteration of organic matter (thermogenic methane) (Schoell, 1988). Abiogenic methane, that is methane not originating from organic matter but from chemical reaction of inorganic compounds, is formed in the Earth's crust by alteration of rock material, e.g. at mid oceanic ridges (Horita and Berndt, 1999).

The predominant sink for atmospheric methane (>80% of total) is photochemical oxidation initiated by a hydroxyl radical reaction in the troposphere (Cicerone and Oremland, 1988; Lelieveld *et al.*, 1998; Conrad, 2009). However, the majority of methane is consumed by aerobic and anaerobic microbial methane oxidation before it even reaches the atmosphere, thereby preventing major global warming effects (Hanson and Hanson, 1996; Reeburgh, 2007). Aerobic methane oxidation, performed by methanotrophic bacteria is coupled to oxygen consumption, while anaerobic methane oxidation is coupled to alternative electron acceptors such as nitrate, nitrite, metal ions or sulfate and is mediated by either bacteria or

archaea or supposedly their combined effort (Hanson and Hanson, 1996; Boetius *et al.*, 2000; Raghoebarsing *et al.*, 2006; Beal *et al.*, 2009; Haroon *et al.*, 2013).

The ocean is assigned a central role in the global methane cycle. In marine anoxic subsurface sediments, methane is produced by microbial methanogenesis and by thermal alteration processes at mid ocean ridges and spreading centers. The seabed, which covers 70% of Earth's solid surface, contains large reservoirs of methane (estimates range between 5000 Gt of carbon (Buffett and Archer, 2004) and 1000 to 22000 Gt of carbon (Dickens, 2003)), found either in solid gas hydrates (≥455 Gt carbon (Wallmann *et al.*, 2012)), or in its dissolved and gaseous form (Boetius and Wenzhöfer, 2013). The exchange of methane between the marine realm and the atmosphere is small: only 10% of the methane produced in the marine environment reaches the atmosphere, the rest consumed by microbial methane oxidation (Reeburgh, 2007). Methane that from subsurface sources or from microbial activity migrates through the sediment by diffusion and advective transport is largely oxidized in the sediments themselves under anaerobic conditions. Indeed, more than 80% of the methane consumption in the ocean occurs in subsurface sediments through microbially-mediated anaerobic oxidation coupled to sulfate reduction, giving this process global significance (Hinrichs and Boetius, 2002). The remainder is released into the water column at methane seeps or vents and a portion of this is oxidized aerobically, again by microbial activity (Boetius and Wenzhöfer, 2013). Owing to this efficient microbial methane filter oceanic methane emission contributes only 2% to the global methane budget (Reeburgh, 2007).

1.2. Anaerobic mineralization of organic matter

Under anoxic conditions, microorganisms are the exclusive drivers of biologic organic matter degradation, ultimately leading to methane formation. Microbial processes involved in this degradation feature a complex network of chemical reactions which link diverse microbial communities by shared metabolic intermediates, necessitating interspecies cooperation.

In the marine ecosystem, the majority of organic matter is synthesized by phototrophic primary producers in the illuminated epipelagic zone and is mineralized in the upper water column by aerobic respiratory processes. The small fraction of organic matter (Hedges and Keil, 1995) that sinks to the ocean floor is, through sedimentation and burial processes, introduced into the marine subsurface ecosystem where oxygen is rapidly depleted with depth and microorganisms thrive by fermentation and anaerobic respiration. Electron acceptors for

anaerobic respiration are consumed in a sequence tied to the energy yield of the reactions they allow (Canfield, 1993). In marine sediments typically the electron acceptor are consumed in a sequence from nitrate, manganese(IV) oxides, iron(III) oxides to sulfate and finally carbon dioxide, which is only reduced in the absence of any other electron acceptor. The corresponding respiratory processes are, nitrate reduction, manganese reduction, iron reduction, sulfate reduction and methanogenesis. The high availability of sulfate (seawater concentration of 28 mM) make sulfate reduction the most quantitatively important respiratory process in anoxic marine sediments, where it accounts for up to 50% of total organic carbon degradation (Kasten and Jørgensen, 2000).

A succession of metabolic processes accomplishes the anaerobic degradation of organic matter. The different redox reactions involve functionally diverse groups of organisms, as no single organism is capable of complete mineralization of complex organic matter in the absence of oxygen (Schink and Stams, 2006; McInerney *et al.*, 2009). In a network of reactions the product of one process usually is the substrate for others, creating a layering of microbial ecosystems (Fig. 1). In the first of these layers, large organic polymers like proteins, polysaccharides or lipids are broken down by extracellular enzymes secreted by members of the resident microbial communities. The resulting monomers such as sugars, organic acids and amino acids are consumed by primary fermentative organisms which couple their oxidation to the reduction of an endogenous electron acceptor (Müller, 2008). In fermentation substrates are only partially oxidized, and a diverse range of organic products (e.g. fatty acids and alcohols) and hydrogen is released. In marine sediments where different external electron acceptors are available, the fermentation products serve as substrates for various anaerobically respiring prokaryotes, predominantly sulfate reducers, which eventually complete the oxidation of organic matter to carbon dioxide (Canfield, 2005; Schink and Stams, 2006). In environments that lack sulfate or other terminal electron acceptors the products of primary fermentation are further oxidized by secondary fermenters (also termed syntrophic metabolizers) that release acetate, formate and hydrogen (Schink, 1997). Such compounds are suitable substrates for methanogens. Acetate, a common intermediate in the anaerobic degradation processes is also formed by homoacetogenic bacteria from hydrogen and carbon dioxide (Diekert and Wohlfarth, 1994). Under specific conditions microorganisms also thrive on the reverse process, the conversion of acetate to hydrogen and carbon dioxide (Schink, 1997).

Methanogenesis is the final step of anaerobic organic matter mineralization that utilizes only the least complex products of previous steps and is exclusively mediated by anaerobic

methanogenic archaea (Thauer, 1998; Thauer *et al.*, 2008). Methanogens mainly reduce carbon dioxide with hydrogen or ferment acetate to methane and carbon dioxide. Moreover, formate, methyl compounds and carbon monoxide serve as their substrates. As methanogenesis has an extremely low energy yield methanogens are outcompeted by sulfate reducers that utilize the same substrates (Cicerone and Oremland, 1988).

Metabolic cooperation of microorganisms is apparent in the successive anaerobic degradation of complex organic matter (McInerney *et al.*, 2009), where fermentation depends on polymer hydrolysis and the consumption of fermentation products by methanogens and other anaerobes eventually drives fermentation. Such a nutritional interdependency of microorganisms occurs in diverse manifestations whenever the achievement of an overall reaction depends on two or more metabolically distinct organisms and is generally referred to as microbial syntrophy (Schink and Stams, 2006; McInerney *et al.*, 2009).

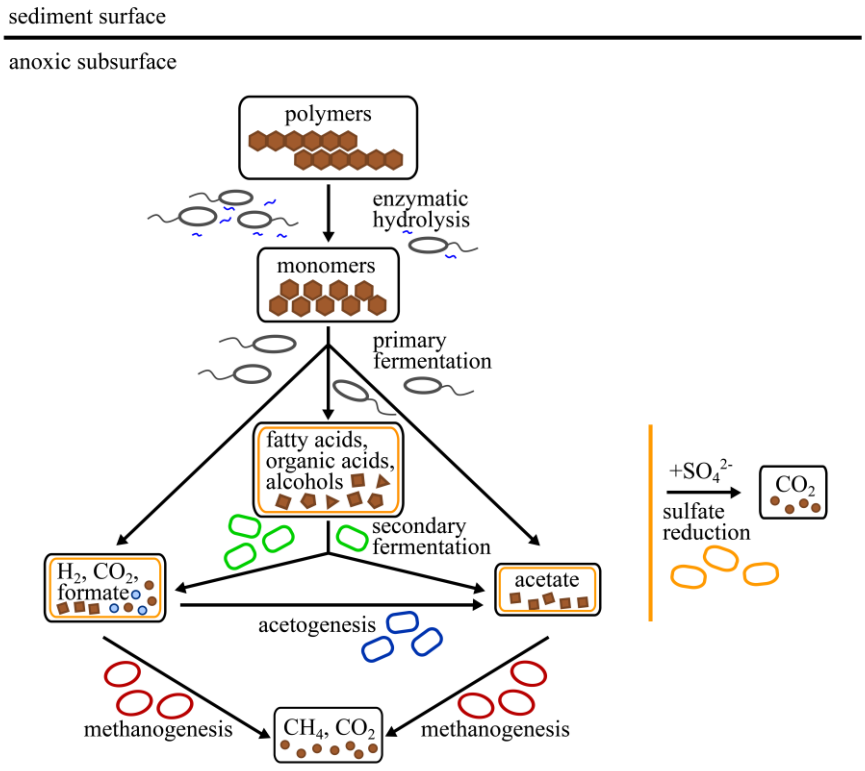

Figure 1 Illustration of the network of microbial processes involved in the degradation of complex organic matter to methane in the absence of oxygen (modified from Schink and Stams, 2006). The different groups of microorganisms involved are: primary fermenters (grey) with extracellular hydrolytic enzymes, secondary fermenters also known as syntrophic metabolizers (green), methanogens (red) and acetogens (blue). Filled symbols indicate complexity of compounds: organic carbon molecules (brown), non-carbon molecules (blue), dissolved/solid molecules (rectangular), gaseous molecules (round); symbol size indicates relative compound size. Yellow frame and line to the right show the range of compounds used by sulfate reducers.

1.3. Microbial syntrophy

Microorganisms of different species frequently interact with one another or with other organisms such as plants and animals. If this interaction is tight and persistent the organisms are thought to be in a symbiosis. The definition of symbiosis includes mutualistic, commensalistic and parasitic interactions (de Bary, 1879), of both obligatory and facultative character (Martin and Schwab, 2012). If symbiosis is based on obligatory mutualistic metabolism it is defined as syntrophy (Morris *et al.*, 2013), also referred to as cross-feeding or "eating together". In a syntrophy a compound is degraded by two or more organisms in a combined metabolic action, where one lives off the products of another's metabolism, thereby allowing its partner to sustain metabolism by preventing product inhibition. Syntrophic lifestyles are adopted by microorganisms within diverse phylogenetic groups including several *Firmicutes*, *Deltaproteobacteria* and *Euryarchaeota*, and are unlikely to have a common evolutionary origin (Sieber *et al.*, 2012). A syntrophic association may occur between closely related organisms, but also between members of different phyla or even domains. A famous example illustrating classical microbial syntrophy is the conversion of ethanol to methane by a co-culture of *Methanobacillus omelianskii*, a methanogenic archaeon and a fermenting bacterium, called the S-strain (Bryant *et al.*, 1967; Reddy *et al.*, 1972). The fermenter converts ethanol to acetate and hydrogen. This reaction is unfavorable (endergonic) under standard conditions but becomes favorable (exergonic) when hydrogen concentrations are kept low. The methanogen consumes hydrogen by converting carbon dioxide to methane, thereby keeping the hydrogen concentration low enough for fermentation to be favorable. This metabolic cooperation via interspecies hydrogen transfer promotes a reaction that neither of the partners could perform alone.

Syntrophic processes are particularly important under anoxic conditions. In these energy-limited ecosystems syntrophy is a strategy to exploit energy resources and expand habitable niches (Morris *et al.*, 2013). As a consequence of energy limitation, syntrophic organisms grow slowly and have low growth yields (McInerney *et al.*, 2009). Syntrophic metabolism often operates close to the thermodynamic equilibrium with a free energy yield of −15 to −20 kJ mol^{-1} or less (Scholten and Conrad, 2000; Adams *et al.*, 2006; Schink and Stams, 2006). This yield is far below the energy requirement for the synthesis of ATP (−60 to −70 kJ mol^{-1}). However, since ATP synthesis can be coupled to the translocation of up to five protons, the minimum energetic increment can be lowered to −12 to −20 kJ mol^{-1}, depending on thermodynamic conditions.

When syntrophically growing organisms form tight spatial associations they may be referred to as a consortium. A microbial consortium is defined as a close association of two or more different microbial types that are in permanent cellular contact and form an organized structure (Schink, 1991, 2002). This term was established for the highly-structured syntrophic association between several phototrophic green sulfur bacteria (*Chlorobium chlorochromatii*) and a rod-shaped central bacterium of the *Comamonadaceae* (*Betaproteobacteria*) (Overmann, 2006, 2010). The complexity these phototrophic consortia encompass is highlighted by interspecies signaling: light sensed by the phototrophic partner is translated into the movement of the entire consortium by the flagellated central bacterium, and by synchronous cell division of all consortium members. Notably, formation of cell aggregations or consortia is not a prerequisite for syntrophy. Syntrophy may involve individual cells or expand to entire communities that metabolically cooperate such as in the example of anaerobic organic matter degradation.

Mechanisms of microbial syntrophy

Syntrophy involves oxidation and reduction reactions which are physically separated in cells of functionally distinct organisms, thus requiring the extracellular transfer of reducing equivalents. In a classical syntrophic cooperation the organism that provides the reducing equivalents by performing the initial oxidative process, such as fermentation, is referred to as the syntrophic metabolizer or the S organism. The organism that carries out the reductive process, thereby consuming the products of the initial fermentation, is referred to as product scavenger. It should be noted that alternative strategies for the exchange of reducing equivalents are known, however, their diversity has not been fully explored.

The most common syntrophic exchange of metabolic intermediates involves hydrogen, carbon, sulfur or nitrogen compounds. Many syntrophies, especially those involving methanogens as the product scavenger, rely on interspecies transfer of molecular hydrogen. Hydrogen's small size, rapid diffusion and relevance to a broad range of metabolic processes render it an electron carrier preferred by many microbes. In aqueous environments formate, the simplest carboxylic acid, is also an important intermediate. For example, *Syntrophobacter fumaroxidans* grows syntrophically on propionate with a formate-utilizing methanogen (Dong *et al.*, 1994). A switch between formate and hydrogen transfer has been observed (Wu *et al.*, 1993; Bleicher and Winter, 1994) and both electron carriers may even be transferred simultaneously (Schink, 1991). Based on diffusion kinetics, hydrogen was

proposed as a preferred intermediate in dense cell aggregates (Boone *et al*., 1989a; Boone *et al*., 1989b), whereas formate exchange might be favored in dispersed cells, where longer distances need to be bridged (Schink and Stams, 2006). Acetate is another intermediate featured in syntrophic partnerships (Platen and Schink, 1987; Schink and Stams, 2006). In the syntrophic degradation of longer chain fatty acids, acetate is consumed by acetoclastic methanogens or sulfate reducers (Schink, 2002). Sulfur cycling as being described for co-cultures of green sulfur bacteria (*Chlorobium)* and the sulfur-reducing partner bacteria (*Desulfuromonas)* is another mechanism of interspecies electron transfer (Biebl and Pfennig, 1978). Such diverse examples show that various molecules fulfill intermediate function in syntrophic metabolism.

In addition to the formation and consumption of a molecular intermediate, reducing equivalents may be shuttled by redox-active mediator molecules. A cysteine/cystine shuttle system, similar to that used in the cycling of sulfur, is the basis of the syntrophy between the acetate-oxidizing *Geobacter sulfurreducens* and the nitrate-reducing *Wolinella succinogenes* (Cord-Ruwisch *et al.*, 1998; Kaden *et al.*, 2002). Another class of electron carriers abundant in soils and sediments are humic acids, and their analog anthraquinone-2,6-disulfonate (AQDS). Several bacteria are able to reduce the quinone moieties in humic substances and thereby transfer electrons (indirectly) to insoluble electron acceptors (iron oxides) or to other bacteria (Lovley *et al.*, 1996). Recently, syntrophic growth via quinone mediated interspecies electron transfer was demonstrated for the ethanol-oxidizing *G. metallireducens* and the fumarate-reducing *G. sulfurreducens* (Smith *et al.*, 2015). Outer surface c-type cytochromes were suggested to be crucial at the site of quinone reduction, while the identities of the outer surface proteins, required to derive electrons from extracellular reduced quinones, remained unclear. The experimental determination of electron transfer systems in microbial syntrophies remains difficult. A broader variety of electron carrier systems may exist and syntrophic communities may utilize several different systems either separately or in parallel.

Furthermore, as another syntrophic strategy, organisms may directly transfer electrons via cell-cell contacts or conductive structures. So far direct interspecies electron exchange has only been described for microbial consortia of *G. metallireducens* and *G. sulfurreducens* or *G. metallireducens* and methanogens. In such associations *G. metallireducens* donates electrons from ethanol oxidation to either of the electron-accepting partners (Summers *et al.*, 2010; Rotaru *et al.*, 2014). Recently, also *G. hydrogenophilus* was found to form consortia with methanogens and Rotaru and colleagues (2015) suggested they likewise interact via direct electron transfer. In these syntrophies, *Geobacter* spp. are proposed to form cell-cell

connections via self-conductive type IV pili that resemble nanowires (Reguera *et al.*, 2005; Vargas *et al.*, 2013; Malvankar *et al.*, 2014). Moreover, Summers and colleagues (2010) proposed that c-type cytochromes associated with the outer cell membrane and the pili themselves were crucial for electron transport. However, the role of pili and cytochromes in direct interspecies electron transfer remains debated. Pili and c-type cytochromes can be substituted by conductive materials such as biochar, carbon cloth, granular activated carbon (Liu *et al.*, 2012; Chen *et al.*, 2014) and magnetite (Liu *et al.*, 2014), respectively. Next to interspecies electron transfer, the extracellular transfer of electrons to insoluble electron acceptors such as iron oxides was also observed in *Geobacter* spp. and *Shewanella* spp.; however, different mechanisms for the direct transfer of electrons are discussed for these organisms (Reguera *et al.*, 2005; Gorby *et al.*, 2006; Lovley *et al*., 2015). Although examples of direct electron transfer in syntrophic communities are limited, this mechanism may constitute an important but yet overlooked process as it remains difficult to be experimentally proven.

Cultivation of syntrophic organisms

To date, only a small fraction (<1%) of the estimated microbial diversity on Earth has been obtained in laboratory cultures (Schink and Stams, 2006). As described above, the strong and necessary interactions between some collections of microbes may provide partial explanation for the limited success of traditional isolation techniques. For example, the disruption of syntrophic relationships may be one reason that prevents cultivation of environmentally relevant organisms. In contrast, co-culture approaches, allowed cultivation of important but previously overlooked syntrophic metabolizers. For instance, anaerobic syntrophic sugar degraders could only be cultured when the culture medium was substituted with a reducing equivalent scavenger (Müller *et al*., 2008). Importantly, not all syntrophic growing organisms are restricted to syntrophic growth. In many cases, the syntrophic metabolizer can be isolated with an alternative fermentable substrate, usually a more oxidized form of the compound used in syntrophic growth. Other syntrophic metabolizers, such as *Desulfovibrio* spp. or *Geobacter* spp. (Sieber *et al*., 2012), are capable of anaerobic respiration. Still, for some syntrophic metabolizers, viable conditions for cultivation could not be established. The same applies to the reducing equivalent scavenger, which often can be grown independently of its partner by providing it with the compound it would ordinarily receive from its syntrophic partner. As shown for methanogens of the rice cluster I which require constant hydrogen

supply at very low concentration (Sakai *et al.,* 2007), initial co-cultivation with a syntrophic metabolizer might be necessary to complete isolation. However, if the syntrophic intermediate or the mechanism of interaction is unknown, cultivation of syntrophs remains impossible. Examples of syntrophic associations in which neither partner has been isolated and physiological understanding is incomplete include the "string of pearls" consortia of SM1 *Euryarchaeota* and sulfur-oxidizing bacteria (Henneberger *et al*., 2006) and the anaerobic methane-oxidizing consortia of ANME *Euryarchaeota* and sulfate-reducing bacteria (Boetius *et al.*, 2000).

While cultivation remains central to the study and understanding of microbial physiology, enrichment-based approaches and culture-independent methods, such as metagenomics or stable isotope probing, have also advanced the knowledge on syntrophic organisms (Morris *et al*., 2014). The anaerobic methane-oxidizing consortium (Boetius *et al.*, 2000) is probably the most prominent example of an unexplained interspecies association. This consortium performs anaerobic methane oxidation which, as describe above (see 1.1.), is central to methane dynamics in the marine ecosystem.

1.4. Anaerobic oxidation of methane

Methane oxidation is prevalent among aerobic bacteria; however, methane also serves as an energy source for microorganisms in anoxic environments where it is oxidized with electron acceptors other than oxygen. Sulfate-dependent, nitrate/nitrite-dependent and metal ion-dependent anaerobic oxidation of methane are examples of such alternative oxidation processes, each associated with a distinct microbial mechanism. The nitrite-dependent methane-oxidizing bacterium, *Candidatus* Methylomirabilis oxyfera, likely produces molecular oxygen intracellularly, which is fed into a canonic aerobic methane oxidation pathway (Ettwig *et al.*, 2010), resembling that of aerobic methanotrophic bacteria. Sulfate-, nitrate- and metal ion-dependent methane oxidizers supposedly utilize a reversed methanogenesis pathway. Further, anaerobic oxidation of methane coupled to nitrate reduction is so far known to be performed by a single archaeon *Candidatus* Methanoperedens nitroreducens and methane oxidation coupled to sulfate or metal ion reduction is proposed to be mediated by a combined effort of anaerobic methane-oxidizing archaea (ANME) and sulfate reducers or metal reducers, respectively (Boetius *et al.*, 2000; Beal *et al.*, 2009: Haroon *et al.*, 2013). The sulfate-dependent anaerobic oxidation of methane (henceforth,

AOM) is, thermodynamically, the least favorable of these processes; however, due to the abundance of sulfate in the marine ecosystem, AOM is the most globally consequential process. The following sections will focus on AOM: the sulfate-dependent anaerobic oxidation of methane.

Sulfate-dependent anaerobic oxidation of methane

Methane oxidation in the absence of oxygen was first observed in porewater profiles which showed the concurrent disappearance of methane and sulfate in oxygen-free marine sediment horizons (Barnes and Goldberg, 1976; Reeburgh, 1976). Later, a direct and stoichiometric link of methane oxidation and sulfate reduction was revealed by radio tracer experiments showing coinciding maxima of methane oxidation and sulfate reduction rates (Reeburgh, 1980; Iversen and Jørgensen, 1985), according to the following reaction:

$$CH_4 + SO_4^{2-} + 2\ H^+ \rightarrow CO_2 + H_2S + 2\ H_2O \quad (1)$$

Since AOM relies on the availability of sulfate and methane, the process is particularly widespread in anoxic, methane-rich marine environments, such as methane-rich sediments (Niemann *et al.*, 2005; Harrison *et al.*, 2009) or anoxic water bodies (Michaelis *et al.*, 2002; Reitner *et al.*, 2005a) and methane seeps (Hinrichs *et al.*, 1999; Orphan *et al.*, 2001a; Knittel *et al.*, 2005; Lloyd *et al.*, 2006). AOM has also been observed in freshwater (Segarra *et al.*, 2015) and terrestrial (Alain *et al.*, 2006) environments. Sulfate methane transition zones (SMTZ), sediment layers where sulfate-rich seawater diffusing through the sediment meets a methane-rich region, are the characteristic environments for AOM to completely consume any available methane (Fig. 2) (Reeburgh, 1980; Regnier *et al.*, 2011). AOM is also the dominant process at marine methane seeps, mud volcanoes and hydrothermal vents where methane-rich fluids from a deep source such as gas hydrate migrate upwards into sulfate-rich sediments (Boetius and Wenzhöfer, 2013). In the anoxic, methane-rich bottom water of the Black Sea, AOM activity is associated with large, microbially-generated carbonate precipitates known as microbial reefs (Fig. 2 C, D) (Michaelis *et al.*, 2002). While AOM is restricted to oxygen-free environments, it can occur across a range of salinity, pH and methane fluxes. Further, AOM has been measured across a wide range of *in situ* temperatures from <20°C (at cold methane seeps, where it is most prevalent) to 90°C (in hydrothermal environments) (Holler *et al.*, 2011b; Wankel *et al.*, 2012). Consequently classes of AOM are defined according to the temperature they occur at; these are psychrophilic (<20°C),

mesophilic (20-50°C) and thermophilic (>50°C) AOM. To date, thermophilic AOM has only been described in the hydrothermal seep sediments in Guaymas Basin (Gulf of Mexico) (Holler *et al.*, 2011b) and Middle Valley (Juan de Fuca Ridge) (Wankel *et al.*, 2012). Examples for studied AOM habitats include Hydrate Ridge seeps (Pacific Ocean), Gulf of Mexico seeps (Gulf of Mexico), Tommeliten and Gullfaks (North Sea), Haakon Mosby mud volcano (Barents Sea) and Amon mud volcano (Mediterranean Sea).

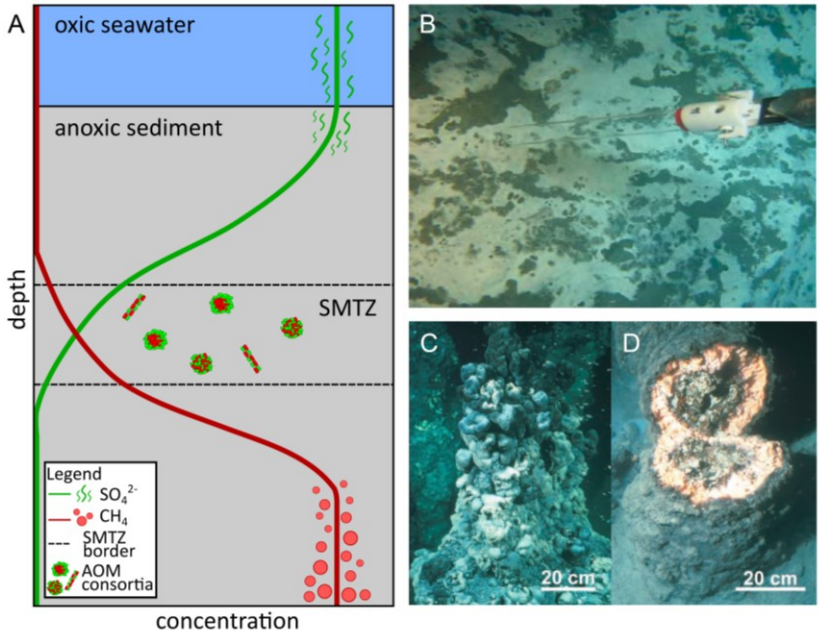

Figure 2 AOM-associated environments. (**A**) Schematic illustration of a sulfate methane transition zone (SMTZ) in marine sediments. The SMTZ is created where upward-migrating methane and downward-diffusing sulfate meet. This area is inhabited by consortia performing AOM. (**B**) Bacterial mats above a zone of active AOM at Haakon Mosby mud volcano (adapted from Boetius and Knittel, 2010). (**C,D**) Microbial reef structures in the Black Sea (adapted from Michaelis *et al.*, 2002). (**D**) View inside a microbial reef tower showing pink microbial mats.

Organisms involved in AOM

The microorganisms responsible for AOM were first identified by their lipid biomarkers which have characteristic depleted carbon isotope signatures. These biomarkers co-occurred with 16S rRNA gene sequences of a novel archaeal group of anaerobic methanotrophic archaea (ANME; Hinrichs *et al.*, 1999). Subsequently these archaea were visualized in association with bacteria as large consortia (Hinrichs *et al*., 1999; Boetius *et al*., 2000; Knittel *et al*., 2005).

The anaerobic methane-oxidizing archaea (ANME) are phylogenetically related to their methane-producing counterpart, the methanogenic archaea within the *Euryarchaeota*. To date three lineages of ANME with their subgroups have been described. These lineages are polyphyletic and share as little as 75% 16S rRNA gene sequence identity (Knittel and Boetius, 2009). ANME of clade 1 (ANME-1) are distant relatives of the order *Methanomicrobiales,* while ANME of clade 2 (ANME-2) and 3 (ANME-3) form distinct

lineages within the *Methanosarcinales* (Hinrichs *et al.*, 1999; Orphan *et al.*, 2001b; Knittel *et al.*, 2005; Niemann *et al.*, 2006). Subgroups have been described within ANME-1 (a, b, c) and ANME-2 (a, b, c, (d)) (Orphan *et al.*, 2001a; Orphan *et al.*, 2001b; Knittel *et al.*, 2005; Wankel *et al.*, 2012). The cell morphology of ANME varies: ANME-1 is often of rectangular shape while ANME-2 and -3 are of coccoidal shape. As shown by transmission electron microscopy, rectangular ANME-1 cells are surrounded by an external sheath of biopolymeric substance and contain internal stacks of cytoplasmic membranes similar to those of methanotrophic *Gammaproteobacteria* (Reitner *et al.*, 2005b). ANME-2 cells were found to store sulfur internally (Milucka *et al.*, 2012). With respect to the environment they occur in ANME-2 and -3 seem restricted to AOM-associated environments with cold to moderate temperatures (<40°C), while ANME-1 was reported to thrive under cold and hot conditions and high salinities (Maignien *et al.*, 2013).

The three distinct lineages of ANME described above have been observed in association with sulfate-reducing bacteria (SRB) of different groups within the *Deltaproteobacteria*. The most frequent partner of ANME-1 and ANME-2 are of the Seep-SRB-1a and Seep-SRB-2 groups related to the *Desulfococcus/Desulfosarcina* (DSS) cluster (Knittel *et al*., 2003, 2005; Kleindienst *et al*., 2012). Four Seep-SRB cluster are distinguished of which only Seep-SRB-1 and -2 were shown to associate with ANME (Knittel *et al*., 2003). Seep-SRB-1 was further subdivided into 6 groups (a-f) of which Seep-SRB-1a appears to be the predominant ANME partner (Schreiber *et al.*, 2010). The known morphologies of the DSS-related bacterial partner are diverse, including coccoidal, rod-shaped and vibroid shapes. Intracellular inclusions of polyhydroxyalkanoates, likely storage compounds, and iron sulfides were identified in DSS cells associated with ANME-2 (Reitner *et al.*, 2005a). The dominant partner bacteria of ANME-3 relate to *Desulfobulbus* (DBB) (Niemann *et al.*, 2006). Bacteria of the HotSeep-1 cluster present a deep-branching lineage within the *Deltaproteobacteria* and are neither related to DSS nor to DBB. This cluster is found in association with ANME-1 at high temperatures (>50°C) (Holler *et al.*, 2011b). To date, HotSeep-1 was exclusively reported at high temperatures while occurrence of the DSS and DBB groups was restricted to environments with cold to moderate oceanic temperatures.

In rare cases, aggregation of ANME archaea with other bacteria has been reported. For instance, ANME-2c was shown in aggregates with *Alpha*- and *Betaproteobacteria* (Pernthaler *et al.*, 2008). Furthermore, ANME-1 were repeatedly found as single cells, in monospecies aggregates or in cell chains while ANME-2 and -3 tend not to occur without a partner bacterium.

Association of ANME and partner bacteria in AOM consortia

Associations of ANME and SRB have diverse morphology, structure and composition. These associations are generally referred to as consortia, because of their multispecies nature and varied structural organization (Boetius *et al.*, 2000; Knittel and Boetius, 2009). The first consortia visualized by fluorescence *in situ* hybridization were aggregates containing an inner archaeal core and an outer bacterial cell layer (shell-type consortium) (Boetius *et al.*, 2000). Subsequently, additional forms of consortia were described (Fig. 3). The ANME-2c/DSS and ANME-3/DBB associations have been observed in the shell-type consortium, while ANME-2a/DSS, ANME-1/Seep-SRB-2 and ANME-1/HotSeep-1 associations were observed as well mixed structures (mixed-type consortium) (Knittel and Boetius, 2009, 2011). ANME-1/HotSeep-1 associations were as well observed as filamentous consortia in which pairs of archaeal and bacterial cells formed long chains (Holler *et al.*, 2011b). The observed ratio of ANME:SRB cells varies from 1:1 to 1:7, the latter ratio observed in shell-type consortia of ANME/DSS, while ANME-3/DBB consortia are strongly ANME-3 dominated (Cui *et al.*, 2015). Little is known about the mechanisms which initialize consortia formation and sustain the structurally-aligned propagation of archaeal and bacterial cells. It is thought that a small number of archaeal and bacterial cells initiate consortia that develop into large aggregations of several hundred thousand to millions of cells (Knittel and Boetius, 2009). Spherical consortia with diameters of a few micrometers to 50 µm have been reported, as well as filamentous consortia of up to 100 µm length (Nauhaus *et al.*, 2007; Holler *et al.*, 2011b). Shell-type consortia were proposed to divide into smaller aggregates once the bacteria grow into the inner archaeal core (Knittel and Boetius, 2009). Alternatively, consortia that reach a specific size may burst, thereby releasing single cells into the environment which eventually initiate new consortia (Knittel and Boetius, 2009).

To date, AOM consortia have been detected in all environments within which AOM occurs either visually or by sequence-based methods. AOM consortia from diverse environmental sources could be enriched into sediment-free *in vitro* cultures, but isolation into axenic co-cultures or isolation of either of the partners into pure culture has never been achieved.

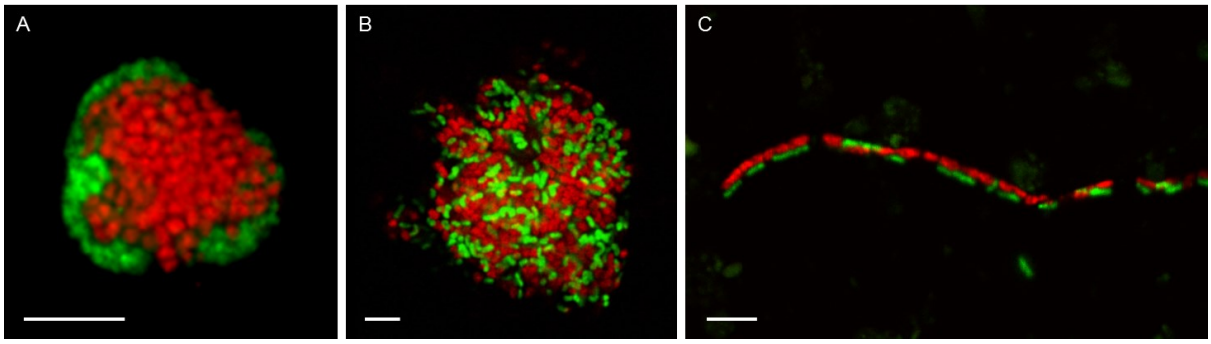

Figure 3 Anaerobic methane-oxidizing consortia visualized by fluorescence *in situ* hybridization. (**A**) Shell-type aggregate (adapted from Boetius *et al.*, 2000). (**B**) Mixed-type aggregate (provided by Katrin Knittel). (**C**) Filament-type consortium (adapted from Holler *et al.*, 2011b). Red: ANME archaea; green: bacterial partner. Scale bars: 5 µm.

Interaction of archaea and bacteria in methane-oxidizing consortia

The co-occurrence of ANME and bacterial cells in consortia indicated that syntrophy may be linked to AOM; however, the mechanisms coupling methane oxidation and sulfate reduction remained unresolved. Fundamentally different models describing the archaea-bacteria interaction have been proposed, yet all assume that ANME are responsible for methane oxidation (Fig. 4).

In the syntrophic depiction of AOM with bacterial sulfate reduction, methane-derived intermediates or reducing equivalents are scavenged by the bacterial partner. The following mediators of reaction-level coupling have been proposed: a molecular intermediate such as an organic carbon compound derived from methane oxidation (A), molecular hydrogen formed from reducing equivalents of methane oxidation (B), interspecies electron transfer via redox active compounds (C), or interspecies electron transfer via direct cell-to-cell contacts such as conductive nanowires (D). An alternative model has been proposed by Milucka and colleagues (2012) with partial sulfate reduction in ANME cells followed by transfer of a sulfur intermediate which is disproportionated by the bacterial partner (E). In this model, AOM based on sulfur cycling would not be an obligate syntrophic process: ANME does not directly rely on interspecies interaction and the metabolic activity of a partner to conduct methane oxidation. Lastly, a non-syntrophic interaction model within AOM consortia was also suggested whereby ANME cells perform complete sulfate reduction and bacteria thrive from their metabolic by-products (F) (Widdel *et al.*, 2007; Thauer and Shima, 2008).

No experimental evidence for rejecting the hypothesis of syntrophy in AOM has been reported, however also the experimental support of syntrophy is limited: sulfur cycling is the only mechanism observed *in vitro* (Milucka *et al.*, 2012). Despite all AOM consortia

presumably carrying out the same net reaction, consortia vary in the phylogenetic identity of their members and their structure. It is thus reasonable to expect that a diversity of interaction mechanisms occur, rather than a single mode.

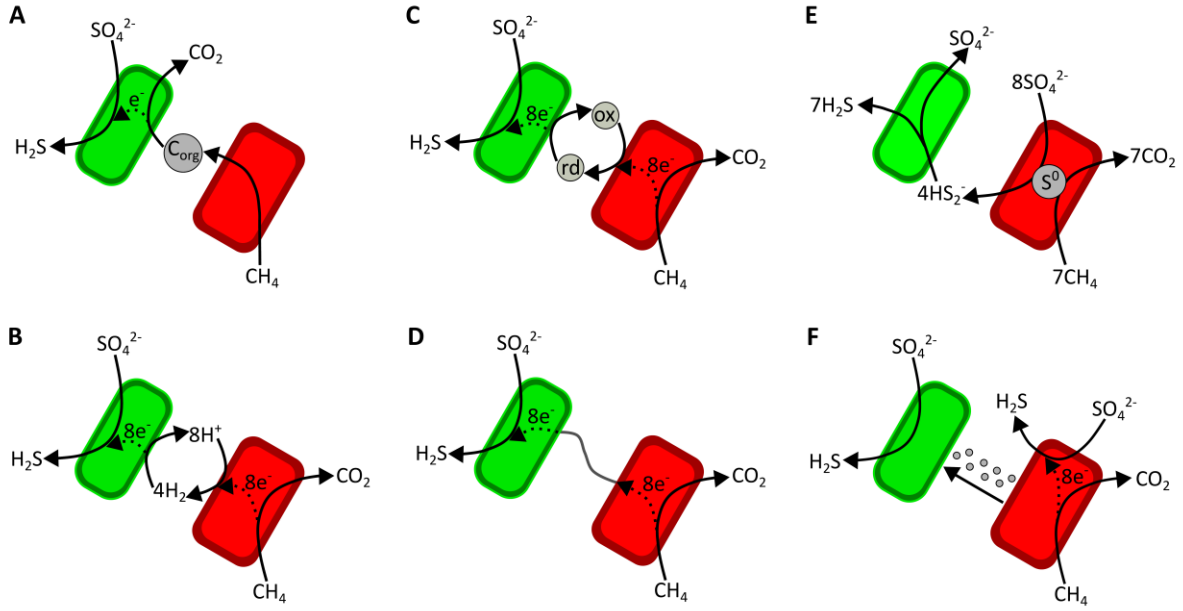

Figure 4 Schematic illustration of various models proposed for the archaeal-bacterial interaction in AOM. (**A**) Transfer of a methane-derived organic carbon intermediate produced by ANME and completely oxidized by the bacterial partner. (**B**) Interspecies transfer of hydrogen produced by reverse methanogenesis in ANME cells. (**C**) Transfer of reducing equivalents by a reduced mediator compound. (**D**) Direct interspecies electron transfer by conductive structures. (**E**) Transfer of zero-valent sulfur produced by partial sulfate reduction in ANME cells and disproportionated by the bacterial partner. (**F**) Transfer of metabolic by-products. Note that, strictly speaking, (E) and (F) present non-syntrophic interactions. See text for details.

Evidence for molecular intermediate transfer in AOM

Molecular compounds such as hydrogen, formate, acetate, methyl compounds and carbon monoxide are considered to be intermediates in syntrophic processes thus they were also considered to be involved in AOM (Nauhaus *et al.*, 2002, 2005; Moran *et al.*, 2008) (Fig. 4 A, B). Physiological studies testing for the existence of potential intermediates used classical substrate experiments assuming that the addition of a molecular intermediate to a syntrophic consortium would stimulate the growth of the product scavenger while inhibiting the syntrophic oxidizer (Schink, 1997; Stams and Plugge, 2009). However, in AOM none of these substrates did significantly enhance sulfide production compared to methane-dependent sulfide production and none of the bacterial partner could be enriched using this strategy (Nauhaus *et al.*, 2002, 2005; Moran *et al.*, 2008; Lens, 2010). Further, most of the compounds tested did not repress AOM as would be expected from intermediates. As

exceptions methyl sulfide and carbon monoxide repressed methane oxidation (Moran *et al.*, 2008), however a pure toxicity effect of these compounds as shown for some methanogens and sulfate reducers (Lens, 2010) could not be excluded. Molecular intermediates in AOM were further excluded by kinetic reasoning (Spormann and Widdel, 2000) and diffusion modelling (Sørensen *et al.*, 2001). For instance, efficient intermediate transfer and intermediate concentrations of less than 10 nM would be required for an AOM energy yield of −31 kJ mol^{-1} (Spormann and Widdel, 2000). Presuming direct ANME-SRB attachments, formate transfer was predicted to be feasible. Instead all the other considered intermediates (including molecular hydrogen) were excluded as effective diffusion distances of less than the thickness of two cell walls would be required (Sørensen *et al.*, 2001).

Evidence for direct interspecies electron transfer in AOM

Direct interspecies electron transfer (DIET) requires either direct contacts or a mediator molecule between the two cells of the partner (Fig. 4 C, D). As DIET does not involve the production of a molecular intermediate AOM would be insensitive to an external supply of substrates. Hence, DIET was proposed as possible mechanism of species interaction in AOM, possibly involving conductive cell-to-cell connections (Thauer and Shima, 2008; Summers *et al.*, 2010). Experimental evidence for the formation of such nanowire-like structures in AOM consortia was however lacking and direct contact between cells was not observed. Furthermore, DIET via redox-active compounds such as phenazines and humic acids or their analog AQDS was tested but ruled out as the experimental supply of mediators to capture electrons did not promote methane oxidation (Nauhaus *et al*., 2005; Basen, 2009). A toxic effect of such mediator compounds, which would obscure their influence *in situ*, however could not be excluded (Nauhaus *et al.*, 2005). Currently available genomes of ANME-1 and -2 organisms encode extracellular cytochromes, and several authors have speculated that these are involved in electron transfer reactions either in association with pili or possibly through the formation of a conductive extracellular matrix (Meyerdierks *et al.*, 2010; Wang *et al.*, 2014). A frequently observed pinkish color of Black Sea AOM mats supports this proposal, the color being attributed to high cytochrome content (Michaelis *et al.*, 2002).

Evidence for internal sulfur cycling in AOM

Adopting the model of AOM driven by internal sulfur cycling, an exchange of a sulfate-derived intermediate between consortium partners would be expected (Fig. 4 E). ANME cells

couple methane oxidation to the partial reduction of sulfate to zero-valent sulfur, which accumulates intracellularly. Zero-valent sulfur that leaves the ANME cell by diffusion or transport reacts with extracellular sulfide to form polysulfide which, in turn, is taken up (mainly as disulfide) by the bacterial partner to be disproportionated into sulfate and sulfide. This mechanism was demonstrated *in vitro* for ANME-2/DSS consortia in physiological experiments and by the presence of sulfur inclusions in the ANME cells (Milucka *et al.*, 2012). There are still a number of open questions associated with this model as the enzymes currently understood as essential for dissimilatory sulfate reduction were exclusively localized in the bacterial partner (Milucka *et al.*, 2013). Additionally, so far the required alternative sulfate reduction in ANME-2 has not been identified. Furthermore, yet the evidence of this sulfur cycling is limited to a single culture and remains to be demonstrated for other AOM consortia types.

Evidence for commensalistic interaction in AOM

A commensalistic relationship in AOM suggests the ANME perform methane oxidation and sulfate reduction while the bacteria benefit from the ANME metabolism without affecting it (Fig. 4 F). The bacteria were proposed to utilize unknown metabolites or components of the exopolymeric matrix surrounding the consortium (Widdel *et al.*, 2007; Thauer and Shima, 2008). However, a transfer of organic carbon compounds is unlikely based on stable isotope labeling studies that showed autotrophic growth of the bacterial partner (Wegener *et al.*, 2008; Kellermann *et al.*, 2012). Although the ANME are not known to perform complete sulfate reduction, repeatedly found ANME-1 without partner bacteria challenge the idea of an obligate syntrophic AOM process.

Physiology of organisms involved in the anaerobic oxidation of methane

Knowledge concerning the metabolic processes involved in AOM, an area of intense research for some 40 years, appears remarkably limited. AOM yields a Gibbs free energy of −16.86 kJ per mol CH_4 oxidized under standard state conditions and −20 to −40 kJ per mol CH_4 oxidized under *in situ* conditions. Assuming AOM is dependent on syntrophic interactions, this energy yield would be shared among the partners in a given consortium. Thus, the organisms performing AOM operate close to the minimum energy which allows ATP synthesis. The consequence of such energy limitation is the extremely slow growth of

these organisms, which have doubling times of 2 to 6 months (Nauhaus *et al.*, 2007; Holler *et al.*, 2009, 2011a) and low biomass yields with only about 1% of reducing equivalents transferred into biomass (Nauhaus *et al.*, 2007; Wegener *et al.*, 2008).

The characteristics of AOM described above restrict cultivation efforts and limit physiological experiments. Cultivation independent methods, then, are particularly promising in furthering our physiological understanding of AOM. Isotope labeling, metagenomics and metatranscriptomics conducted on enrichment cultures or samples naturally enriched in AOM consortia hold much promise in this pursuit.

Methane metabolism in AOM consortia

The proposed biochemical pathway of methane oxidation is reverse methanogenesis, featuring the same enzymes as the classical methanogenesis pathway. In the following paragraphs, the key enzyme of this pathway, the pathway itself, the possible occurrence of methanogenesis in ANME cells, and carbon assimilation by AOM consortia are described.

Methyl-coenzyme M reductase (Mcr) is the key enzyme of methanogenesis and catalyzes the formation of methane from methyl-coenzyme M (CoM) and coenzyme B (CoB). In methanogens, Mcr is a heterodimeric enzyme ($\alpha_2\beta_2\gamma_2$) with a nickel porphinoid (coenzyme F_{430}) as a prosthetic group (Jaun and Thauer, 2007). The detection of methanogen-related, but deeply-branching, *mcrA* sequences in AOM-associated environments has suggested the involvement of Mcr in AOM. This is supported by the extraction of highly abundant Mcr protein homologs from ANME-dominated Black Sea microbial mats (Krüger *et al.*, 2003), and the subsequent localization of Mcr in ANME cells by immunolabeling (Heller *et al.*, 2008). ANME-1 and ANME-2 contain two distinct types of Mcr. The nickel protein I is found in ANME-1 and contains a modified F_{430} cofactor with higher molecular weight relative to that found in methanogens. The nickel protein II is found in ANME-2 and contains the same F_{430} cofactor present in methanogens (Krüger *et al.*, 2003). The hypothesis of reversed methanogenesis in ANME was further supported by metagenome and metatranscriptome studies. These revealed the presence and expression of genes of the methanogenesis pathway in ANME (Hallam *et al*., 2003; Krüger *et al*., 2003; Hallam *et al*., 2004; Meyerdierks *et al*., 2005, 2010; Stokke *et al*., 2012; Wang *et al.*, 2014).

In AOM itself, methane is proposed to be activated by Mcr and bound as a methyl group to CoM via the reduction of the disulfide CoM-CoB bond (see Chapter IV Fig. 4 for details of the reverse methanogenesis pathway). The activation of a carbon-hydrogen bond in the

methane molecule requires 439 kJ per mol (Thauer and Shima, 2008) and the activation mechanism is not fully understood. The subsequent methyl group transfer to the coenzyme tetrahydromethanopterin (H4MPT) is catalyzed by membrane-bound methyl-H4MPT-coenzyme M methyltransferase; this releases CoM which is rebound to CoB via the regeneration of their disulfide linkage. Cytoplasmic enzymes subsequently oxidize the methyl group stepwise via the H4MPT-bound intermediates methylene, methenyl and formyl. These steps involve, respectively, the enzymes methylene-H4MPT reductase (Mer), methylene-H4MPT dehydrogenase (Mtd) and methenyl-H4MPT cyclohydrolase (Mch). The formyl group is transferred to the coenzyme methanofuran (MFR) by the formyl methanofuran H4MPT transferase (Ftr) and subsequently reduced to CO_2 by formyl methanofuran H4MPT dehydrogenase (Fmd). However, the ANME-1 metagenome lacks a Mer enzyme. To account for this, a bypass was proposed via methanol and formaldehyde to methylene-H4MPT (Meyerdierks *et al.*, 2010). As genomic and proteomic data on ANME is still limited, it is unclear whether the AOM pathway may differ among ANME types.

It has been proposed that ANME-1 cells are able to operate as both methanotrophs and methanogens (Lloyd *et al.*, 2011). The numerous similarities between members of the ANME group and methanogens, including phylogenetic relatedness and consistent enzymatic inventory, as well as the detection of active ANME cells in methanogenic environments (Lloyd *et al.*, 2011) supported the hypothesis of methanogenesis by ANME cells. In fact, in radio tracer experiments with natural AOM enrichments, methane production rates amounting to 13% of the rates of simultaneous methane oxidation were measured (Treude *et al*., 2007; Orcutt *et al*., 2008). Likewise, methanogens show trace methane oxidation of 0.001 to 0.3% of methane formation (Zehnder and Brock, 1979). Further, a complete reversibility of all enzymatic reactions involved in reverse methanogenesis was recently shown through isotope labeling experiments with AOM consortia (Holler *et al.*, 2011a). This enzymatic reversibility explains the trace reactions observed as isotope exchanges (a backflux) from the product to substrate pool. This is particularly pronounced in AOM, as the process operates close to thermodynamic equilibrium and reaction reversibility is likely to increase. Importantly, this reaction does not yield net methane production and does not yield energy (Holler *et al.*, 2011a; Yoshinaga *et al.*, 2014). The possibility of methanogenesis in ANME cells cannot be fully excluded, however no single organism has been found to sustain growth from both methanogenesis and reverse methanogenesis.

The assimilation of carbon into AOM consortial biomass is dependent on the presence of methane as an energy source (Wegener *et al.*, 2008). The bacterial partner predominantly

assimilates carbon dioxide, and thus is an autotroph. While ANME-2 cells were shown to assimilate larger portions of methane, ANME-1 cells predominantly incorporated carbon dioxide-derived carbon (Wegener *et al.*, 2008; Kellermann *et al.*, 2012). Therefore, Kellerman and colleagues (2012) suggested that the ANME-1 group should not be considered methanotrophic, as this would imply methane assimilation, but rather considered chemorganoautotrophic. Genomic data suggest that the ANME group utilizes the reverse acetyl CoA pathway to assimilate carbonyl and methyl groups derived from either carbon dioxide or carbon dioxide and methane (Meyerdierks *et al.*, 2010; Wang *et al.*, 2014). While methane is central to the energy metabolism, current knowledge suggests that carbon dioxide is the carbon source for the organisms in the ANME groups.

Sulfur metabolism in AOM consortia

Sulfate reduction in AOM consortia is methane-dependent and classically was thought to proceed in the bacterial partner. Since the proposal of an internal cycling of sulfur in AOM consortia this view has changed by attributing partial sulfate reduction to ANME and sulfur disproportionation to the bacterial partner. Dissimilatory sulfate reduction is carried out by a series of cytoplasmic enyzmes. Initially sulfate is activated by sulfate adenylyltransferase (Sat) to adenosine-5'-phosphosulfate (APS). Two reduction steps then convert APS to sulfite and further to sulfide. These reactions are catalyzed by APS reductase (Apr) and dissimilatory sulfite reductase (Dsr). Electrons are supplied to the reductases via different membrane-bound or via cytoplasmic enzyme complexes. These contain subunits of heterodisulfide reductases which are essential in electron transfer reactions (Pereira *et al.*, 2011). The heterodisulfide reductases of sulfate reducers are related to the CoM-CoB specific-heterodisulfide reductases found in methanogens and ANME. To date key enzymes of the canonical sulfate reduction pathway were localized exclusively in the bacteria as shown by immunolabeling of Dsr and Sat in ANME-2/DSS consortia (Milucka *et al.*, 2013). Possible specific modifications of the sulfate reduction pathway can presently not be inferred as no genomic data are available for the bacterial partner. The so far available draft genomes of ANME do not encode canonical sulfate reduction genes (Meyerdierks *et al.*, 2010; Wang *et al*., 2014). However, sulfate reduction in ANME may proceed via yet unknown enzymes. The presence of a supposedly non-CoM-CoB specific heterodisulfide reductase in the ANME-1 genome was interpreted as potentially relevant for sulfate reduction (Meyerdierks *et al.*, 2010). Moreover, Meyerdierks and colleagues (2010) reported an almost complete set

of genes for assimilatory sulfate reduction in ANME-1. However, ANME are expected to assimilate sulfide and thus a potential dissimilatory function of these assimilatory sulfate reduction genes was not excluded (Meyerdierks *et al.*, 2010). Further investigations are needed to derive a more complete picture of the sulfur metabolism in AOM consortia, the processes and genes involved and their spatial localization.

1.5. Research outline and objectives

The sulfate-dependent anaerobic oxidation of methane is of global importance as it converts methane, a potent greenhouse gas, to the less impactful carbon dioxide before it reaches the atmospheric methane pool. The investigations summarized in this thesis focused on the marine microbial consortium that couples sulfate reduction to methane oxidation in order to perform AOM. The interaction between methane-oxidizing archaea and sulfate-reducing bacteria is still not fully understood, but it is thought to be a case of syntrophy. This thesis includes reports on enrichment-based physiological investigations combined with metagenomic and metatranscriptomic analyses, which provide insight into the metabolism and the genomic profile of the organisms involved in AOM. The organisms that perform AOM at elevated temperatures and which belong to the ANME-1 clade and the HotSeep-1 cluster were the primary focus of these investigations.

The unifying objective of the investigations described in this thesis was to deepen the physiological understanding of the organisms involved in sulfate-dependent anaerobic oxidation of methane as well as their interspecies interactions within AOM consortia. More specifically, the aims were i) to understand the physiology of thermophilic AOM consortia and the interspecies interaction of ANME-1 and HotSeep-1, ii) to elucidate the physiology and genomic potential of the bacterial partner HotSeep-1, iii) to provide a comparison of the metabolic potential of different ANME-1 subtypes and iv) to determine the metabolic capabilities of different AOM enrichments. Based on these objectives, the research hypotheses and key questions of this thesis were outlined as follows:

- *Syntrophy in thermophilic AOM involves the exchange of a molecular intermediate or direct electron transfer.*

Thermophilic AOM is the analog to the more studied, cold-adapted AOM process and the organisms involved in the former are only distantly related to those involved in the latter. Therefore, like their cold-adapted counterparts, thermophilic AOM consortia may have unique physiological capabilities. The content of **Chapter II** focuses on the physiology of thermophilic AOM and the question of how ANME-1 and HotSeep-1 perform AOM.

- *The bacterial participant in thermophilic AOM is a novel species of sulfate reducer and is not restricted to growth in AOM consortia.*

Specific groups of *Deltaproteobacteria* have been shown to act as the bacterial partners in AOM consortia. However, little is known about their physiology and metabolic potential as no representatives could be isolated and maintained in pure culture. Further, genomic information on these organisms is limited. **Chapter III** summarizes work which has addressed the lack of knowledge concerning the specific physiological capabilities and genomic features of HotSeep-1, the bacterial partner in thermophilic AOM.

- *Anaerobic methanotrophs of clade I (ANME-1) share a central set of metabolic capabilities.*

The organisms classified as ANME-1 constitute a large phylogenetic group, distantly related to methanogens within the *Methanomicrobia*. The physiologic and metabolic characteristics of ANME-1 are largely unexplored, as is their diversity among members of the group. **Chapter IV** summarizes the results of a comparative genomic analysis which addressed the question: Do the genomes of different ANME-1 types encode similar or different metabolic potentials?

- *The microorganisms involved in AOM or associated with the AOM process have diverse metabolic capabilities.*

AOM is performed by a diverse set of consortia composed of ANME and SRB cells; however, the consortia members may not be restricted to AOM and may be capable of alternative metabolisms such as methanogenesis or sulfur disproportionation. Furthermore, in environments associated with AOM and laboratory enrichments, AOM consortia are accompanied by a smaller community whose metabolic potential is not well understood. Consequently, the microbial communities present in environments where AOM occurs require broader characterization. **Chapter V** is a comparative analysis of the community composition of several long-term AOM enrichments. In addition to questions of community composition, it addresses questions regarding the metabolic capabilities of specific community members.

1.6. Material and methods

The following section will provide an overview of the microbial material studied and the most relevant methods employed in this thesis. The enrichments of anaerobic methane-oxidizing consortia and the sulfate-reducing bacterial partner obtained in long-term cultivation approaches prior to and during the work of this thesis are introduced including information on their specific origin, growth conditions and phylogenetic composition. The strong dominance of AOM organisms in those enrichments provided a system that allowed applying culture-dependent methods while also benefiting culture-independent techniques. The methods employed combine microbiological approaches such as substrate tests with molecular techniques like isotope labeling, metagenomics and gene expression studies.

Microbial enrichments

Spatial and temporal agglomeration of specific microorganisms occurs naturally triggered by environmental parameters that favor growth of one or several types over others. Similarly the laboratory enrichment of microorganisms is achieved by providing defined culture media and selective conditions for the growth of subpopulations with specific metabolic traits from a bulk environmental sample. The principle of enrichment dates back to the early 1900's and the work of the microbiologists Berjerink and Winogradski. It refers to the process of selection and accumulation of organisms compatible with the given conditions and often is an initial step in the process of isolation. An enrichment culture opposed to a pure culture is composed of a community of multiple organisms of which some may be more abundant than others but community composition is not necessarily stable over time. Microbial enrichments are important when studying the "unculturable" ones, those microorganisms for which yet no pure culture growth conditions were found or which may depend on other organisms for sustained metabolism. The enrichments central to this thesis are anaerobic methane-oxidizing and hydrogenotrophic sulfate-reducing enrichments.

Anaerobe methane-oxidizing enrichments

Anaerobe methane-oxidizing enrichments are here defined as microbial enrichments obtained and maintained with methane and sulfate as sole energy source and electron acceptor and with carbon dioxide as sole carbon source. The selective conditions promote growth of anaerobic methane-oxidizing archaea and sulfate-reducing bacteria, the AOM consortia. All organisms

in the enrichments rely on methane as primary energy source; however metabolic by- and end-products may allow sustaining a side population of secondary consumers in the enrichment. The AOM enrichments studied here were originally initiated with environmental samples from methane-rich habitats: shallow water seeps off the coast of Elba, Italy and deep-sea hydrothermal vent sediments in the Guaymas Basin, Gulf of California, Mexico.

The Guaymas Basin is part of the Gulf of California, an ocean basin formed by active seafloor spreading. The Guaymas Basin is characterized by strong sedimentation of organic matter-rich material, which results in thick sediment layers of 100-500 m, covering the hydrothermally active center (Teske *et al*., 2002). Due to fluctuations in the hydrothermal activity the subsurface sediment temperatures are highly variable and reach temperatures of up to 300°C (Welhan, 1988). The steep temperature gradients lead to thermogenic alteration of organic matter and release organic acids, methane and diverse hydrocarbons (Simoneit and Lonsdale, 1982; Jørgensen *et al*., 1990; Martens, 1990). Thermal fluids, enriched in methane (up to 16 mM), hydrocarbons and sulfide percolate the sediment and create a system of focused and diffusive vents. A diverse anaerobic microbial community including thermophilic methanogens, methanotrophs, thermophilic and hyperthermophilic sulfate-reducers as well as hyperthermophilic fermenters thrives on these fluids (Jannasch *et al*., 1988; Burggraf *et al*., 1990; Teske *et al*., 2002; Schouten *et al*., 2003). Sulfate reduction and AOM were measured at temperatures from 60 to 95°C and between 35 to 90°C, respectively (Kallmeyer and Boetius, 2004). To further study the organisms responsible for thermophilic AOM, Guaymas Basin hydrothermally heated sediments were sampled during the RV Atlantis cruise AT15-56 in November/December 2009 (Alvin Dive 4570; 27°00.437 N, 111°24.548 W; water depth 1999 m). The sampling procedure and initial AOM enrichment preparation is described by Holler and colleagues (2011a) and in Chapter V of this thesis. Briefly, a sediment core was sampled from an area covered with *Beggiatoa* mats, indicative of AOM activity in the underlying sediment. Following *in situ* temperature profiling, the core was sectioned into horizons reflecting distinct temperature regimes: 2-13 cm (4-30°C; horizon A), 14-25 cm (30-60°C; horizon B) and 26-45 cm (60-85°C; horizon C). Sediment sections were diluted 1:1 with artificial seawater medium (Widdel and Bak, 1992) and stored under methane headspace until further processing (Holler *et al.*, 2011b). For enrichment of AOM consortia, samples were incubated under AOM conditions (sulfate-reducing bacteria medium (Widdel and Bak, 1992) containing 28 mM sulfate, 0.225 MPa methane and 0.025 MPa carbon dioxide) at temperatures respective to the *in situ* temperature in the depth horizon: 37°C for sediment of horizon A and 50°C or 60°C for sediment of horizon B. Activity of enrichments was

monitored by sulfide production. Culture medium was exchanged when sulfide concentrations reached 12 mM and the enriched biomass was regularly diluted. In long-term approaches (>1.5 years), sediment-free enrichments were obtained from the Guaymas Basin samples.

The seeps off the island Elba are located in shallow water depth (12 m) and are characterized by *in situ* temperatures of 12 to 27°C. Thermal fluids diffusing through the sandy sediments are rich in methane and other hydrocarbons. Sediment for AOM enrichments was sampled in 2010 by scuba diving. The microbial AOM enrichments established were initially sediment-free due to the sampling procedure and sediment texture (see Chapter V). Activity was monitored and biomass was diluted as described above.

The diversity of the enrichment was assessed using molecular biological tools including 16S rRNA gene sequencing and CARD-FISH (see below). The main community members were ANME-2c/Seep-SRB-2 in the Elba enrichment, ANME-1/Seep-SRB-2 in Guaymas Basin 37°C, and ANME-1/HotSeep-1 in the Guaymas Basin 50°C and 60°C enrichments (Fig. 5). Enrichment subsamples were used for physiological experiments including substrate tests, and isolation approaches as well as metagenome and metatranscriptome sequencing.

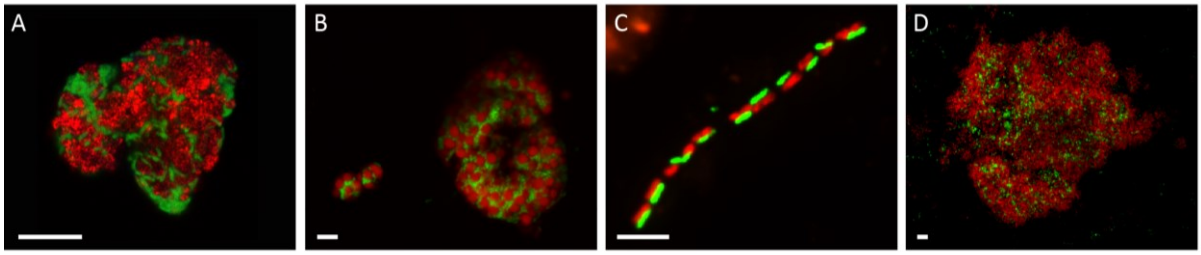

Figure 5 AOM consortia types from enrichments studied in this thesis. Cells are visualized by fluorescence *in situ* hybridization. (**A**) ANME-2c/Seep-SRB-2 aggregate from Elba enrichment (20°C). (**B**) ANME-1/Seep-SRB-2 aggregates from Guaymas Basin enrichment (37°C). (**C**) ANME-1/HotSeep-1 filament from Guaymas Basin enrichment (50/60°C). (**D**) ANME-1/HotSeep-1 aggregate from Guaymas Basin enrichment (50/60°C). Red: ANME archaea; green: bacterial partner. Scale bars: 5 µm.

In the main focus of this thesis are the thermophilic AOM enrichments from Guaymas Basin (50°C and 60°C). These enrichments were shown to be initially dominated by filamentous AOM consortia (Fig. 5 C) (Holler *et al.*, 2011b), but growth morphology of consortia changed over time to large aggregates that reached sizes of 500 µm in diameter (Fig. 5 D, 6). These aggregates are of brownish-red color and contain crystal needles and iron sulfide precipitates. The contained biomass shows, when excited with fluorescence light of specific wavelength distinct autofluorescence patterns indicative of ANME-1 and HotSeep-1 cells (Fig. 6).

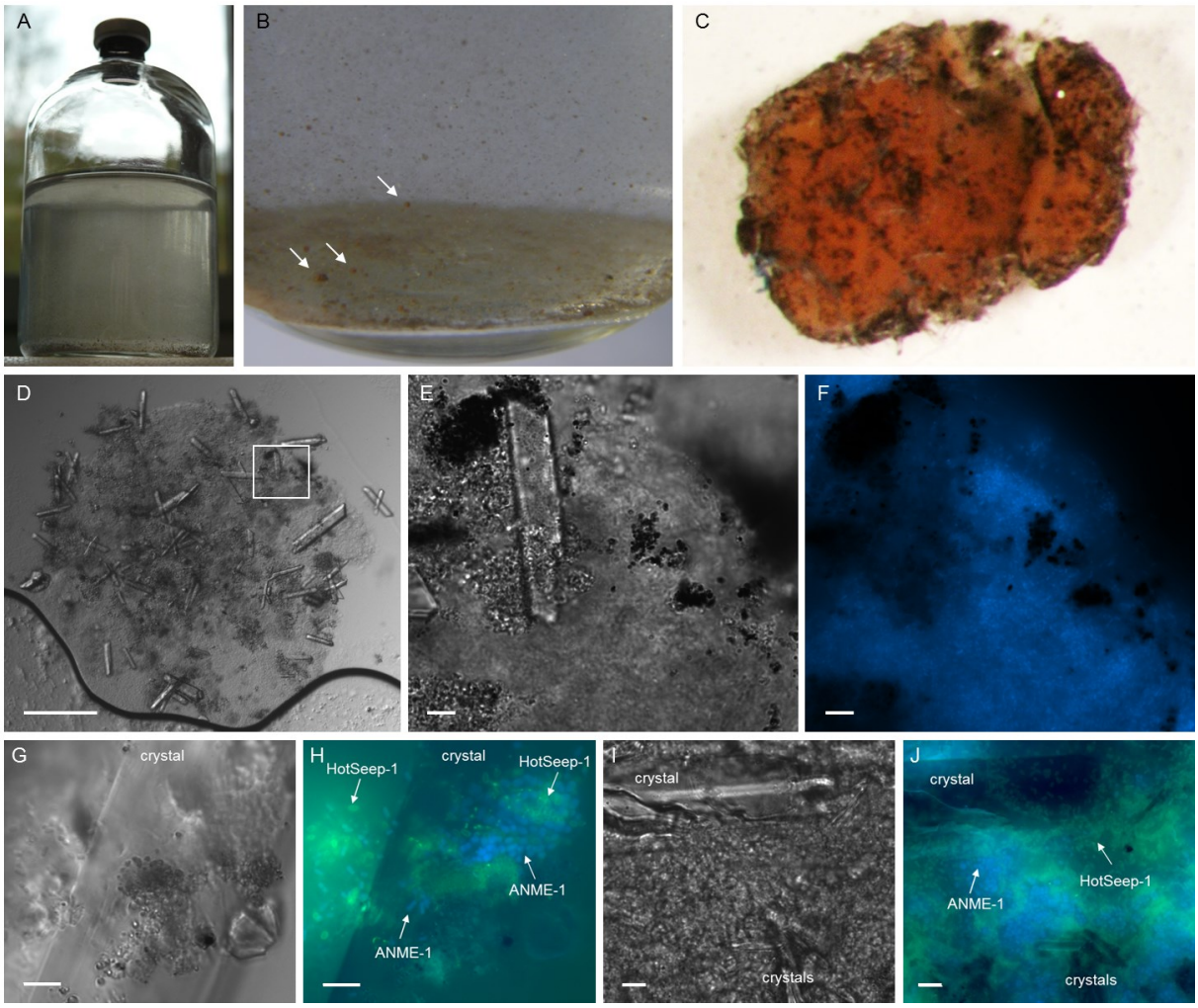

Figure 6 Visualization of thermophilic anaerobic methane-oxidizing enrichment. (**A**) Long-term enrichment incubated for 2 years at 50 or 60°C. Enrichment is sediment-free but contains crystals and precipitates originating from culture medium and microbial activity. (**B**) Close up view on the enrichment depicted in (A). Microbial biomass occurs in aggregates, some are marked by arrows. (**C**) Image of a microbial aggregate from enrichment depicted in (A). Brownish-red color likely originates from presence of c-type cytochromes; dark spots are inorganic iron sulfide precipitates. (**D**) Bright field image of a microbial aggregate from (A). Large crystals are visible. Scale bar: 100 µm. (**E**) Bright field image of area marked in (D) showing crystal and iron sulfide precipitates (dark spots). (**F**) Fluorescence image of (E). Cells (blue) are stained with DAPI to show microbial biomass. (**G,I**) Bright field images obtained from (A). (**H,J**) Fluorescence image of (G) and (I), respectively. ANME cells are identified by blue autofluorescence which is attributed to the presence of the methanogenic cofactor F_{420} (Doddema and Vogels, 1978). HotSeep-1 cells are identified by green autofluorescene. Source of autofluorescence in HotSeep-1 is not known. Scale bars in (E-J): 5 µm.

Hydrogenotrophic sulfate-reducing enrichments

Hydrogenotrophic enrichments of sulfate-reducing bacteria were obtained and maintained with hydrogen and sulfate as energy source and electron acceptor and with carbon dioxide as sole carbon source. Hydrogen is a common electron donor for sulfate reducers and the selective conditions favor growth of chemolithoautotrophic sulfate reducers. The hydrogenotrophic enrichments studied here were obtained with AOM enrichment subsamples as inoculum and by subsequent dilution-to-extinction series (see Chapter II and III).

Enrichments were provided with sulfate reducer medium (28 mM sulfate), hydrogen (0.18 MPa) and carbon dioxide (0.02 MPa). The enrichment central to this thesis is the thermophilic hydrogenotrophic enrichment, obtained from the thermophilic AOM enrichment that is highly dominated by HotSeep-1 cells (95%; Fig. 7; see Chapter II and III). The diversity of the enrichment was assessed using molecular biological tools including 16S rRNA gene sequencing and CARD-FISH (see below). Enrichment subsamples were used for physiological experiments including substrate tests, as well as metagenome and metatranscriptome sequencing.

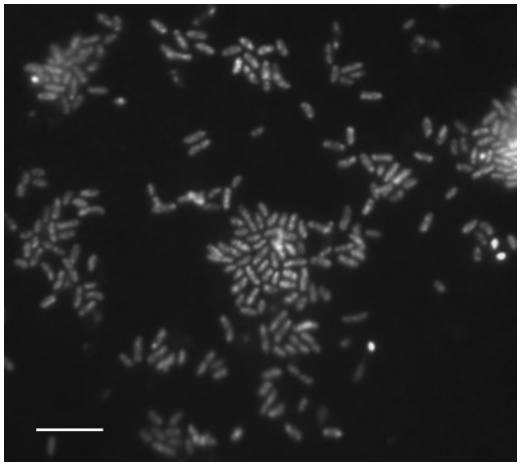

Figure 7 HotSeep-1 enrichment growing on hydrogen. Fluorescence image of DAPI stained cells. Colors are changed to black and white for better contrast. Scale bar: 5 µm.

Methods applied to characterize the physiology of microorganisms

The field of microbial physiology concerns the study of the metabolism, structure, growth and genetic basis of the cell and its interrelation with the environment. Classic microbiological approaches require a rather defined system (pure cultures). Here we studied slow-growing enrichments with substantial contaminations of microorganisms that are not directly involved in AOM. Thus, the AOM enrichments needed constant maintenance and experimental approaches required optimization for limited biomass and accountance for the presence of multiple responsible organisms.

Substrate tests

Classically the metabolic capabilities of an isolate are determined by following the consumption of a provided substrate and the production of a metabolic product. When applied to enrichments such substrate tests aid to identify the possible alternative metabolic capabilities of all organisms present. Studying syntrophic associations, the response to artificial substrates is indicative for the substrate being an intermediate of the syntrophy or an

alternative substrate for one of the partners. We performed substrate tests with enrichment aliquots of either the AOM enrichments or the HotSeep-1 enrichment. The enrichments were tested for alternative sulfur metabolism, alternative organic and inorganic electron donors and alternative organic carbon sources to carbon dioxide. The culture medium was sulfate reducer medium, optionally omitting sulfate when testing for alternative electron acceptors or disproportionation. All soluble compounds tested were supplemented in defined portion from sterile anoxic stock solutions. Metabolic activity was followed by sulfide production, methane production and selectively by cell counts. Incubations showing a positive response to the substrate were analyzed for the enriched organisms using molecular tools.

^{14}C tracer incubations

Incubation with radiolabeled substrates are advantageous when studying slow growing organisms as already trace activities can be measured as tracer turnover. In ^{14}C tracer assays the sample is incubated with a ^{14}C-labeled substrate, here ^{14}C-bicarbonate or ^{14}C-methane in the presence of unlabeled substrate for a defined period of time. To measure methane oxidation rates, samples were incubated with carrier-free ^{14}C-methane tracer in the presence of methane, sulfate and carbon dioxide. At the incubation end, samples were transferred to NaOH and immediately sealed. To determine activity of ^{14}C-methane, the headspace gas was combusted and trapped as carbon dioxide as previously described (Treude *et al*., 2003; Holler *et al*., 2011a). Radioactivity was subsequently measured by liquid scintillation counting. To determine transfer of ^{14}C from methane to the product pool (CO_2) the sample was acidified and in a closed system the emerging carbon dioxide was trapped as carbamide following previously reported protocols (Treude *et al*., 2003; Holler *et al*., 2011a). The activity of the $^{14}CO_2$ fraction was determined by liquid scintillation counting. The rate of methane oxidation was calculated from the tracer turnover, the methane concentration and incubation time.

To measure the enzymatic back reaction of methane oxidation samples were incubated with ^{14}C-bicarbonate in the presence of methane, sulfate and carbon dioxide. At the incubation end, the activity of the carbon dioxide and methane pool was determined as described above. The back reaction rate was calculated from the tracer transfer considering the concentration of bicarbonate and the incubation time.

To quantify carbon assimilation and determine the carbon source assimilated in AOM enrichments samples were incubated with either ^{14}C-methane or ^{14}C-bicarbonate in the presence of methane, sulfate and carbon dioxide for a defined period of time. Uptake of labeled carbon into biomass was determined by transferring the sample onto filters. After

removal of residual inorganic carbon by exposure to HCl atmosphere, radioactivity was determined by liquid scintillation counting. Assimilation rates of methane or carbon dioxide were calculated from the tracer turnover, considering the concentrations of methane or bicarbonate, respectively and incubation time.

Carbon assimilation by the hydrogenotrophic HotSeep-1 enrichment was determined by incubation of samples with ^{14}C-bicarbonate following the same approach as described above but instead of methane supplying hydrogen as energy source.

Methods to identify and visualize microorganisms

The identification and classification of microorganisms has been largely based on the comparison of their genetic material since classification systems based on physiological and morphological properties were found to be inapplicable. The phylogenetic classification of the microbial world has been revolutionized by the use of the 16S rRNA gene as evolutionary marker, which was initially introduced by Woese in the 1970's and remains in use to date. The detection of the 16S rRNA *in situ* applying fluorescently labeled oligonucleotides has been widely used to link phylogenetic identification and quantification. We used sequencing of the 16S rRNA gene to identify the microbial community in enrichments and applied CARD-FISH to show spatial arrangement of dominant groups.

Amplification, sequencing and analysis of 16S rRNA genes

The 16S rRNA gene, because of its ubiquitous presence, its conserved function and interspaced conserved and variable sequence regions allows inferring phylogenetic relatedness of organisms based on comparative analysis of their sequence. We used a clone library based approach to identify the dominant members of enrichment cultures based on their 16S rRNA gene phylogeny. The employed protocol starts with the PCR amplification of the 16S rRNA gene from a bulk DNA extract, using general primer pairs for archaea and bacteria. Amplicons were purified in a gel, ligated into a vector and cloned into competent *Escherichia coli* cells. Separation of *E. coli* cells by plating and subsequent PCR amplification and Sanger sequencing of separate colonies allows retrieval of the 16S rRNA gene of a specific community member. Sequences were phylogenetically classified using the SILVA SSU reference database (Quast *et al.*, 2013) and the ARB software package (Ludwig *et al.*, 2004). The number of sequences obtained by this method is rather small (~100 clones per library) when compared to next generation sequencing techniques that allow to deeply

sequence microbial communities. However, it is sufficient to describe the dominant community members and importantly provides full length sequences of those.

Application of 16S rRNA targeted fluorescence probes (CARD-FISH)

The rRNA targeted fluorescence *in situ* detection of microorganisms applies fluorescently labeled oligonucleotide probes designed to complementarily bind on a region of the 16S rRNA of a specific taxonomic group. Those probes may be general to match all bacteria or specific to target classes like *Deltaproteobacteria* or even smaller clades. A more sensitive alternative to FISH is CARD-FISH which combines horseradish peroxidase labeled oligonucleotide probes with catalyzed reporter deposition of fluorescently labeled tyramides (Amann and Fuchs, 2008). The standard CARD-FISH protocol according to Pernthaler and colleagues (2002) was used here with some modification. In short, cells were fixed with formaldehyde to stabilize cell morphology followed by embedding in agarose and inactivation of endogenous peroxidases by hydrogen peroxide treatment. Cell wall permeabilization is required for probe penetration into the cells and depends on the type of sample. Cell wall permeabilization was achieved by treatment with lysozyme, proteinase K or a combination of both. Subsequently, the probe was applied to the sample at stringent temperature and formamide concentration in a hybridization buffer. After probe hybridization, remaining unbound probe was washed away. Signal amplification was achieved by incubation with fluorescently labeled tyramides. The tyramides are converted to a radical stage by the horseradish peroxidase enzyme and bind to the cell wall to give a strong signal (Amann and Fuchs, 2008). In a final washing step unbound probe was removed. In case of a double hybridization the peroxidases are inactivated prior to application of the second probe, which follows the same subsequent steps as described. Samples were visualized using epifluorescence microscopy with filter sets for excitation and emission respective to the applied tyramides. Optionally confocal laser scanning microscopy was applied to obtain images of consortia.

Methods to study genomic potential and gene expression

The term genome, first proposed 1920 by the botanist Hans Winkler refers to the total hereditary information of an organism encoded in DNA, or RNA in viruses. Genomics broadly describes the study of genes and their functions in an organism. The related term transcriptomics describes the study of RNA, the expressed part of the genome while

proteomics describes the study of proteins, the translated part of the genome of an organism. Genomics and related 'omics' fields have greatly improved the understanding of the functioning of single, isolated organisms. In contrast the emerging fields of metagenomics, metatranscriptomics or metaproteomics facilitate the study of the collective of the genomes, transcriptomes or proteomes of a microbial community. These approaches allow insights into the metabolic potential of organisms that remain unculturable and also allow studying the metabolic functioning and activity of complex assemblages in their natural environment. We used metagenome sequencing of enrichments to reconstruct the draft genomes of dominant community members. This genomic information allowed insight into the metabolic potential of the organisms. We performed metatranscriptome sequencing of the same enrichments to obtain information of the actively expressed genes and in combination with substrate incubation experiments determined gene expression patterns.

From metagenomes to draft genomes

The metagenome of a sample contains the sum of the genetic information of its members. To obtain a metagenome a sample of genomic DNA is randomly fragmented and, in a so called shot gun approach, sequenced using next generation sequencing technologies. Subsequently bioinformatic tools are required to assemble the short sequence fragments into larger fragments (contigs) and assign those genome fractions to members of the community.

In this approach we used the Illumina sequencing technology for metagenome sequencing of AOM enrichments and sulfate-reducing enrichments. The principle workflow of DNA library preparation starts with the fragmentation of high molecular weight genomic DNA. DNA fragments of the required length for library preparation are selected via the Solid Phase Reversible Immobilization (SPRI) bead method or by extracting them from a preparative agarose gel (Fig. 8). The two general types of libraries used here are distinguished as paired end and mate pair library. For paired end libraries a fragment size of ~500 bp was selected using SPRI beads. The protocol of paired end library preparation includes several steps to prepare the DNA fragment for adapter ligation including end repair and attachment of a 5' A overhang base. Two different adapters are ligated to the 5' and 3' end of a fragment to facilitate sequencing of the same fragment from both sides. Paired end sequencing generates two reads per fragment that represent the 5' end of the forward and reverse DNA strand, respectively, and point towards each other. In contrast to paired end libraries, mate pair libraries are prepared from larger fragments excised from an agarose gel, here >5000 bp. The principle workflow encompasses the attachment of biotin-labeled adapters to both ends of the

DNA fragment followed by fragment circularization and re-fragmentation. Fragments containing the biotin tag are enriched. Those fragments represent the two ends of the initial long fragment in an inverted direction. After further steps to prepare the fragment for adapter ligation, the sequencing adapters are attached. Paired end sequencing of these fragments produces reads that point away from one another on the original DNA fragment. While paired end reads may overlap to produce a larger fragment mate pair reads do not and are referred to as jump libraries as the read pairs represent distant regions on the genome. Mate pair data in combination with paired end reads are usually beneficial for the assembly and scaffolding process.

Illumina technology bases on sequencing by synthesis meaning that the base pair composition of a DNA strand is captured base-by-base while being synthesized. Prior to sequencing the adapter ligated DNA fragments are immobilized on a solid surface, the flow cell, and are clonally amplified generating clusters of millions of identical sequences. Illumina platforms use the cyclic reversible termination technology with color labeled dNTPs to determine base composition of the DNA fragment. In this process, the polymerase enzyme reads along the DNA fragment and incorporates a fluorescently labeled dNTP complement to the template's base, which is subsequently detected by fluorescence signal. As each base has a unique fluorescence emission the detected color converts to its identity. After cleavage of the 3' end blocking group and dye the next sequencing cycle starts. Number of cycles determines the read length which currently is limited to a maximum of 300 bp. In paired end sequencing runs, two reads are generated in subsequent sequencing steps. Illumina sequencing is one of the several next generation sequencing technologies which because of its principle of sequencing claims low error rate and allows high throughput and massive data production in short time and to moderate costs.

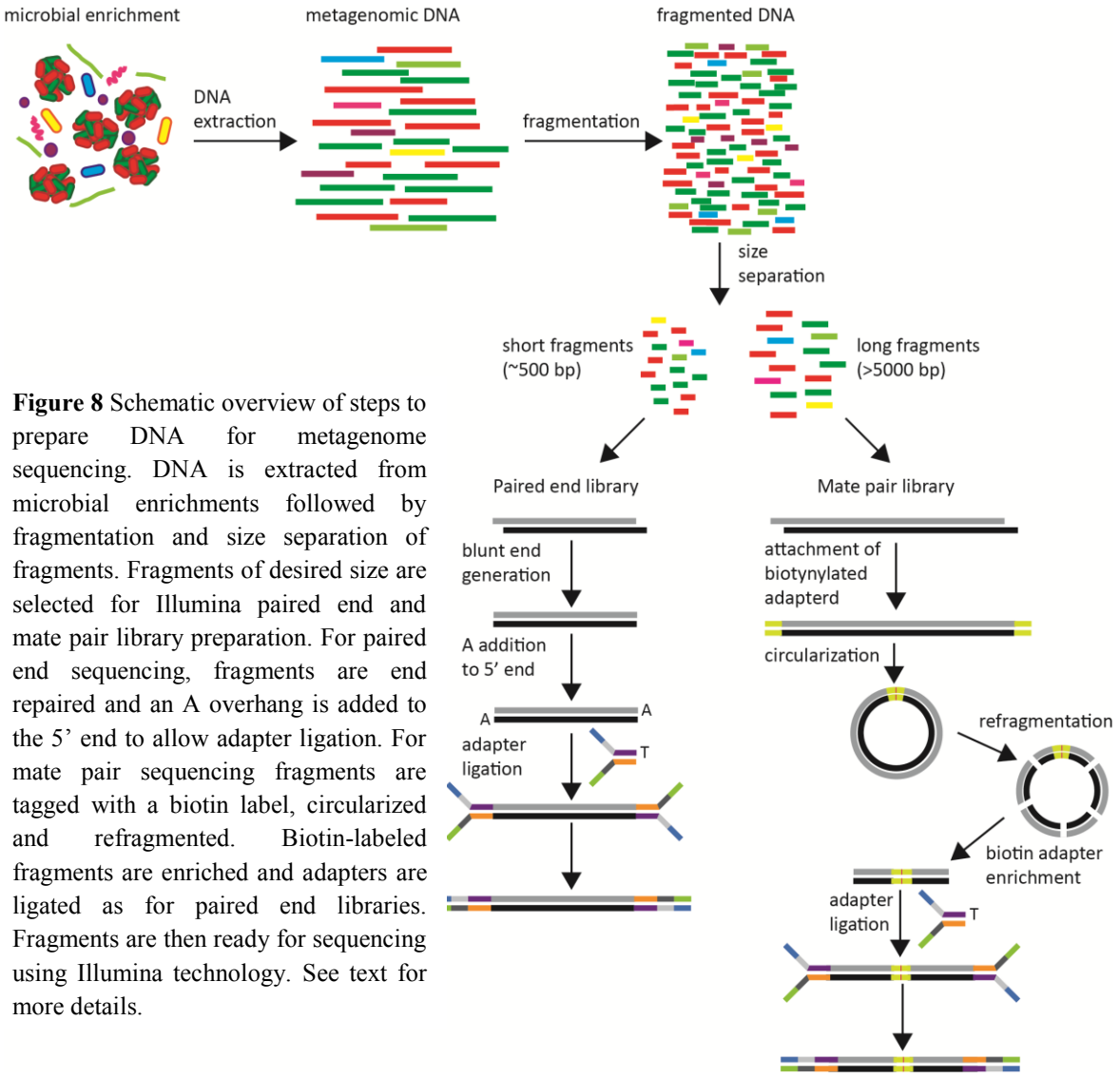

Figure 8 Schematic overview of steps to prepare DNA for metagenome sequencing. DNA is extracted from microbial enrichments followed by fragmentation and size separation of fragments. Fragments of desired size are selected for Illumina paired end and mate pair library preparation. For paired end sequencing, fragments are end repaired and an A overhang is added to the 5' end to allow adapter ligation. For mate pair sequencing fragments are tagged with a biotin label, circularized and refragmented. Biotin-labeled fragments are enriched and adapters are ligated as for paired end libraries. Fragments are then ready for sequencing using Illumina technology. See text for more details.

Assembly is the process of joining together the small fragments (reads) to reconstruct the larger DNA fragments that they originate from and which eventually represent the genome of an organism. Assemblies of metagenome datasets are complicated by the fact that the fragments originate from several organisms, and hence the reconstruction process becomes more complex. Genome assembly and metagenome assembly especially is a compute intensive process that is prone to errors as often fragments are joined wrongly or discarded besides being part of the assembly. Repeat elements and missing data eventually limit the ability to reconstruct the complete fragment initially sequenced and hence often prevent complete genome assembly. *De novo* assemblies (assemblies of genomes for which no reference is available) are evaluated based on general metrics such as contig number, contig length, assembly length or N50 value. N50 is the contig size above which 50% of the assembly is represented. Other measures to judge genome assembly quality are estimates of the completeness based on single copy genes, tRNAs or other functional marker genes. In our

approach we used the metagenome assembly as a basis to extract and reconstruct the genomes of abundant community members (Fig. 9). The initial metagenome assembly was binned, a process in which contigs belonging to the same organism are grouped together, according to tetranucleotide frequency, GC content and coverage. The bins of organisms of interest were extracted for targeted bin reassembly. This included mapping of the original reads to the bin, reassembly using mapped reads and re-binning. This process was repeated until no further increase of assembly quality was achieved. Contigs were arranged into larger fragments so called scaffolds and were annotated using protein domain models, blastp hits and subcellular localization patterns. The annotated draft genomes were analyzed for the encoded metabolic potential and genetic basis involved in cellular functions.

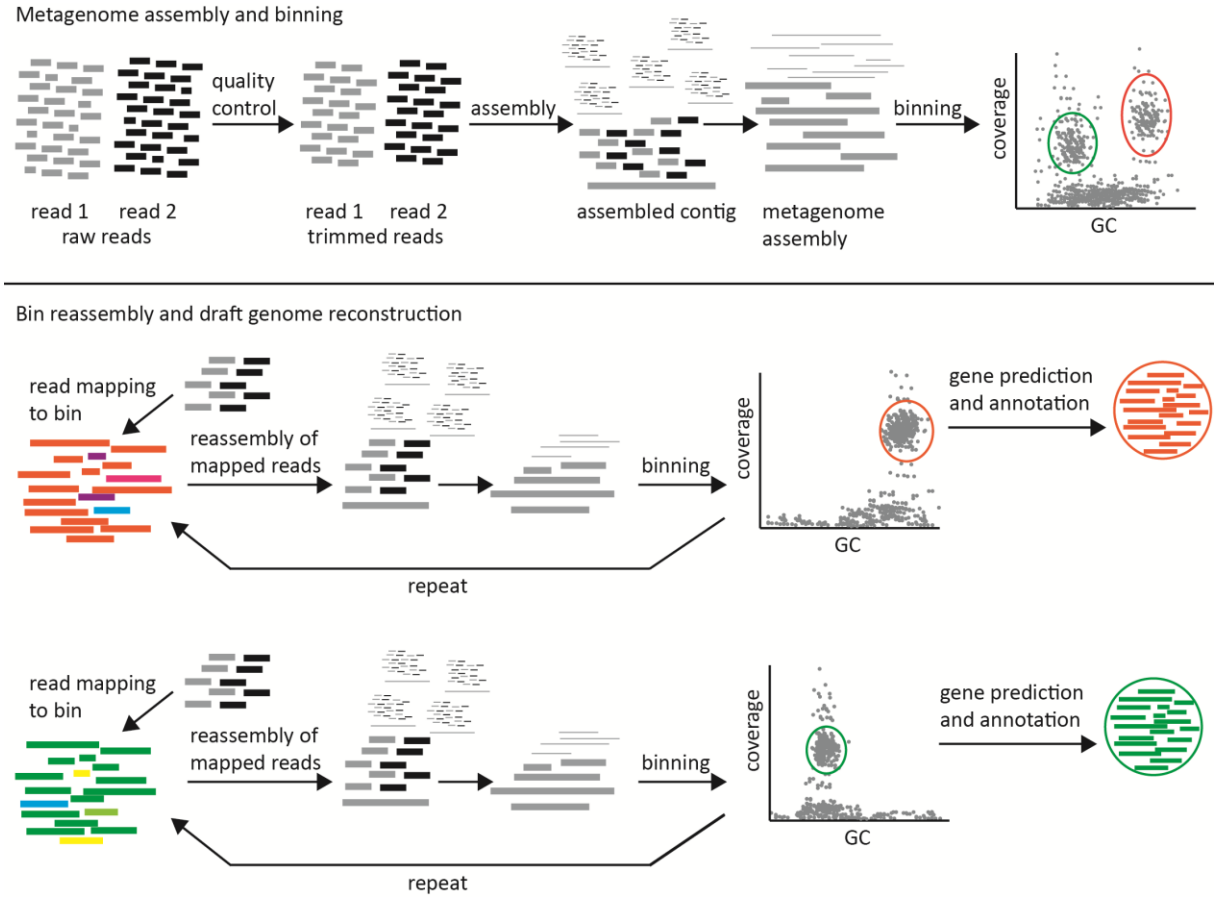

Figure 9 Schematic overview of metagenome assembly and draft genome reconstruction. Illumina raw reads are quality controlled and then assembled to reconstruct larger fragments (contigs) which altogether represent the metagenome. Contigs of the metagenome assembly are assigned to separate bins (potentially presenting the genome of an organism) in a process called binning. Bins can be selected based on GC and coverage spread of contigs. To obtain improved assembly of a selected bin, reads are mapped to the respective contigs and reassembly followed by binning of contigs is repeated. The process is iterated until assembly quality is not improved anymore. The final bin is annotated and considered a draft genome. Color coding: grey and black for forward and reverse Illumina read, respectively and larger assembled fragments (contigs); red and green indicate contigs of two different bins; other colors indicate contigs not belonging to the target bin (e.g. contamination from genomes of other organisms).

Metatranscriptomics – studying gene expression in a diverse culture

A metatranscriptome captures the genes expressed by a community of microorganisms at a certain time point and therewith provides a snapshot of the active microbial community and its metabolism. Because RNA and especially mRNA, the template for protein synthesis, are easily degradable, preservation of RNA at the moment of sampling is crucial to avoid RNA loss and artificial changes in the gene expression profile. In our studies we worked with thermophilic anaerobes for which a transition from their growth temperature and anaerobic milieu is likely to affect gene expression patterns. Furthermore, because biomass of enrichment cultures was limited, the method for RNA extraction had to be optimized for low input samples. For RNA expression experiments we therefore used a protocol that included initial sample preservation in RNAlater (Sigma, Aldrich) under *in situ* conditions (60°C and specific headspace gas composition). This step was crucial since omitting it resulted in low quantity and poor quality of RNA. RNAlater was subsequently removed by transferring the sample onto a 0.2 μm pore size polycarbonate filter using a vacuum filtration set up. RNA was immediately extracted from the filter using a commercial RNA extraction kit (see also Chapter II).

We performed Illumina sequencing on total RNA extracts from AOM enrichments and HotSeep-1 enrichments using strand-specific library preparation and paired end or single end sequencing. Because of the low amount of total RNA input, an enrichment of mRNA was omitted and total RNA was sequenced. The protocol for RNA Seq library preparation starts with fragmentation of input RNA. Next, RNA fragments are reverse transcribed into cDNA, a step called first strand synthesis. In the next step, the second strand is synthesized using the cDNA as template. Finally, adapters are ligated to the cDNA fragments to allow Illumina sequencing as described above.

The reads obtained were mapped to draft genomes and quantified as counts per genome feature (gene). Several ways exist to represent RNA Seq data. To quantify and compare gene expression, the transcript counts per genome feature were first normalized to the length of the feature (bp). To obtain its relative transcription value (T), the normalized counts value of a genome feature *i* was put into relation with the normalized counts values of all other genome features using the following equation, according to Li and colleagues (2010):

$$\mathrm{T_i} = X_\mathrm{i} / l_\mathrm{i} \times (\sum X_\mathrm{j} / l_\mathrm{j})^{-1} \qquad (2)$$

where X = counts and l = length of the feature (bp). For ease of notation, the relative transcription values were multiplied by 10^6, and are given in terms of transcripts per million (TPM). When comparing data from replicate substrate incubation experiments, differential gene expression was tested using ANOVA-like statistics and applying a compositionality correction to the dataset.

1.7. Overview of enclosed manuscripts

Chapter II

Intercellular wiring enables electron transfer between methanotrophic archaea and bacteria

Gunter Wegener, Viola Krukenberg, Dietmar Riedel, Halina E. Tegetmeyer & Antje Boetius

Published in Nature 526, 587-590 (22. October 2015)

This study reports on the physiology of thermophilic methane-oxidizing enrichments consisting of consortia of ANME-1 and HotSeep-1. Based on results from substrate experiments in combination with gene expression analysis and electron microscopic visualization techniques a model of direct interspecies electron transfer is proposed for the archaeal-bacterial interaction in thermophilic AOM.

The study was cooperatively designed by G. Wegener, V. Krukenberg and A. Boetius. G. Wegener, V. Krukenberg and H.E. Tegetmeyer performed experiments and data analysis. D. Riedel performed electron microscopy. G. Wegener, V. Krukenberg and A. Boetius wrote the manuscript with contributions from the other co-authors.

Chapter III

***Candidatus* Desulfofervidus auxilii, a hydrogenotrophic sulfate-reducing bacterium involved in the thermophilic anaerobic oxidation of methane**

Viola Krukenberg, Katie Harding, Michael Richter, Frank Oliver Glöckner, Harald Gruber-Vodicka, Birgit Adam, Jasmine Berg, Katrin Knittel, Halina E. Tegetmeyer, Antje Boetius & Gunter Wegener

Submitted to Environmental Microbiology (21. October2015)

This study describes the first ANME-free enrichment of an AOM partner bacterium, HotSeep-1. The physiology and genome of this representative of the HotSeep-1 cluster are analyzed and its deep-branching phylogenetic position is discussed with the proposal to name this chemolithoautothrophic sulfate-reducing bacterium *Candidatus* Desulfofervidus auxilii.

The study was designed by V. Krukenberg, A. Boetius and G. Wegener. Experiments were performed by V. Krukenberg and K. Harding. Data were analyzed by V. Krukenberg, K. Harding, M. Richter, H. Gruber-Vodicka, K. Knittel and G. Wegener. Microscopic imaging was performed by V. Krukenberg, B. Adam, J. Berg and H. Gruber-Vodicka. V. Krukenberg, A. Boetius and G. Wegener wrote the manuscript with contributions from all co-authors.

Chapter IV

Comparative analysis of the metabolic potential of different subgroups of anaerobic methanotrophic archaea of clade 1

Viola Krukenberg, Harald Gruber-Vodicka, Halina E. Tegetmeyer & Gunter Wegener

In preparation for submission

In this study the draft genomes of meso- and thermophilic ANME-1 are analyzed and compared to the available draft genome of psychrophilic ANME-1. The general metabolic potential is shown to be shared among ANME-1 and a modified reverse methanogenesis pathway is proposed to be a likely characteristic of the ANME-1 clade. We found indication for the capability of direct interspecies electron transfer in all analyzed ANME-1 subclades suggesting similar metabolic interspecies interaction as described in the thermophilic subclade.

The study was designed by V. Krukenberg and G. Wegener. Experiments and data analysis were performed by V. Krukenberg, H.E. Tegetmeyer and H. Gruber Vodicka. The manuscript was written by V. Krukenberg and G. Wegener and with contributions from all co-authors.

Chapter V

Metabolic capabilities of microorganisms involved in and associated with the anaerobic oxidation of methane

Gunter Wegener, Viola Krukenberg, S. Emil Ruff, Matthias Y. Kellermann & Katrin Knittel

Submitted to Frontiers in Microbiology; Special issue: Living on gas – microbial degradation of gaseous alkanes, from mud to genes (23. October 2015)

In this study we compared the phylogenetic composition and metabolic capabilities of sediment-free anaerobic methane-oxidizing enrichments. We found distinct dominating AOM consortia types and a differing phylogenetic composition including the presence of species that are unlikely directly involved in AOM. We could show that alternative catabolic processes such as methanogenesis and sulfur disproportionation are not performed by ANME and their partner bacteria but by less abundant background community members.

This study was designed by G. Wegener and V. Krukenberg. Experiments and data analysis were performed by G. Wegener and V. Krukenberg with contributions of M.Y. Kellermann, S.E. Ruff and K. Knittel. The manuscript was written by G. Wegener and V. Krukenberg with contributions from all co-authors.

Chapter II

Intercellular wiring enables electron transfer between methanotrophic archaea and bacteria

Gunter Wegener[1,2*], Viola Krukenberg[1*], Dietmar Riedel[3], Halina E. Tegetmeyer[4,5] and Antje Boetius[1,2,4]

[1]Max-Planck Institute for Marine Microbiology, Bremen, Germany

[2]MARUM, Center for Marine Environmental Sciences, University Bremen, Germany

[3]Max Planck Institute for Biophysical Chemistry, Göttingen, Germany

[4]Alfred Wegener Institute, Helmholtz Center for Polar and Marine Research, Bremerhaven, Germany

[5]Center for Biotechnology, Bielefeld University, Bielefeld, Germany

Nature 526, 587-590

Correspondence to: gwegener@mpi-bremen.de, vkrukenb@mpi-bremen.de

[*]These authors contributed equally to this work.

Abstract

The anaerobic oxidation of methane (AOM) with sulfate controls the emission of the greenhouse gas methane from the ocean floor[1,2]. In marine sediments, AOM is performed by dual-species consortia of anaerobic methanotrophic archaea (ANME) and sulfate-reducing bacteria (SRB) inhabiting the methane-sulfate transition zone[3-5]. The biochemical pathways and biological adaptations enabling this globally relevant process are not fully understood. Here we studied the syntrophic interaction in thermophilic AOM (TAOM) between ANME-1 archaea and their sulfate-reducing partner bacteria HotSeep-1[6] thriving at 60°C, to test the hypothesis of a direct interspecies exchange of electrons[7,8]. The activity of TAOM consortia was compared to the first ANME-free culture of an AOM partner bacterium that grows on hydrogen as sole electron donor. The thermophilic ANME-1 do not produce sufficient hydrogen to sustain the observed growth of the HotSeep-1 partner. Enhancing the growth of the HotSeep-1 partner by hydrogen addition represses methane oxidation and metabolic activity of the ANME-1. Further supporting the hypothesis of direct electron transfer between both partners, we observed that under TAOM conditions, both the ANME and the HotSeep-1 bacteria overexpress genes for extracellular cytochrome production, and form cell-to-cell connections resembling the nanowire structures for interspecies electron transfer between syntrophic consortia of Geobacter[9,10]. HotSeep-1 highly expresses genes for pili production only during consortial growth on methane, and the nanowire-like structures are absent in HotSeep-1 cells isolated on hydrogen. These observations suggest that direct electron transfer is a principle mechanism in thermophilic AOM, which may also explain the enigmatic functioning and specificity of other methanotrophic ANME-SRB consortia.

Main text

The anaerobic oxidation of methane with sulfate (AOM) controls the emission of methane from the seabed[1,3,4]. At environmental conditions the net reaction (Eq. 1)

$$CH_4(aq) + SO_4^{2-} \rightarrow HS^- + HCO_3^- + H_2O \quad (1)$$

allows an energy yield of only –20 to –40 kJ per mol methane oxidized, shared between the two partner organisms. Generally, AOM consortia show exceptionally slow growth with generation times >2 months, which has so far impeded their cultivation[6,11]. Sulfate-coupled AOM in marine habitats is performed by members of three different ANME clades (ANME-1,-2,-3), which associate physically with specific partner bacteria of the *Desulfosarcina*/*Desulfococcus* or the *Desulfobulbus* cluster[11-13], suggesting an obligate functional role of the sulfate-reducing bacteria in AOM. Early studies had already suggested a syntrophic coupling of both partners via a transfer of reducing equivalents[4,14]. Yet, the underlying mechanisms remain unknown. Biochemically, the anaerobic oxidation of methane appears in the ANME and involves a reversal of the enzymatic machinery of the methanogenesis pathway[15-18]. However, reversing an energy-yielding process is per se endergonic, and hence AOM requires an efficient transfer of reducing equivalents from methane to sulfate, so that the ANME can gain energy by AOM[14,19]. Previous results indicate that the sulfate reducing partner bacteria[4,20] act as electron sink of AOM, but recently also members of the ANME-2 clade were suggested to perform incomplete sulfate reduction by a yet unknown pathway[21].

In this study we focused on the hypothesis of syntrophic growth in thermophilic AOM consortia by direct interspecies electron transfer, and tested this and alternative hypotheses (mechanisms illustrated in Extended Data Fig. 1). The studied sediment-free TAOM enrichment was cultivated at 60°C supplied with 28 mM sulfate and 0.2 MPa methane, allowing an energy yield (ΔG_R) of −34 kJ mol^{-1}, and resulting in doubling times of approx. 68 days (Fig. 1a) and growth efficiencies of 2% (see Methods). The culture is dominated by consortia of ANME-1 and HotSeep-1 appearing in an approximate 1:1 stoichiometry. Due to their larger size ANME account for around 75% of the consortial biomass (Fig. 1b; Extended Data Table 1). Using a dilution-to-extinction approach (1:10 to $1:10^9$) with hydrogen (0.2 MPa) and sulfate (28 mM), we were able to separate a strain of HotSeep-1 identical with the partner bacterium of the TAOM consortium (>99% identity in 16S rRNA gene and internal transcribed spacer region (ITS); and (genomic) average nucleotide identity (ANI) of >99%; Extended Data Table 2). This strain grows without ANME-1 as single cells or in

monospecies aggregates (Extended Data Fig. 2a) and with a single contaminant, *Archaeoglobus* sp. (1-5% of all cells), which does not form consortia with HotSeep-1. Substrate tests with the HotSeep-1 culture showed that it is an obligate chemolithoautotroph with hydrogen and sulfate as sole molecular redox couple and doubling times of 4 to 6 days (see Methods and Extended Data Fig. 2b,c). Although the supplied hydrogen (0.2 MPa) could provide a tenfold higher energy yield to HotSeep-1 than syntrophy in TAOM (ΔG_R=−151 kJ mol^{-1} vs. −17 kJ mol^{-1}, i.e. half of the net energy yield of TAOM consortia), its carbon assimilation remained similarly low (approx. 1.5% of converted reducing equivalents).

We compared the activity of the TAOM consortia and the hydrogenotrophic HotSeep-1 by physiological experiments combined with metagenomic and metatranscriptomic analyses and electron microscopy of the involved organisms. A classical experiment for the study of syntrophy in dual-species consortia is the addition of potential intermediates that could be theoretically produced by the ANME as a by-product of methane oxidation, and consumed as electron donor by the partner SRB (mechanisms illustrated in Extended Data Fig. 1). If these compounds were relevant in interspecies transfer of reducing equivalents, their amendment to the medium should favour the electron-accepting partner, and should repress the electron transfer between the consortial partners[14,21-23]. In contrast, a model of direct electron transfer via nanowires as proposed by 7,8,10, would be insensitive to such external additions of potential intermediates, if the amendments do not represent an alternative, preferred substrate for one of the partner organisms.

With the exception of hydrogen, none of the potential intermediates added as sole electron donor caused significant microbial sulfide production in the TAOM enrichment (Extended Data Table 3). Carbon monoxide and methyl sulfide even inhibited sulfide production when added together with methane. Carbon monoxide is known to inhibit type-c cytochrome activity, which may play an important role in intra- and intercellular transfer of reducing equivalents in AOM[17]. Methylated substrates may interfere with the reverse, oxidative operation of the methanogenesis pathway[24]. The addition of colloidal zero-valent sulfur to the TAOM culture (supplied in concentrations from 1 to 25 mM, Extended Data Fig. 3a) did not result in production of sulfide and sulfate as reported in a previous study with ANME2a/DSS consortia[21]. However, with hydrogen as electron donor (0.16 MPa), sulfide production rates increased 3 to 8 fold compared to replicate incubations with methane as sole electron donor at TAOM conditions (Fig. 1c; Extended Data Table 3). We investigated further the influence of hydrogen on the oxidation of methane using headspace-free incubations (Extended Data Fig. 4). In incubations with methane and hydrogen, hydrogen was first selectively consumed

and methane oxidation was repressed. When hydrogen was consumed, methane oxidation rates recovered to the same level as in replicate incubations with only methane, suggesting an inhibition of methane oxidation in the presence of hydrogen. To investigate the influence of hydrogen on the consortial partners, we mapped total RNA reads to the genome drafts of ANME-1 and HotSeep-1 after exposure to different substrate conditions (Fig. 1d, for read numbers see Supplementary Information Table 1). Under TAOM conditions, relative RNA expression patterns reflected the biomass ratio between the ANME and their partner bacteria (3:1) (Fig. 1d). The addition of hydrogen caused a strong relative increase of HotSeep-1 over ANME gene expression, even in the presence of methane. This indicates that if the partner SRB does not act as electron sink for reverse methanogenesis, ANME activity is repressed; an effect of syntrophic cooperation that was predicted previously[14].

To test the hypothesis of hydrogen production by the ANME as direct intermediate in TAOM (Extended Data Fig. 1) that would be consumed by HotSeep-1, we assessed the presence and production of hydrogen under TAOM conditions. Maximal hydrogen concentrations were only about 2 Pa in the TAOM enrichments, and re-established within 7 hours after gas phase exchange (Fig. 2a). Thermodynamically, HotSeep-1 could thrive on these low hydrogen concentrations with an energy yield of approx. −24 kJ mol^{-1}. However the production of hydrogen in TAOM cultures corresponded to only ~0.5% of the theoretical hydrogen production rates as reflected by sulfide production (according to the stoichiometry of reverse methanogenesis; Fig. 2b). This is insufficient to explain consortial growth of HotSeep-1. Furthermore, we could not detect catalytic subunits of (Fe,Fe) or (Ni,Fe)hydrogenases in the ANME-1 draft genome. In conclusion, hydrogen appears to be an alternative growth substrate for HotSeep-1 when available externally, but is not provided by ANME-1 as intermediate in TAOM.

An alternative explanation of the TAOM interaction could be the direct interspecies electron transfer (DIET) between ANME-1 and HotSeep-1, also hypothesized as principle mechanism for syntrophic growth of AOM consortia[8,10,17,25]. A switch from interspecies hydrogen transfer to DIET has been previously shown for the dual-species interaction between *Geobacter sulfurreducens* and *Geobacter metallireducens*, benefiting both consortial partners, as evidenced by their increased growth rates via DIET[10,26]. In their tightly packed consortia, a dense network of cell-cell connections was detected by transmission electron microscopy and immunogold labeling, likely serving in electron transfer[10]. This finding supports recent observations of redox-dependent staining of the intercellular matrix of ANME-2/SRB consortia[8]. The functioning of electron transfer via conductive cell-to-cell

connections (nanowires) is not fully understood, but apparently involves the expression of the pilin protein PilA of the TypeIV pili (T4P) together with certain c-type cytochromes[9,10,27,28].

To find evidences for DIET in TAOM we analysed the genome and specific gene expression of ANME-1 and HotSeep-1, with the focus on similarities to the Geobacter consortia using DIET as main electron transfer mechanism. The ANME-1 draft genome also contains several potentially extracellular multiheme c-type cytochromes, some of which are highly expressed during TAOM, but no genes for pili formation (Extended Data Table 4, Supplementary Information Table 2). However, HotSeep-1 comprises the genes for the biosynthesis and assembly of TypeIV pili, as well as large multiheme c-type cytochromes, both with high amino acid similarity to respective proteins in *Geobacter* spp.[29] (Extended Data Table 4, Supplementary Information Table 3-4). We further investigated expression patterns of these potentially DIET-related genes, in comparison to genes for AOM (*mcrA*) and sulfate reduction (*dsrA*), representing key catabolic processes in ANME-1 and HotSeep-1 (Fig. 3a, for statistical analyses see Supplementary Information Table 5). In agreement with the results from total RNA expression (Fig. 1d), a switch from methane to hydrogen (or methane plus hydrogen) as energy sources caused an immediate drop in *mcrA* and cytochrome expression in the ANME, as well as a reduction of the expression of the HotSeep-1 pili and cytochromes. Comparing relative gene expression of HotSeep-1 in consortial growth on methane, versus single growth on hydrogen, both *pilA* and cytochrome c are clearly overexpressed under TAOM conditions, also when compared to *dsrA* (Extended Data Fig. 5, for statistical analyses see Supplementary Information Table 5).

This observation is supported independently by transmission electron microscopy on thin sections of TAOM consortia. Using two different embedding techniques we found a dense network of pili-like structures connecting HotSeep-1 to ANME-1 cells (Fig. 3b-c, Extended Data Fig. 6a), resembling the nanowire structures found in Geobacter consortia (visualized with the same methods, see Extended Data Fig. 6b). In TAOM consortia the nanowires are larger, and appear more dense, with diameters of approx. 10 nm and apparent lengths of 100 to >1000 nm. In agreement with the genomic patterns, these wires seem to be formed by the partner bacteria, connecting to the ANME-1 at their polar sides (Fig. 3b-d). In contrast, HotSeep-1 cells in mono-species aggregates isolated on hydrogen show smooth surfaces without such extracellular extensions (Fig. 3e,f), indicating that the observed intercellular structures are specific to consortial growth under TAOM conditions, and not only related to cellular attachment.

In conclusion, our data show that consortial growth of the thermophilic ANME-1 archaea and HotSeep-1 bacteria is likely based on similar principles as those in Geobacter consortia, where direct interspecies electron transfer is mediated by intercellular wiring by pili-like structures and outer-membrane multi-heme cytochromes. The underlying biophysics and biochemistry of intercellular wiring for direct electron transfer needs further investigation. If this mode of syntrophic cooperation between the electron-generating archaea and nanowire-producing bacteria is also the underlying mechanism for other types of AOM consortia as suggested recently[8], it may explain the enigmatic specificity of the dual-species partnerships in AOM in general.

Methods

Cultivation of TAOM consortia

Sediment-free, thermophilic AOM enrichment cultures were obtained after 1.5 years by semi-continuous incubation of hydrothermal vent sediments from Guaymas Basin with sulfate reducer medium[31] and 0.225 MPa CH_4 (+0.025 MPa CO_2) as sole energy source at 60°C as described by ref. 6. Culture medium was replaced and samples were diluted 1:2 when sulfide concentrations exceeded 12 mM. For the different experiments, subsamples of the main culture (biological replicates) were incubated in parallel.

DNA extraction, sequencing and phylogenetic classification of TAOM partners

Genomic DNA was extracted as described before[32] from an active TAOM culture. The protocol encompassed three cycles of freezing and thawing, chemical lysis in a high-salt extraction buffer (1.5 M NaCl) by heating of the suspension in the presence of sodium dodecyl sulfate and hexadecyltrimethylammonium bromide, and treatment with proteinase K. To amplify bacterial 16S rDNA genes the primer pair GM3/GM4[33] was used. For archaeal 16S rDNA genes the primers 20F[34] and Arc1492R[35] were selected. PCR reactions were performed according to ref. 6. The phylogenetic affiliation was inferred with the ARB software package[36] and release 115 of the ARB SILVA database[37]. Representative 16S rRNA gene sequences are deposited at NCBI with the accession numbers KT152859-KT152885.

Visualization of TAOM aggregates by fluorescence *in situ* hybridisation

Cell aliquots were fixed in 2% formaldehyde for 2 h at room temperature, washed with 1x phosphate buffered saline (PBS; pH 7.4). Fixed cell suspensions were treated with mild sonication (Sonoplus HD70; Bandelin) and aliquots of 50-250 µl were filtered onto GTTP filter (0.2 µm pore size, 20 mm diameter). CARD-FISH was performed as described previously[38] with the following modifications: For cell wall permeabilization, filters were sequentially incubated in lysozyme solution (10 mg ml^{-1} lysozyme powder, 0.1 M Tris–HCl, 0.05 M EDTA, pH 8) for 15-30 min at 37°C and proteinase K solution (0.45 mU ml^{-1}, 0.1 M Tris–HCl, 0.05 M EDTA, pH 8, 0.5 M NaCl) for 2 min at room temperature. Endogenous peroxidases were inactivated by incubating the filters in 0.15% H_2O_2 in methanol (30 min, room temperature). The oligonucleotide probes ANME-1-350 and HotSeep-1-590 were applied with formamide concentrations according to ref. 6. For dual CARD-FISH, peroxidases of the first hybridization were inactivated by 0.3% H_2O_2 in methanol (30 min, room temperature). Catalysed reporter deposition was combined with the fluorochromes Alexa Fluor 488 and Alexa Fluor 594. Filters were stained with DAPI (4,6-diamidino-2-phenylindole). Micrographs were obtained by confocal laser scanning microscopy (LSM 780; Zeiss; Oberkochen, Germany).

Influence of potential AOM intermediates/alternative HotSeep-1 substrates on sulfide production rates

All experiments were performed with artificial seawater medium containing 30 mM of carbonate buffer at TAOM cultivation temperature (60°C), except when specified otherwise. To ensure equilibration of gas phases, samples were agitated on shaking tables. Highly pure gases and chemicals were used as amendments to the incubations. Standard TAOM conditions are defined here as 0.2 MPa methane and 28 mM sulfate. To test the TAOM enrichment for substrate specific sulfide production, triplicate culture aliquots (10 ml in 20 ml Hungate tubes) were supplemented with different substrates (Extended Data Table 2) at concentrations of 20 mM, except of methyl sulfide and carbon monoxide (both 0.05 MPa), and hydrogen (0.16 MPa) with and without methane (0.2 MPa). Zero-valent sulfur was prepared according to ref. 39 and was supplied as dissolved species. For this compound we additionally tested sulfide development via disproportionation in a concentration gradient from 1-12 mM final S^0 concentration (Extended Data Fig. 6a). As positive reference, methane was provided at 0.2 MPa (at 60°C roughly equivalent to 1.6 mM in solution). Sulfide production in the experiments was repeatedly measured every 3 to 4 days using the copper

sulfide assay[40] and absorption spectrometry at 480 nm. TAOM rates with methane as sole energy source (0.2 MPa) reached approx. 0.100 +/− 0.030 μM d^{-1}, compared to a negative control (nitrogen; <0.001 μM d^{-1}). Rates determined for other substrates were compared to those under TAOM conditions.

Influence of hydrogen addition on methane oxidation in TAOM cultures

To determine the effect of hydrogen addition on methane oxidation rates, TAOM culture aliquots were supplemented with methane:hydrogen (0.15 MPa and 0.05 MPa), and only methane as control (0.15 MPa). Cultures were incubated headspace-free at 50°C for this experiment, because hydrogen was too rapidly consumed at 60°C for time-course experiments. To determine concentrations of methane and hydrogen, 1 ml medium was sampled with gas-tight glass syringes, and the sampled medium was concurrently replaced with substrate-free medium to avoid the formation of a headspace. The sampled medium was injected through the septum of 10 ml Exetainer® filled with 1 ml NaOH and concentrations of CH_4 and H_2 were measured as described below.

Presence and production of hydrogen in active TAOM cultures with and without inhibition of sulfate reduction

To determine hydrogen concentrations at TAOM conditions, 20 ml culture were transferred into 156 ml bottles at 60°C and gas phases were repeatedly sampled using glass syringes (1 ml) combined with direct measurements on the gas chromatograph. Cultures incubated ≥3 days reached stable hydrogen concentrations. A comparison to molybdate addition is provided in Extended Data Fig. 6b,c. To quantify molecular hydrogen production in TAOM, 20 ml culture was supplied with sodium molybdate (10 mM final conc.). This molybdate concentration assured complete inhibition of hydrogen-dependent sulfate reduction as shown in replicate incubations of TAOM culture (1 to 25 mM molybdate) with hydrogen (0.1 MPa) as sole electron donor (Extended Data Fig. 6d). Samples were stored at 60°C on a shaking table and repeatedly sampled by glass syringes. Concentrations of methane and hydrogen were measured via gas chromatography coupled to flame ionization detection (Focus GC, Thermo) and via reducing compound photometry (RCD; Peak Performer 1 RCP; Peak Laboratories; Mountain View, CA, USA).

Determination of carbon fixation by TAOM consortia

Replicate culture aliquots (n=5) were incubated in 5 ml Hungate tubes supplemented with methane, sulfate and ^{14}C-labeled inorganic carbon (380 kBq). AOM-independent carbon fixation was determined under N_2 atmosphere (n=5). To determine methane oxidation rates, replicate vials were incubated with ^{14}C-methane (14 kBq). Incubations were performed at 60°C for 24 hours. Samples were blotted onto 0.2 µm mixed cellulose esters membrane filters (Millipore, Merck, Darmstadt, Germany). Filters were dried and potential residual inorganic carbon was removed by exposing the filters to an HCl atmosphere for 24 hours. Radioactivity in liquid aliquots (0.1 ml) and filters was determined by liquid scintillation counting (scintillation mixture; Filtercount; Perkin Elmer, Waltham, MA, USA; scintillation counter 2900TR LSA; Packard, Waltham, MA, USA).

Cultivation of HotSeep-1 on molecular hydrogen

To isolate the hydrogenotrophic sulfate reducers in the TAOM enrichment, aliquots were transferred to Hungate tubes (20 ml) and diluted 1:10 to 1:10^9 with marine sulfate reducer medium. All vials were amended with 0.2 MPa H_2:CO_2 (80:20) gas phase, and additionally stored in N_2 atmosphere to prevent oxygen flux into the culture vials. Vials were stored at the TAOM temperature optimum (60°C) and measured for sulfide production using the copper sulfate assay[40]. To identify cultivated microorganisms, the 16S rRNA gene of active hydrogenotrophic cultures was directly amplified from freeze-thawed pellets of culture aliquots (primer pair GM3/GM4) and sequenced as described above. The phylogenetic affiliation was inferred with the ARB software package[36] and release 115 of the ARB SILVA database[37]. Representative sequences are deposited at NCBI with the accession numbers KT152886-KT152887.

Physiology experiments with HotSeep-1

Electron acceptor tests. Culture aliquots (1 ml 10 fold diluted in artificial anoxic seawater medium) were supplied with different potential electron acceptors (colloidal sulfur, sulfite, thiosulfate) with and without addition of hydrogen. Potential growth on alternative carbon sources (i.e. acetate, butyrate, peptone, methyl sulfide) was tested. *Growth rates*. Growth rates were independently determined from the development of sulfide concentrations and cell counts (from DAPI stained cells for total cell numbers and from fluorescence *in situ* hybridized cells for specific cell numbers) from replicate cultures (grown from 10% inoculum). *Growth efficiencies*. Growth efficiencies were determined in a ^{14}C-DIC radiotracer

assay. Replicate cultures were spiked with ^{14}C-DIC (~5.4 MBq) and incubated with H_2:CO_2 or, as control with N_2:CO_2 headspace. Sulfate-dependent hydrogen consumption was determined as by the increase of sulfide (colorimetrically[40]) and by the decrease of sulfate (via ion chromatography) in the medium. Fixed carbon was measured from culture aliquots (5 ml volume) blotted on filters as described above. Concentrations of radioactivity on the filter and the medium were determined via scintillation counting. The total carbon fixation was calculated as ^{14}C uptake into particulate organic carbon multiplied by total DIC [^{14}C-POC (Bq $ml_{culture}^{-1}$) / ^{14}C-total (Bq $ml_{culture}^{-1}$) × DIC (mmol $ml_{culture}^{-1}$)] and values are compared normalized to reducing equivalents with the consumption of sulfide.

Metagenome sequencing and draft genome assembly of ANME-1 and HotSeep-1

Genomic DNA was extracted from TAOM and HotSeep-1 enrichment cultures (as described above) and prepared for Illumina sequencing using the Nextera mate pair sample preparation kit (Illumina, CA, USA), following the Gel-Plus protocol of the manufacturer's user guide. DNA fragments with a length of approx. 5-8 kb were extracted from a preparative gel prior to circularization. Additionally a paired end read library with insert size of 500 bp was constructed for the TAOM enrichment using the TruSeq library preparation kit. Libraries were sequenced on a MiSeq instrument (MiSeq, Illumina), in a 2x250 bases paired end run. Quality controlled mate pair reads were assembled using the SPAdes genome assembler v.3.5.0[41] with default values of k and the --hqmp option. Assembled contigs from the TAOM metagenome were binned based on tetranucleotide frequency using the Metawatt software[42]. ANME-1 and HotSeep-1 specific bins were extracted for targeted reassembly using the SPAdes genome assembler v.3.5.0[41] with mapped mate pair and paired end read data and default values of k and subsequently were used as draft genomes. A HotSeep-1 draft genome was also obtained from the assembled contigs of the highly enriched HotSeep-1 culture metagenome (hydrogenotrophic HotSeep-1).

Draft genome analysis

Draft genomes were annotated with prokka[43], and the draft genome of HotSeep-1 (obtained from the hydrogenotrophic HotSeep-1 enrichment) was additionally annotated with an in house pipeline and analysed using GenDB[44] and JCoast[45]. The annotation of reported genes was manually curated. An expectation (E)-value cut-off of 10^{-5} was considered for all predictions of putative protein functions. Identity of the enriched hydrogenotrophic HotSeep-1 and the TAOM partner HotSeep-1 was evaluated by pairwise blast search of the

nucleotide sequence of the 16S and 23S rRNA genes, functional and housekeeping genes and the intergenic spacer region (ITS) (see Exteded Data Table 2) derived from the draft genome of the TAOM partner HotSeep-1 (query) vs the hydrogenotrophic HotSeep-1 (subject). To verify that the organisms belong to the same species the average nucleotide identity (ANI) and the tetranucleotide frequency correlation of the two draft genomes were determined using JSpecies[46] (v.1.2.1). Analyses resulted in tetranucleotide frequency correlation of 0.999 and ANI of >99%. To check for absence of ANME-1 in the hydrogenotrophic HotSeep-1 culture metagenomic reads were mapped to the SILVA SSU 119 reference database (bbmap v.35 and pyhloflash v.1.5) for phylogenetic classification at minimum identities of 90%, 95% and 97% resulting in approx. 3500, 2100, 1500 classified 16S rRNA gene fragments, respectively which were screened for hits to ANME related sequences.

To identify potential cytochrome c and T4P genes in the draft genomes of ANME-1 and HotSeep-1 protein domains were predicted using hmmscan (HMMER 3.0[47]) with the PfamA[48] and TIGRFAM[49] reference databases. Potential cytochromes were identified by the CXXCH motive and cytochrome c specific protein domain models. Potential T4P genes were identified using protein models related to T4P. ANME-1 cytochrome and HotSeep-1 cytochrome and pili genes were compared for their best matching hits in the *G. sulfurreducens* (strain PCA) and *G. metallireducens* genome and the NCBI non-redundant protein database using blastp. Cytochrome annotation based on detected protein domains in PfamA, pili annotation based on detected protein domains and amino acid sequence. Subcellular localization was predicted with PSORTb[50] (v.3.0.2). For cytochromes the number of potential heme-binding sites was derived from the abundance of the CXXCH motif. For sequence comparison to the NCBI non-redundant protein database and *Geobacter* spp. and for details on protein domains and subcellular localization prediction see Supplementary Information Table 2a,b (ANME-1 cytochromes), Supplementary Information Table 3a,b (HotSeep-1 cytochromes), and Supplementary Information Table 4a,b for HotSeep-1 TypeIV pili biogenesis.

The ANME-1 draft genome was searched for genes encoding catalytic subunits of hydrogenases using blastp search against known genes of catalytic subunits of NiFe and FeFe hydrogenases (MvhA, EchA, FrhA, VhuA, VhtA, EhaO, HymC). Annotation of genes with hits was evaluated by blastp search against the NCBI non-redundant protein database for best matching reference sequences related to hydrogenases, but none were found.

Transcriptome analysis of TAOM and HotSeep-1

To harvest cells for transcriptome analyses a 3.5 days experiment with replicates of 20 ml culture in 60 ml vials was carried out (Fig. 1). From triplicate TAOM cultures incubated on methane as control, on hydrogen, on methane/hydrogen mixture, or nitrogen as negative control, ~80% of the enrichment medium was removed and RNA was preserved using pre-heated RNA later (Life Technologies, ThermoFisher Scientific). Total RNA was extracted using the Quick-RNA MiniPrep kit (Zymo Research, Irvine, CA, USA), treated with DNase I (Roche, Rotkreuz, Switzerland) and purified using the RNeasy MinElute Cleanup kit (Qiagen, Hilden, Germany) following manufacturer recommendations. Removal of rRNA was omitted and total RNA was prepared for sequencing using the TruSeq stranded mRNA library prep kit (Illumina CA, USA) following the manufacturer's guidelines. The cDNA library was sequenced on a MiSeq instrument (MiSeq, Illumina) generating between 2 to 3 Mio 150 bp single end reads per library. Quality controlled reads were mapped to the draft genomes of HotSeep-1 and ANME-1 using bbmap (v. 35) with minimum mapping identity of 98%. To quantify gene expression unambiguously mapped reads per gene were counted using bedtools multicov (v.2.24.0). To compare relative expression patterns within each organism across treatments, read counts per feature were converted to transcripts per million (TPM, which is the number of a transcript (i) in a million sequenced transcripts taking into account the abundance of all other transcripts) calculated according to ref. 51

$$TPM_i = X_i/l_i \times (1 / \sum_j X_j/l_j) \times 10^6 \quad (2)$$

with X=counts, l=length (bp). Relative changes in expression of selected genes were calculated by comparing TPM normalized expression data of the H_2 and H_2+CH_4 treatment to those under TAOM (control) conditions. Differential expression (p-value, fold change and effect size) between control (TAOM condition) and treatment (H_2 or H_2+CH_4) was computed with the aldex2 R package[52] for ANOVA-like differential expression analysis. Raw read numbers, read mapping data and statistical analysis are provided in Supplementary Table 1 (total expression) and Supplementary Table 5 (specific gene expression).

For HotSeep-1 transcriptomes total RNA was extracted from triplicate cultures (50 ml) grown on hydrogen/CO_2 following the same procedure as described for TAOM enrichments (see above). Removal of rRNA was omitted and total RNA was prepared for sequencing using the TruSeq stranded mRNA library prep kit (Illumina CA, USA) following the manufacturer's guidelines. The cDNA library was sequenced on a MiSeq instrument (MiSeq, Illumina) generating between 6.4 to 6.9 Mio 75 bp paired end reads per library. Quality controlled reads were mapped to the draft genome of HotSeep-1 using bbmap (v. 35) with

minimum mapping identity of 98%. To quantify gene expression unambiguously mapped reads per gene were counted using featureCount[53] (part of Subread, v. 1.4.6.) with the –p option to count fragments instead of reads. Fragment counts per gene were converted to transcripts per million (TPM) as described above for TAOM transcriptome analyses.

Cultivation of Geobacter consortia

Active cultures of *G. sulfurreducens* (strain PCA; DSM 12127) and *G. metallireducens* strain (GS-15; DSM 7210) were mixed in fresh medium (DSM Medium 826) supplied with Na_2-fumarate (50 mM) and ethanol (20 mM) according to reference 10 and cultivated anaerobically at 33°C. After subsequent transfers (1% inoculum) a well growing culture consisting of reddish microbial aggregates developed, which was used for thin-sectioning and electron microscopy.

Transmission electron microscopy

The cell material was harvested at 2000 rpm using a Stat Spin Microprep 2 table top centrifuge. After centrifugation the pellet was fixed by immersion using 2% glutaraldehyde in 0.1 M cacodylate buffer at pH 7.4. Fixation was performed for 60 min at room temperature. The fixed pellet was immobilized with 2% agarose in cacodylate buffer at pH 7.4. The pellet was cubed and the pieces carefully washed with buffer and further fixed in 1% osmium tetroxide. After pre-embedding staining with 1% uranyl acetate, samples were dehydrated and embedded in Agar 100. As independent complementary method (shown in Extended Data Fig. 5a) samples were placed in aluminium platelets of 150 µm depth containing 1-hexadecene[54]. The platelets were frozen using a Leica Em HPM100 high pressure freezer (Leica Mikrosysteme Vertrieb GmbH, Wetzlar, Germany). The frozen samples were transferred to an Automatic Freeze Substitution Unit Leica EM AFS2 and substituted at −90°C in a solution containing anhydrous acetone, 0.1% tannic acid for 24 h and in anhydrous acetone, 2% OsO4, 0.5% anhydrous glutaraldehyde (EMS Electron Microscopical Science, Ft. Washington, USA) for additional 8 h. After a further incubation over 20 h at −20°C samples were warmed up to +4°C and washed with anhydrous acetone subsequently. The samples were embedded at room temperature in Agar 100 (Epon 812 equivalent) at 60°C over 24 h. Thin sections (30-60 nm) were counterstained with uranyl acetate and lead citrate and examined using a Philips CM 120 transmission electron microscope (Philips Inc. Eindhoven, The Netherlands). In total, we recorded more than 200 views on TAOM consortia, 64 views on HotSeep-1 and 90 views of Geobacter consortia.

Thermodynamic calculations

Free energy yields (ΔG_{rxn}) were calculated according to equation 3

$$\Delta G_{rxn} = \Delta G^{\circ}_{(T)} + RT \times \ln \frac{[Pi]^n}{[Ri]^n} \quad (3)$$

including the gas constant R, the temperature T (K) and the measured activities/partial pressures of the respective products [P_i] and reactants [R_i] in their respective stoichiometric appearance (n) in the reaction. Values consider activities and fugacity of respective compounds. The temperature corrected standard free energy $\Delta G^{\circ}_{(T)}$ were determined according to ref. 55.

Acknowledgements

We thank Katie Harding, Ines Kattelmann, Andreas Ellrott and Mirja Meiners for technical and Michael Richter, Harald Gruber-Vodicka and Pier Luigi Buttigieg for bioinformatic support, and Katrin Knittel, Nicole Dubilier, Marcel M.M. Kuypers and Friedrich Widdel for helpful discussions. Furthermore we thank chief scientist Andreas Teske and the RV ATLANTIS and ALVIN team of cruise AT15-56 in 2009 for providing the initial sediment material. The project was funded by the DFG Leibniz program to A.B., and by the DFG excellence cluster MARUM, Center of Marine Environmental Sciences, Bremen. Further support was provided by the Max Planck Society to D.R. and A.B.

Author information

Representative full length 16S sequences of TAOM and HotSeep-1 enrichment have been submitted to NCBI. Sequencing projects are registered at NCBI under the BioProject IDs PRJNA286178 (TAOM enrichment) and PRJNA276404 (HotSeep-1 enrichment). The authors declare no competing financial interests. Readers are welcome to comment on the online version of the paper. Reprints and permissions information is available at www.nature.com/reprints. Correspondence should be addressed to G.W. (gwegener@mpi-bremen.de) and V.K. (vkrukenb@mpi-bremen.de).

Author contributions

G.W. V.K. and A.B designed the experiments, G.W. V.K., H.E.T. and D.R. performed experiments and data analyses, G.W. V.K. and A.B. wrote the manuscript with contributions of D.R. and H.E.T.

References

1 Reeburgh, W. S. Oceanic methane biogeochemistry. *Chem. Rev.* **107**, 486−513 (2007).

2 Boetius, A. & Wenzhöfer, F. Seafloor oxygen consumption fuelled by methane from cold seeps. *Nat. Geosci.* **6**, 725−734 (2013).

3 Hinrichs, K.-U., Hayes, J. M., Sylva, S. P., Brewer, P. G. & DeLong, E. F. Methane-consuming archaebacteria in marine sediments. *Nature* **398**, 802−805 (1999).

4 Boetius, A. *et al.* A marine microbial consortium apparently mediating anaerobic oxidation of methane. *Nature* **407**, 623−626 (2000).

5 Orphan, V. J. *et al.* Comparative analysis of methane-oxidizing archaea and sulfate-reducing bacteria in anoxic marine sediments. *Appl. Environ. Microbiol.* **67**, 1922−1934 (2001).

6 Holler, T. *et al.* Thermophilic anaerobic oxidation of methane by marine microbial consortia. *ISME. J.* **5**, 1946−1956 (2011).

7 Thauer, R. K. & Shima, S. Methane as fuel for anaerobic microorganisms. *Ann. N. Y. Acad. Sci.* **1125**, 158−170 (2008).

8 McGlynn, S. E., Chadwick, G. L., Kempes, C. P. & Orphan, V. J. Single cell activity reveals direct electron transfer in methanotrophic consortia. *Nature* (in press).

9 Reguera, G. *et al.* Extracellular electron transfer via microbial nanowires. *Nature* **435**, 1098−1101 (2005).

10 Summers, Z. M. *et al.* Direct exchange of electrons within aggregates of an evolved syntrophic coculture of anaerobic bacteria. *Science* **330**, 1413−1415 (2010).

11 Knittel, K. & Boetius, A. Anaerobic oxidation of methane: progress with an unknown process. *Annu. Rev. Microbiol.* **63**, 311−334 (2009).

12 Niemann, H. *et al.* Novel microbial communities of the Haakon Mosby mud volcano and their role as a methane sink. *Nature* **443**, 854−858 (2006).

13 Schreiber, L., Holler, T., Knittel, K., Meyerdierks, A. & Amann, R. Identification of the dominant sulfate-reducing bacterial partner of anaerobic methanotrophs of the ANME-2 clade. *Environ. Microbiol.* **12**, 2327−2340 (2010).

14 Hoehler, T. M., Alperin, M. J., Albert, D. B. & Martens, C. S. Field and laboratory studies of methane oxidation in an anoxic marine sediment: evidence for a methanogen-sulfate reducer consortium. *Glob. Biogeochem. Cycles* **8**, 451−463 (1994).

15 Krüger, M. *et al.* A conspicuous nickel protein in microbial mats that oxidize methane anaerobically. *Nature* **426**, 878−881 (2003).

16 Hallam, S. J. *et al.* Reverse methanogenesis: testing the hypothesis with environmental genomics. *Science* **305**, 1457−1462 (2004).

17 Meyerdierks, A. *et al.* Metagenome and mRNA expression analyses of anaerobic methanotrophic archaea of the ANME-1 group. *Environ. Microbiol.* **12**, 422−439 (2010).

18 Kojima, H., Moll, J., Kahnt, J., Fukui, M. & Shima, S. A reversed genetic approach reveals the coenzyme specificity and other catalytic properties of three enzymes putatively involved in anaerobic oxidation of methane with sulfate. *Environ. Microbiol.* **16**, 3431−3442 (2014).

19 Thauer, R. K. Anaerobic oxidation of methane with sulfate: on the reversibility of the reactions that are catalyzed by enzymes also involved in methanogenesis from CO_2. *Curr. Opin. Microbiol.* **14**, 292−299 (2011).

20 Milucka, J., Widdel, F. & Shima, S. Immunological detection of enzymes for sulfate reduction in anaerobic methane-oxidizing consortia. *Environ. Microbiol.* **15**, 1561−1571 (2013).

21 Milucka, J. *et al.* Zero-valent sulphur is a key intermediate in marine methane oxidation. *Nature* **491**, 541−546 (2012).

22 Schink, B. Energetics of syntrophic cooperation in methanogenic degradation. *Microbiol. Mol. Biol. Rev.* **61**, 262−280 (1997).

23 Stams, A. J. M. & Plugge, C. M. Electron transfer in syntrophic communities of anaerobic bacteria and archaea. *Nat. Rev. Microbiol.* **7**, 568−577 (2009).

24 Moran, J. J. *et al.* Methyl sulfides as intermediates in the anaerobic oxidation of methane. *Environ. Microbiol.* **10**, 162−173 (2008).

25 Stokke, R., Roalkvam, I., Lanzen, A., Haflidason, H. & Steen, I. H. Integrated metagenomic and metaproteomic analyses of an ANME-1-dominated community in marine cold seep sediments. *Environ. Microbiol.* **14**, 1333−1346 (2012).

26 Nagarajan, H. *et al.* Characterization and modelling of interspecies electron transfer mechanisms and microbial community dynamics of a syntrophic association. *Nat. Commun.* **4**, 2809 (2013).

27 Rotaru, A.-E. *et al.* A new model for electron flow during anaerobic digestion: direct interspecies electron transfer to *Methanosaeta* for the reduction of carbon dioxide to methane. *Energ. Environ. Sci.* **7**, 408−415 (2014).

28 Malvankar, N. S. *et al.* Structural basis for metallic-like conductivity in microbial nanowires. *mBio* **6**, e00084−15 (2015).

29 Methe, B. *et al.* Genome of *Geobacter sulfurreducens*: metal reduction in subsurface environments. *Science* **302**, 1967−1969 (2003).

30 Reitner, J. *et al.* Concretionary methane-seep carbonates and associated microbial communities in Black Sea sediments. *Palaeogeogr. Palaeoclimatol. Palaeoecol.* **227**, 18−30 (2005).

References methods

31 Widdel, F. & Bak, F. in *The Prokaryotes* Vol. 4 (eds Trüper, H. G., Balows, A., Dworkin, M., Harder, W., Schleifer, K. H.) 3352−3378 (Springer, 1992).

32 Zhou, J., Bruns, M. A. & Tiedje, J. M. DNA recovery from soils of diverse composition. *Appl. Environ. Microbiol.* **62**, 316−322 (1996).

33 Muyzer, G., Teske, A., Wirsen, C. O. & Jannasch, H. W. Phylogenetic relationships of *Thiomicrospira* species and their identification in deep-sea hydrothermal vent samples by denaturing gradient gel electrophoresis of 16S rDNA fragments. *Arch. Microbiol.* **164**, 165−172 (1995).

34 Massana, R., Murray, A., Preston, C. & DeLong, E. Vertical distribution and phylogenetic characterization of marine planktonic *Archaea* in the Santa Barbara Channel. *Appl. Environ. Microbiol.* **63**, 50−56 (1997).

35 Teske, A. *et al.* Microbial diversity of hydrothermal sediments in the Guaymas Basin: evidence for anaerobic methanotrophic communities. *Appl. Environ. Microbiol.* **68**, 1994−2007 (2002).

36 Ludwig, W. *et al.* ARB: a software environment for sequence data. *Nucleic Acids Res.* **32**, 1363−1371 (2004).

37 Pruesse, E. *et al.* SILVA: a comprehensive online resource for quality checked and aligned ribosomal RNA sequence data compatible with ARB. *Nucleic Acids Res.* **35**, 7188−7196 (2007).

38 Pernthaler, A., Pernthaler, J. & Amann, R. Fluorescence *in situ* hybridization and catalyzed reporter deposition for the identification of marine bacteria. *Appl. Environ. Microbiol.* **68**, 3094−3101 (2002).

39 Steudel, R., Göbel, T. & Holdt, G. The molecular composition of hydrophilic sulfur sols prepared by decomposition of thiosulfate. *Z. Naturforsch. B* **43**, 203−218 (1988).

40 Cord-Ruwisch, R. A quick method for the determination of dissolved and precipitated sulfides in cultures of sulfate-reducing bacteria. *Microbiol. Meth.* **4**, 33−36 (1985).

41 Bankevich, A. *et al.* SPAdes: a new genome assembly algorithm and its applications to single-cell sequencing. *J. Comput. Biol.* **19**, 455−477 (2012).

42 Strous, M., Kraft, B., Bisdorf, R. & Tegetmeyer, H. E. The binning of metagenomic contigs for microbial physiology of mixed cultures. *Front. Microbiol.* **3**, 410 (2012).

43 Seemann, T. Prokka: rapid prokaryotic genome annotation. *Bioinformatics* **30**, 2068–2069 (2014).

44 Meyer, F. *et al.* GenDB-an open source genome annotation system for prokaryote genomes. *Nucleic Acids Res.* **31**, 2187−2195 (2003).

45 Richter, M. *et al.* JCoast - A biologist-centric software tool for data mining and comparison of prokaryotic (meta)genomes. *BMC Bioinformatics* **9**, 177 (2008).

46 Richter, M. & Rosselló-Móra, R. Shifting the genomic gold standard for the prokaryotic species definition. *Proc. Natl. Acad. Sci. USA* **106**, 19126−19131, (2009).

47 Eddy, S. HMMER User's Guide. Biological sequence analysis using profile hidden Markov models. (Howard Hughes Medical Institute, 2003).

48 Finn, R. D., Miller, B. L., Clements, J. & Bateman, A. iPfam: a database of protein family and domain interactions found in the Protein Data Bank. *Nucleic Acids Res.* **42**, D364−D373 (2014).

49 Haft, D. H., Selengut, J. D. & White, O. The TIGRFAMs database of protein families. *Nucleic Acids Res.* **31**, 371−373 (2003).

50 Yu, N. Y. *et al.* PSORTb 3.0: improved protein subcellular localization prediction with refined localization subcategories and predictive capabilities for all prokaryotes. *Bioinformatics* **26**, 1608−1615 (2010).

51 Li, B., Ruotti, V., Stewart, R. M., Thomson, J. A. & Dewey, C. N. RNA-Seq gene expression estimation with read mapping uncertainty. *Bioinformatics* **26**, 493−500, (2010).

52 Fernandes, A. D. *et al.* Unifying the analysis of high-throughput sequencing datasets: characterizing RNA-seq, 16S rRNA gene sequencing and selective growth experiments by compositional data analysis. *Microbiome* **2**, 1−13 (2014).

53 Liao, Y., Smyth, G. & Shi, W. featureCounts: an efficient general purpose program for assigning sequence reads to genomic features. *Bioinformatics* **30**, 923−930 (2014).

54 Studer, D., Michel, M. & Müller, M. High pressure freezing comes of age. *Scanning Microsc. Suppl.* **3**, 253−268 (1989).

55 Conrad, R. & Wetter, B. Influence of temperature on energetics of hydrogen metabolism in homoacetogenic, methanogenic, and other anaerobic bacteria. *Arch. Microbiol.* **155**, 94−98 (1990).

Figures

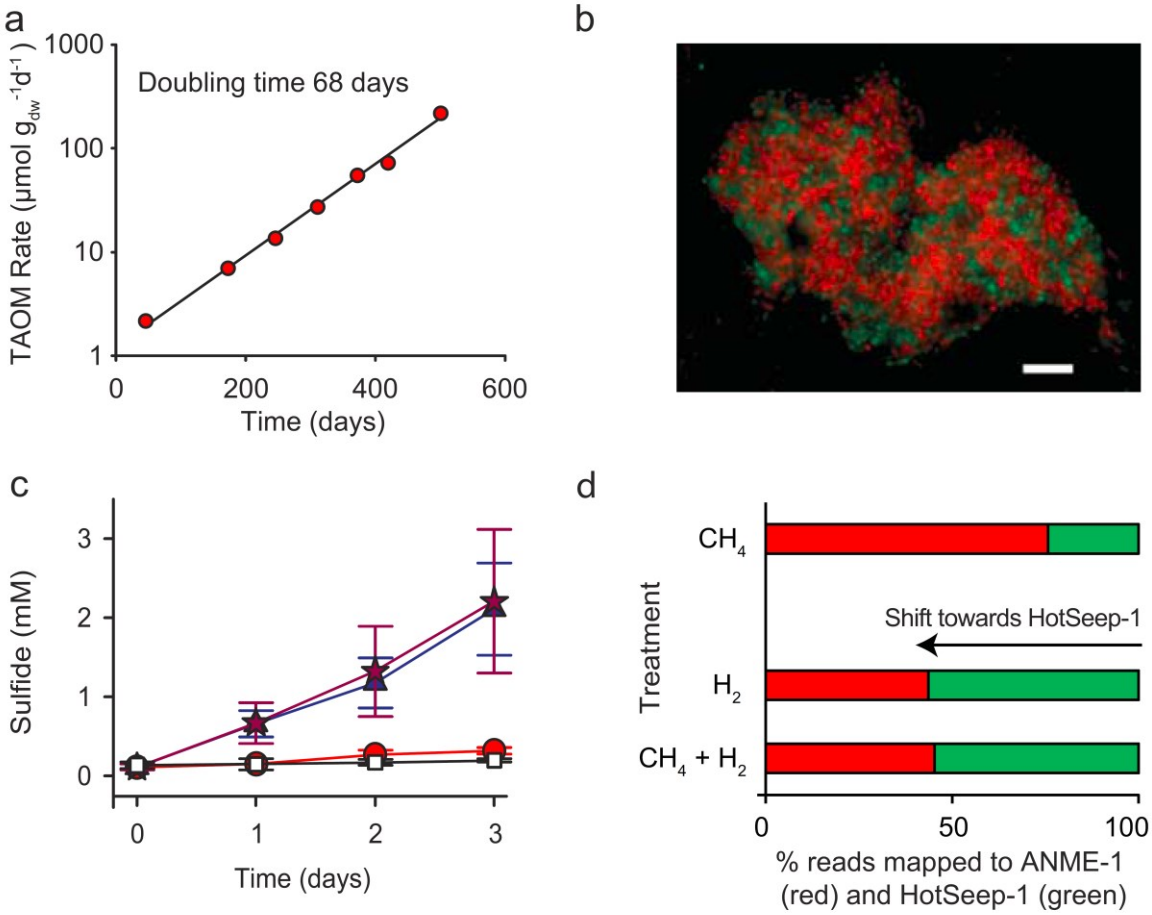

Figure 1 Activity of the TAOM consortia in culture. **a**, The exponential increase of sulfide production translates to a doubling time of 68 days (biological replicates; n=4). **b**, Fluorescence micrograph of TAOM consortia from (a), hybridization see methods; white bar scales 10 µm. **c**, Sulfide production under TAOM conditions (red circles; 0.07 mM sulfide per day) versus a control (white squares; 0.02 mM per day). Hydrogen (blue triangles), or hydrogen plus methane (purple stars) increased sulfide production (both 0.55 mM per day; biological replicates n=3; symbols=mean values; error bars=s.d.). **d**, Percent total RNA reads mapped to ANME-1 (red) and HotSeep-1 (green) after 3 days incubation (c), biological replicates n=3, bars=means, for statistical analyses see Supplementary Table 1.

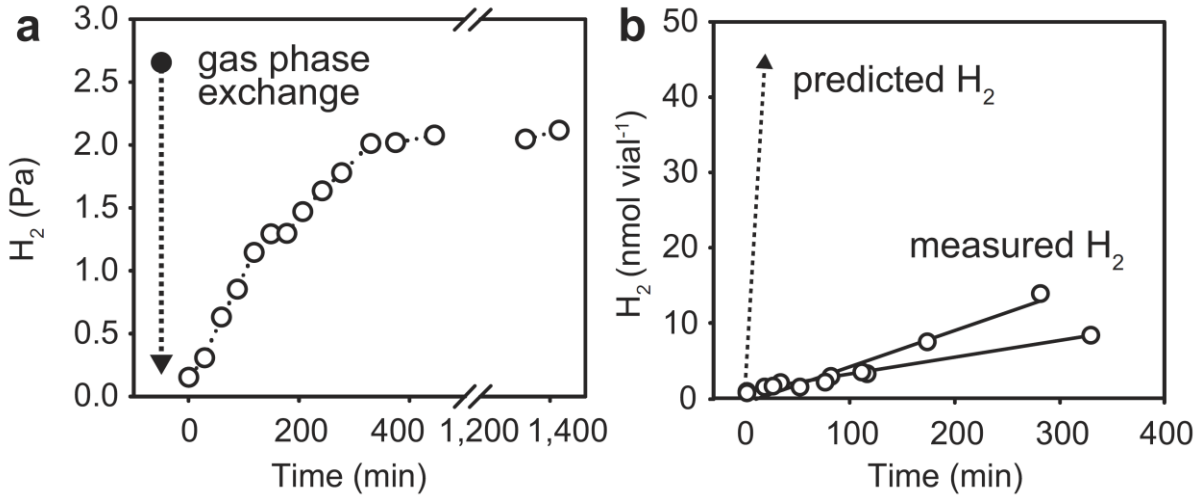

Figure 2 Hydrogen in TAOM cultures. **a**, Hydrogen gas pressure under TAOM conditions (methane 0.2 MPa; sulfate 28 mM; 5 day incubation (filled circle)). The dashed arrow depicts gas phase exchange with methane. Open circles show equilibration of hydrogen in the headspace (n=1; experiment repeated with same results (not shown)). **b**, Hydrogen production in 10 ml TAOM culture supplied with 0.2 MPa methane after headspace exchange and addition of 10 mM molybdate (final concentration) to inhibit hydrogen consumption. Open circles are replicate measurements with hydrogen production of 2 and 3 nmol l^{-1} min^{-1}. Dotted line: Predicted hydrogen production for reverse methanogenesis ($CH_4+2H_2O \rightarrow CO_2+4H_2$) = 420 nmol H_2 l^{-1} min^{-1} culture, for an observed sulfide production rate of 104 nmol l^{-1} min^{-1}).

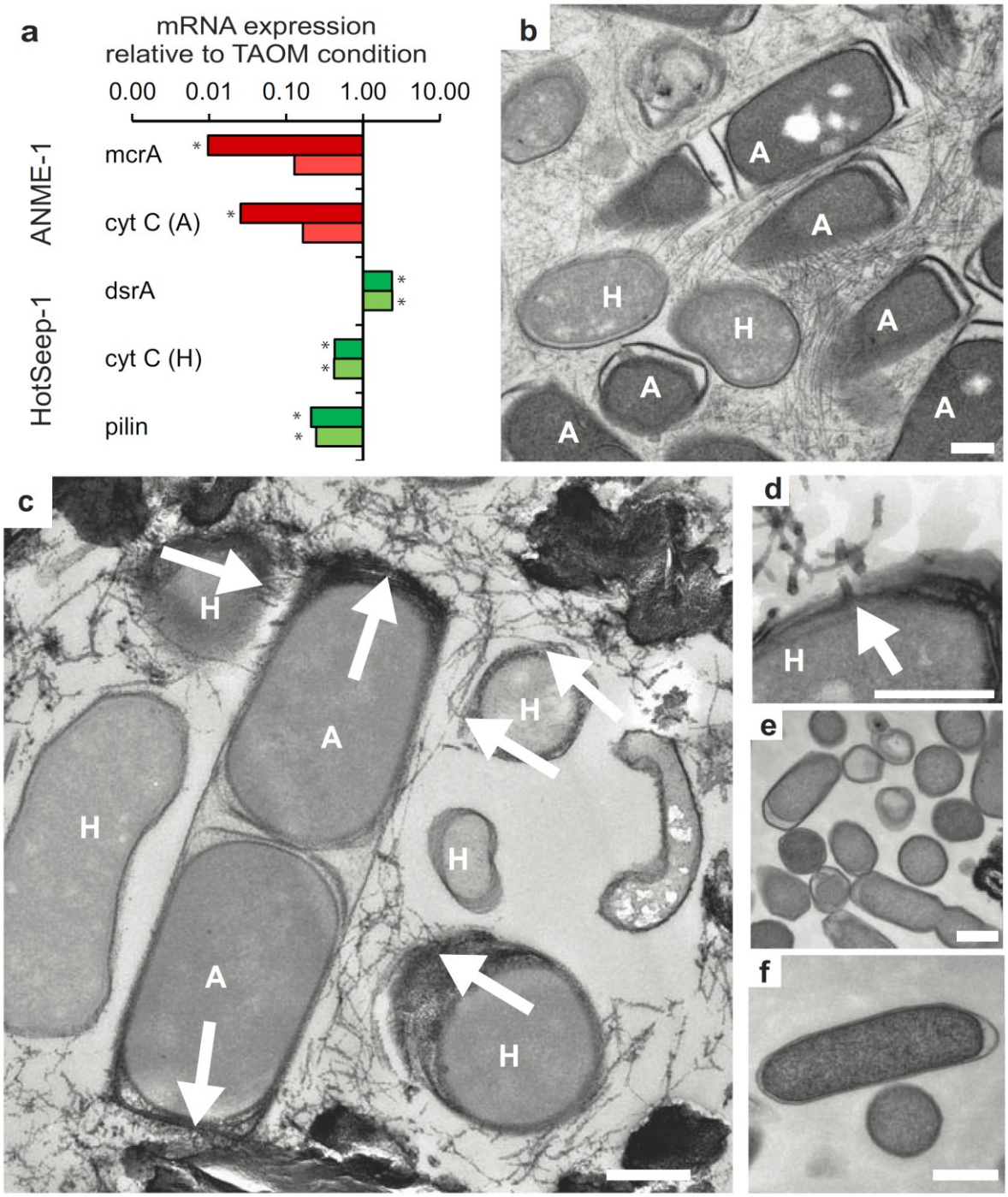

Figure 3 Expression of genes and visualisation of structures attributed to interspecies electron transfer in TAOM. **a**, Expression of archaeal (red) and bacterial genes (green) in incubations with hydrogen (dark shade), or hydrogen plus methane (light shade), relative to methane alone (expression under TAOM condition = 1; biological replicates; n=3; *p-value <0.05; for statistics see Supplementary Table 5b). **b-f**, Micrographs of thin-sections; bar scales 300 nm. **b-d**, TAOM consortia with HotSeep-1 cells (H; rod-shaped; approx. 1×0.5 µm) and ANME-1 cells (A; cylindrical shape with envelope[30]; 1.5×0.8 µm). Nanowires of 10 nm diameter and up to several 1000 nm length connect both species. **c,d**, Arrows mark the apparent origin of the wires from the membrane of HotSeep-1 bacteria to the polar sites of ANME-1 cells. **d**, HotSeep-1 cell with nanowires crossing the cell membrane (marked by the arrow). **e,f**, Aggregated HotSeep-1 cells grown on hydrogen do not develop nanowires.

Extended data

Extended data figures

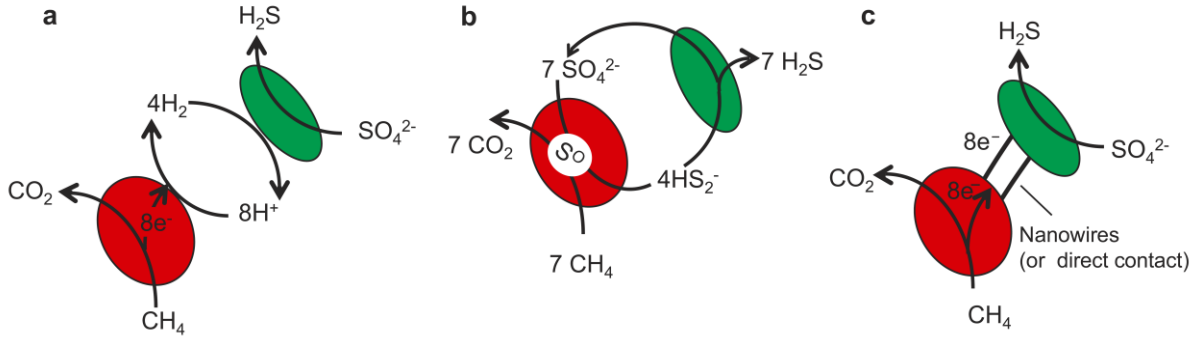

Extended Data Figure 1 Models of possible species interaction mechanisms in TAOM tested in this study. **a**, Transfer of molecular intermediates such as hydrogen; **b**, incomplete reduction of sulfate in ANME and zero-valent sulfur transfer to the partner bacteria; **c**, direct interspecies electron transfer via conductive nanowires.

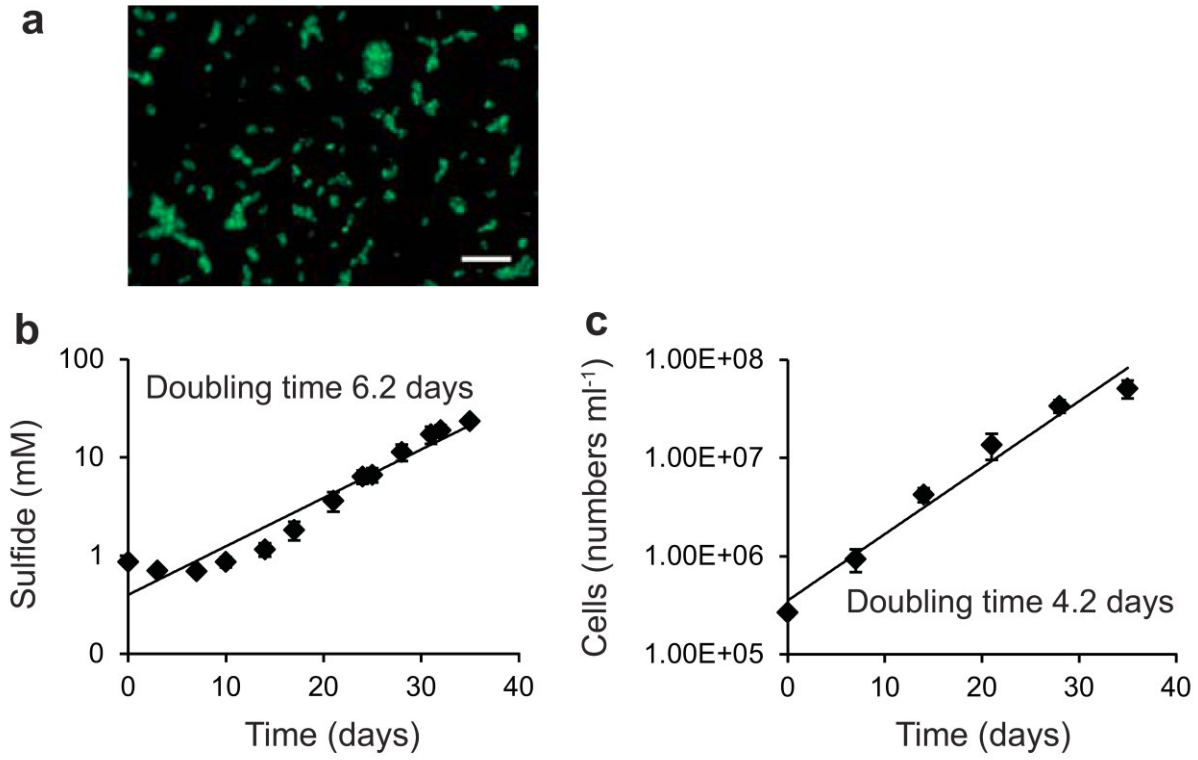

Extended Data Figure 2 Visualisation of and growth experiments with HotSeep-1. **a**, Fluorescence micrograph of HotSeep-1 culture (probe HotSeep-1-590). Cells are solitary or form small aggregates, bar scales 10 µm. **b,c**, Semi-logarithmic illustration of the development of (b) sulfide, or (c) numbers of cells and resulting doubling times (doubling time = ln(2)/exponential factor of the regression curve) during incubation of the HotSeep-1 culture with hydrogen as sole energy source and sulfate. (b,c) biological replicates n=3, circles=mean values, error bars=s.d.

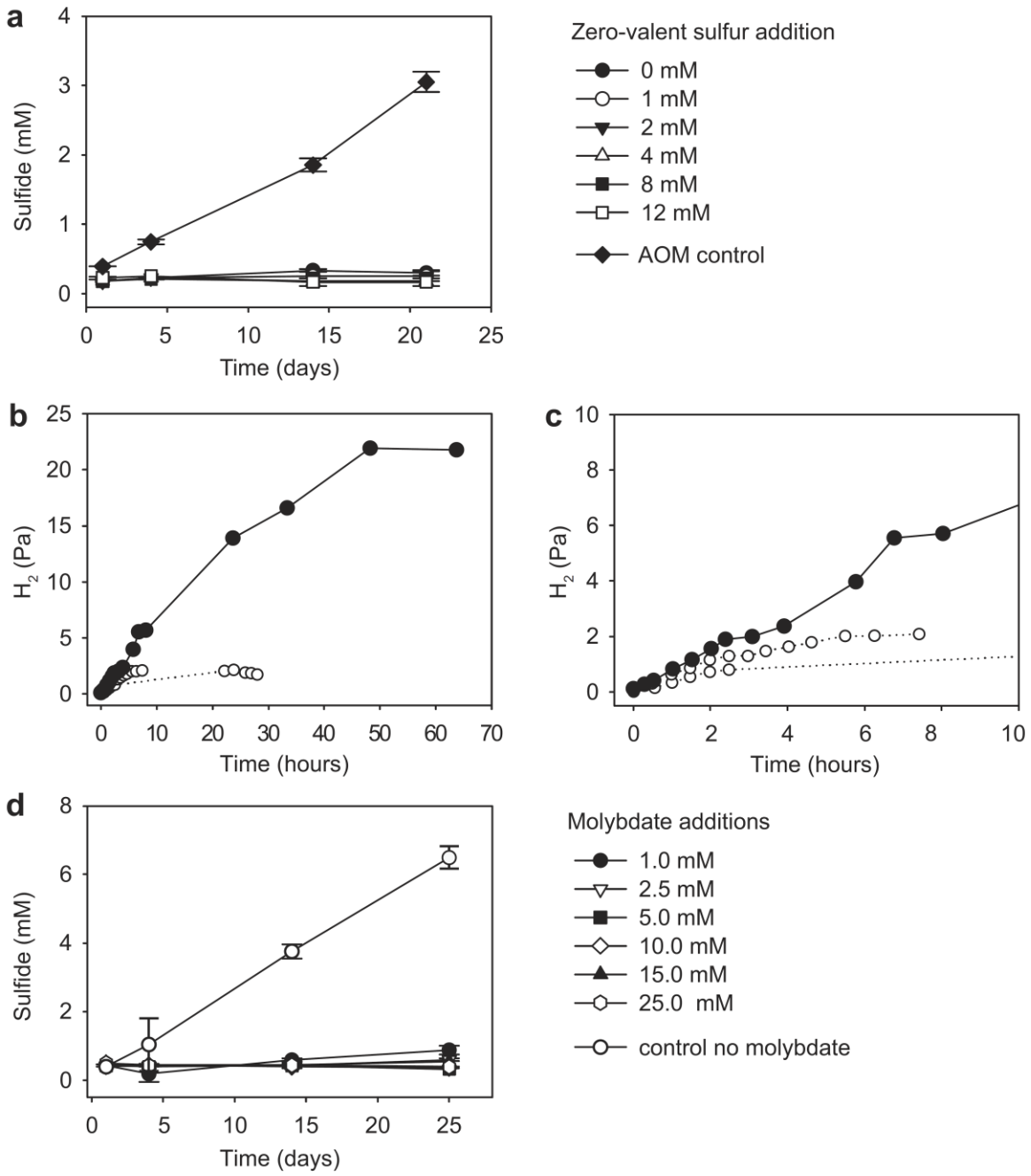

Extended Data Figure 3 Effect of zero-valent elemental sulfur and molybdate additions on TAOM. **a**, Sulfide production in response to zero-valent (colloidal) sulfur amendments versus TAOM conditions; zero-valent sulfur did not cause sulfide formation. **b,c**, Monitoring of hydrogen partial pressures at TAOM conditions (open circles) versus extra addition of 10 mM molybdate (filled circles); (b) full times series, (c) subset first 10 hours. Molybdate addition caused 10 times higher hydrogen concentrations than TAOM condition. **d**, Inhibition of methane-dependent sulfide production at different molybdate concentrations. (a,d) biological replicates n=3, symbols=mean values, error bar=s.d.; (b, c) single time series with the same culture.

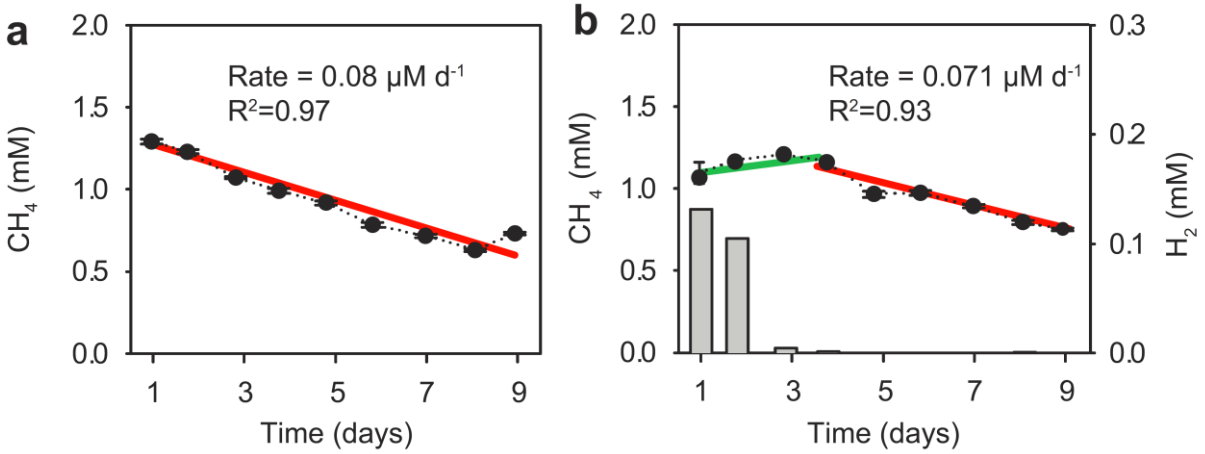

Extended Data Figure 4 Effect of hydrogen on microbial methane oxidation. **a**, Methane (0.15 MPa) supplied as sole electron source was steadily consumed with time by TAOM. **b**, When both methane (0.15 MPa) and hydrogen (0.05 MPa) were added, hydrogen was rapidly consumed (grey bars), whereas methane consumption was reversely inhibited (green line) until hydrogen was fully consumed. Afterwards methane consumption occurred at the same rate as in the control with only methane (a). Technical replicates n=3, symbols=mean values, error bar=s.d. Experiment was replicated once in the laboratory.

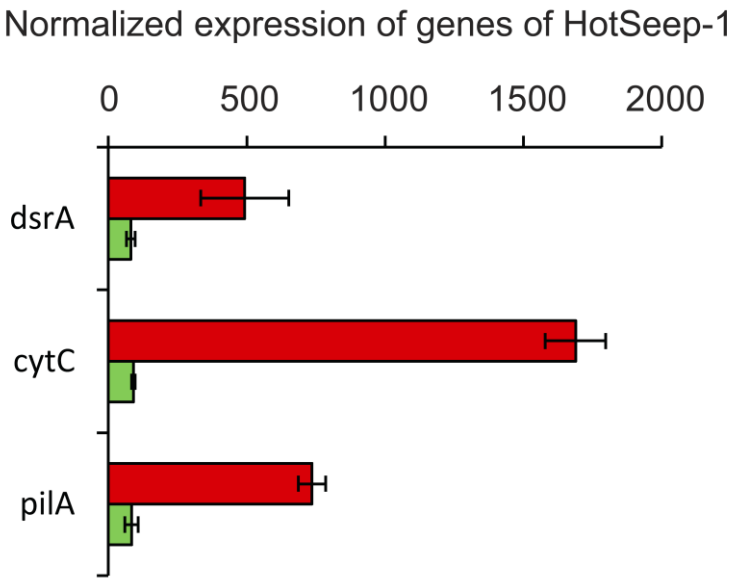

Extended Data Figure 5 Relative expression of marker genes of HotSeep-1 in consortial growth on methane (TAOM) versus enrichment on hydrogen. Genes encoding proteins apparently involved in direct interspecies electron transfer (cytC and PilA) are strongly overexpressed during TAOM (red) compared to hydrogenotrophic growth (green). Biological replicates n=3, error bars=s.d.

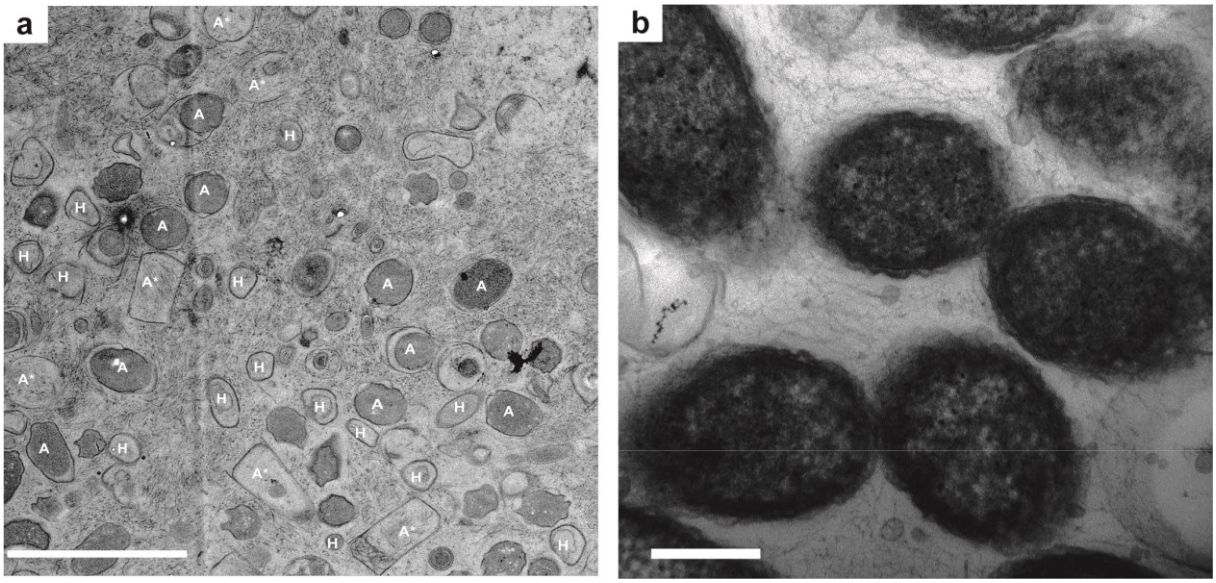

Extended Data Figure 6 Thin-sections of TAOM and dual species *Geobacter* spp. aggregates. **a**, TAOM culture. High-pressure frozen ANME-1 cells (A) have a cylindrical shape and a size of 1.5×0.8 µm, looking circular in cross-sections, and rectangular when cut along the axis. Their cell content shows a high contrast. A* shows cell envelopes. HotSeep-1 cells (H) are smaller (approx. 1×0.5 µm), of rod-like shape, and have lower contrast. The matrix between the cells is largely filled with filaments. Bar scales 3 µm. **b**, Thin-sections of Geobacter consortia and their intercellular nanowires using the same embedding techniques as for TAOM consortia. Bar scales 300 nm.

Extended data tables

Extended Data Table 1 Phylogenetic affiliation of cloned 16S rRNA gene sequences obtained from TAOM enrichments in 2010 (compiled from ref. 6) and after 1.5 years of cultivation in 2012 (this study).

Phylogenetic Group	No of clones	
	2010, slurry	2012, sediment-free
Archaea		
Euryarchaeota		
ANME-1		
ANME-1-Guaymas cluster	**46 (82%)**	**148 (89%)**
Other related ANME-1	-	7
Thermoplasmatales (19c-33 related)	6	7
Thermococcales	-	1
Others	4	3
Sum	**56**	**166**
Bacteria		
Proteobacteria		
Betaproteobacteria	3	1
Gammaproteobacteria	11	-
Deltaproteobacteria		
HotSeep-1-Cluster	**124 (60%)**	**89 (59%)**
DSS group	1	1
Others	16	4
Acidobacteria	1	-
Actinobacteria	3	-
Candidate Division OD1	6	1
Candidate Division OP3	5	40
Candidate Division OP8	21	6
Chloroflexi	8	-
Others	8	9
Sum	**207**	**151**

Extended Data Table 2 Pairwise comparison of nucleotide sequences from the HotSeep-1 draft genomes derived from the TAOM culture versus the HotSeep-1 culture on hydrogen.

Feature	Identity (bp)	Identity (%)	Gaps	Query coverage	E value
16S rRNA	1554/1555	99	0/1555	100	0
23S rRNA	3025/3029	99	0/2029	100	0
ITS (23S-16S)	270/271	99	0/271	100	3.00E-145
dsrA	1406/1438	98	0/1438	100	0
aprA	1905/1905	100	0/1905	100	0
Hydogenase small subunit	1437/1437	100	0/1437	100	0
Hydrogenase large subunit	916/918	100	0/918	99	0
dnaK	1884/1893	99	0/1893	100	0

Extended Data Table 3 Effect of potential intermediates in AOM on sulfide production (SP) of TAOM culture (3 replicates, 20 day incubation). '−' SP at level of negative control; '+' SP similar to TAOM under standard conditions; '+++' SP tripled compared to TAOM standard conditions.

	Sulfide production	
Substrate	plus substrate	plus methane
Control (no donor)	−	
Methane	+	
Colloidal sulfur	−	+
Hydrogen	+++	+++
Carbon monoxide	−	−
Methyl sulfide	−	−
Methanol	−	+
Acetate	−	+
Formate	−	+

Extended Data Table 4 Genes encoding for c-type cytochromes identified in thermophilic ANME-1 and HotSeep-1 genome draft, and for Type IV pili (T4P) biogenesis identified in the HotSeep-1 genome draft with expression >20 TPM. Genes in bold are presented in Fig. 3a.

Cytochrome c type based on PfamA domain prediction	**Predicted cellular localization (PSORTb)**	**Predicted heme groups**	**Expression in TAOM (TPM)**	**Expression change in H_2 treatment**
ANME-1				
Cytochrom_c3_2	**Unknown (CM,CW,E)**	**8**	1,063	↓
Cytochrome_C7	Unknown (CM,CW,E)	4	603	↓
Cytochrome_C7	Extracellular	4	506	↓
Cytochrom_NNT	Cytoplasmic	5	73	↓
HotSeep-1				
Paired_CXXCH_1	**Extracellular**	**6**	2,485	↓
Cytochrom_CIII	Periplasmic	4	1,011	-
Paired_CXXCH_1	Unknown (CM,OM,P,E)	7	974	-
Cytochrome_C554	Unknown (CM,OM,P,E)	5	881	-
Cytochrom_CIII	Periplasmic	4	179	-
Cytochrome_C7	Cytoplasmic Membrane	5	95	-
Paired_CXXCH_1	Cytoplasmic	10	95	-
Cytochrom_c3_2	Unknown (CM,P,E)	12	86	-
Cytochrom_c3_2	Periplasmic	12	74	-
Cytochrome_C554	Unknown (CM,P,E)	4	24	↓
Predicted pili protein	**Predicted cellular localization (PSORTb)**	**% identity to *G. sulfurreducens***	**Expression in TAOM (TPM)**	**Expression change in H_2 treatment**
HotSeep-1				
assembly protein (*pil*A)	**Extracellular**	**74**	**1084**	↓
retraction ATPase (*pil*T)	Cytoplasmic	40	51	↓
assembly protein (*pil*Y)	Extracellular	26	46	↓
assembly ATPase (*pil*B)	Cytoplasmic	47	26	-
secretion (*pil*Q)	Unknown (OM, C)	32	26	-
assembly protein (*pil*A)	Cytoplasmic Membrane	41	23	↓
retraction ATPase (*pil*T)	Cytoplasmic	55	21	-
assembly protein (*pil*M)	Cytoplasmic	35	21	-
assembly protein (*pil*O)	Cytoplasmic Membrane	35	21	↓

(E=Extracellular, CM=Cytoplasmic Membrane, CW=cell wall, OM=Outer Membrane, P=Periplasm); ↑ up-regulated by factor 2; ↓ down-regulated by factor 2; - no change.

Supplementary information

Supplementary information is available in the online version of the paper.

Chapter III

Candidatus Desulfofervidus auxilii, a hydrogenotrophic sulfate-reducing bacterium involved in the thermophilic anaerobic oxidation of methane

Viola Krukenberg[1*], Katie Harding[1], Michael Richter[1], Frank Oliver Glöckner[1,5], Harald Gruber-Vodicka[1], Birgit Adam[1], Jasmine Berg[1], Katrin Knittel[1], Halina E. Tegetmeyer[2,3], Antje Boetius[1,2,4] and Gunter Wegener[1,4]

[1]Max Planck Institute for Marine Microbiology, Bremen, Germany

[2]Alfred Wegener Institute, Helmholtz Center for Polar and Marine Research, Bremerhaven, Germany

[3]Center for Biotechnology, Bielefeld University, Bielefeld, Germany

[4]MARUM, Center for Marine Environmental Sciences, University Bremen, Germany

[5]Jacobs University Bremen gGmbH, Bremen, Germany

Submitted to Environmental Microbiology

[*]Correspondence: Viola Krukenberg, Max Planck Institute for Marine Microbiology, Celsiusstrasse 1, 28359 Bremen; email: vkrukenb@mpi-bremen.de; Tel.: 0049 421 2028 984; Fax: 0049 421 2028 870

Running title: The partner bacterium in thermophilic methanotrophy

Summary

The anaerobic oxidation of methane (AOM) is mediated by consortia of anaerobic methane-oxidizing archaea (ANME) and their specific partner bacteria. In thermophilic AOM consortia enriched from Guaymas Basin, members of the ANME-1 clade are associated with bacteria of the HotSeep-1 cluster, which likely perform direct electron exchange via nanowires. The partner bacterium was enriched with hydrogen as sole electron donor and sulfate as electron acceptor. Based on phylogenetic, genomic and metabolic characteristics we propose to name this chemolithoautotrophic sulfate reducer *Candidatus* Desulfofervidus auxilii. *Ca.* D. auxilii grows on hydrogen at temperatures between 50°C and 70°C with an activity optimum at 60°C and doubling time of four to six days. Its genome draft encodes for canonical sulfate reduction, periplasmic and soluble hydrogenases and autotrophic carbon fixation via the reductive tricarboxylic acid cycle. The presence of genes for pili formation and cytochromes, and their similarity to genes of *Geobacter* spp., indicate a potential for syntrophic growth via direct interspecies electron transfer when the organism grows in consortia with ANME. This first ANME-free enrichment of an AOM partner bacterium and its characterization opens the perspective for a deeper understanding of syntrophy in anaerobic methane oxidation.

Introduction

The microbially mediated anaerobic oxidation of methane (AOM) is a key process in anoxic methane-rich marine habitats, controlling methane efflux from the seabed (Boetius and Wenzhöfer, 2013). Marine AOM is performed by consortia of anaerobic methanotrophic archaea (ANME) and partner bacteria coupling the oxidation of methane to the reduction of sulfate in a syntrophic process (Boetius *et al.*, 2000; Orphan *et al.*, 2001b). The oxidation of methane is mediated by the archaea, involving the reversal of the methanogenesis pathway (Hoehler *et al.*, 1994; Hallam *et al.*, 2004). Previous studies have assigned canonical sulfate reduction to the consortial partner bacteria (Boetius *et al.*, 2000; Milucka *et al.*, 2013). The mode of interspecies transfer of electrons from the ANME to the partner SRB remains uncertain. Exchange of metabolic intermediates, hydrogen or direct interspecies electron transfer have been discussed (Hoehler *et al.*, 1994; Widdel *et al.*, 2007; Moran *et al.*, 2008; McGlynn *et al.*, 2015). Alternatively, it was suggested that archaea could carry out partial sulfate reduction, with the bacterial partner disproportionating zero-valent sulfur species (Milucka *et al.*, 2012). AOM is mediated by members of three different phylogenetic clades (ANME-1, ANME-2 and ANME-3; Knittel and Boetius, 2009) which comprise a substantial diversity of subgroups (Ruff *et al.*, 2015). Although the consortia formed by the different ANME are highly specific associations with only one type of partner bacterium, there is a considerable diversity of *Deltaproteobacteria* that can form AOM consortia. The Seep-SRB-1 cluster (*Desulfosarcina*/*Desulfococcus*) prevails in most natural and laboratory psychro- and mesophilic enrichments dominated by ANME-2 (Boetius *et al.*, 2000; Orphan *et al.*, 2001a; Michaelis *et al.*, 2002; Knittel *et al.*, 2003). The Seep-SRB-2 cluster is frequently observed as partner of psychro- and mesophilic ANME-1 and -2 (Kleindienst *et al.*, 2012) and *Desulfobulbus*-relatives as partners of ANME-3 (Niemann *et al.*, 2006). None of the psychro- to mesophilic ANME or their partner bacteria has yet been obtained as pure culture hence some of these organisms might be obligate syntrophs.

Here we studied the bacterial partner in thermophilic AOM (growth range 50 to 65°C), HotSeep-1, recently enriched from the methane-rich hydrothermal system of Guaymas Basin, Gulf of California (Holler *et al.*, 2011). In thermophilic AOM enrichments HotSeep-1 bacteria associate with ANME-1 archaea to form filamentous or densely packed spherical consortia. So far, sequences similar to those of this bacterial partner have only been reported from hydrothermal vent systems (Teske *et al.*, 2002; Biddle *et al.*, 2011), and thermophilic short-chain hydrocarbon-degrading enrichments originating from the Guaymas Basin (butane-degrading) and from Middle Valley, Juan de Fuca Ridge (butane- and propane-degrading)

(Kniemeyer *et al.*, 2007; Adams *et al.*, 2013). In thermophilic AOM, HotSeep-1 retrieves reducing equivalents from its ANME partner through the oxidation of methane (Holler *et al.*, 2011) likely via direct interspecies electron transfer (Wegener *et al.*, 2015).

Here we studied the metabolic and genomic features of a representative of the HotSeep-1 cluster, proposed as *Candidatus* Desulfofervidus auxilii, with the focus on its potential role as syntrophic partner in hydrocarbon degradation.

Results and discussion

Enrichment and cultivation of HotSeep-1

During thermophilic anaerobic oxidation of methane (TAOM), HotSeep-1 formed dense cell aggregates with ANME-1 archaea in the form of filaments or large spherical aggregates (Fig. 1). In filaments, HotSeep-1 and ANME-1 cells associated in close proximity and often 1:1 stoichiometry within a sheath-like structure (Holler *et al*., 2011) (Fig. 1 B). Spherical aggregates reaching sizes of 0.5 mm contained well-mixed, approximately equal portions of HotSeep-1 and ANME-1 cells and were the dominant consortia growth type in long-term, sediment-free TAOM enrichments (>2 years of enrichment by continuous dilution) (Fig. 1 A). When the energy supply to the TAOM enrichment was switched from methane to hydrogen, the enrichment responded with a fivefold increase of the sulfide production rate within nine days (Fig. 2 A). Other substrates including a variety of organic compounds including acetate, formate, alcohols, benzoate, dicarboxylic acids, pyruvate, methyl sulfide, and carbon monoxide did not lead to sulfide production. Serial dilution-to-extinction cultivation of this enrichment at 60°C with sulfate and hydrogen as the energy source, and inorganic carbon as the sole carbon source, resulted in separation of HotSeep-1 cells from the ANME partner in initial dilutions of up to $1:10^6$. Continuous dilution yielded an enrichment of >95% HotSeep-1 cells (Fig. 2 B-D). A persistent archaeal contaminant, identified as *Archaeoglobus* sp. by 16S rRNA gene sequencing, accounted for around 5% of all cells during exponential growth phase (Fig. S1). Classification of metagenomic 16S rRNA gene fragments (approx. 2000 reads) obtained from the enrichment estimated HotSeep-1 to *Archaeoglobus* sp. 16S rRNA genes in a ratio >100:1. Accordingly, the from the metagenome assembled nearly full length 16S rRNA gene sequences related to HotSeep-1 and *Archaeoglobus fulgidus* showed coverages of 108x and 3x, respectively. ANME-1 was not detected in the hydrogenotrophic HotSeep-1 enrichment. Based on phylogenetic, genomic and metabolic data we propose that

the enriched HotSeep-1 represents a novel species, *Candidatus* Desulfofervidus auxilii, referring in denotation to the bacterium's sulfate-reducing metabolism in thermophilic syntrophic consortia.

Physiological characterization of *Ca.* D. auxilii

Hydrogen-dependent sulfate-reducing activity of *Ca.* D. auxilii cultures was observed at temperatures between 50-70°C. Sulfate reduction rates were highest at 60°C (Fig. S2). The cell specific sulfate reduction rate at 60°C was 46 fmol sulfate reduced per day per cell (Fig. S1). No activity was observed below 50°C and above 70°C, matching the temperature optimum in consortial growth with ANME-1 (Holler *et al.*, 2011). Freshly inoculated *Ca.* D. auxilii cultures showed a relatively long lag phase of approximately 12 days followed by an exponential increase of sulfate-reducing activity, carbon fixation and cell numbers until sulfate was depleted (after about 32-35 days) (Fig. S1). *Ca.* D. auxilii tolerates high sulfide concentrations of up to 25 mM (Fig. S1), which is an advantage in its highly sulfidic natural habitat in subsurface sediments of methane-rich hydrothermal vents (Jørgensen *et al.*, 1990; Vigneron *et al.*, 2014). The calculated doubling time of 4-6 days is slow compared to other hydrogenotrophic sulfate reducers (doubling time of 12-24 h (Brysch *et al.*, 1987; Alazard *et al.*, 2003; Audiffrin *et al.*, 2003; Rabus *et al*., 2006)). However, compared to the inherently slow growth as partner bacterium in thermophilic AOM (doubling time approx. 50 days as estimated from the increase in sulfide production), growth dynamics were 12 times faster in single culture on hydrogen. Organic compounds (including acetate, formate, alcohols, benzoate, dicarboxylic acids, pyruvate, methyl sulfide, carbon monoxide) were not used as energy source for sulfate reduction (Fig. S3) which is in agreement with the absence of sulfide production in TAOM enrichments supplemented with organic compounds other than methane (see above). Notably, no sulfate-reducing activity of *Ca.* D. auxilii was observed on methane and short-chain hydrocarbons (butane, propane), which contrasts earlier reports of HotSeep-1-dominated hydrocarbon (propane)-degrading enrichments (Adams *et al.*, 2013) (Fig. S3, S4). Further, tested organic compounds did not stimulate the sulfate-reducing activity of *Ca.* D. auxilii during growth on hydrogen suggesting that *Ca.* D. auxilii grows autotrophically. Autotrophic growth of *Ca.* D. auxilii is in line with earlier studies on other sulfate-reducing AOM partner bacteria also showing carbon dioxide fixation (Wegener *et al.*, 2008; Kellermann *et al.*, 2012). Autotrophic carbon fixation by *Ca.* D. auxilii accounts for on average 0.03 to 0.04 mol carbon dioxide fixed per mol sulfate reduced (Fig. S5) with a carbon fixation rate of 1.3 fmol per day per cell. This corresponds to the use of only 1.5% of the

reducing equivalents derived from hydrogen oxidation for carbon fixation. This carbon fixation capacity is much lower than in other studied hydrogenotrophic sulfate reducers (Brandis and Thauer, 1981; Cypionka and Pfennig, 1986), which explains the comparatively low growth rates and limited cell densities of the *Ca.* D. auxilii culture. It compares well to the carbon fixation capacity in TAOM of 2%, when determined as reducing equivalents derived from methane oxidation (Wegener *et al.*, 2015). Furthermore, alternative sulfur sources (i.e. sulfite, thiosulfate and elemental sulfur) were neither reduced nor disproportionated by *Ca.* D. auxilii (Tab. 1), indicating that *Ca.* D. auxilii is an obligate sulfate reducer.

Phylogenetic position of *Ca.* D. auxilii

Ca. D. auxilii is the first cultured representative of its 16S rRNA gene sequence cluster (>97.5% similarity) which to date comprises almost full-length sequences (>1400 bp) obtained from Guaymas Basin environmental samples (Teske *et al.*, 2002) and methane- and butane-degrading enrichments (Kniemeyer *et al.*, 2007; Holler *et al.*, 2011), and additionally assigned partial sequences retrieved from Middle Valley hydrocarbon-degrading enrichments (NCBI SRA066151) (Adams *et al.*, 2013). The first sequences of this cluster were identified by Teske and colleagues (2002) as “Guaymas-specific sequence cluster”. Later, when Holler and colleagues (2011) assigned similar sequences to the bacterial partner in thermophilic AOM the cluster was denoted “HotSeep-1”. The genomic 16S rRNA gene obtained from the hydrogenotrophically grown *Ca.* D. auxilii is identical or highly similar to sequences of the HotSeep-1 cluster (see Tab. S1). Our 16S rRNA gene phylogenetic analysis confirmed the previously described deep-branching position of this cluster (Holler *et al.*, 2011) and showed that its affiliation within the bacterial phylogenetic tree varied highly depending on the set of reference sequences used for tree calculation (Fig. S6). This unstable phylogenetic placement is also reflected in earlier discordant classifications of the cluster as related to the *Thermodesulfobacteria* phylum or as a member of the *Deltaproteobacteria* with *Desulfurella* and *Hippea* as distant relatives (Teske *et al.*, 2002; Holler *et al.*, 2011). Accordingly, a database comparison with the genomic 16S rRNA gene of *Ca.* D. auxilii shows among the top 10 hits (84-86% identity) members of *(Delta)Proteobacteria* and *Thermodesulfobacteria*, with the best scoring hit (86% similarity) to *Thermodesulforhabdus norvegica* (*Deltaproteobacteria*) (Tab. S2). According to recent taxonomic thresholds defined in Yarza and colleagues (2014), a 16S rRNA gene sequence similarity of ≤86.2% suggests a

membership in different families. Hence, we propose that *Ca.* D. auxilii and related sequences in the HotSeep-1 cluster represent a novel family, *Candidatus* Desulfofervidaceae.

To further resolve the phylogenetic classification of *Ca.* D. auxilii we reconstructed a 23S rRNA gene based phylogeny. This placed *Ca.* D. auxilii within the *Deltaproteobacteria*. Notably, *Ca.* D. auxilli's relatives were *Desulfobacca acetoxidans*, *Geobacter* spp. and *Syntrophobacter fumaroxidans*, with the latter two being known to grow syntrophically (Fig. S7). We furthermore used a genome-based phylogenetic approach. Phylotyping of 30 single copy genes identified in the *Ca.* D. auxilii genome assigned 47% (14) of these genes to the *Deltaproteobacteria*, and 40% (12) to *Thermodesulfobacteria* (Tab. S3). The phylogenetic tree reconstructed from a subset of 19 ubiquitous single copy genes (detected in all here analysed genomes) revealed a sister relationship of *Ca.* D. auxilii to members of the *Thermodesulfobacteria*, namely *Thermodesulfatator indicus* and *Thermodesulfobacterium geofontis*, and an affiliation of this cluster as sister clade of the *Deltaproteobacteria* (Fig. 3). In contrast based on 16S rRNA gene phylogeny the *Thermodesulfobacteria* represent a phylum distantly related to the *Deltaproteobacteria*. A discrepancy between 16S rRNA gene and whole genome-based phylogeny of the *Thermodesulfobacteria* has been previously described (Lang *et al.*, 2013) and the authors suggested that *Thermodesulfobacteria* may not represent a distinct phylum but were to be included in the *Deltaproteobacteria*. The observed placement of *Ca.* D. auxilii may suggest a basal position within the *Thermodesulfobacteria*. It however also indicates that *Ca.* D. auxilii affiliates with both *Thermodesulfobacteria* and *Deltaproteobacteria*, which may be interpreted as an intermediate position between these groups. In addition to the phylogenetic resolution of conserved single copy genes we also compared the taxonomic assignment (on phylum and species level) of all *Ca.* D. auxilii proteins (using the in house genomesDB as a reference (Richter *et al.*, 2008)). Consistently with the observation on single copy gene level the highest number of best hits was assigned to *Thermodesulfatator indicus* (Tab. S4). Subsequent reciprocal best match blast analysis of the *Ca.* D. auxilii genome versus selected genomes (see Tab. S5) consistently showed highest similarity to *T. indicus*. Although to some degree *Ca.* D. auxilii resembles *T. indicus* in lifestyle (thermophilic chemoautotrophic metabolism) and habitat (deep-sea vents) (Moussard, 2004), they share only 958 genes, representing 37% of the genes of *Ca.* D. auxilii and including only 195 genes with similarity above 60%. Among the *Deltaproteobacteria*, *Ca.* D. auxilii shows most genomic similarity to another syntrophic organism, the propionate-oxidizer *Syntrophobacter fumaroxidans,* with 912 shared orthologous genes (36% of the *Ca.* D. auxilii genes). This comparative genomic analysis revealed that *Ca.* D. auxilii affiliates

with both thermophilic sulfate-reducing and syntrophic organisms and concordantly with the results from 23S rRNA gene and single copy gene analysis suggests that, both, *S. fumaroxidans* and *T. indicus* were among the closest relatives of *Ca.* D. auxilii. The observed moderate genomic similarity (<40% based on shared orthologous genes) to members of both *Thermodesulfobacteria* and *Deltaproteobacteria*, may further indicate a basal position of *Ca.* D. auxilii in either of the two groups. At the time of writing the genomes of the thermophilic sulfate reducers *T. norvegicus, Dissulfuribacter thermophilus* and *Desulfosoma caldarium*, which are more closely related on 16S rRNA gene level, were not available. The remarkably low genomic similarity of the *Ca.* D. auxilii genome to any genome analyzed here (Tab. S4, S5) might be due to its phylogenetic isolation; however it might also point towards metabolic characteristics which impede cultivation of close relatives.

On a functional level, the dissimilatory sulfite reductase gene (Dsr), encoding a key enzyme of sulfate reduction, is also a functional marker gene for sulfate reducers (Klein *et al.*, 2001; Müller *et al.*, 2014). The amino acid sequence of the Dsr subunit A (DsrA) of *Ca.* D. auxilii affiliates with DsrA sequences from *Desulfatiglans anilini* (formerly *Desulfobacterium anilini*), *Moorella thermoacetica* and *Desulfotomaculum* spp. (Fig. S8), with highest amino acid sequence similarity of 75% to *D. anilini*. The *drsA* gene is prone to lateral gene transfer and *Desulfotomaculum* species (*Firmicutes*) are proposed to have acquired their *dsrA* gene through lateral transfer from *D. anilini* (Klein *et al.*, 2001; Zverlov *et al.*, 2005). A placement of the *Ca.* D. auxilii *dsrA* in this cluster might indicate an involvement of this deep-branching bacterium in lateral gene transfer events. The identification of the genomic *dsrA* of *Ca*. D. auxilii as reported here allows for its detection in functional gene-based surveys of sulfate reducers.

Based on our phylogenetic analysis and whole genome comparison as well as physiologic characteristics we suggest a tentative classification of *Ca.* D. auxilii in the *Deltaproteobacteria*. A clear classification on higher taxonomic level (above family) awaits clarification by isolating and describing further members of this novel deep-branching lineage.

General genome features

The here described draft genome of *Ca.* D. auxilii has a size of 2.55 Mbp and a GC content of 37%. The obtained sequencing data provided an estimated 430 fold coverage of the genome. In total, 2528 open reading frames (ORFs) were identified of which about 66% (1658 ORFs) could be assigned to COG (clusters of orthologous genes) categories (see Tab. S6 for an

overview of observed COG categories). The genome contains one 16S-23S-5S rRNA operon and 47 tRNAs. Genome completeness was almost reached, based on estimations by (i) the checkM software (Parks *et al.*, 2015) using 340 markers (97% completeness with 4% contamination and without detected strain heterogeneity) and (ii) the AMPHORA2 package with 31 bacterial markers (all detected, DnaG duplicated) (Wu and Scott, 2012), and (iii) based on the detection of tRNAs for all amino acids. The general genome features are summarized in Table 2. The draft genome of *Ca.* D. auxilii is comparable in size and GC content to genomes of other sulfate- and sulfur-reducing bacteria retrieved from hydrothermal habitats such as *Thermodesulfatator indicus* (2.5 Mbp, GC content 40%), *Thermodesulfobacterium geofontis* (1.3 Mbp, GC content 30%), and *Hippea maritima* (1.7 Mbp, GC content 37%) (Anderson *et al.*, 2004; Huntemann *et al.*, 2011; Elkins *et al.*, 2013). In the course of evolution genome reduction might occur as a result of adaptation to specific environmental niches, thus *Ca.* D. auxilii's limited metabolic versatility is presumably reflected in its small genome size.

Genomic basis for hydrogenotrophic growth of *Ca.* D. auxilii

Ca. D. auxilii's draft genome encodes a complete set of proteins required for hydrogen-dependent sulfate-reduction (see Supplementary Information Annotation Tables for an overview of annotated genes). It includes a soluble (HS1_002313-HS1_002314) and a periplasmic (HS1_000162-HS1_000163) NiFe hydrogenase, and proteins required for its maturation and expression (HS1_000157-HS1_000161, HS1_000149-HS1_000151). The predicted non-membrane-bound periplasmic hydrogenase is proposed to transfer electrons from hydrogen oxidation to periplasmic c-type cytochromes (Matias *et al.*, 2005). The identified soluble NiFe methyl viologen hydrogenase (MvhA) may form a cytoplasmic complex with subunits of the heterodisulfide reductase (HS1_001272-HS1_0001274) as previously suggested (Thauer *et al.*, 2008). This HdrABC/MvhADG complex may couple hydrogen oxidation to the endergonic reduction of the low-potential redox-carrier ferredoxin and the exergonic reduction of a heterodisulfide bond in a flavin-based electron bifurcation mechanism (Buckel and Thauer, 2013).

As a terminal electron sink, *Ca.* D. auxilii has a complete dissimilatory sulfate reduction pathway. It is located in the cytoplasm and consists of ATP sulfurylase (Sat, HS1_002311), APS-reductase (AprAB, HS1_000253-HS1_000254), and a dissimilatory sulfite reductase complex (DsrABCD, HS1_002180-HS1_002182, HS1_000090). Electrons derived through the periplasmic oxidation of molecular hydrogen are proposed to reduce the periplasmic

cytochrome pool and enter the sulfate reduction pathway via cytochrome- and menaquinone-interacting membrane-bound electron transfer complexes, several of which are known from sulfate-reducing bacteria and archaea (Pereira *et al.*, 2011). The quinone reductase complex (QrcABCD, HS1_000675-HS1_000678) was proposed to reduce the membrane menaquinone pool via electrons from periplasmic cytochromes (Venceslau *et al.*, 2010). The menaquinone-interacting oxidoreductase complex (QmoABC, HS1_002183-HS1_002185) then delivers electrons from the reduced menaquinone pool to the APS reductase complex (Pires *et al.*, 2003; Ramos *et al.*, 2012; Grein *et al.*, 2013). The TmcABCD complex (HS1_001244-HS1_001247) and DsrMKOPJ or HmeABCDE complex (HS1_002291-HS1_002295) were suggested to directly deliver electrons from the periplasmic cytochrome pool to the cytoplasmic DsrAB complex through a reduction of the disulfide bond in DsrC via heterodisulfide reductases (Venceslau *et al.*, 2014). Electrons derived through cytoplasmic hydrogen oxidation by HdrABC/MvhADG (HS1_002313-HS1_002314/HS1_001272-HS1_0001274) possibly enter the dissimilatory sulfate reduction pathway also at the level of DsrAB via reduction of DsrC by HdrB (Pereira *et al.*, 2011; Grein *et al.*, 2013).

Energy conservation during hydrogenotrophic growth of *Ca.* D. auxilii could occur via electron transport phosphorylation utilizing the electrochemical gradient created by periplasmic hydrogen oxidation for synthesis of ATP via ATP synthase (F-type ATPase, HS1_001679-HS1_001682, HS1_001898-HS1_001904). Alternatively, *Ca.* D. auxilii may utilize a membrane-associated ion translocating complex (Rnf complex, HS1_001621-HS1_001626) (Buckel and Thauer, 2013) which was suggested to couple the exergonic re-oxidation of reduced ferredoxin with NAD^+ to the translocation of protons (Na^+ or H^+) across the membrane, creating an electrochemical gradient for ATP synthesis (Biegel and Müller, 2010). Thus *Ca.* D. auxilii potentially conserves energy via two mechanisms: electron transport phosphorylation and electron bifurcation. However, ferredoxin is a central electron carrier and reduced ferredoxin is crucial for autotrophic carbon fixation in anaerobes. *Ca.* D. auxilii may generate reduced ferredoxin from hydrogen through cytoplasmic electron bifurcation at the MvhADG/HdrABC complex as suggested before for other sulfate reducers (Thauer *et al.*, 2008; Buckel and Thauer, 2013). Another possibility would be a reverse-functioning Rnf complex to generate additional reduced ferredoxin (e.g. for carbon fixation) with NADH (endergonic) utilizing energy conserved in the proton gradient (Schmehl *et al.*, 1993; McInerney *et al.*, 2007).

As generally observed in genomes of sulfate reducers (Strittmatter *et al.*, 2009; Pereira *et al.*, 2011) several (16) genes encoding putative heterodisulfide reductase (Hdr) subunits

were identified in the *Ca.* D. auxilii draft genome. Besides the Hdr-containing membrane-bound electron transfer complexes Tmc, Dsr and Qmo an additional gene cluster was identified that potentially encodes another membrane-bound complex with Hdr-related subunits. The genes of this cluster were annotated as an integral membrane protein with a HdrB-related domain and a potential c-type cytochrome (HS1_002398), two electron transfer flavoproteins (HS1_002399-HS1_002400) and two proteins with HdrA- and HdrB-related domains, respectively (HS1_002397, HS1_002401). Encoded directly upstream of this cluster were genes for another HdrA-like protein (HS1_002394), for two delta subunits of the methyl viologen-reducing hydrogenase (HS1_002393, HS1_002395) and for two beta subunits of formate dehydrogenase (HS1_002392, HS1_002396), which may be involved in electron transfer reactions. Together these proteins could form an additional electron transport complex directly interacting with the reduced periplasmic cytochrome pool and possibly via HdrB reduce DsrC or transfer electrons onto cytoplasmic electron transfer proteins.

Possible mechanisms for syntrophic growth in the anaerobic oxidation of methane via direct electron transfer

Microbial syntrophy can occur by transfer of a molecular intermediate such as hydrogen or formate that is produced by a syntrophic metabolizer, e.g. a fermenting bacterium and scavenged by a single or multiple partners that oxidize the compound. The activity of the latter prevents product inhibition (McInerney *et al*., 2009). Alternatively, some organisms have the capability to directly transfer electrons (Summers *et al*., 2010; Rotaru *et al*., 2014). Consequently, common features such as systems for reverse electron flow, hydrogenases, formate dehydrogenases, pili and outer membrane cytochromes have been highlighted in the genomes of syntrophic metabolizers (Sieber *et al*., 2012). *Ca.* D. auxilii grows as syntrophic partner of ANME-1 archaea, both in the environment and *in vitro* (Holler *et al*., 2011; Wegener *et al*., 2015). Formate can be excluded as substrate of *Ca.* D. auxilii as it does not grow on formate and its genome does not encode a complete formate dehydrogenase, necessary to metabolize formate. In contrast, *Ca.* D. auxilii grows on hydrogen and could theoretically utilize its hydrogenases during syntrophic growth via interspecies hydrogen transfer. During TAOM, production of molecular intermediates was however not observed (Wegener *et al*., 2015). Instead direct electron transfer via excreted multi-heme cytochrome c and nanowire-like structures was proposed for the syntrophic coupling in AOM consortia (McGlynn *et al*., 2015; Wegener *et al*., 2015). DIET is the preferred mode of syntrophic interaction between the syntrophic ethanol metabolizer *G. metallireducens* and its product

scavenger *G. sulfurreducens* (Summers *et al*., 2010). They can switch between interspecies hydrogen transfer and DIET, which may indicate that only a few genetic adaptations are required to alternate between the two modes. In TAOM consortia a dense network of nanowire-like structures was observed that might enable direct interspecies electron transfer (Wegener *et al*., 2015). The *Ca.* D. auxilii genome encodes a set of genes required for biogenesis and assembly of type IV pili (HS1_000117, HS1_000600-HS1_000604, HS1_002000, HS1_002454). Although type IV pili may have various functions including attachment, they seem to play a crucial role in mediating direct electron transfer in syntrophically growing dual-species *Geobacter* consortia (Summers *et al*., 2010). Recent studies indicated that the *Geobacter*-specific geopilins are self-conductive and that the PilA protein contains aromatic amino acids that are the key to electron transport along pili via delocalized charges (Liu *et al*., 2014; Malvankar *et al*., 2014, 2015). Comparison of the amino acid sequences of PilA prepilins from *Ca.* D. auxilii (HS1_000117) and *G. sulfurreducens* revealed that the *Ca.* D. auxilli pilin contains 3 of the 5 aromatic amino acids found in the N-terminal domain of geopilin. Furthermore, in *Geobacter* spp. highly expressed multi-heme c-type cytochromes (OmcS) were proposed to play an important role in electron transfer. *Ca.* D. auxilii lacks this specific cytrochrome, but harbors a variety of c-type cytochromes (24), several (10) of which have orthologs in the *G. sulfurreducens* genome and could possibly fulfill similar functions. Three potentially secreted multi-heme c-type cytochromes were related to OmcT (HS1_000545, HS1_000649, HS1_000650), which in *G. sulfurreducens* was suggested to be involved in DIET. Further, seven multi-heme c-type cytochrome encoding genes (HS1_000540 (10 heme), HS1_000543 (12 heme), HS1_000544 (12 heme), HS1_000545 (7 heme), HS1_000548 (7 heme), HS1_000555 (26 heme), HS1_000556 (16 heme)) were located in a large cluster together with other genes, including one encoding an outer-membrane channel cytochrome c (HS1_000541 (1 heme)), related to OmcL of *G. sulfurreducens*, and two encoding lipoproteins. Although the mechanisms of extracellular electron transfer by *Ca.* D. auxilii remain unknown, these cytochromes may be candidates for the extracellular transfer of electrons between pili and outer-membrane and the channeling of electrons into the periplasm via a porin outer-membrane protein. Once transferred to the periplasmic cytochrome pool electrons may be delivered to membrane-bound electron transport complexes via a cytochrome-interacting periplasmic subunit (see above) and subsequently fuel sulfate reduction. *Ca.* D. auxilii could possibly utilize the same redox components to pass electrons between the periplasmic cytochrome pool and cytoplasmic sulfate reduction complexes during DIET-based syntrophic and

hydrogenotrophic growth (Fig. 4). This would allow a rather quick transition between both growth modes and may explain its fast response to hydrogen as alternative substrate. Syntrophic growth via DIET would circumvent hydrogenases; hence during syntrophic growth in AOM *Ca.* D. auxilii would not reduce ferredoxin via electron bifurcation at the MvhADG/HdrABC complex. Under these conditions ferredoxin reduction could be driven by proton translocation at the reverse working Rnf complex (see above).

Furthermore, flagella have previously been reported to be an important feature of syntrophy establishment (Shimoyama *et al.*, 2009). *Ca.* D. auxilii includes an almost complete set for flagella assembly and movement (HS1_000713-HS1_000715, HS1_000723-HS1_000730, HS1_000732-HS1_000750, HS1_000753-HS1_000763). Although not observed during growth in consortia (Wegener *et al.*, 2015) or in the solitary growth mode in the hydrogen enrichment (Fig. 2 D), flagella might be important to initiate the contact between *Ca.* D. auxilii and ANME-1, or other suitable syntrophic partners. It further contains a variety of genes encoding for chemotaxis and response regulation, which possibly play a role in interspecies signaling during syntrophic growth or syntrophy establishment.

Carbon and nitrogen metabolism

Autotrophic carbon fixation in *Ca.* D. auxilii likely proceeds via the reductive tricarboxylic (citric) acid cycle (rTCA) as the complete enzyme set is encoded in its draft genome. In contrast only an incomplete set of genes for carbon fixation via the Wood-Ljundahl pathway (reductive acetyl CoA pathway) was identified, lacking the key enzyme of this pathway, the carbon monoxide dehydrogenase/acetyl CoA synthase. The reductive TCA cycle which forms one molecule acetyl CoA from the fixation of two molecules of CO_2, is a central metabolic pathway in the cell that generates precursors for lipid and protein biosynthesis (Fuchs, 2011). In sulfate reducers this mechanism of carbon fixation was first described in the hydrogenotrophic *Desulfobacter hydrogenophilus* (Schauder *et al.*, 1987). In the *Ca.* D. auxilii genome the key enzymes of the reductive TCA cycle, fumarate reductase (HS1_001279, HS1_001733, HS1_001734, HS1_001735), ferredoxin-dependent 2-oxoglutarate oxidoreductase (HS1_001275-HS1_001277) and ATP citrate lyase (HS1_001265-HS1_001266) are encoded in one cluster together with genes for other enzymes of the cycle (HS1_001263, HS1_001268-HS1_001271, HS1_001275, HS1_001281-HS1_001282). This cluster also comprises genes encoding a heterodisulfide reductase (HdrABC, HS1_001272-HS1_001274), adjacent to the ferredoxin-dependent 2-oxoglutarate oxidoreductase genes. The potential electron bifurcating function of Hdr within the

MvhADG/HdrABC enzyme complex (Buckel and Thauer, 2013) may provide reduced ferredoxin to the 2-oxoglutarate oxidoreductase during hydrogenotrophic growth. As indicative from the draft genome, *Ca.* D. auxilii converts the product of the reductive TCA cycle, acetyl CoA, further to pyruvate in a ferredoxin-dependent reductive carboxylation reaction that leads to the fixation of another molecule of CO_2. Genes encoding the responsible enzyme, pyruvate ferredoxin oxidoreductase (HS1_001566, HS1_001571-HS1_001573), were observed in a cluster with genes for an aldehyde ferredoxin reductase (HS1_001562, HS1_001567) two proteins containing 4Fe-4S ferredoxin (HS1_001563, HS1_001568) and proteins with similarity to HdrA (HS1_001564-HS1_001565), HdrB (HS1_001570) and HdrC (HS1_001569). These proteins could be involved in electron transfer reactions and regeneration of reduced ferredoxin. Genes for further conversion of pyruvate to oxalacetate, either via phosphoenolpyruvate (PEP; PEP synthase, HS1_001176 and PEP carboxylase, HS1_002476-HS1_002477) or directly (pyruvate carboxylase, HS1_000172), were present and link carbon fixation to carbohydrate biosynthesis via gluconeogenesis. Although growth of *Ca.* D. auxilii on acetate was not observed, its genome encodes genes for the conversion of acetate to acetyl CoA by acetyl CoA synthetase (HS1_001676, HS1_001693).

Ammonium is likely to be used as inorganic nitrogen source by *Ca.* D. auxilii. Its genome encodes glutamine synthetase (HS1_000233) for the condensation of ammonium and glutamate to glutamine and glutamate synthase (HS1_001956-HS1_001957) to further convert glutamine and 2-oxoglutarate to yield two glutamate molecules. Genes encoding enzymes to catalyze the formation of ammonium from nitrate, nitrate reductase and nitrite reductase, were not found. Further, genes for a nitrogenase complex were not identified; only two genes for a nitrogen fixation protein (*nifU*, HS1_000655, HS1_001433) were present. This confirms earlier studies which indicated that partner bacteria in AOM consortia do not fix molecular nitrogen but assimilate ammonia (Dekas *et al.*, 2009).

Implications for the lifestyle of *Ca.* D. auxilii in the environment

In solitary growth mode in our enrichment, *Ca.* D. auxilii thrives as an obligatory thermophilic, hydrogenotrophic and autotrophic sulfate reducer. However, in natural hydrothermally heated hydrocarbon-rich sediments as well as in thermophilic methane-amended enrichments, *Ca.* D. auxilii cells generally appear to be associated with ANME-1 (Fig. 1), implying that close proximity is crucial for dual-species syntrophic growth (Holler *et al*., 2011). A tight cell-to-cell association seems characteristic for DIET-performing syntrophic consortia. As previously shown in the *Geobacter* dual-species consortium, the two

partners require direct contact; a partner capable of alternating between hydrogen uptake and DIET would only aggregate during DIET but not during interspecies hydrogen transfer (Summers *et al.*, 2010; Rotaru *et al.*, 2014). Despite *Ca.* D. auxilii's inability to utilize hydrocarbons, highly affiliated 16S rRNA gene sequences were also detected in anaerobic enrichments with butane or propane as sole energy source (Kniemeyer *et al.*, 2007; Adams *et al.*, 2013). Hence, in its natural environment, *Ca.* D. auxilii may not be restricted to TAOM syntrophy, but may act as syntrophic partner to a variety of thermophilic organisms, which lack complete oxidative pathways. Its fast (within a few days) response to hydrogen addition together with its rather small genome size indicates that switching between solitary or consortial growth does not require major transformations in the proteome, but may be mediated by similar redox components and enzyme complexes. In hydrothermal sediments *Ca.* D. auxilii therefore possibly also grows non-syntrophically using naturally abundant hydrogen as the energy source for sulfate reduction. The flexibility to transition between growth strategies might be of selective advantage in dynamic hydrothermal systems and allow for sustained metabolism on changing substrates.

Description of '*Candidatus* Desulfofervidus auxilii' and '*Candidatus* Desulfofervidaceae'

'*Candidatus* Desulfofervidus auxilii' (De.sul.fo.fer'vi.dus, N.L. prefix Desulfo used in taxonomic names for sulfate-reducing bacteria, *fervidus* L. adj. hot, L. n. the hot one, N.L. n. *Desulfofervidus* hot sulfate reducer; au.xi' li.i, L. neut. n. *auxilium* help/support, *auxilii,* L. gen. n. of help/support indicating that the organism is capable of a syntrophic life style).

The bacterium was enriched from a thermophilic anaerobic methane-oxidizing enrichment obtained with hydrothermal sediments of the Guaymas Basin, Gulf of California, Mexico. The bacterium grows chemolithoautotrophically with sulfate and hydrogen in a temperature range between 50 and 70°C, optimal at 60°C. No heterotrophic growth was observed. Syntrophic growth (chemoorganoautotrophic) is observed on methane with thermophilic ANME-1 archaea. Cell morphology is rod shaped with a length of 1.0-2.0 µm and width of 0.5-1.0 µm. The bacterium is proposed to belong to the *Candidatus* Desulfofervidaceae (-*aceae* ending to denote a family), a novel family of sulfate-reducing bacteria tentatively placed in the *Deltaproteobacteria*.

Material and methods

Enrichment and maintenance of *Ca.* D. auxilii

Ca. D. auxilii was obtained from a sediment-free, thermophilic (60°C) AOM enrichment from Guaymas Basin sediments (Gulf of California) (see Holler *et al*., 2011). It has been separated from its methanotrophic partner by dilution-to-extinction series with sulfate and hydrogen as sole energy sources. Dilution-to-extinction series were prepared in 20 ml Hungate tubes filled with 10 ml artificial seawater medium for sulfate-reducing bacteria (Widdel and Bak, 1992). Hungate tubes were supplied with a 250 kPa H_2:CO_2 (80:20) headspace. Dilution series were inoculated with 10% of the anaerobic methanotrophic enrichment and serial dilutions of 1:10 were performed resulting in effective dilutions from 10^2 to 10^{10}. To determine microbial sulfate reduction, sulfide concentration in the medium was repeatedly measured using a colorimetric test (Cord-Ruwisch, 1985). After three months the highest active dilutions were analyzed for the presence of *Ca.* D. auxilii cells. The purest enrichments were maintained by transfer into fresh medium (5-10% culture). The latter procedure was repeated when sulfide concentration exceeded 15 mM.

DNA extraction, 16S rRNA gene amplification and clone library construction

DNA was extracted from 40 ml of the thermophilic AOM enrichment (50 and 60°C) and from 100 ml of *Ca.* D. auxilii culture following the protocol by Zhou and colleagues (1996). For 16S rRNA gene amplification the bacterial specific primer set GM3 and GM4 was employed (Muyzer *et al.*, 1995). The *dsrA* gene, encoding dissimilatory sulfate reductase subunit A, was amplified using the primer set DSR1Fmix (containing DSR1F, DSR1Fa, DSR1Fb, DSR1Fc, DSR1Fd) (Wagner *et al.*, 1998; Loy *et al.*, 2004; Zverlov *et al.*, 2005) and DSR1334R (Santillano *et al.*, 2010). The archaeal primer pair Arch20F (Massana *et al.*, 1997) and Arch958 (DeLong, 1992) was used to identify the archaeal contaminant in the *Ca.* D. auxilii culture. PCR reactions were performed in a 20 µl reaction volume, containing 0.5 µM of each primer, 200 µM of each deoxyribonucleoside triphosphate, 6 µg bovine serum albumin, 1x PCR buffer (5'Prime, Hamburg, Germany), 0.25 U Taq DNA Polymerase (5'Prime) and 1 µl of template (20-30 ng). The cycle conditions were as follows: initial step at 95°C for 5 min; 26 cycles, each at 95°C for 1 min, 46°C (GM3/GM4) or 52°C (DSR1Fmix/DSR1334R) for 1.5 min, and 72 °C for 3 min; and final step at 72°C for 10 min. PCR amplicons from 3 reactions were pooled, purified and concentrated using the QIAquick PCR Purification Kit (Qiagen, Hilden, Germany), gel excised and purified again using the

QIAquick Gel Purification Kit (Qiagen) according to the manufacturer's recommendations. Ligation was carried out with the pGEM-T Easy vector system (Promega, Madison, WI, USA) followed by transformation of *Escherichia coli* One Shot Top10 cells (Invitrogen, Carlsbad, CA, USA) according to the manufacturer's recommendations. Clones were screened using the M13F/R primer pair and a standard PCR procedure. Positive inserts were sequenced using ABI BigDye Terminator chemistry and an ABI377 sequencer (Applied Biosystems, Foster City, CA, USA). The PCR product obtained with the archaeal-specific primer pair was purified and sequenced directly.

Probe design

An oligonucleotide probe specifically targeting *Ca.* D. auxilii, probe HotSeep1_1465 (probe sequence 5'-CCCAAGGUGUGGUCGGCG-3') was designed using the probe design tool in the ARB software package (Ludwig *et al.*, 2004). The oligonucleotide probe (HRP labeled) was synthesized by Biomers (Ulm, Germany). The probe was *in silico* tested for sensitivity (target group hits) and specificity (outgroup hits) with the ARB probe match tool (Quast *et al.*, 2013). Probe HotSeep1_1465 covers sequences currently assigned to the *Ca.* D. auxilii cluster (97% similarity threshold) with the exception of three sequences (NCBI acc. no.'s KJ569680, FR682643, FR682645; compare Tab. S1) and has at least one mismatch to non-target group sequences (sequences less than 97% similar to the *Ca.* D. auxilii cluster). The stringency of the newly designed probe was tested in a CARD-FISH experiment by increasing the formamide concentration in the hybridization buffer from 0% to 70%.

Catalyzed reporter deposition fluorescence *in situ* hybridization

CARD-FISH (catalyzed reporter deposition fluorescence *in situ* hybridization) was applied to detect *Ca.* D. auxilii cells in AOM enrichments and to repeatedly analyze the purity of *Ca.* D. auxilii cultures. Cells for CARD-FISH were fixed in 2% formamide for 2 h at room temperature and filtered onto polycarbonate filters, 0.2 µm pore size (GTTP, Whatman). CARD-FISH was performed following the standard procedure as described previously (Pernthaler and Amann, 2004) with some modifications. In short: filters were embedded in 0.2% low melting agarose prior to the CARD-FISH procedure. Optimized cell wall permeabilization for probe HotSeep-1_1465 was achieved with lysozyme treatment for 7 min at 37°C (10 mg ml^{-1} lysozyme, lyophilized powder (SigmaAldrich) in 0.1 M Tris–HCl, 0.05 M EDTA, pH 8) followed by proteinase K digestion for 2 min at RT (4.5 mU ml^{-1} proteinase K (Merck) in 0.1 M Tris−HCl, 0.05 M EDTA and 0.5 M NaCl, pH 8). Endogenous

peroxidases were inactivated with 0.15% H_2O_2 in methanol (30 min, RT). For hybridization the following oligonucleotide probes were applied with respective formamide concentration (according to original publication or derived from the melting curve for probe HotSeep-1_1465): EUB338I-III, 35%, Arch915, 35%, ANME-1-350, 40%, HotSeep-1_1456, 35%. Catalyzed reporter deposition was performed using tyramides labeled with the fluorochromes Alexa Fluor 594 or Alexa Fluor 488. When performing double hybridizations (e.g. for the AOM consortia) the peroxidase enzymes of the first hybridization were inactivated with 0.3% H_2O_2 in methanol (30 min, RT) prior to the application of the HRP probe in the second hybridization. For archaeal cell wall permeabilization only 7 min lysozyme at 37°C was used as proteinase K treatment resulted in damage of archaeal cells. Hence in dual CARD-FISH experiments targeting HotSeep-1 and *Archaea* permeabilization was restricted to lysozyme treatment resulting in less bright signals in HotSeep-1 cells. Samples were stained with DAPI (4,6-diamidino-2-phenylindole) and visualized using epifluorescence microscopy.

Physiological experiments

To analyze the response of *Ca.* D. auxilii to different substrates and temperatures 1 ml aliquots of cultures pre-grown at 60°C with sulfate, hydrogen and carbon dioxide were inoculated to 20 ml Hungate tubes filled with 10 ml artificial seawater medium (28 mM sulfate). The medium and/or headspace composition was modified with respect to electron donor, electron acceptor/sulfur compound and carbon source to be tested (see below). Sulfate-reducing activity was determined by measuring the sulfide concentrations in the medium using the copper-sulfide formation assay (Cord-Ruwisch, 1985).

To test the temperature range and optimum of sulfate-reducing activity, cultures were incubated between 20°C and 80°C (9 temperatures: 20°C, 27°C, 37°C, 50°C, 55°C, 60°C, 65°C, 70°C and 80°C; with triplicates for each temperature). The incubations were provided with 28 mM sulfate and a 250 kPa H_2:CO_2 (80:20) headspace. Sulfide production at each temperature was determined over a period of three weeks.

To test an influence of organic substrates (carbon sources) cultures were incubated with 28 mM sulfate and 150 kPa H_2:CO_2 (80:20) plus the potential substrate: acetate, formate, ethanol, lactate, benzoate, dicarboxylic acid mixture (succinate, fumarate, malate), fructose, methanol, pyruvate, methyl sulfide; all 2 mM, yeast extract and peptone; both 0.01% (w/v), carbon monoxide, methyl sulfide; both 10 kPa or methane; 150 kPa. CO_2 was present as additional carbon source in all incubations. Control experiments were performed under

standard conditions with CO_2 as sole carbon source. All substrates were tested in duplicates and incubation was performed at 60°C. The sulfide production was determined over a period of three weeks.

To test activity of *Ca.* D. auxilii on alternative electron donors substrates were added to incubations containing sulfate (28 mM) and a N_2:CO_2 (90:10) headspace, except gaseous electron donors (see below). Acetate, formate, ethanol, lactate, benzoate, dicarboxylic acid mixture (succinate, fumarate, malate), fructose, methanol, pyruvate were supplied in concentration of 10 mM, yeast extract and peptone as 0.1% (w/v). The following gaseous substrates were tested (% atmosphere added): methyl sulfide (10%), carbon monoxide (10%), methane (90%), butane (90%) and propane (90%). Control experiments were performed under standard conditions with hydrogen as sole electron donor (250 kPa H_2:CO_2 (80:20)). All substrates were tested in duplicates and incubation was performed at 60°C with sulfide production measured over three weeks. To test for fermentation of organic carbon sources the headspace was tested for hydrogen production after three weeks of incubation by gas chromatography coupled to mercury reduction detection (Shimadzu).

The capability to utilize alternative sulfur compounds as electron acceptors or to disproportionate was tested in sulfate-free incubations supplemented with either sulfite (0.5 mM), thiosulfate (5 mM), sulfate (10 mM), elemental sulfur and colloidal sulfur. In disproportionation experiments the headspace contained 250 kPa N_2:CO_2 (80:20) while in experiments testing for the capability of reduction hydrogen was supplied as electron donor (250 kPa H_2:CO_2 (80:20)). Sulfide production was measured over three weeks.

Growth characteristics were determined from replicate cultures (7.5% inoculum) incubated in 256 ml bottles containing 150 ml artificial seawater medium and a H_2:CO_2 headspace. To measure inorganic carbon fixation in a ^{14}C-DIC radiotracer assay replicates (3 of 6 cultures) were spiked with ^{14}C-DIC (~5.4 kBq). Controls were supplied with a N_2:CO_2 headspace (80:20; 2 replicates, 1 ^{14}C spiked, 1 non-spiked). To provide an abiotic control a sterilized (121°C, 25 min) culture aliquot served as inoculum (2 replicates, 1 ^{14}C spiked, 1 non-spiked). All incubations were performed at 60°C. Incubations were sampled repeatedly for sulfide (copper sulfide formation assay) and sulfate (ion chromatography) concentrations, for DIC concentrations, for ^{14}C-tracer content and for cell counts over a period of 5 weeks. To measure carbon fixation aliquots of spiked cultures (3 to 5 ml volume) were blotted on filters (0.2 µm, GSWP). Inorganic carbon was removed via exposure to HCl atmosphere and fixed radiocarbon was determined by scintillation counting. The total carbon fixation was calculated as ^{14}C uptake into particulate organic carbon multiplied by total DIC

[^{14}C-POC (kBq $ml_{culture}^{-1}$) / ^{14}C-total (kBq $ml_{culture}^{-1}$) × DIC (mmol $ml_{culture}^{-1}$)]. Cell numbers were determined from non-labeled replicates by counting DAPI-stained cells to obtain total cell numbers and specific CARD-FISH-stained cells to determine the fraction of *Ca.* D. auxilii cells.

Scanning electron microscopy

Culture aliquots of *Ca.* D. auxilii were blotted onto gold/palladium sputtered polylysine coated glass slides and single TAOM aggregates were picked from the enrichment culture. Samples were dehydrated in an ethanol series, dried and mounted on electrically conductive, adhesive tags (Leit-Tab; Plano GmbH, Wetzlar, Germany). Specimens were investigated with a FEI environmental field emission SEM Quanta 250 FEG (FEI, Eindhoven, Netherlands) at electron energy of 2 keV using the Everhart-Thornley secondary electron detector (ETD).

Atomic force microscopy

Samples were retrieved from the supernatant of a TAOM enrichment, fixed in 20 g l^{-1} formaldehyde for 30 min at RT and directly filtered onto 0.2 µm pore size GTTP polycarbonate filter, 25 mm diameter (Millipore, Germany) sputtered with a gold palladium (20%/80%) layer (~40 nm). Filters were stored at −20°C or directly analyzed using an atomic force microscope (AFM) (NT-MDT Co., Russia) in semi-contact mode with a gold coated silicon cantilever (NSG10). Images were processed using NT-MDT Image Analysing 3.5. Image color and contrast was optimized using conventional image processing software (Adobe Photoshop CS5, version 12.0.4).

Metagenome sequencing and assembly

Genomic DNA was extracted according to the protocol by Zhou and colleagues (1996) from a cell pellet of 100 ml *Ca.* D. auxilii culture (harvested by centrifugation at 5000×g for 15 min, 4°C). 2 µg of high molecular weight DNA was subjected to fragment library construction using the Nextera Mate Pair Library Preparation Kit, following the Gel-Plus protocol of the manufacturer's user guide. DNA fragments of approx. 5-8 kb were extracted from a preparative gel prior to circularization. The mate pair library was sequenced on a MiSeq instrument (MiSeq, Illumina) in a 2x300 bases paired end run.

To estimate the taxonomic composition of the metagenomic dataset raw reads were mapped to the SILVA database (release 119) (Quast *et al.*, 2013) using bbmap v.35 implemented in phyloflash v.1.5 with minimum identity of 95%. For quantification only

unambiguously mapped reads were counted. Nearly full length 16S rRNA gene sequences assembled by phyloflash were classified as HotSeep-1 (99.4% identity, 1530 bp, coverage 107.5) and *Archaeoglobus fulgidus* (98% identity, 1035 bp, coverage 2.5).

Quality of raw read data was assessed using FastQC and raw reads were processed, including adapter clipping, trimming of bases with quality below Q30 and removal of reads shorter 50 bp using bbduk2 (bbmap v.35). *De novo* assembly was performed with quality controlled mate pair reads using the SPAdes genome assembler v. 3.5.0. (Bankevich *et al.*, 2012) with default values for k and the option for high quality mate pairs (--hqmp). In total 2,577,039 bp were assembled into 57 contigs >1000 kb, representing 31 scaffolds (N50 2,540,211 bp). The largest, final scaffold of 2,540,211 bp was used for all further analysis. Small and low coverage scaffolds (on average <5 kb length and <2x coverage) were excluded from the analysis.

Completeness of the draft genome assembly was evaluated with checkM (Parks *et al.*, 2015) using the lineage-specific workflow. In addition completeness was also estimated with the AMPHORA2 package using the 31 bacterial marker genes (Wu and Scott, 2012).

ORF prediction and annotation

Gene prediction was carried out using the Glimmer3 software package (Delcher *et al*., 2007). Ribosomal RNA genes were detected by using the RNAmmer 1.2 software (Lagesen *et al*., 2007) and transfer RNAs by tRNAscan-SE (Lowe and Eddy, 1997). Batch cluster analysis was performed by using the GenDB (version 2.2) system (Meyer *et al*., 2003). Annotation and data mining were done with the tool JCoast, version 1.7 (Richter *et al*., 2008), using observations from similarity searches against several sequence databases (NCBI nr, Swiss-Prot, KEGG-Genes, genomesDB) and to the protein family databases InterPro (Mulder *et al*., 2005) and Pfam (Bateman *et al*., 2004) for each coding region. Predicted protein coding sequences were automatically annotated by the software tool MicHanThi (Quast, 2006). Briefly, the MicHanThi software infers gene functions based on similarity searches against the NCBI nr (including Swiss-Prot) and InterPro databases using fuzzy logic. The annotation of proteins highlighted within the scope of this study was subject of manual inspection. For all observations regarding putative protein functions, an expectation (E)-value cut-off of 10^{-5} was applied. For proteins of interest the subcellular localization was predicted by PSORTb v.3.0.2. (Yu *et al*., 2010) and transmembrane helices were identified by TMHMM scan v.2.0 (Krogh *et al*., 2001). Further for selected proteins signal peptides and alternative secretion (without signal peptide) were predicted with SignalP 4.1 (Petersen *et al*., 2011) and

SecretomP 2.0 (Bendtsen *et al*., 2005), respectively. Potential c-type cytochromes and type IV pili were identified by protein domain models related to cytochrome c or type IV pili, respectively. For cytochromes the number of hemes was derived from the number of detected CXXCH motifs, which are indicative for heme-binding sites. An overview of the observations made for selected proteins including the ones discussed is provided as Supplementary Information Annotation Tables.

Comparison of the shared gene content by reciprocal best matches (RBMs)

Determination of the shared orthologous gene content has been performed by a blast 'all-versus-all' search between selected organisms (*Deltaproteobacteria* and *Thermodesulfobacteria* and *Nitrospira*). Reciprocal best matches were counted by a blast result with E-values of $<10^{-5}$ each and a subject coverage of over 65%.

Taxonomic distributions

To analyze the *Ca.* D. auxilii genome for the taxonomic distribution of best matches the genome was compared against the genomesDB database (Richter *et al.*, 2008), an in house protein database based on the NCBI Reference Sequence database (RefSeq) containing protein sequences from all sequenced bacterial and archaeal genomes. Each predicted protein of *Ca.* D. auxilii was searched against the genomesDB and the best match was recorded on phyla and species level. Only those proteins with significant hits (E-value $>10^{-5}$) were considered.

Functional classification with KEGG

For metabolic pathway identification, genes were searched for similarity against the KEGG database. A match was counted if the similarity search resulted in an E-value below 10^{-5}. All occurring KO (KEGG Orthology) numbers were mapped against KEGG pathway functional hierarchies and statistically analyzed.

Functional classification with COG

All predicted ORFs were also searched for similarity against the COGs database (Tatusov *et al.*, 2003). A match was counted if the similarity search resulted in an E-value below 10^{-5}.

16S rRNA gene sequence analysis

The genomic 16S rRNA gene sequence of *Ca.* D. auxilii was compared to the NCBI database of reference sequences (rna-RefSeq, containing curated, non-redundant sequences; 17,765 database entries, 15.10.2015) and the NCBI nucleotide collection database (nt/nr, including environmental sequences; 28,723,871 database entries, 27.10.2014) using NCBI blastn (2.2.30) (Zhang *et al.*, 2000) under default settings. Phylogenetic analysis was performed using the ARB software package (Ludwig *et al.*, 2004) and the SILVA database (release 119) (Quast *et al.*, 2013). Sequence selection for analysis was based on the initial blast hits to *Ca.* D. auxilii (see above); the 100 top scoring rna-RefSeq database entries (query coverage >85%) were included and used as references to guide further sequence selection from related classes/phyla. In addition, sequences in the nt/nr database with similarity >90% to *Ca.* D. auxilii as well as sequences obtained from the thermophilic Guaymas Basin AOM enrichments and *Ca.* D. auxilii culture were considered. The *Ca.* D. auxilii sequence cluster was defined based on 97.5% sequence similarity. Similarity was determined from a similarity matrix (neighbour joining algorithm) considering nearly full length sequences (>1300 bp). For phylogenetic reconstruction 654 nearly full length sequences (>1300 bp) covering several bacterial classes and phyla including *Deltaproteobacteria*, *Nitrospira*, *Thermodesulfobacteria* were aligned using the SINA aligner implemented in ARB (Pruesse *et al.*, 2012) and the alignment was manually curated. Distance matrix trees were calculated with the neighbour joining algorithm (Saitou and Nei, 1987) and Jukes Cantor correction. Maximum likelihood based trees were calculated using RAxML (version 8.0.26) (Stamatakis, 2006) with GTRGAMMA as nucleotide substitution model and PhyML based trees with GTR as nucleotide substitution model. A base frequency filter was employed for each tree calculation to consider only alignment regions which are 50% conserved. 1000 bootstrap replicates were used to estimate branch support.

23S rRNA gene sequence analysis

Phylogenetic analysis of the genomic 23S rRNA of *Ca.* D. auxilii was performed with the SILVA LSU reference database (release 119) (Quast *et al.*, 2013) and the ARB software package (Pruesse *et al.*, 2012). The sequence alignment was manually curated and phylogenetic trees were calculated with the maximum likelihood algorithm using RAxML (version 8.0.26) (Stamatakis, 2006) with GTRGAMMA as nucleotide substitution model or PhyML with GTR as nucleotide substitution model. To include only conserved alignment

regions a 50% base frequency filter was employed. Branch support was estimated by 100 bootstrap replicates.

DsrA sequence analysis

For functional gene based phylogenetic analysis the *dsrA* gene sequence of *Ca.* D. auxilii was obtained from its genome sequence. Additional *dsrA* gene sequences were retrieved from the thermophilic AOM enrichments (50°C and 60°C) and the *Ca.* D. auxilii culture. Related sequences were obtained from the NCBI nr database using a blastp search of the genomic DsrA amino acid sequence of *Ca.* D. auxilii. For phylogenetic analyses sequences were added to the *dsrAB*/DsrAB database constructed by Müller and colleagues (2014) and aligned using the ARB software package (Ludwig *et al.*, 2004). A phylogenetic tree was calculated from 256 aligned amino acid sequences with the maximum likelihood algorithm (RAxML version 8.2.4.) using the rate distribution model PROTGAMMA and LG as substitution matrix. The best suited substitution model was determined by RAxML using the –m PROTGAMMAAUTO option. Employing a 30% base frequency filter to exclude highly variable regions a total of 260 alignment positions were included in the phylogenetic reconstruction. Branch support was estimated from 100 bootstrap replicates.

Single copy gene analysis

Single copy gene analysis of *Ca.* D. auxilii was carried out with the AMPHORA2 software package which uses a set of 31 universal bacterial single copy genes as marker (Wu and Scott, 2012). Single copy genes were identified from the nucleotide sequence, aligned with references and assigned to phylotypes by maximum likelihood algorithm. To reconstruct the phylogenetic affiliation of *Ca.* D. auxilii on the level of multiple single copy genes the AMPHORA2 MarkerScanner and MarkerAlignTrim tools were used to identify, align and trim single copy genes present in *Ca.* D. auxilii and selected reference genomes. As references genomes of organisms that had been used in 16S rRNA gene based phylogenetic analysis (if available) and additionally those that were of interest based on the results from comparative genomic analysis were included. A marker gene was excluded if not present in all analyzed genomes resulting in ubiquitous 19 single copy genes (Tab. S3). The trimmed protein alignments of each marker were concatenated using SequenceMatrix (Vaidya *et al.*, 2011) and phylogenetic trees were calculated from the multi-protein alignment (2857 positions) using the maximum likelihood algorithm (RAxML version 8.2.4.) applying PROTGAMMA and LG as substitution model and 100 bootstrap replicates to estimate branch support (Stamatakis,

2006). The best suitable substitution model for the concatenated multi gene alignment was selected by using the –m PROTGAMMAAUTO option provided by RAxML. The iTOL software (Letunic and Bork, 2011) was used for tree visualization.

Nucleotide sequence accession numbers

The Whole Genome Shotgun project has been deposited in INSDC (DDBJ/EBI-ENA/GenBank) under the BioProject PRJNA276404. The sequence associated contextual (meta)data are MIxS (Yilmaz *et al.*, 2011) compliant. Representative *dsrA* sequences are deposited in INSDC (DDBJ/EBI-ENA/GenBank) under accession numbers KT819174-KT819177.

Acknowledgements

We thank Susanne Menger and Ines Kattelmann for technical assistance and Ulrich Fischer for valuable discussion. We are grateful to Hans G. Trüper, University of Bonn, Germany, for his precious help with the etymology. Furthermore we thank chief scientist Andreas Teske and the RV ATLANTIS and ALVIN team of cruise AT15-56 in 2009 for providing the initial sediment material. The project was funded by the DFG Leibniz program to A.B., the DCO Deep Life program to G.W., and by the DFG excellence cluster MARUM, Center of Marine Environmental Sciences, Bremen.

References

Adams MM, Hoarfrost AL, Bose A, Joye SB, Girguis PR. (2013). Anaerobic oxidation of short-chain alkanes in hydrothermal sediments: potential influences on sulfur cycling and microbial diversity. *Front Microbiol* **4**: 110.

Alazard D, Dukan S, Urios A, Verhe F, Bouabida N, Morel F, *et al*. (2003). *Desulfovibrio hydrothermalis* sp. nov., a novel sulfate-reducing bacterium isolated from hydrothermal vents. *Int J Syst Evol Microbiol* **53**: 173–178.

Anderson I, Saunders E, Lapidus A, Nolan M, Lucas S, Tice H, *et al.* (2004). Genome sequence of the thermophilic sulfate-reducing ocean bacterium *Thermodesulfatator indicus* type strain (CIR29812^{T}). *Stand Genomic Sci* **6**: 155–164.

Audiffrin C, Cayol J, Joulian C, Casalot L, Thomas P, Garcia J, *et al.* (2003). *Desulfonauticus submarinus* gen. nov., sp. nov., a novel sulfate-reducing bacterium isolated from a deep-sea hydrothermal vent. *Int J Syst Evol Microbiol* **53**: 1585–1590.

Bankevich A, Nurk S, Antipov D, Gurevich AA, Dvorkin M, Kulikov AS, *et al.* (2012). SPAdes: a new genome assembly algorithm and its applications to single-cell sequencing. *J Comput Biol* **19**: 455–477.

Bateman A, Coin L, Durbin R, Finn RD, Hollich V, Griffiths-Jones S, *et al.* (2004). The Pfam protein families database. *Nucleic Acids Res* **32**: D138–D141.

Bendtsen JD, Kiemer L, Fausbøll A, Brunak S. (2005). Non-classical protein secretion in bacteria. *BMC Microbiol* **13**: 1–13.

Biddle JF, Cardman Z, Mendlovitz H, Albert DB, Lloyd KG, Boetius A, *et al.* (2011). Anaerobic oxidation of methane at different temperature regimes in Guaymas Basin hydrothermal sediments. *ISME J* **6**: 1018–1031.

Biegel E, Müller V. (2010). Bacterial Na^{+}-translocating ferredoxin:NAD^{+} oxidoreductase. *Proc Natl Acad Sci USA* **107**: 18138–13142.

Boetius A, Ravenschlag K, Schubert CJ, Rickert D, Widdel F, Gieseke A, *et al*. (2000). A marine microbial consortium apparently mediating anaerobic oxidation of methane. Nature **407**: 623–626.

Boetius A, Wenzhöfer F. (2013). Seafloor oxygen consumption fuelled by methane from cold seeps. *Nat Geosci* **6**: 725–734.

Brandis A, Thauer RK. (1981). Growth of *Desulfovibrio* species on hydrogen and sulphate as sole energy source. *J Gen Microbiol* **126**: 249–252.

Brysch K, Schneider C, Fuchs G, Widdel F. (1987). Lithoautotrophic growth of sulfate-reducing bacteria, and description of *Desulfobacterium autotrophicum* gen. nov., sp. nov. *Arch Microbiol* **148**: 264–274.

Buckel W, Thauer RK. (2013). Energy conservation via electron bifurcating ferredoxin reduction and proton/$Na^{(+)}$ translocating ferredoxin oxidation. *Biochim Biophys Acta* **1827**: 94–113.

Cord-Ruwisch R. (1985). A quick method for the determination of dissolved and precipitated sulfides in cultures of sulfate-reducing bacteria. *J Microbiol Meth* **4**: 33–36.

Cypionka H, Pfennig N. (1986). Growth yields of *Desulfotomaculum orientis* with hydrogen in chemostat culture. *Arch Microbiol* **143**: 396–399.

Dekas AE, Poretsky RS, Orphan VJ. (2009). Deep-sea archaea fix and share nitrogen in methane-consuming microbial consortia. *Science* **326**: 422–426.

Delcher AL, Bratke KA, Powers EC, Salzberg SL. (2007). Identifying bacterial genes and endosymbiont DNA with Glimmer. *Bioinformatics* **23**: 673–679.

DeLong EF. (1992). Archaea in coastal marine environments. *Proc Natl Acad Sci USA* **89**: 5685–5689.

Elkins JG, Hamilton-Brehm SD, Lucas S, Han J, Lapidus A, Cheng J, *et al.* (2013). Complete genome sequence of the hyperthermophilic sulfate-reducing bacterium *Thermodesulfobacterium geofontis* $OPF15^{T}$. *Genome Announc* **1**: e00162–13.

Fuchs G. (2011). Alternative pathways of carbon dioxide fixation: insights into the early evolution of life? *Annu Rev Microbiol* **65**: 631–658.

Grein F, Ramos AR, Venceslau SS, Pereira IAC. (2013). Unifying concepts in anaerobic respiration: insights from dissimilatory sulfur metabolism. *Biochim Biophys Acta* **1827**: 145–160.

Hallam SJ, Putnam N, Preston CM, Detter JC, Rokhsar D, Richardson PM, *et al*. (2004). Reverse methanogenesis: testing the hypothesis with environmental genomics. *Science* **305**: 1457–1462.

Hoehler TM, Alperin MJ, Albert DB, Martens S, Field A. (1994). Field and laboratory studies of methane oxidation in an anoxic marine sediment: evidence for a methanogen-sulfate reducer consortium. *Global Biogeochem Cycles* **8**: 451–463.

Holler T, Widdel F, Knittel K, Amann R, Kellermann MY, Hinrichs K-U, *et al.* (2011). Thermophilic anaerobic oxidation of methane by marine microbial consortia. *ISME J* **5**: 1946–1956.

Huntemann M, Lu M, Nolan M, Lapidus A, Lucas S, Deshpande S, *et al.* (2011). Complete genome sequence of the thermophilic sulfur-reducer *Hippea maritima* type strain (MH_2^T). *Stand Genomic Sci* **4**: 303–311.

Jørgensen BB, Zawacki LX, Jannasch HW. (1990). Thermophilic bacterial sulfate reduction in deep-sea sediments at the Guaymas Basin hydrothermal vent site (Gulf of California). *Deep-Sea Res* **37**: 695–710.

Kellermann MY, Wegener G, Elvert M, Yoshinaga MY, Lin Y-S, Holler T, *et al.* (2012). Autotrophy as a predominant mode of carbon fixation in anaerobic methane-oxidizing microbial communities. *Proc Natl Acad Sci USA* **109**: 19321–19326.

Klein M, Friedrich M, Roger AJ, Hugenholtz P, Fishbain S, Abicht H, *et al.* (2001). Multiple lateral transfers of dissimilatory sulfite reductase genes between major lineages of sulfate-reducing prokaryotes. *J Bacteriol* **183**: 6028–6035.

Kleindienst S, Ramette A, Amann R, Knittel K. (2012). Distribution and *in situ* abundance of sulfate-reducing bacteria in diverse marine hydrocarbon seep sediments. *Environ Microbiol* **14**: 2689–2710.

Kniemeyer O, Musat F, Sievert SM, Knittel K, Wilkes H, Blumenberg M, *et al.* (2007). Anaerobic oxidation of short-chain hydrocarbons by marine sulphate-reducing bacteria. *Nature* **449**: 6–10.

Knittel K, Lemke A, Lochte K. (2003). Activity, distribution, and diversity of sulfate reducers and other bacteria in sediments above gas hydrate (Cascadia Margin, Oregon). *Geomicrobiol J* **20**: 269–294.

Knittel K, Boetius A. (2009). Anaerobic oxidation of methan: progress with an unknown process. *Annu Rev Microbiol* **6**: 311–334.

Krogh A, Larsson B, von Heijne G, Sonnhammer EL. (2001). Predicting transmembrane protein topology with a hidden markov model: application to complete genomes. *J Mol Biol* **305**: 567–580.

Lagesen K, Hallin P, Rødland EA, Stærfeldt H, Rognes T, Ussery DW. (2007). RNAmmer: consistent and rapid annotation of ribosomal RNA genes. *Nucleic Acids Res* **35**: 3100–3108.

Lang JM, Darling AE, Eisen JA. (2013). Phylogeny of bacterial and archaeal genomes using conserved genes: supertrees and supermatrices. *PLoS One* **8**: e62510.

Letunic I, Bork P. (2011). Interactive Tree Of Life v2: online annotation and display of phylogenetic trees made easy. *Nucleic Acids Res* **39**: 1–4.

Liu X, Tremblay P, Malvankar NS, Nevin KP, Lovley DR. (2014). A *Geobacter sulfurreducens* strain expressing *Pseudomonas aeruginosa* type IV pili localizes OmcS on pili but is deficient in Fe(III) oxide reduction and current production. *Appl Environ Microbiol* **80**: 1219–1224.

Lowe TM, Eddy SR. (1997). tRNAscan-SE: a program for improved detection of transfer RNA genes in genomic sequence. *Nucleic Acids Res* **25**: 955–964.

Loy A, Küsel K, Lehner A, Harold L, Wagner M, Ku K, *et al.* (2004). Microarray and functional gene analyses of sulfate-reducing prokaryotes in low-sulfate, acidic fens reveal cooccurrence of recognized genera and novel lineages. *Appl Environ Microbiol* **70**: 6998–7009.

Ludwig W, Strunk O, Westram R, Richter L, Meier H, Buchner A, *et al.* (2004). ARB: a software environment for sequence data. *Nucleic Acids Res* **32**: 1363–1371.

Malvankar NS, Yalcin SE, Tuominen MT, Lovley DR. (2014). Visualization of charge propagation along individual pili proteins using ambient electrostatic force microscopy. *Nat Nanotechnol* **9**: 1012–1017.

Malvankar NS, Vargas M, Nevin K, Tremblay P-L, Evans-Lutterodt K, Nykypanchuk D, *et al*. (2015) Structural basis for metallic-like conductivity in microbial nanowires. *mBio* **6**: e00084−15.

Massana R, Murray AE, Preston CM, Delong EF. (1997). Vertical distribution and phylogenetic characterization of marine planktonic *Archaea* in the Santa Barbara Channel. *Appl Environ Microbiol* **63**: 50–56.

Matias PM, Pereira IAC, Soares CM, Carrondo MA. (2005). Sulphate respiration from hydrogen in *Desulfovibrio* bacteria: a structural biology overview. *Prog Biophys Mol Biol* **89**: 292–329.

McGlynn SE, Chadwick GL, Kempes CP, Orphan VJ. (2015). Single cell activity reveals direct electron transfer in methanotrophic consortia. *Nature* **526**: 531–535.

McInerney MJ, Rohlin L, Mouttaki H, Kim U, Krupp RS, Rios-Hernandez L, *et al.* (2007). The genome of *Syntrophus aciditrophicus*: life at the thermodynamic limit of microbial growth. *Proc Natl Acad Sci USA* **104**: 7600–7605.

McInerney MJ, Sieber JR, Gunsalus RP. (2009). Syntrophy in anaerobic global carbon cycles. *Curr Opin Biotechnol* **20**: 623–632.

Meyer F, Goesmann A, McHardy AC, Bartels D, Bekel T, Clausen J, *et al.* (2003). GenDB-an open source genome annotation system for prokaryote genomes. *Nucleic Acids Res* **31**: 2187–2195.

Michaelis W, Seifert R, Nauhaus K, Treude T, Thiel V, Blumenberg M, *et al.* (2002). Microbial reefs in the Black Sea fueled by anaerobic oxidation of methane. *Science* **297**: 1013–1015.

Milucka J, Ferdelman TG, Polerecky L, Franzke D, Wegener G, Schmid M, *et al.* (2012). Zero-valent sulphur is a key intermediate in marine methane oxidation. *Nature* **491**: 541–546.

Milucka J, Widdel F, Shima S. (2013). Immunological detection of enzymes for sulfate reduction in anaerobic methane-oxidizing consortia. *Environ Microbiol* **15**: 1561–1571.

Moran JJ, Beal EJ, Vrentas JM, Orphan VJ, Freeman KH, House CH. (2008). Methyl sulfides as intermediates in the anaerobic oxidation of methane. *Environ Microbiol* **10**: 162–173.

Moussard H. (2004). *Thermodesulfatator indicus* gen. nov., sp. nov., a novel thermophilic chemolithoautotrophic sulfate-reducing bacterium isolated from the Central Indian Ridge. *Int J Syst Evol Microbiol* **54**: 227–233.

Mulder NJ, Apweiler R, Attwood TK, Bairoch A, Bateman A, Binns D, *et al.* (2005). InterPro, progress and status in 2005. *Nucleic Acids Res* **33**: 201–205.

Müller AL, Kjeldsen KU, Rattei T, Pester M, Loy A. (2014). Phylogenetic and environmental diversity of DsrAB-type dissimilatory (bi)sulfite reductases. *Int J Syst Evol Microbiol* **9**: 1152–1165.

Muyzer G, Teske A, Wirsen CO. (1995). Phylogenetic relationships of *Thiomicrospira* species and their identification in deep-sea hydrothermal vent samples by denaturing gradient gel electrophoresis of 16S rDNA fragments. *Arch Microbiol* **164**: 165–172.

Niemann H, Lösekann T, de Beer D, Elvert M, Nadalig T, Knittel K, *et al.* (2006). Novel microbial communities of the Haakon Mosby mud volcano and their role as a methane sink. *Nature* **443**: 854–858.

Orphan VJ, Hinrichs K-U, Ussler W III, Paull CK, Taylor LT, Sylva SP, *et al.* (2001a). Comparative analysis of methane-oxidizing archaea and sulfate-reducing bacteria in anoxic marine sediments. *Appl Environ Microbiol* **67**: 1922–1934.

Orphan VJ, House CH, Hinrichs K-U, McKeegan KD, DeLong EF. (2001b). Methane-consuming archaea revealed by directly coupled isotopic and phylogenetic analysis. *Science* **293**: 484–487.

Parks DH, Imelfort M, Skennerton CT, Hugenholtz P, Tyson GW, Centre A, *et al.* (2015). CheckM: assessing the quality of microbial genomes recoverd from isolates, single cells, and metagenomes. *Genome Res* **25**: 1043−1055.

Pereira IAC, Ramos AR, Grein F, Marques MC, da Silva SM, Venceslau SS. (2011). A comparative genomic analysis of energy metabolism in sulfate reducing bacteria and archaea. *Front Microbiol* **2**: 69.

Pernthaler A, Amann R. (2004). Simultaneous fluorescence *in situ* hybridization of mRNA and rRNA in environmental bacteria. *Appl Environ Microbiol* **70**: 5426–5433.

Petersen TN, Brunak S, von Heijne G, Nielsen H. (2011). SignalP 4.0: discriminating signal peptides from transmembrane regions. *Nat Methods* **8**: 785–786.

Pires RH, Lourenço AI, Morais F, Teixeira M, Xavier AV, Saraiva LM, *et al.* (2003). A novel membrane-bound respiratory complex from *Desulfovibrio desulfuricans* ATCC 27774. *Biochim Biophys Acta* **1605**: 67–82.

Pruesse E, Peplies J, Glöckner FO. (2012). SINA: accurate high-throughput multiple sequence alignment of ribosomal RNA genes. *Bioinformatics* **28**: 1823–1829.

Quast C. (2006). MicHanThi - design and implementation of a system for the prediction of gene functions in genome annotation projects. Diploma Thesis. University of Bremen. Germany.

Quast C, Pruesse E, Yilmaz P, Gerken J, Schweer T, Glöckner FO, *et al.* (2013). The SILVA ribosomal RNA gene database project: improved data processing and web-based tools. *Nucleic Acids Res* **41**: 590–596.

Rabus R, Hansen TA, Widdel F. (2006). Dissimilatory sulfate- and sulfur-reducing prokaryotes. In: *The Prokaryotes*. Dworkin M, Falkow S, Rosenberg E, Schleifer K-H, Stackebrandt E (eds). New York: Springer, pp 659–768.

Ramos AR, Keller KL, Wall JD, Pereira IAC. (2012). The membrane QmoABC complex interacts directly with the dissimilatory adenosine 5'-phosphosulfate reductase in sulfate reducing bacteria. *Front Microbiol* **3**: 137.

Richter M, Lombardot T, Kostadinov I, Kottmann R, Duhaime MB, Peplies J, *et al.* (2008). JCoast - A biologist-centric software tool for data mining and comparison of prokaryotic (meta)genomes. *BMC Bioinformatics* **9**: 177.

Rotaru A, Malla P, Liu F. (2014). Direct interspecies electron transfer between *Geobacter metallireducens* and *Methanosarcina barkeri*. *Appl Environ Microbiol* **80**: 4599–4605.

Ruff SE, Biddle JF, Teske AP, Knittel K, Boetius A, Ramette A. (2015). Global dispersion and local diversification of the methane seep microbiome. *Proc Natl Acad Sci USA*. **112**: 4015–4020.

Saitou N, Nei M. (1987). The neighbor-joining method: a new method for reconstructing phylogenetic trees. *Mol Biol Evol* **4**: 406–425.

Santillano D, Boetius A, Ramette A. (2010). Improved *dsrA*-based terminal restriction fragment length polymorphism analysis of sulfate-reducing bacteria. *Appl Environ Microbiol* **76**: 5306–5311.

Schauder R, Widdel F, Fuchs G. (1987). Carbon assimilation pathways in sulfate-reducing bacteria II. Enzymes of a reductive citric acid cycle in the autotrophic *Desulfobacter hydrgenophilus*. *Arch Microbiol* **3**: 218–225.

Schmehl M, Jahn A, Meyer zu Vilsendorf A, Hennecke S, Masepohl B, Schuppler M, *et al.* (1993). Identification of a new class of nitrogen fixation genes in *Rhodobacter capsulatus*: a putative membrane complex involved in electron transport to nitrogenase. *Mol Gen Genet* **241**: 602–615.

Shimoyama T, Kato S, Ishii S, Watanabe K. (2009). Flagellum mediates symbiosis. *Science* **323**: 1574.

Sieber JR, McInerney MJ, Gunsalus RP. (2012). Genomic insights into syntrophy: the paradigm for anaerobic metabolic cooperation. *Annu Rev Microbiol* **66**: 429–452.

Stamatakis A. (2006). RAxML-VI-HPC: maximum likelihood-based phylogenetic analyses with thousands of taxa and mixed models. *Bioinformatics* **22**: 2688–2690.

Strittmatter AW, Liesegang H, Rabus R, Decker I, Amann J, Andres S, *et al.* (2009). Genome sequence of *Desulfobacterium autotrophicum* HRM2, a marine sulfate reducer oxidizing organic carbon completely to carbon dioxide. *Environ Microbiol* **11**: 1038–1055.

Summers ZM, Fogarty HE, Leang C, Franks AE, Malvankar NS, Lovley DR. (2010). Direct exchange of electrons within aggregates of an evolved syntrophic coculture of anaerobic bacteria. *Science* **330**: 1413–1415.

Tatusov RL, Fedorova ND, Jackson JD, Jacobs AR, Kiryutin B, Koonin E V, *et al.* (2003). The COG database: an updated version includes eukaryotes. *BMC Bioinformatics* **14**: 1–14.

Teske A, Hinrichs K-U, Edgcomb V, Gomez DV, Kysela D, Sylva SP, *et al.* (2002). Microbial diversity of hydrothermal sediments in the Guaymas Basin: evidence for anaerobic methanotrophic communities. *Appl Environ Microbiol* **68**: 1994–2007.

Thauer RK, Kaster A-K, Seedorf H, Buckel W, Hedderich R. (2008). Methanogenic archaea: ecologically relevant differences in energy conservation. *Nat Rev Microbiol* **6**: 579–591.

Vaidya G, Lohman DJ, Meier R. (2011). SequenceMatrix: concatenation software for the fast assembly of multi-gene datasets with character set and codon information. *Cladistics* **27**: 171–180.

Venceslau SS, Lino RR, Pereira IAC. (2010). The Qrc membrane complex, related to the alternative complex III, is a menaquinone reductase involved in sulfate respiration. *J Biol Chem* **285**: 22774–22783.

Venceslau SS, Stockdreher Y, Dahl C, Pereira IAC. (2014). The 'bacterial heterodisulfide' DsrC is a key protein in dissimilatory sulfur metabolism. *Biochim Biophys Acta* **1837**: 1148–1164.

Vigneron A, Cruaud P, Pignet P, Caprais J-C, Gayet N, Cambon-Bonavita M-A, *et al.* (2014). Bacterial communities and syntrophic associations involved in anaerobic oxidation of methane process of the Sonora Margin cold seeps, Guaymas Basin. *Environ Microbiol* **16**: 2777–2790.

Wagner M, Roger AJ, Flax JL, Gregory A, Stahl DA, Brusseau GA. (1998). Phylogeny of dissimilatory sulfite reductases supports an early origin of sulfate respiration. *J Bacteriol* **180**: 2975–2982.

Wegener G, Niemann H, Elvert M, Hinrichs K-U, Boetius A. (2008). Assimilation of methane and inorganic carbon by microbial communities mediating the anaerobic oxidation of methane. *Environ Microbiol* **10**: 2287–2298.

Wegener G, Krukenberg V, Riedel D, Tegetmeyer HE, Boetius A. (2015). Intercellular wiring enables electron transfer between methanotrophic archaea and bacteria. *Nature* **526**: 587–590.

Widdel F, Bak F. (1992) Gram negative mesophilic sulphate-reducing bacteria. In: *The Prokaryotes.* Balows A, Trüper HG, Dworkin M, Harder W, and Schleifer K-H (eds). New York: Springer, pp 3352–3378.

Widdel F, Musat F, Knittel K, Galushko A. (2007). Anaerobic degradation of hydrocarbons with sulphate as electron acceptor. In: *Sulphate-Reducing Bacteria: Environmental and Engineered Systems*. Barton LL, Hamilton WA (eds). Cambridge (UK): Cambridge University Press, pp 265–303.

Wu M, Scott AJ. (2012). Phylogenomic analysis of bacterial and archaeal sequences with AMPHORA2. *Bioinformatics* **28**: 1033–1034.

Yarza P, Yilmaz P, Pruesse E, Glöckner FO, Ludwig W, Schleifer K, *et al.* (2014). Uniting the classification of cultured and uncultured bacteria and archaea using 16S rRNA gene sequences. *Nat Rev Microbiol* **12**: 635–645.

Yilmaz P, Kottmann R, Field D, Knight R, Cole JR, Amaral-Zettler L, *et al.* (2011). Minimum information about a marker gene sequence (MIMARKS) and minimum information about any (x) sequence (MIxS) specifications. *Nat Biotechnol* **29**: 415–420.

Yu NY, Wagner JR, Laird MR, Melli G, Rey S, Lo R, *et al.* (2010). PSORTb 3.0: improved protein subcellular localization prediction with refined localization subcategories and predictive capabilities for all prokaryotes. *Bioinformatics* **26**: 1608–1615.

Zhang Z, Schwartz S, Wagner L, Miller W. (2000). A greedy algorithm for aligning DNA sequences. *J Comput Biol* **7**: 203–214.

Zhou J, Bruns MA, Tiedje JM. (1996). DNA recovery from soils of diverse composition. *Appl Environ Microbiol* **62**: 316–322.

Zverlov V, Klein M, Lücker S, Friedrich W, Kellermann J, Stahl DA, *et al.* (2005). Lateral gene transfer of dissimilatory (bi)sulfite reductase revisited. *J Bacteriol* **187**: 2203–2208.

Figures and tables

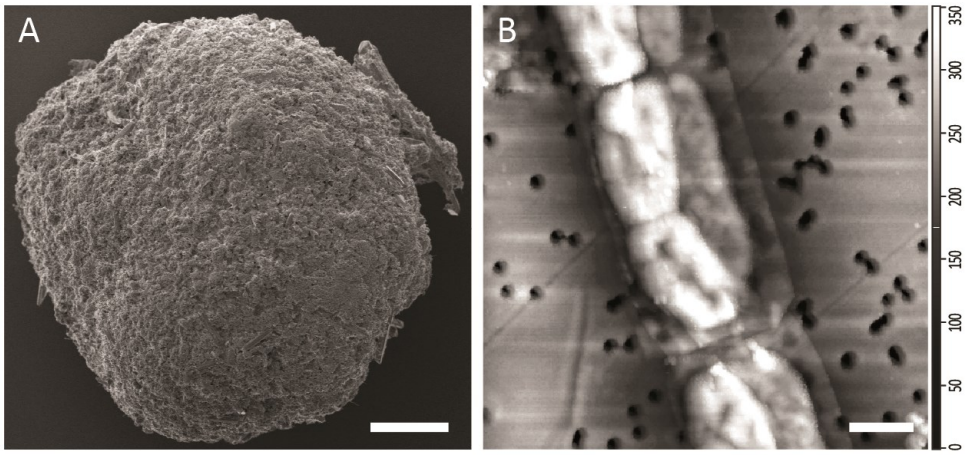

Figure 1 Microbial consortia from thermophilic AOM enrichments. (**A**) SEM image of a spherical TAOM aggregate, scale 100 µm. (**B**) AFM image of a component of a TAOM filament showing close proximity of archaeal (left) and bacterial (right) cells in a common envelope, visualized on a 0.2 µm pore-size filter, scale 1 µm, color bar indicates object height in nm.

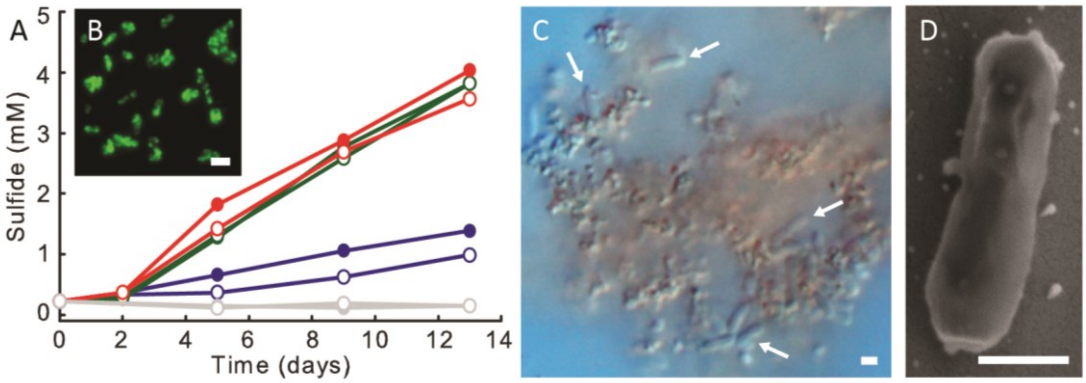

Figure 2 Effect of hydrogen on TAOM enrichment (**A**) and visualization of *Ca*. D. auxilii cells (**B-D**). (**A**) Sulfide production in thermophilic AOM consortia enrichment supplied with methane (blue), methane plus hydrogen (green) or hydrogen (red), and without energy source (grey) in replicate incubation per condition (filled and empty circle). (**B**) *Ca*. D. auxilii cells in a highly enriched culture on hydrogen; cells were visualized with the specific CARD-FISH probe HotSeep-1_1465, scale 2 µm. (**C**) Differential interference contrast micrograph of *Ca*. D. auxilii cells (marked by arrow) aggregating around inorganic precipitates (brownish color), scale 1 µm. (**D**) Scanning electron microscopy image of a *Ca*. D. auxilii cell grown on hydrogen, scale 500 nm.

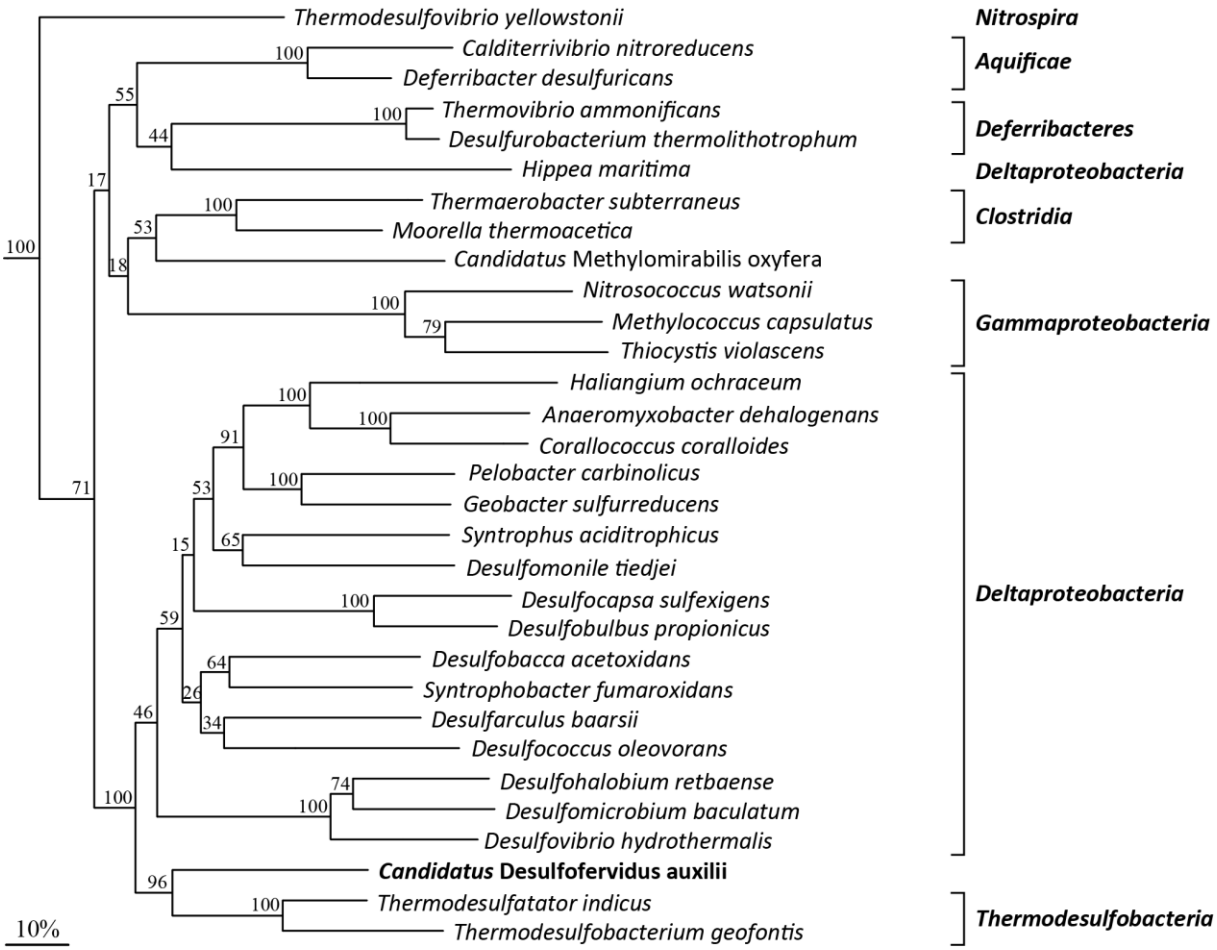

Figure 3 Phylogenetic affiliation of *Ca*. D. auxilii reconstructed from the concatenated protein alignment of 19 universal single copy marker genes. The phylogenetic tree was calculated using the maximum likelihood algorithm (RAxML). For clarity only a subset of the tree is depicted. Values at nodes indicate bootstrap support calculated from 100 replicates. The 16S rRNA gene based phylogeny is indicated to the right and is not fully congruent with the clustering observed in the depicted single copy gene tree. *Ca*. D. auxilii branches off at the root of the *Thermodesulfobacteria*, which form a sister clade to the *Deltaproteobacteria*.

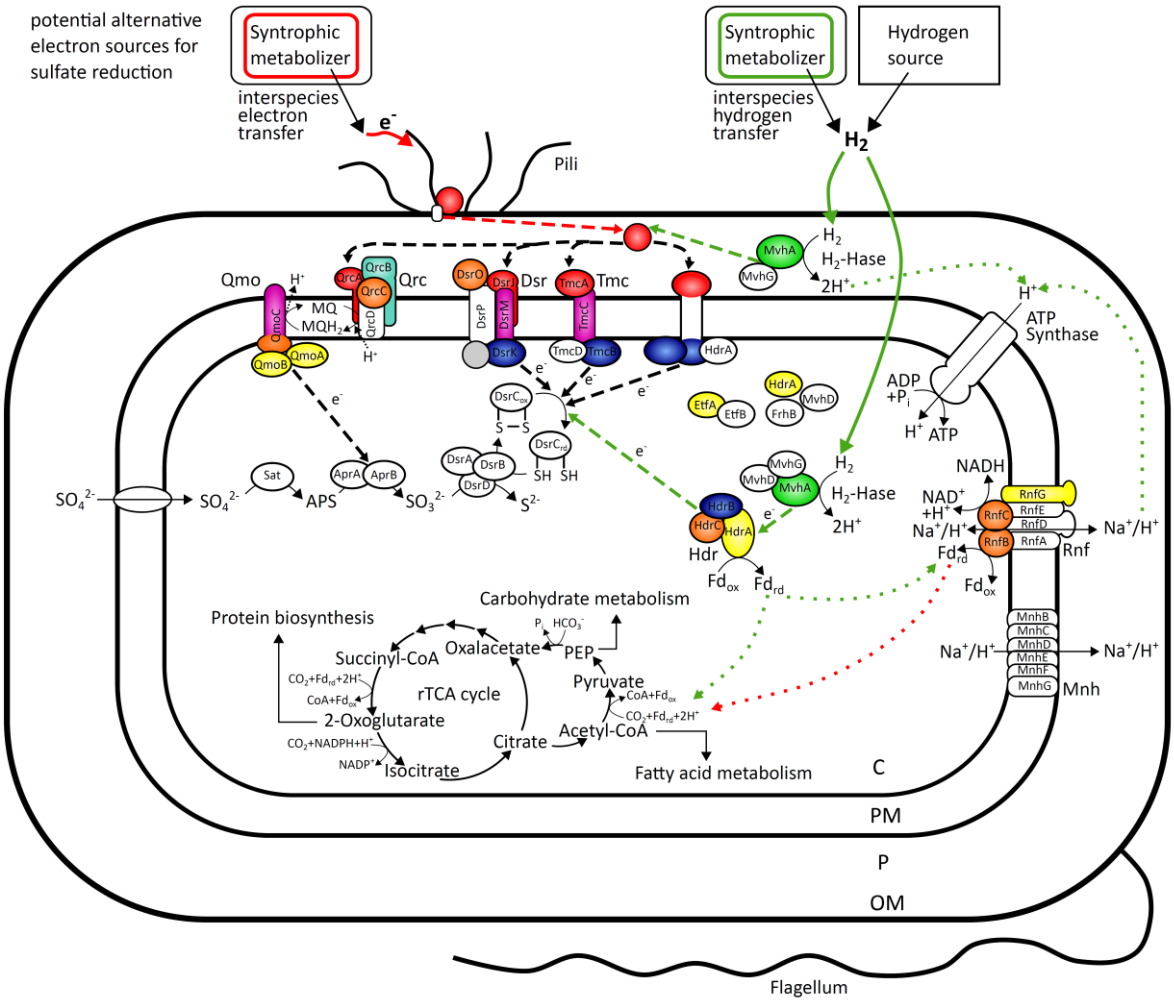

Figure 4 Scheme of energy metabolism and autotrophic carbon fixation in *Ca*. D. auxilii reconstructed from its draft genome. Depicted are the proposed reducing equivalent entry points during the possible alternative growth strategies of *Ca*. D. auxilii via hydrogen, green arrows (either supplied hydrogen or syntrophic interspecies hydrogen transfer) or via direct electron transfer, red arrow. Color coding: red for c-type cytochrome, purple for b-type cytochrome, orange for FeS proteins, turquoise for molybdopterin family proteins, dark blue for CCG proteins, yellow for flavoproteins, green for hydrogenase (catalytic subunit), white means not assigned and grey indicates protein may represent an additional subunit. Protein complex structure is adapted from previous models (Pereira *et al*., 2011). Dashed lines represent potential electron flow pathways. Dotted lines represent proton flow pathways or possible ferredoxin linkage. Black line color: path predicted to exist during growth with hydrogen and DIET; red line color: path predicted to only exist during growth via DIET; green line color: path predicted to exist only during growth on hydrogen. Rnf complex is depicted as working in both directions. C: Cytoplasm, PM: Periplasmic membrane, P: Periplasm, OM: Outer membrane.

Table 1 Morphological and physiological characteristics of *Ca.* D. auxilii.

Characteristic	*Ca.* D. auxilii
Cell morphology	rod
Cell size (μm)	1.5-2.0 x 0.5
Doubling time (days)	4-6
Temperature range (°C)	50-70
Activity optimum (°C)	60
Carbon source	CO_2
Electron acceptors	
Sulfate	+
Sulfite	−
Thiosulfate	−
Sulfur[1]	−
Electron donors	
H_2	+
Formate	−
Acetate	−
Hydrocarbons[2]	−
Other organic compounds[3]	−
Disproportionation	
Sulfite	−
Thiosulfate	−
Sulfur[1]	−
Syntrophic growth[4]	+

[1] Sulfur was provided in form of either S° powder or as colloidal S°

[2] Methane, propane and butane were tested

[3] Other organic electron donors tested: pyruvate, lactate, benzoate, succinate, fumarate, malate, ethanol, methanol, fructose, peptone, yeast extract, carbon monoxide, methyl sulfide

[4] Determined as consortial growth in AOM enrichments with methane as substrate

Table 2 Draft genome sequence information.

Feature	Value
Scaffolds	1
Genome size (bp)	2,540,211
Coding DNA sequence (bp)	2,286,941
Coding DNA sequence (%)	>90
N (%)	<1
GC content (%)	37
ORFs	2528
Genes assigned to COGs	1658
rRNAs (5S, 16S, 23S)	3
tRNAs	47
tRNA completeness (%)[1]	100
Single copy genes[2]	31
Single copy gene completeness (%)[2]	97-100

[1] Estimate of completeness based on identification of at least one tRNA for each amino acid; tRNAscan-SE v.1.21 (Lowe and Eddy, 1997).

[2] Estimate of completeness based on single copy gene analysis using AMPHOR2 (Wu and Scott, 2012) and checkM (Parks *et al.,* 2015) pipeline (see material and method, and results and discussion).

Supplementary information

Supplementary figures and tables

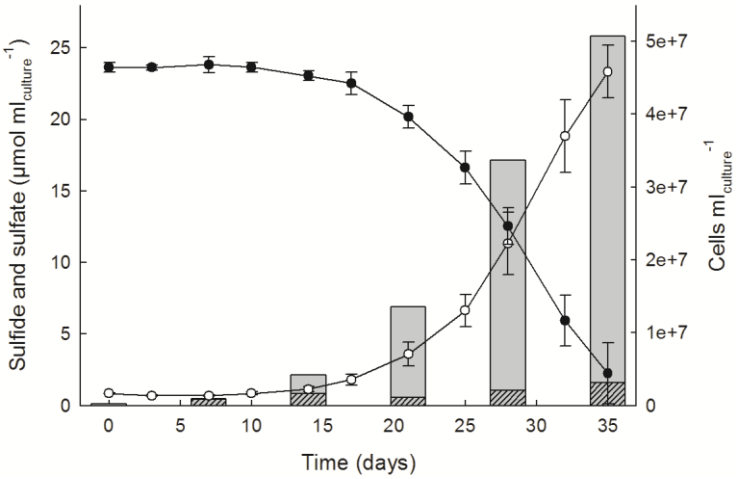

Figure S1 Evolution of sulfide (white symbols), sulfate (black symbols) and cell numbers (bars) in triplicate *Ca.* D. auxilii cultures grown with hydrogen and sulfate. Total cell numbers were determined by DAPI stained cell counts, fractions of *Ca.* D. auxilii and the contaminating archaeal cells were determined after dual CARD-FISH treatment with the *Ca.* D. auxilii specific probe (HotSeep-1_1465) and a general *Archaea*-targeting probe (Arch915). During exponential growth phase 90 to 95% of all cells were identified as *Ca.* D. auxilii (grey bar area). The contaminating species (patterned bar area) was identified as *Archaeoglobus* sp..

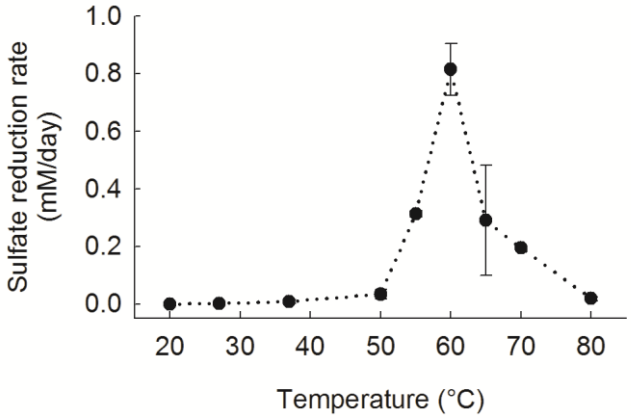

Figure S2 Temperature dependency of sulfate reduction in *Ca.* D. auxilii. Sulfate reduction rates were calculated from sulfide production observed in triplicates over three weeks of incubation at the designated temperature.

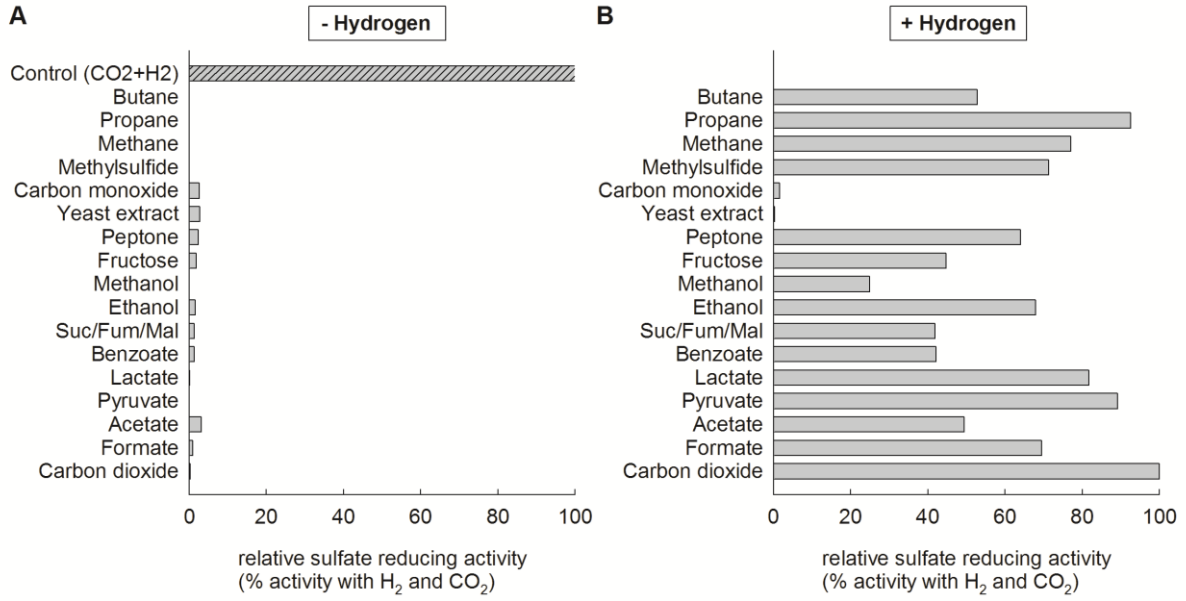

Figure S3 Effect of organic electron donors (**A**) and carbon sources (**B**) on the sulfate-reducing activity of *Ca.* D. auxilii. Activity of the culture is shown as % of sulfate reduction rates observed in incubations under standard conditions (hydrogen as electron source and carbon dioxide as carbon source). Activity was low in incubations with alternative electron donors (**A**) accounting for less than 5% of the sulfate reduction rate observed in controls supplemented with hydrogen, CO_2 and sulfate (patterned bar). Activity in the presence of alternative carbon sources (**B**) and hydrogen as electron donor varied with the organic compound supplied from less than 3% (CO and yeast extract) to about 90% (pyruvate and propane) of the sulfate reduction rate observed in incubations supplemented with hydrogen, CO_2 and sulfate (lowest bar in chart). Incubations testing the effect of organic carbon sources also included carbon dioxide (as it is part of the buffering system). As activity was not increased by additional organic carbon compounds heterotrophic growth of *Ca.* D. auxilii is unlikely.

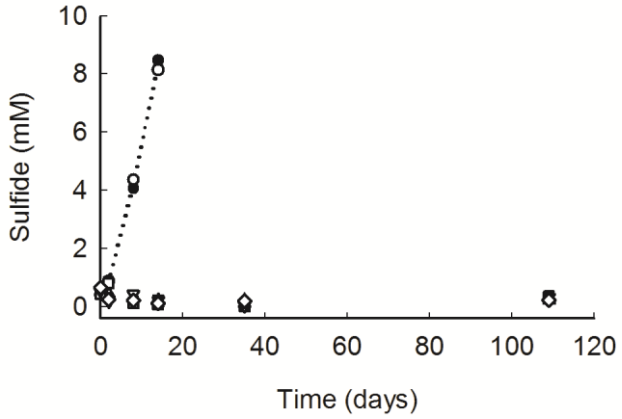

Figure S4 Sulfide production in long-term incubations of *Ca*. D. auxilii with different hydrocarbons (methane, propane, butane) and in control incubations with hydrogen (circles) and without electron donor (diamonds). Incubations were performed in duplicates (filled and open symbols). Sulfide production in hydrocarbon amended cultures was comparable to the control without electron donor over 3 months. Incubations supplemented with hydrogen showed high sulfide concentrations after approximately 3 weeks proving that the culture used as inoculum was active.

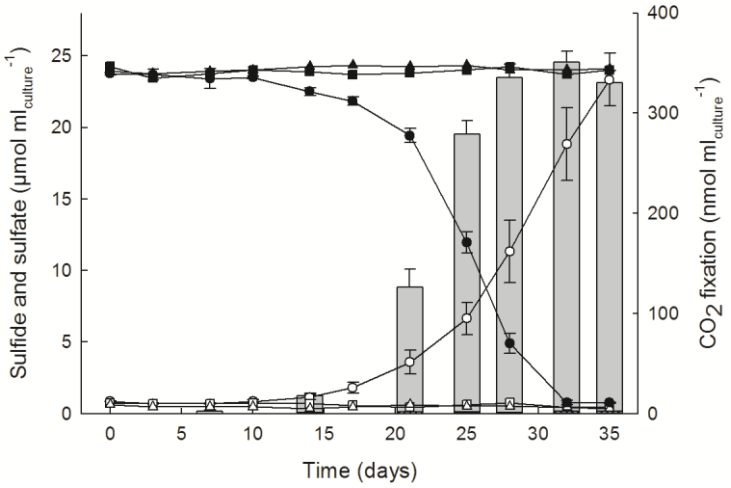

Figure S5 Correlation of sulfate reduction and carbon fixation. Sulfate consumption (black symbols) and sulfide production (white symbols) in triplicate *Ca*. D. auxilii cultures grown with sulfate and hydrogen (circles) and in control incubations without electron donor (triangles) and abiotic control (squares). CO_2 fixation (bars) was determined by ^{14}C-bicarbonate uptake into particulate organic material. CO_2 fixation in control experiments (without electron donor and in abiotic controls) is not visible. Sulfide development was determined in parallel incubations without ^{14}C-labeling. During exponential growth phase CO_2 fixation accounts for 2.4 to 4.1% of the sulfate reduction rate (3% on average).

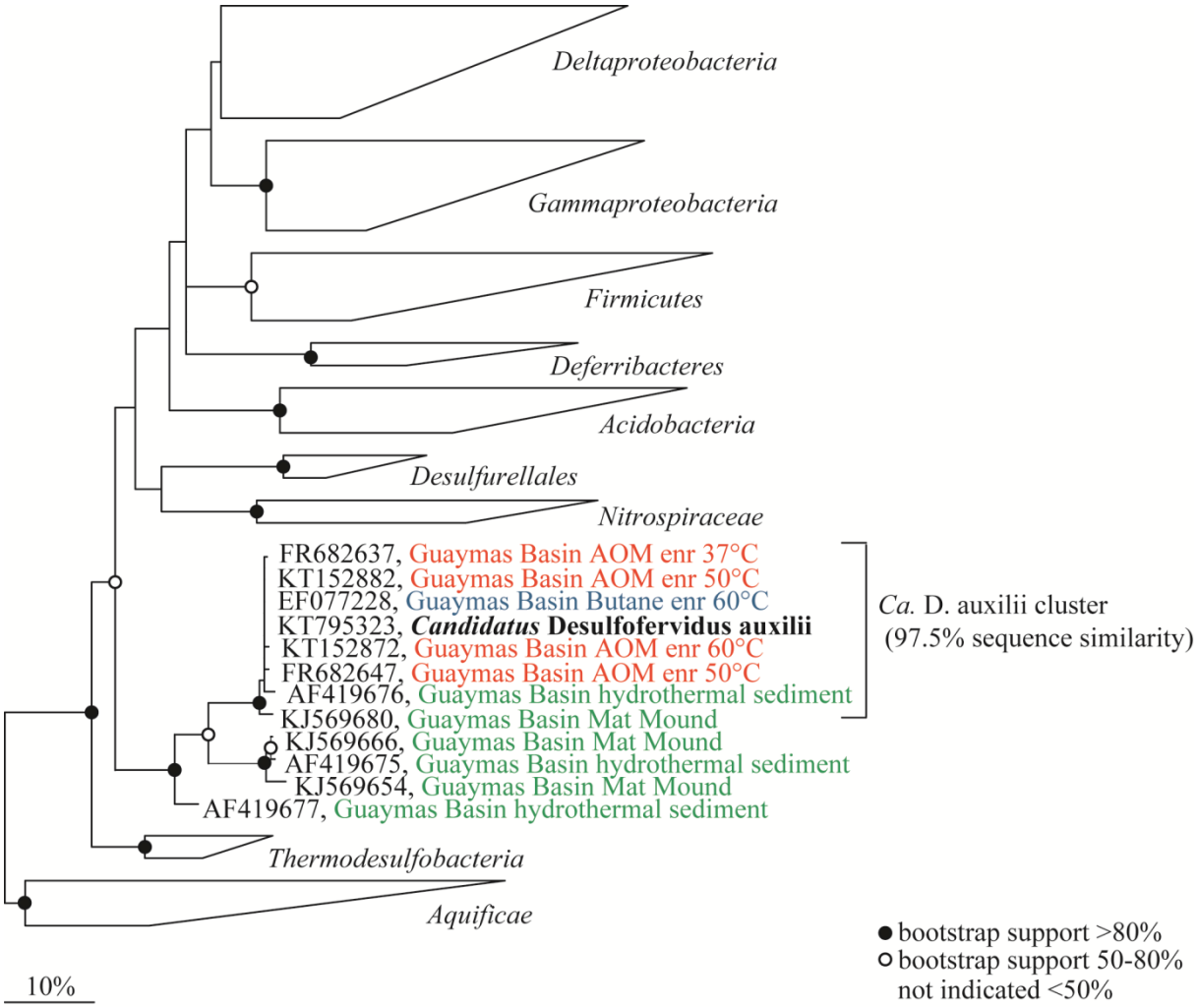

Figure S6 16S rRNA gene based phylogenetic classification of *Ca*. D. auxilii and representative related sequences. The phylogenetic tree was calculated applying the maximum likelihood algorithm (RAxML) with a 50% base frequency filter and 100 replicates to estimate branch support. The phylogenetic position of the 16S rRNA gene of *Ca*. D. auxilii was not stable as indicated by a comparison of trees calculated by different methods (RAxML, PhyML, Neighbor Joining, and Maximum Parsimony). Other observed relationships were within *Thermodesulfobacteria* or *Desulfurellales*. Sequences in the *Ca*. D. auxilii cluster share >97.5% sequence similarity and affiliate with environmental sequences currently exclusively retrieved from the Guaymas Basin. Indicated are the accession numbers and the source of the sequence, for more details on these and other HotSeep-1 related sequences see Tab. S1. Colour coding: black, genomic 16S rRNA of *Ca*. D. auxilii; red, obtained from Guaymas Basin enrichments on methane (Holler *et al*., 2011; Kellermann *et al*., 2012); blue, obtained from Guaymas Basin enrichment on butane (Kniemeyer *et al*., 2007); green, obtained from Guaymas Basin sediments (Teske *et al*., 2002 and Dowell *et al*., unpublished).

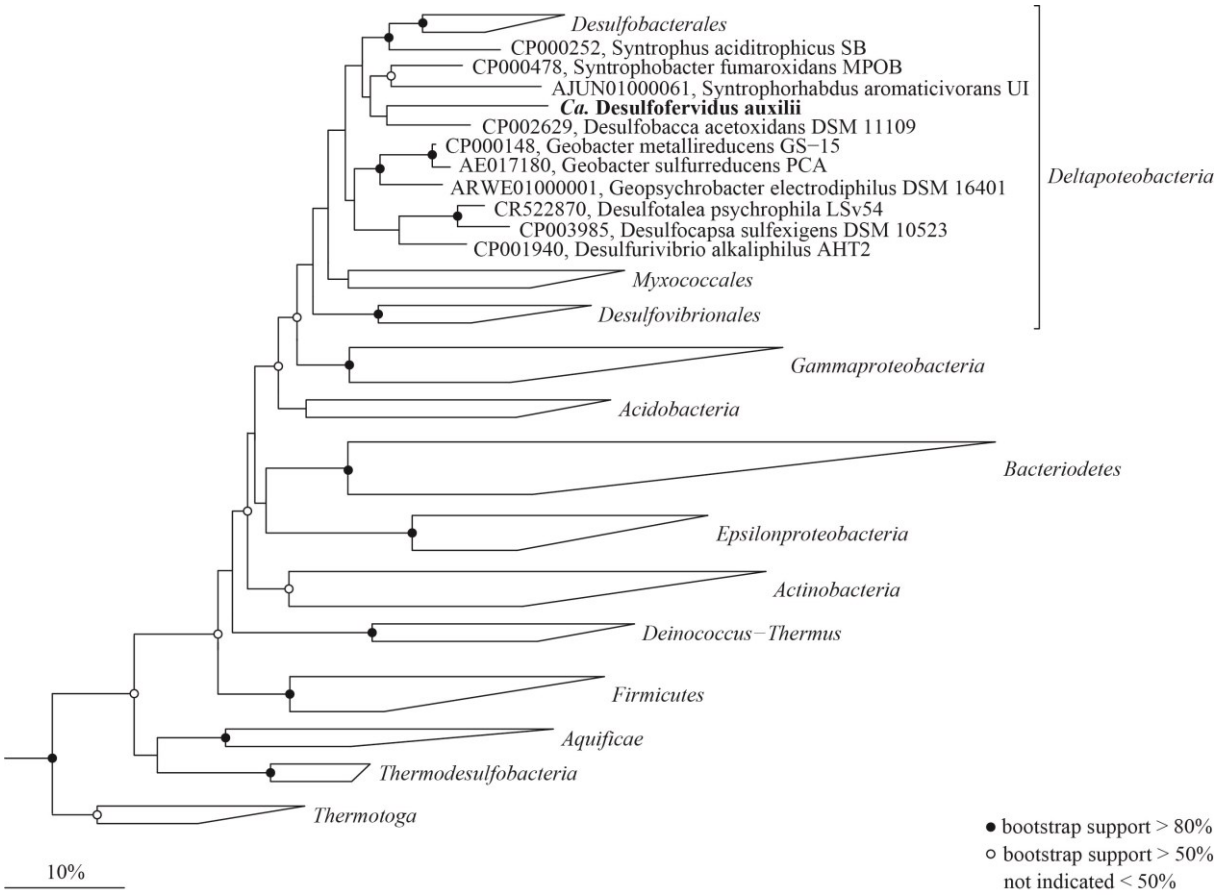

Figure S7 Phylogenetic classification based on the 23S rRNA gene. The phylogenetic tree was calculated with the RAxML algorithm and application of a 50% variability filter to exclude highly variable alignment regions. It is shown that the genomic 23S rRNA gene of *Ca.* D. auxilii affiliates with known syntrophically growing organisms of the class *Deltaproteobacteria*.

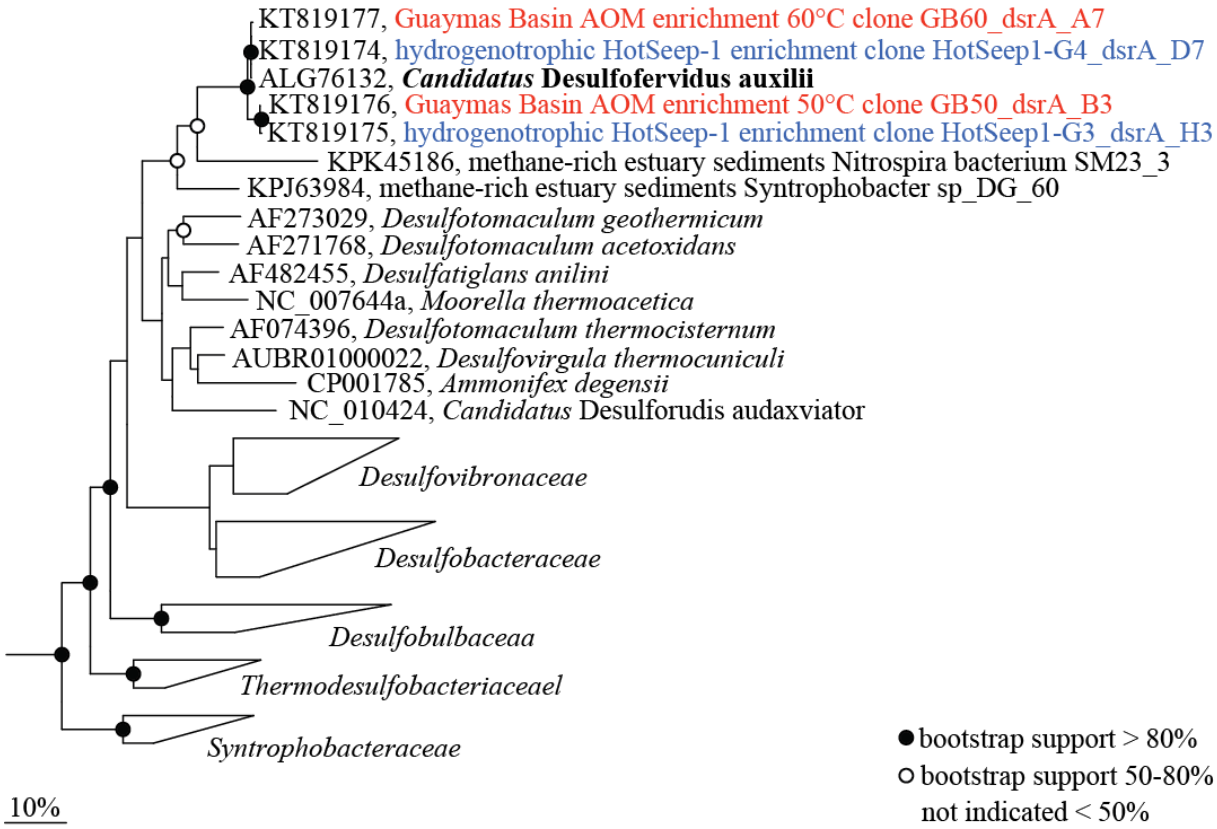

Figure S8 Phylogenetic classification of the dissimilatory sulfite reductase gene, subunit A of *Ca*. D. auxilii. The phylogenetic tree was calculated from the amino acid sequence alignment of 219 sequences applying the maximum likelihood algorithm (RAxML) with the LG substitution model and employing a 30% variability filter to exclude highly variable alignment regions. Branch support was calculated from 100 replicates. The genomic *dsrA* of *Ca*. D. auxilii clusters with sequences from Guaymas Basin AOM enrichments incubated at 50°C and 60°C (red) and sequences from early hydrogenotrophic-growing HotSeep-1 enrichments (blue) with >95% amino acid sequence similarity. The *Ca*. D. auxilii *dsrA* cluster affiliates with environmental sequences obtained from methane-rich estuary sediments (Baker *et al*., 2015) and relates to the *dsrA* sequences of *Desulfatiglans anilini* (formerly *Desulfobacterium anilini*), *Moorella thermoacetica* and *Desulfotomaculum* spp..

Table S1 Overview of available 16S rRNA gene sequences (full length) related to *Ca*. D. auxilii, their isolation source, sequence similarity to the genomic 16S rRNA gene of *Ca*. D. auxilii and relative abundance of related sequences in thermophilic AOM enrichments (GB50 and GB60). Sequences >99% similar are marked by black lines and relative abundance of clones is given for each cluster observed in the thermophilic AOM enrichments. Grey shaded sequences are considered the closest related environmental sequences but are not classified as *Ca*. D. auxilii (based on 97% sequence similarity threshold).

GenBank ID	Isolation source	Sequence description	Author year	Similarity to genomic 16S (%)	% of clones	
					GB50 AOM	GB60 AOM
KT795323	Guaymas Basin H2 enr 60°C	Genomic 16S rRNA	Wegener 2015			
KT152887	Guaymas Basin H2 enr 60°C	clone HotSeep1_G4_Bac_G5	Wegener 2015	100.0		
KT152872	Guaymas Basin AOM enr 50°C	clone GB50_Bac_F2	Wegener 2015	99.9		
EF077228	Guaymas Basin Butane enr 60°C	clone Butane60-GuB	Kniemeyer 2007	99.9		
KT152886	Guaymas Basin H2 enr 60°C	clone HotSeep1_G3_Bac_C4	Wegener 2015	99.9	40	69
FR682637	Guaymas Basin AOM enr 37°C	clone GUAY_enr37_Bac26	Kellermann 2012	99.7		
KT152882	Guaymas Basin AOM enr 60°C	clone GB60_Bac_F4	Wegener 2015	99.7		
FR682647	Guaymas Basin AOM enr 50°C	clone GUAY_enr50_Bac31	Holler 2011	99.7		
AF419676	Guaymas Basin hydroth sed	clone a2b002	Teske 2002	99.7		
FR682650	Guaymas Basin AOM enr 50°C	clone GUAY_enr50_Bac6	Holler 2011	98.8		
KJ569680	Guaymas Basin Mat Mound	clone BAC2_60	Dowell 2014	98.7		
FR682648	Guaymas Basin AOM enr 50°C	clone GUAY_enr50_Bac3	Holler 2011	98.5		
KT152874	Guaymas Basin AOM enr 50°C	clone GB50_Bac_C2	Wegener 2015	98.5	6	2
KT152884	Guaymas Basin AOM enr 60°C	clone GB60_Bac_B9	Wegener 2015	98.5		
KJ569657	Guaymas Basin Mat Mound	clone BAC2_45	Dowell 2014	98.4		
FR682643	Guaymas Basin AOM enr 37°C	clone GUAY_enr37_Bac9	Kellermann 2012	98.3		
FR682645	Guaymas Basin AOM enr 50°C	clone GUAY_enr50_BAC18	Holler 2011	98.0		
AF419677	Guaymas Basin hydroth sed	clone a2b033	Teske 2002	93.6		
KJ569666	Guaymas Basin Mat Mound	clone BAC2_21	Dowell 2014	91.5		
AF419675	Guaymas Basin hydroth sed	clone a1b020	Teske 2002	91.4		
KJ569654	Guaymas Basin Mat Mound	clone BAC1_24	Dowell 2014	91.4		

Table S2 Top scoring hits from blastn search of the genomic *Ca*. D. auxilii 16S rRNA gene sequence (1560 bp) against the NCBI database of 16S ribosomal RNA (*Archaea* and *Bacteria*); from 13.10.2015; 17762 sequences.

Organism	NCBI acc #	% identity	% query coverage	Bit score	Phylum
Thermodesulforhabdus norvegica strain A8444	NR_025970.1	86	97	1594	*Proteobacteria*
Syntrophobacter fumaroxidans strain MPOB	NR_075002.1	85	100	1585	*Proteobacteria*
Dissulfuribacter thermophilus strain S69	NR_109598.1	86	96	1580	*Proteobacteria*
Syntrophobacter sulfatireducens strain TB8106	NR_043073.1	85	99	1561	*Proteobacteria*
Desulfobacca acetoxidans strain DSM 11109	NR_074955.1	85	99	1559	*Proteobacteria*
Desulfovirga adipica strain TsuA1	NR_036764.1	85	98	1531	*Proteobacteria*
Desulfosoma caldarium strain USBA-053	NR_116707.1	86	92	1526	*Proteobacteria*
Anaeromyxobacter dehalogenans strain 2CP-1	NR_027547.1	84	99	1524	*Proteobacteria*
Desulfosoma profundi strain SPDX02-08	NR_117786.1	86	93	1517	*Proteobacteria*
Thermodesulfatator indicus strain DSM 15286	NR_075021.1	84	99	1515	*Thermodesulfo-bacteria*

Table S3 Overview of single copy marker genes identified in the *Ca*. D. auxilii genome and their assigned phylotypes on phylum and order level. Single copy genes were identified from a set of 31 universal bacterial marker genes and phylogenetically classified using the AMPHORA2 software package (Wu and Scott, 2012). Marker genes in bold were used for phylogenetic reconstruction.

Marker gene	Phylotype phylum level	Phylotype order level
frr	*Proteobacteria*	*Desulfovibrionales*
nusA	*Proteobacteria*	*Desulfovibrionales*
rplC	*Proteobacteria*	*Syntrophobacterales*
rplE	*Proteobacteria*	*Desulfarculales*
rplN	*Proteobacteria*	*Desulfovibrionales*
rplP	*Proteobacteria*	*Desulfobacterales*
rpsB	*Proteobacteria*	*Syntrophobacterales*
rpsC	*Proteobacteria*	*Desulfobacterales*
rpsS	*Proteobacteria*	*not assigned*
tsf	*Proteobacteria*	*Syntrophobacterales*
Pgk	*Proteobacteria*	*Desulfarculales*
rplA	*Proteobacteria*	*Desulfovibrionales*
rplL	*Proteobacteria*	*Syntrophobacterales*
smpB	*Proteobacteria*	*Desulfarculales*
rplB	*Thermodesulfobacteria*	*Thermodesulfobacteriales*
rplD	*Thermodesulfobacteria*	*Thermodesulfobacteriales*
rpmA	*Thermodesulfobacteria*	*Thermodesulfobacteriales*
rpsE	*Thermodesulfobacteria*	*Thermodesulfobacteriales*
rpsJ	*Thermodesulfobacteria*	*Thermodesulfobacteriales*
rpsK	*Thermodesulfobacteria*	*Thermodesulfobacteriales*
rpsM	*Thermodesulfobacteria*	*Thermodesulfobacteriales*
pyrG	*Thermodesulfobacteria*	*Thermodesulfobacteriales*
rplK	*Thermodesulfobacteria*	*Thermodesulfobacteriales*
rplS	*Thermodesulfobacteria*	*Thermodesulfobacteriales*
rpoB	*Thermodesulfobacteria*	*Thermodesulfobacteriales*
rpsI	*Thermodesulfobacteria*	*Thermodesulfobacteriales*
rplF	*Spirochaetes*	*Spirochaetales*
rplT	*Aquificae*	*Aquificales*
rplM	*Fusobacteria*	*Fusobacteriales*
dnaG	*Planctomycetes*	*Planctomycetales*

Table S4 Distribution of best scoring database hits of *Ca*. D. auxilii proteins across phyla and species.

Phylum/Species	**# of *Ca.* D. auxilii proteins (E-value $1.0E^{-5}$)**	**% of total best hits**
Proteobacteria	1020	53.1
Desulfobacca acetoxidans	147	7.65
Syntrophobacter fumaroxidans	100	5.21
deltaproteobacterium NaphS2	85	4.42
Syntrophus aciditrophicus	59	3.07
Desulfatibacillum alkenivorans	55	2.86
Desulfarculus baarsii	41	2.13
Desulfococcus oleovorans	35	1.82
Desulfobacterium autotrophicum	30	1.56
Geobacter uraniireducens	29	1.51
Pelobacter carbinolicus	26	1.35
Geobacter metallireducens	23	1.2
Desulfonatronospira thiodismutans	23	1.2
Geobacter sp. FRC-32	21	1.09
Thermodesulfobacteria	210	10.93
Thermodesulfatator indicus	**171**	**8.9**
Thermodesulfobacterium sp. OPB45	39	2.03
Euryarchaeota	97	5.05
Nitrospirae	66	3.44
Thermodesulfovibrio yellowstonii	47	2.45
Aquificae	59	3.07
Cyanobacteria	35	1.82
Chloroflexi	34	1.77
Bacteroidetes	23	1.2
Other phyla (with <1% of total matches)	143	7.44
Other species (with >1% of total matches)	24	1.25
Desulfotomaculum kuznetsovii	24	1.25
Other species (with <1% of total matches)	966	50.29

Table S5 Reciprocal best match analysis of the *Ca*. D. auxilii genome versus selected organisms.

Species	Phylum	# of shared genes	% of total *Ca.* D. auxilii genes	# of shared genes with similarity >60%	% of total shared *Ca.* D. auxilii genes
Thermodesulfatator indicus	*Thermodesulfobacteria*	958	37	195	20
Syntrophobacter fumaroxidans	*Proteobacteria*	912	36	143	16
Desulfobacca acetoxidans	*Proteobacteria*	882	34	160	18
Desulfobacterium autotrophicum	*Proteobacteria*	881	34	91	10
deltaproteobacterium NaphS	*Proteobacteria*	880	34	125	14
Thermodesulfovibrio yellowstonii	*Nitrospira*	857	34	121	14
Thermodesulfobacterium geofontis	*Thermodesulfobacteria*	852	33	148	17
Geobacter metallireducens	*Proteobacteria*	850	33	105	12
Desulvovibrio hydrothermalis	*Proteobacteria*	848	33	88	10
Desulfovibrio vulgaris	*Proteobacteria*	801	31	93	11
Syntrophus aciditrophicus	*Proteobacteria*	798	31	112	14

Table S6 Classification of *Ca*. D. auxilii genes according to COG categories.

COG category	No of genes
[J] Translation, ribosomal structure and biogenesis	142
[A] RNA processing and modification	1
[K] Transcription	69
[L] Replication, recombination and repair	152
[B] Chromatin structure and dynamics	2
[D] Cell cycle control, cell division, chromosome partitioning	26
[Y] Nuclear structure	0
[V] Defense mechanisms	26
[T] Signal transduction mechanisms	87
[M] Cell wall/membrane/envelope biogenesis	153
[N] Cell motility	48
[Z] Cytoskeleton	0
[W] Extracellular structures	0
[U] Intracellular trafficking, secretion, and vesicular transport	54
[O] Posttranslational modification, protein turnover, chaperones	80
[C] Energy production and conversion	146
[G] Carbohydrate transport and metabolism	68
[E] Amino acid transport and metabolism	127
[F] Nucleotide transport and metabolism	56
[H] Coenzyme transport and metabolism	87
[I] Lipid transport and metabolism	49
[P] Inorganic ion transport and metabolism	73
[Q] Secondary metabolites biosynthesis, transport and catabolism	33
[R] General function prediction only	227
[S] Function unknown	117
ORFs with COGs	1658
ORFs	2528
COGs	1823

Annotation Tables are not displayed.

Chapter IV

Comparative analysis of the metabolic potential of different subgroups of anaerobic methanotrophic archaea of clade 1

Viola Krukenberg[1], Halina E. Tegetmeyer[2,3], Harald Gruber-Vodicka[1] and Gunter Wegener[1,4]

[1]Max Planck Institute for Marine Microbiology, Bremen, Germany

[2]Alfred Wegener Institute, Helmholtz Center for Polar and Marine Research, Bremerhaven, Germany

[3]Center for Biotechnology, Bielefeld University, Bielefeld, Germany

[4]MARUM, Center for Marine Environmental Sciences, University Bremen, Germany

Manuscript in preparation

Abstract

The anaerobic oxidation of methane is an efficient microbial methane sink in marine environments. The responsible anaerobic methanotrophic archaea (ANME) form consortia with specific partner bacteria. The physiological mechanisms underlying sulfate-dependent methane oxidation are not yet completely understood but presumably involve a syntrophic interaction. Here we performed metagenomic and transcriptomic analyses on sediment-free mesophilic and thermophilic ANME-1 grown at 37°C or 60°C in association with either Seep-SRB-2 or HotSeep-1. We compared the obtained draft genomes of the meso- and thermophilic ANME-1 among one another and also to the published psychrophilic ANME-1 dataset from the Black Sea. Despite differences in growth temperature, cell morphology and partner bacterium, the similarly small genomes of meso- and thermophilic ANME-1 (~1.5 Mbp) share most properties. The ANME-1 encode and express the genes of the reverse methanogenesis pathway. However, consistently with previous studies on ANME-1 lack the *mer* (N^5,N^{10}-methylenetetrahydromethanopterin reductase) gene, which would catalyze the oxidation of the methyl group to methylene. We suggest that this step is instead adopted by a tetrahydrofolate reductase that may allow similar function but is commonly not expressed in a canonical methanogenesis pathway. Genes for dissimilatory sulfate reduction or hydrogen metabolism were not found in any of the ANME-1 draft genomes, hence the ANME-1 require an efficient alternative pathway for the removal of electrons. We found highly expressed membrane-associated and extracellular cytochromes in ANME-1, which indicates their central role in ANME-1 and likely in an interspecies electron transfer to partner bacteria. Archaeal cytochromes may not only promote electron transfer within specific AOM consortia, they may play a prominent role in the archaeal-bacterial interactions in general.

Introduction

The sulfate-dependent anaerobic oxidation of methane (AOM), an efficient methane sink in anoxic marine environments, regulates oceanic methane emissions to the atmosphere (Boetius and Wenzhöfer, 2013). The responsible microbial consortia of anaerobic methanotrophic archaea (ANME) and their specific partner bacteria couple the oxidation of methane to the reduction of sulfate in an interspecies effort (Boetius *et al.*, 2000; Orphan *et al.*, 2001b). The overall process of AOM yields a minimal amount of energy (ΔG_r) of approx. −30 kJ mol^{-1} to be shared among the partners, resulting in low growth yields and doubling times of 2 to 7 months of the involved organisms (Knittel and Boetius, 2009; Holler *et al.*, 2011). The methane-consuming ANME are relatives of methanogenic archaea and have reversed the methanogenesis pathway to oxidize methane (Hoehler *et al.*, 1994; Hallam *et al.*, 2004). ANME are classified into three main phylogenetic clades (ANME-1, -2, -3) and several subclades, but none of these clades has cultured representatives (Knittel and Boetius, 2009; Ruff *et al.*, 2015). The ANME form consortia with specific bacterial groups. While ANME-1 and -2 archaea associate with partner bacteria of the Seep-SRB-1a or Seep-SRB-2 cluster (*Desulfosarcina*/*Desulfococcus*) (Orphan *et al.*, 2001a; Michaelis *et al.*, 2002; Knittel *et al.*, 2003; Kleindienst *et al.*, 2012), ANME-3 form consortia with bacteria of the *Desulfobulbus* cluster (Niemann *et al.*, 2006), and the deep-branching HotSeep-1 cluster associates in consortia with thermophilic ANME-1 (Holler *et al.*, 2011).

The metabolic interaction between ANME and their partner bacteria in AOM is explained in different models. For ANME-2/DSS consortia an internal cycling of zero-valent sulfur was suggested that proposed partial sulfate reduction in ANME-2 and sulfur disproportionation by DSS (Milucka *et al.*, 2012). Alternatively, ANME-2 was proposed to directly transfer reducing equivalents from methane oxidation to sulfate-reducing partner bacteria via redox active extracellular c-type cytochromes (McGlynn *et al.*, 2015). In thermophilic ANME-1/HotSeep-1 consortia the bacterial partner was suggested to additionally produce nanowire-like connections to retrieve the electrons from the ANME-1 (Wegener *et al.*, 2015). Yet the general applicability of these proposed models to the complete ANME clades and bacterial partners is unknown.

Here we focus on the molecular basis of methane oxidation and electron transfer in ANME-1-dominated consortia. The ANME-1 clade comprises a large group of environmental sequences obtained from >50 AOM habitats that form a distinct phylogenetic branch within the *Methanomicrobia* (Knittel and Boetius, 2009). Based on 16S rRNA gene similarity ANME-1 was classified into ANME-1a and ANME-1b. Central aspects of the physiology of

ANME-1 were revealed in culture-independent studies (Wegener *et al.*, 2008; Kellermann *et al.*, 2012). Metagenomic approaches, together with transcriptomic and proteomic data, have provided detailed insights into the potential metabolic capabilities of the clade (Hallam *et al.*, 2004; Meyerdierks *et al.*, 2005, 2010; Stokke *et al.*, 2012). As physiologic and genomic information on ANME-1 is still limited, little is known about the potential metabolic diversity within this large group. Consequently, the general characteristics of ANME-1 that distinguish them from other methanotrophic archaea such as ANME-2 or methanogenic archaea are difficult to determine. We obtained draft genomes from two members of the ANME-1 clade that are characterized by distinct growth temperatures and specific bacterial partners. We performed comparative analysis of our datasets and previous ANME-1 genome drafts focusing on their central metabolisms and commenting on potential interaction mechanisms with their bacterial partners.

Material and methods

AOM enrichments

Material for AOM enrichments was sampled during the RV Atlantis cruise AT15-56 in November/December 2009 (Alvin Dive 4570) from hydrothermal vent sediments in the Guaymas Basin, Gulf of California, Mexico (27°00.437 N, 111°24.548 W). Enrichments were initiated as described by Holler and colleagues (2011) and were incubated with sulfate reducer medium (28 mM sulfate; Widdel and Bak, 1992). The electron donor was CH_4 (0.225 MPa CH_4) and sulfate served as the sole energy source and CO_2 (0.025 MPa CO_2; 30 mM dissolved inorganic carbon) as additionally offered carbon source. Parallel enrichments were incubated at 37°C and 60°C. Culture medium was exchanged when sulfide concentrations exceeded ~12 mM and samples were regularly diluted (1:2; 1:4) to obtain sediment-free enrichments after ~2 years. The phylogenetic composition and metabolic capabilities of the two enrichments was described previously (Wegener *et al*., submitted).

Catalyzed reporter deposition fluorescence *in situ* hybridization

Aliquots of AOM enrichments were fixed in 2% formaldehyde for 2 h at room temperature and washed with 1x phosphate buffered saline (PBS; pH 7.4). Fixed cell suspensions were treated with mild sonication (Sonoplus HD70; Bandelin) and aliquots of 50-250 µl were filtered onto GTTP filters (0.2 µm pore size, 20 mm diameter). CARD-FISH was performed

as described previously (Pernthaler and Amann, 2004) with some modifications. For cell wall permeabilization, filters were sequentially incubated in lysozyme solution (10 mg ml^{-1} lysozyme powder, 0.1 M Tris–HCl, 0.05 M EDTA, pH 8) for 15-30 min at 37°C and proteinase K solution (0.45 mU ml^{-1}, 0.1 M Tris–HCl, 0.05 M EDTA, pH 8, 0.5 M NaCl) for 2 min at room temperature. To inactivate endogenous peroxidases filters were incubated in 0.15% H_2O_2 in methanol (30 min, room temperature). The oligonucleotide probes ANME-1-350, HotSeep-1-1456 and SEEP2-658 were applied with formamide concentrations of 40%, 35% and 45%, respectively. To specifically target Seep-SRB-2 cells a competitor (unlabeled DSS658) was included with probe SEEP2-658 to avoid cross hybridization to cells of the DSS clade (Kleindienst *et al*., 2012). For dual CARD-FISH, peroxidases of the first hybridization were inactivated by incubation of filters in 0.3% H_2O_2 in methanol (30 min, room temperature). Catalyzed reporter deposition was combined with the fluorochromes Alexa Fluor 488 and Alexa Fluor 594. Filters were stained with DAPI (4,6-diamidino-2-phenylindole). Micrographs were obtained by confocal laser scanning microscopy (LSM 780; Zeiss; Oberkochen, Germany).

Visualization of ANME by autofluorescence

To visualize autofluorescence of cofactor F_{420} AOM aggregates were sampled from the enrichments, transferred to microscopy slides and immediately analyzed using a confocal laser scanning microscope with an excitation light of 390 to 420 nm and a ≥463 nm emission filter.

Extraction of genomic DNA, library preparation and sequencing

Genomic DNA was extracted from 45 ml active TAOM enrichment culture harvested by centrifugation at 5000xg for 15 min. Supernatant was discarded and the pellet resuspended in extraction buffer prepared according to Zhou and colleagues (1996). Cell aggregates were disrupted by 40 cycles of manual grinding in a tissue grinder (Wheaton, 1 ml) followed by 3 cycles of freezing in liquid nitrogen and thawing at 65°C. DNA was extracted according to the protocol by Zhou and colleagues (1996) which includes cell lysis by proteinase K digestion, sodium dodecyl sulfate (SDS) extraction and chloroform:isoamylalcohol extraction. DNA was precipitated with isopropanol at –20°C overnight, pelleted by centrifugation for 1 h at 13000 rpm and washed three times with ice-cold 70% EtOH. The pellet was air dried, resuspended in PCR water and DNA quantity and quality was assessed by Qubit measurements and gel electrophoresis.

For metagenome sequencing 2 µg and 4 µg high molecular weight DNA was used for PCR-free TruSeq paired end and mate pair library preparation, respectively, following the manufacturer guidelines. Paired end libraries were prepared from ~500 bp DNA fragments and mate pair libraries from DNA fragments of ~5000 bp size. Libraries were sequenced on an Illumina MiSeq platform using chemistry to generate 250 bp long reads.

16S rRNA diversity, metagenome assembly and draft genome reconstruction

The taxonomic composition of the metagenomic dataset was estimated by mapping the raw reads to the SILVA database (release 119) (Quast *et al.*, 2013) using bbmap v.35 implemented in phyloflash v.1.5 with minimum identity of 95%. For quantification only unambiguously mapped reads were counted.

Quality of raw read data was assessed using FastQC (v.011.2) and reads were processed, including adapter clipping, trimming of low quality bases from sequence ends and removal of reads with quality <10 and length <50 bp using bbduk (bbmap v.35). Prior to assembly a read error correction was performed using BayesHammer implemented in the SPAdes software package (Bankevich *et al.*, 2012). Mate pair reads were assembled with SPAdes v.3.5.0. using default values of k and the –hqmp option. Binning of the bulk metagenome assembly was performed within the Metawatt software version 3.2 (Strous *et al.*, 2012) combining tetranucleotide frequency binning with manual bin refinement based on coverage and GC spread. Bins of ANME and partner bacteria were extracted from the bulk assembly for targeted reassembly. Mate pair and paired end reads were mapped to the binned contigs using bbmap (v. 35) with minimum mapping identity of 98% and best site of ambiguous reads. Mapped reads including unmapped read pairs were reassembled using SPAdes with default values of k. Binning and bin refinement as described above was repeated. Paired end connections of contigs was assessed using mate pair mapping data and the scripts of the multimetagenome workflow (Albertsen *et al.*, 2013) to further refine the bin. The process of reassembly and binning was repeated until no further improvement was achieved. Then the assembled contigs were subjected to iterative scaffolding and gapfilling using SSPACE (Boetzer *et al.*, 2010) and GapFiller (Boetzer and Pirovano, 2012), respectively. Assembly quality and bin completeness was assessed repeatedly during the assembly process. QUAST (Gurevich *et al.*, 2013) was used to obtain general assembly metrics and single-copy gene analysis provided estimates of the degree of completeness and level of contamination of the bin. Final draft genome completeness was estimated using checkM (Parks *et al.*, 2015) and AMPHORA2 (Wu and Scott, 2012). Draft genomes were annotated using prokka (Seemann,

2014). Protein domains were identified by hmmscan (HMMER 3.0) (Eddy, 1998) using the PfamA (Bateman *et al*., 2004) and TIGRFAM (Haft *et al*., 2003) reference databases. Proteins were compared to the NCBI nr protein database in a blastp (2.2.29+) search (Altschul *et al*., 1990). Subcellular localization of selected proteins was determined with PSORTb 3.0 (Yu *et al*., 2010). Potential c-type cytochromes were identified by the presence of the CXXCH motif, indicative of a heme-binding site and when matching a c-type cytochrome related protein domain were considered as such. Potential type IV pili genes were identified based on the presence of respective protein domains. Annotation of all genes discussed here was manually inspected and curated.

Extraction of RNA, library preparation and sequencing

Total RNA was extracted from 20 ml enrichment aliquots. For thermophilic cultures ~80% culture medium was removed under ambient temperatures and 5 volumes of pre-warmed RNA later (SigmaAldrich) was injected to prevent mRNA degradation. RNAlater amended cultures were kept at ambient temperature and headspace gases for 20 min. Biomass was then collected onto 0.2 μm pore size GTTP polycarbonate filters and total RNA was immediately extracted using the Quick-RNA MiniPrep kit (Zymo Research, Irvine, CA, USA) following manufacturers recommendations. For mesophilic cultures ~95% culture medium was removed, 2 volumes extraction buffer was injected and samples were immediately processed with the Quick-RNA MiniPrep kit (Zymo Research, Irvine, CA, USA) following manufacturers recommendations. RNA extracts were treated with DNase I (Roche, Rotkreuz, Switzerland) in the presence of RNasin for 30 min at 37°C followed by DNase I inactivation at 56°C for 10 min. RNA was then purified with the RNeasy MinElute Cleanup kit (Qiagen, Hilden, Germany) following manufacturer recommendations and eluted with RNase-free water. RNA quality and quantity was measured on a Bioanalyzer instrument using RNA chips. DNA contamination was tested by PCR reaction.

For RNA sequencing 50 ng total RNA was prepared using the TruSeq stranded mRNA library prep kit (Illumina CA, USA) omitting the rRNA depletion step and including a PCR amplification step of 15 cycles. Synthesized cDNA was sequenced on a MiSeq instrument (MiSeq, Illumina) generating between 2 to 3 Mio 150 bp single end reads per library and on a HiSeq generating additionally 30 to 40 Mio 150 bp reads per library.

Gene expression analysis

Quality of raw read data was assessed using FastQC (v.011.2) and reads were processed, including adapter clipping, trimming of low quality bases from sequence ends and removal of reads with quality <10 and length <25 bp using bbduk (bbmap v.35). Reads were mapped to the draft genomes obtained from the respective thermophilic or mesophilic enrichments with a minimum mapping identity threshold of 98%. Unambiguously mapping reads per feature (gene) were quantified with bedtools multicov (v.2.24.0). Count data were converted to transcripts per million mapped reads by first normalizing each count value by the length of its feature. Then, to calculate relative values of transcription (T), the normalized count value of a genome feature *i* was set in relation to the normalized count values of all other genome features using the following equation, according to Li and colleagues (2010)

$$T_i = X_i / l_i \times (\sum X_j / l_j)^{-1} \quad (1)$$

where X = counts and l = length of the gene (bp). The relative transcription values were multiplied by 10^6, and are given in terms of transcripts per million (TPM).

Results and discussion

The meso- and thermophilic AOM enrichment cultures

The studied AOM enrichments were cultivated at mesophilic (37°C; G37) and thermophilic (60°C; G60) conditions, respectively (Holler *et al.*, 2011; Wegener *et al.*, submitted). The G37 enrichment was dominated by ANME-1/Seep-SRB-2 consortia while ANME-1/HotSeep-1 consortia prevailed in G60 (Fig. 1 A, B) (Wegener *et al.*, submitted). Both consortia were observed to grow as aggregates of visible size, however aggregates in G37 were smaller than in G60 (<100 µm and 500 µm in diameter, respectively). Aggregated cells were surrounded by an extrapolymeric matrix, also containing iron sulfide precipitates and in particular in the G60 culture carbonate crystals. The microbial consortia in the G60 culture were easily detectable by their brownish-red color similar to ANME-1-dominated regions of microbial reefs from the Black Sea (Michaelis *et al.*, 2002), which might be attributed to a high cytochrome c content. As for the consortia, differences in morphology between growth temperatures were also observed for ANME-1 cells: The G37 enrichment was dominated by large coccoid ANME-1 cells (~2 µm diameter), whereas ANME-1 in G60 were cylindrical and enclosed in an envelope similar to previous reports (Reitner *et al.*, 2005a; Wegener *et al.*, 2015). In both, G37 and G60 ANME-1 cells showed the characteristic

autofluorescence of the methanogenic cofactor F_{420}, which is indicative for the activity of the methanogenesis pathway (Fig. 1 C, D) (Doddema and Vogels, 1978). The dominant archaeal 16S rRNA gene sequences from the two enrichments (Wegener *et al*., submitted) showed an identity of >98% and represented two clusters of partial sequences with within cluster similarity of >99%. These mesophilic and thermophilic clusters are distinguished by <96% similarity indicating temperature-dependent growth of the two different ANME-1 subtypes. Classification of 16S rRNA gene fragments obtained by metagenome sequencing supported that two distinct and abundant variants of ANME-1 were present (Fig. 2). Further, sequences related to the mesophilic ANME-1 were not detected at thermophilic conditions and vice versa. In both metagenomic libraries, ANME-1 accounted for about 40% of all 16S rRNA gene reads and their bacterial partners for about 30%. From a bulk assembly of the metagenomic datasets, ANME-1-related bins were extracted for targeted assembly of mesophilic and thermophilic ANME-1 draft genomes.

We also compared our data to the available genomic dataset of psychrophilic ANME-1b (Meyerdierks *et al.*, 2010). This ANME-1b dataset was derived from the inner part of microbial reef structures from the Black Sea naturally enriched in ANME-1b cells. With *in situ* temperatures ~8 to 10°C in the Black Sea these ANME-1b represent the cold-adapted (psychrophilic) counterpart to the mesophilic and thermophilic ANME-1 from our Guaymas Basin enrichments.

Classification of ANME-1 draft genomes

ANME-1 comprises a large clade within the *Methanomicrobia*. To resolve the phylogenetic relatedness of the studied ANME-1 we compared their 16S rRNA gene and the functional gene *mcrA*, which encodes the key enzyme of methanogenesis. Each of the ANME-1 draft genome datasets investigated contained only a single 16S rRNA gene; however, the metagenomic dataset of G37 contained at least two further closely related ANME-1 clades (Fig. 2). Furthermore, the 16S rRNA gene sequence of the studied bin showed two insertions which were not observed in any ANME-1-related full length 16S rRNA gene sequence in the NCBI non-redundant sequence database. As the 16S rRNA gene is highly conserved, the insertions observed may result from assembly problems derived from the presence of closely related ANME-1 subtypes in the enrichment.

The genomic 16S rRNA gene of the G37 and the G60 ANME-1 bins showed a similarity of 89% while they shared 90% or 93% similarity with the 16S rRNA gene sequence of the psychrophilic ANME-1b, respectively. Even when masking the regions of insertion in the

mesophilic ANME-1 16S rRNA gene sequence similarities only slightly increased (91% identity to both, thermo- and psychrophilic ANME-1). Hence according to a minimum identity threshold of 94.5% as genus border (Yarza *et al.*, 2014) the ANME-1 analyzed here likely represent different genera of methanotrophic archaea. The 16S rRNA gene based phylogenetic reconstruction showed that the genomic 16S rRNA gene of the G60 ANME-1 affiliates well with cloned sequences amplified from Guaymas Basin sediment samples and the G60 enrichments (Fig. 3 A). In contrast the genomic 16S rRNA gene of the G37 ANME-1 did not affiliate with the dominant sequences retrieved from the G37 enrichment previously (Wegener *et al*., submitted) but formed a cluster with few sequences of the G37 enrichment. Again, the observed insertion in its genomic 16S rRNA gene may impede reliable classification of mesophilic ANME-1. For comparison, the best database hit was observed to a clone from a Guaymas Basin AOM enrichment incubated at 50°C, regardless of masking the insertion or not (identities of 93% and 92%, respectively). As previously shown, the psychrophilic ANME-1 from the Black Sea belongs to a well separated branch including clones from the Black Sea and other cold methane seep sites.

A phylogenetic classification of the Mcr alpha subunit, a part of the key enzyme of methanogenesis, revealed a similar clustering (Fig. 3 B). Thermophilic and mesophilic ANME-1 form distinct branches, however while here the mesophilic ANME-1 affiliates in the same branch as the dominant *mcrA* obtained from Guaymas Basin AOM enrichments (at 37 and 50°C) (Holler *et al.*, 2011), the thermophilic ANME-1 clusters with a single sequence obtained from an AOM enrichment incubated at 50°C. As also observed for the 16S rRNA gene the *mcrA* of ANME-1b formed a distinct cluster. Sequence identities of the analyzed McrA proteins ranged from 89 to 90% among the three ANME-1.

Comparison of ANME-1 draft genomes

Tetranucleotide frequency binning of the initial metagenome assemblies followed by iterative, targeted bin reassembly and bin refinement yielded draft genomes of mesophilic and thermophilic ANME-1a variants. We performed comparative analyses of the two retrieved draft genomes and the draft genome of the psychrophilic ANME-1b (Meyerdierks *et al.*, 2010). The general genome properties and the estimated degree of draft genome completeness of the three datasets are summarized in Table 1. Our meso- and thermophilic ANME-1 have relatively small genomes of about 1.5 Mb, which is approximately half of the assembly size obtained for the psychrophilic ANME-1. The GC content is considerably higher in mesophilic ANME-1 (52%) relative to the thermophilic (41%) or psychrophilic ANME-1 (43%). Such

observations suggest that elevated growth temperatures do not lead to increased GC content in ANME-1, as suggested for other archaea (Merkel *et al.*, 2013). The three genomes encode for 38 to 46 tRNAs, whereas the tRNA for tyrosine is missing in all three genomes. We estimated the completeness of the draft genomes of mesophilic and thermophilic ANME-1 by three independent methods (see Tab. 1). Based on the presence of tRNAs for all except one amino acid, the genomes showed a 95% completeness. Two sets of single-copy genes were used to further evaluate genome completeness. Detection of archaeal-specific single-copy genes indicated a completeness of 90 to 91%. In all three ANME-1 most of the detected marker genes were classified into the *Euryarchaeota* and thereof the largest fraction was assigned to the *Methanosarcinales* (Tab. S1). Based on detected *Euryarchaeota*-specific single-copy genes the genome completeness was 89 to 92%. When comparing the identity of the single copy genes missing, 6 *Archaea*-specific and 8 *Euryarchaeota*-specific genes were absent in all three ANME-1 datasets. This might indicate that the ANME-1 branch lacks some single-copy genes generally thought to be characteristic for *Euryarchaeota* or *Archaea* in general. The degree of contamination observed in the two draft genomes was below 2% for the thermophilic and below 1% for the mesophilic ANME-1 variant. Estimated strain heterogeneity accounted for 75% and 0% of contamination by other organisms, respectively. In comparison, the previously-described ANME-1b dataset (Meyerdierks *et al.*, 2010) represents a less complete (87%) genome that contains a higher degree of contamination (20%), of which 80% are attributed to strain heterogeneity. Hence, this dataset was considered as composite genome of several ANME-1 strains (Meyerdierks *et al.*, 2010; Parks *et al.*, 2015). It probably also provides an at least partial explanation for the observed larger size of this psychrophilic ANME-1 genome relative to the genomes of meso- and thermophilic ANME-1. But the small genome of the meso- and thermophilic ANME-1 may also be interpreted as adaptation to specific environmental conditions or limited metabolic versatility and may be a feature contrasting the Guaymas-specific ANME-1 population from other ANME-1. In contrast to all previous ANME-1 metagenomic datasets, the draft genomes of the mesophilic and thermophilic ANME-1 generated here provide genomic information of two specific ANME-1a subtypes differentiated by their phylogenetic affiliation and also their morphology, growth temperature, and the identity of their bacterial partner. Together, these datasets allow deeper insight into the potential metabolic diversity within the ANME-1 group.

The reverse methanogenesis pathway in ANME-1

Sulfate-dependent methane oxidation by ANME is proposed to proceed via a reversal of the methanogenesis pathway (Hallam *et al*., 2004). The mesophilic and thermophilic ANME-1 types studied here originate from enrichments in which methane and sulfate display the only redox couple for cell catabolism. Despite earlier proposals that ANME-1 may be able to switch to methanogenic metabolism (Lloyd *et al.*, 2011) methane production by ANME-1 was not measureable in the G37 and G60 enrichments (Wegener *et al*., submitted). Hence, we attribute the detection of methanogenesis-related genes in the ANME-1 draft genomes to their utilization in methane oxidation. With the exception of the *mer* gene, encoding N^5,N^{10}-methylenetetrahydromethanopterin (methylene-H4MPT) reductase, we found that both ANME-1 types contain and express all the genes necessary to convert methane to CO_2 via reverse methanogenesis (Fig. 4; compare Tab. S2). Notably, following the 16S and 23S rRNA genes, *mcrA* was the most highly expressed gene in the enrichments, and its expression was almost two orders of magnitudes higher than for all other enzymes of the methanogenesis pathway. Mcr catalyzes the initial activation of methane to methyl-CoM. Due to the endergonic character of methyl-CoM formation this is the rate limiting step of the overall metabolism of ANME (Thauer and Shima, 2008). This limitation explains the high amount of McrA protein in the cells (Krüger *et al.*, 2003) and the respective predominant expression of this gene. The enzymes catalyzing the subsequent steps of methane oxidation were less expressed as they rely on the supply of activated methane which they sequentially turnover. We observed a gradual decrease in gene expression along the pathway, with an increased expression of only the genes catalyzing the last two reaction steps (Fig. 5).

The *mer* gene is not present in G37 and G60, which is in agreement with the earlier findings that showed the absence of a *mer* gene in cold-adapted ANME-1 (Meyerdierks *et al.*, 2010; Stokke *et al.*, 2012). Consequently, a bypass for this enzymatic step was proposed that involves the formation of methanol and formaldehyde which finally re-enters the methanogenesis pathway via oxidation to methylene-H4MPT (Welander and Metcalf, 2008; Meyerdierks *et al.*, 2010). Indeed, we also detected genes encoding the enzymes proposed to catalyze the *mer* bypass reaction sequence, including a fusion protein of formaldehyde-activating enzyme (FaeA) and hexulose-6-phosphate synthase (Hps), and an alcohol dehydrogenase. However, all genes showed low expression in both ANME-1 (Tab. S2), which argues against their involvement in the methane catabolism. Furthermore, the FaeA/Hps enzyme is probably necessary for the ribose phosphate synthesis (Goenrich *et al.*, 2005). As alternative to a bypass Stokke and colleagues (2012) proposed a substitution of Mer

by a methylenetetrahydrofolate (methylene-H4F) reductase (MetF) in ANME-1. MetF is a Mer analog that acts on similar substrates and may be a suitable candidate to replace Mer. Mer catalyzes the F_{420}-dependent conversion of methylene-H4MPT to methyl-H4MPT while in MetF the reduction of methylene-H4F is NADH-dependent and proceeds via two steps in which first NADH reduces FAD and reduced FADH2 reduces methylene-H4T to methyl-H4T (Maden, 2000; Shima *et al.*, 2000). MetF and additionally a MetV gene, which was reported to associate with MetF (Bertsch *et al.*, 2015) is present in the ANME-1b dataset of Meyerdierks and colleagues (2010). Additionally, these genes were present and expressed in the meso- and thermophilic ANME-1. In some organisms MetFV were shown to form a complex with RnfC or with HdrABCD and MvhD. These additional subunits were proposed as alternative electron entry points (Mock *et al.*, 2014; Bertsch *et al.*, 2015). In principle, in ANME-1 such a MetFV/HdrABC complex could exist and engage in electron transport. Together these data support the notion that a modified methanogenesis pathway, lacking the Mer protein and utilizing the MetFV enzyme may operate in ANME-1. Such a modification in the enzyme series of the methanogenesis pathway would be a characteristic of the ANME-1 which distinguishes these methanotrophic archaea from their methanogenic counterparts and also from the related ANME-2 in which a complete methanogenesis pathway was detected (Wang *et al.*, 2014). Tetrahydrofolate-dependent enzymes like MetFV are usually found in non-methanogenic organisms such as *Eukaryotes*, *Bacteria* and some *Archaea* (Thauer, 1998). In *Methanosarcina* spp. these genes are proposed to involve in C1 metabolism from serine/glycine and they seemed to originate from lateral gene transfer from a bacterial donor (Deppenmeier *et al*., 2002; Buchenau and Thauer, 2004). The MetFV in ANME-1 are also likely acquired by horizontal gene transfer from bacteria. This hypothesis is supported by a comparison of the ANME-1 MetV and MetF proteins to the NCBI non-redundant protein database. The closest matches of ANME-1 MetV proteins were to bacterial MetV genes. For the ANME-1 MetF closest matches again included many bacterial MetF genes but the top hits derived from miscellaneous *Crenarchaeota* (unpublished) and *Lokiarchaeota* (Spang *et al.*, 2015), respectively. Currently, ANME-1 seems to be among the few *Archaea* containing a methylene-H4T reductase and unique in that it possibly employs this enzyme in the methanogenesis pathway. Yet, biochemical characterization of MetFV in ANME-1 is required to elucidate its mechanisms and structural composition and to verify the hypothetical function in methane turnover.

Carbon assimilation in ANME-1

The mesophilic and thermophilic ANME-1 studied here produce their biomass from the assimilation of carbon dioxide (Wegener *et al.*, 2008; Kellermann *et al.*, 2012; Wegener *et al*., submitted). Hence it might be more accurate for ANME-1 to be referred to as chemoorganoautotrophs than as methanotrophs, considering that methanotrophy would imply direct assimilation of methane carbon (Kellermann *et al.*, 2012). In the meso- and thermophilic ANME-1 we found expression of the genes encoding a CO dehydrogenase/acetyl CoA synthase (CODH/ACS) complex, the key enzyme of the reductive acetyl CoA pathway for carbon fixation (Fig. 5, Tab. S2). This is in agreement with the previous report of this enzyme in the ANME-1b dataset (Meyerdierks *et al.*, 2005, 2010). The CODH/ACS complex combines a carbonyl and methyl group with CoA to yield acetyl CoA, a central metabolite of the cell (Fuchs, 2011). In methanogens utilizing the reductive acetyl CoA pathway a tetrahydromethanopterin bound methyl group is produced via the enzymatic steps of methanogenesis. In ANME-1, employing the reversal of the methanogenesis pathway, a tetrahydromethanopterin bound methylgroup is produced from methane. However, the observed absence of transfer of methane-derived carbon into biomass implies that also in ANME-1 a carbon dioxide-derived methyl group is assimilated. Hence ANME-1 possibly utilizes the enzymes of the methanogenesis pathway partially in a reductive direction to generate a carbon dioxide-derived methyl group. Indications for CO_2 fixation via an alternative pathway were not found in the present genomic dataset. A characteristic of the reductive acetyl CoA pathway is its simultaneous fixation of CO_2 and generation of ATP, when acetyl CoA is converted to acetate (Fuchs, 2011). Employing such a pathway may be advantageous for the generally energy limited ANME, however the genes required for acetyl CoA conversion to acetate were only partially detected and low expressed (see Tab. S3). It is probably also energy efficient for ANME to utilize the same enzyme complexes for carbon fixation that are already available in the cell for energy metabolism. However, utilizing the same enzymes in opposite directions will require specific mechanisms to regulate the direction or a spatial separation within the cell.

Nitrogen and sulfur metabolism in ANME-1

We further investigated the meso- and thermophilic ANME-1 for their metabolic potential regarding nitrogen and sulfur metabolism. Ammonium is likely the source of nitrogen to the here investigated ANME-1 types as in both draft genomes we identified the genes for glutamate synthase and glutamine synthetase which are required for the two step conversion

of ammonium to glutamate. Next to those genes Meyerdierks and colleagues (2010) identified a branched amino acid transporter in the psychrophilic ANME-1, which they interpreted as second way of nitrogen assimilation in ANME. Also the thermophilic ANME-1 encodes such a five subunit transporter system, of which the ligand binding subunit showed elevated expression (see Tab. S3). The in this subunit identified type I periplasmic ligand binding domain is found in active ABC transport systems predicted to function in the uptake of amino acids, peptides or inorganic ions, but ligand specificity is not experimentally determined. Because of its elevated expression it may be speculated that this protein in ANME-1 is also involved in transport of substrates other than branched amino acids. Such a transporter complex was not detected in the mesophilic ANME-1 draft genome, which may present differences in the nitrogen sources utilized by the ANME-1 types. However, it may also be that the respective genes are hidden in yet missing parts of the genome. Genes encoding nitrate- or nitrite-reducing capabilities (nitrate and nitrite reductase) were not found. All three ANME-1 genomes encode an incomplete set of genes required for nitrogen fixation (*nif* genes) including genes with similarity to *nifH*, encoding dinitrogenase reductase (see Tab. S3). In meso- and thermophilic ANME-1 the *nifH* gene showed almost no expression, as also all other detected nitrogen fixation related genes. This lack of expression together with the incompleteness of the *nif* gene set and the phylogenetic placement of the *nifH* of ANME-1 in *nifH* group IV (representing non-functional *nifH*; Dekas *et al*., 2015) suggest that ANME-1 do not assimilate molecular nitrogen. This contrasts the proposed nitrogen fixation capability of ANME-2 archaea as observed by stable isotope labeling experiments (Dekas *et al*., 2009, 2015). While nitrogen fixation in ANME-1 awaits further experimental elucidation it is intriguing that energy-limited organisms such as ANME should invest into nitrogen fixation (16 ATP per N_2 fixed) as they also inhabit ammonium-rich habitats.

Genes involved in sulfur metabolism in meso- and thermophilic ANME-1 largely correlate with those reported by Meyerdierks and colleagues (2010). Encoded were a sulfur transporter, an ATP sulfurylase, an APS kinase and an assimilatory sulfite reductase (see Tab. S3). All genes showed low expression levels suggesting that they were less important for ANME-1 metabolism under the given growth conditions. As previously suggested, due to energetic reasons and because of the abundance of sulfide ANME may rather assimilate sulfur from its reduced form (Meyerdierks *et al*., 2010). Our results contradict dissimilatory sulfur metabolism in ANME, if present it would need to proceed via yet unknown enzymes.

Intracellular electron transport and energy conversion in ANME-1

The complete oxidation of a molecule of methane by reverse methanogenesis releases eight electrons. To sustain metabolism ANME-1 require efficient mechanisms for electron transport and removal. As an internal terminal electron sink in ANME is not present (Meyerdierks *et al*., 2010; Wang *et al*., 2014; this study) electrons are thought to be transferred across the cell membrane to an external sink (i.e. a syntrophic partner). Electrons liberated during methane oxidation are transferred to the electron carriers ferredoxin (Fd) or F_{420} generating Fd_{red} and $F_{420}H_2$ which are recycled by deposition of electrons to other redox active compounds. The mesophilic and thermophilic ANME-1 genomes encode a membrane-bound $F_{420}H_2$:quinone oxidoreductase (Fqo) complex, previously observed in the ANME-1 dataset (Meyerdierks *et al*., 2010), which was described in *Archaeoglobus fulgidus* and shows similarity to the NADH dehydrogenase complex (Brüggemann *et al*., 2000). This complex supposedly couples the reoxidation of reduced F_{420} to the export of protons across the membrane and the transfer of electrons to a membrane-associated electron carrier. The potential electron carrier is yet not known, but in *A. fulgidus* was proposed as special form of a menaquinone. Proton translocation at the Fqo complex contributes to generation of an electrochemical gradient for ATP synthesis. Furthermore, both here analyzed ANME-1 draft genomes encode a multi-subunit H^+/Na^+ antiporter and a V-type ATP synthase (see Tab. S3) for energy conservation. The reduced Fd produced in the last step of methane oxidation was proposed to be reoxidized at the membrane-bound electron-translocating complex (Rnf complex) in ANME-2 (Wang *et al*., 2014). Genes encoding this complex are however absent in all available ANME-1 datasets and the mechanisms of Fd recycling is yet unknown. In hydrogenotrophic methanogens a membrane-bound Ech hydrogenase couples Fd reduction to hydrogen oxidation (Thauer *et al*., 2008). Consequently a reverse operating reaction in methanotrophs would recycle reduced Fd with the generation of hydrogen. Although a hydrogenase was observed in the ANME-1b dataset (Meyerdierks *et al*., 2010) the draft genomes of meso- and thermophilic ANME-1 as also the ANME-2 genome draft (Wang *et al*., 2014) contain no catalytic subunits of hydrogenases. Hence protons are unlikely the terminal electron acceptor for methane oxidation. The in the initial step of methane oxidation utilized heterodisulfide of CoM and CoB is regenerated by a heterodisulfide reductase complex. The ANME-1 datasets encodes subunits of soluble HdrABC but lack the respective membrane-bound variant (HdrDE) of the complex which was detected in ANME-2 (Meyerdierks *et al*., 2010; Stokke *et al*., 2012; Wang *et al*., 2014). The acceptor for electrons liberated in the heterodisulfide reductase reactions is unknown in ANME-1. Delta subunits of

the methyl viologen hydrogenase, detected in all ANME-1 genomes may function as an electron transferring subunit interacting with HdrABC, hence electrons might be further transferred from the HdrABC complex to a membrane-bound complex as proposed previously (Meyerdierks *et al.*, 2010). The available ANME-1 genomes all encode a set of c-type cytochromes, some predicted to be located extracellular. These cytochromes may play a crucial role in energy metabolism of ANME-1 as they possibly could act as extracellular sink for the methane-derived electrons (Meyerdierks *et al.*, 2010; McGlynn *et al*., 2015; Wegener *et al*., 2015). Electrons deposited in the membrane-associated redox carrier pool (e.g. by the Fqo complex) could be transferred to the extracellular cytochrome pool via an interacting membrane-bound enzyme complex. However, as to date no candidate for such an enzyme could be described, the mechanisms of coupling electron flow to extracellular cytochromes remain unclear.

Interaction of ANME-1 with their partner bacteria

The genomic information obtained here supports functioning of reverse methanogenesis in ANME and sulfate reduction in partner bacteria as suggested before (Boetius *et al*., 2000; Wegener *et al*., 2015). However, a transfer of molecular intermediates including hydrogen could be excluded based on the absence of hydrogenases (see above). This is consistent with previous experiments that found a lack of hydrogen production in ANME or a lack of response of the partner bacteria to hydrogen addition (Nauhaus *et al.*, 2005; Moran *et al.*, 2008; Wegener *et al.*, 2015). Furthermore, genes of dissimilatory sulfur metabolism were not detected (Meyerdierks *et al*., 2010) and disproportionation in the partner bacteria were not observed (Wegener *et al*., 2015; Wegener *et al*., submitted), excluding partial sulfate reduction in ANME-1. In contrast, for thermophilic AOM consortia a direct electron transfer via extracellular cytochromes and conductive structures was suggested (Wegener *et al.*, 2015). Consistently with previous reports from thermophilic ANME-1, we detected expression of c-type cytochromes in the mesophilic ANME-1 (Fig. 6, Tab. S4) (Wegener *et al.*, 2015). In thermophilic ANME-1, the cytochrome with highest expression has a predicted potential extracellular location. For the mesophilic ANME, the localization of the highest expressed cytochromes could not be predicted, however it could be outside the cell. Consistently, also the psychrophilic ANME-1 contains cytochromes with potentially extracellular localization (Meyerdierks *et al.*, 2010). The presence of potentially extracellular cytochromes in the different ANME-1 with high expression suggests that these cytochromes serve in electron shuttling in ANME-1-dominated consortia. When we searched the ANME-1

draft genomes for genes encoding potential extracellular structures, we detected an incomplete set of genes related to the archaeal flagellum (archaellum), which resembles a bacterial type IV pilus (Albers *et al*., 2015), in both datasets. It may be speculated that also the archaellum can exhibit conductive properties just like bacterial nanowires. Genes encoding flagellin (or putative flagellin) showed elevated expression in both ANME-1, while all other archaellum-related genes however showed almost no expression (see Tab. S4). Still this suggests a function of these proteins in AOM consortia and the identification of the origin of nanowire structures in AOM consortia requires further attention.

As expression of cytochrome and pili in the partner bacteria were proposed to enable the archaeal-bacterial interaction in thermophilic AOM (Wegener *et al.*, 2015), we searched the preliminary genome bin (90% complete) of the bacterial partner of mesophilic ANME-1, Seep-SRB-2, for c-type cytochrome and type IV pili-related genes. Indeed, also Seep-SRB-2 encodes several cytochromes and an almost complete set of pili genes. As observed for the bacterial partner in thermophilic AOM cytochrome expression was partially high in Seep-SRB-2. The *pilA* gene, encoding the major pilin subunit, however showed instead lower expression than observed for HotSeep-1 when growing in thermophilic AOM. This finding indicates a generally lower abundance of pili-based nanowire connections in ANME-1/Seep-SRB-2 consortia. This might reflect the internal structuring of ANME-1/Seep-SRB-2 consortia, which appear to be more densely packed and therefore would not require wire-like connections to bridge distances between the partners. Visualization of the intercellular space in mesophilic consortia (e.g. by transmission electron microscopy) is required to complement transcriptomic data and to verify pili-like structures in these consortia. Instead of pili-like connections a direct cytochrome-cytochrome bridge might also be sufficient for electron transfer (Meyerdierks *et al.*, 2010; McGlynn *et al.*, 2015). Large multi-heme cytochromes associated with the archaeal S-layer in ANME-2/DSS consortia were reported to conduct electrons between the partners (McGlynn *et al.*, 2015). We searched the meso- and thermohilic ANME-1 draft genomes for such a cytochrome type but did not detect this kind of cytochrome. This is consistent with the absence of these cytochromes in ANME-1 as reported by McGlynn and colleagues (2015). The largest multi-heme cytochromes we found in ANME-1 contained only 9 hemes, while bacterial partners contained cytochromes with up to 26 hemes. In particular, these multi-heme cytochromes however were only poorly expressed (Tab. S5). We suggest that cytochromes detected in and expressed by ANME-1 and their bacterial partner may fulfill similar functions despite different properties such as cytochrome type, heme content and S-layer fusion. The present

data indicate that mechanisms of the archaeal-bacterial interaction in ANME-1-dominated consortia, including the involvement of different cytochromes, pili and archaellum in electron transfer, might be more diverse than anticipated.

Conclusion

We studied the metagenomic and transcriptomic information of ANME-1 archaea and their partner bacteria in sediment-free meso- and thermophilic AOM consortia. The genomes of meso- and thermophilic ANME-1 are with estimated sizes of 1.5 Mb only half the genome size previously estimated for ANME-1 and ANME-2 (Meyerdierks *et al*., 2010; Wang *et al*., 2014). We showed expression of all methanogenesis pathway genes, except for the *mer* gene, in the meso- and thermophilic ANME-1 and together with previous observations on ANME-1 datasets suggest that ANME-1 employ a modified reverse methanogenesis pathway. This would involve a replacement of Mer by the tetrahydrofolate-dependent enzyme MetFV, which is usually found in non-methanogens. Biochemical analysis will be required to test functioning of MetFV in ANME-1. However, a reverse methanogenesis pathway in ANME-1 employing a gene of likely bacterial origin would present a unique characteristic of these methanotrophs. With respect to recent proposed archaea-bacteria interactions in AOM consortia we showed that both meso- and thermophilic ANME-1 and their bacterial partner express c-type cytochromes. This may indicate a general function of c-type cytochromes in the interspecies interaction in AOM consortia. In contrast to thermophilic AOM, in the mesophilic partner bacterium type IV pili are poorly expressed. The absence of pili structures in the mesophilic consortia remains to be shown by complementary visualization techniques. However, it may as well be that interaction mechanisms in AOM consortia, even within different ANME-1-dominated consortia are versatile and not dependent on one single strategy. The hypothesis of direct electron transfer in AOM and the mechanisms by which diverse ANME/SRB consortia possibly achieve it needs further systematic experimental investigation.

Acknowledgements

We thank Susanne Menger for culture maintenance, Mirja Meiners for laboratory assistance and Ines Kattelmann for supporting library preparation and sequencing. We also thank chief scientist Andreas Teske and the RV ATLANTIS and ALVIN team of cruise AT15-56 (2009) for providing the initial sediment material. Furthermore we greatly appreciate the bioinformatics support from Michael Richter. We acknowledge the funding of this project by the DFG Leibniz program to Antje Boetius, the DCO Deep Life program to Gunter Wegener, and by the DFG excellence cluster MARUM, Center of Marine Environmental Sciences, Bremen.

References

Albertsen M, Hugenholtz P, Skarshewski A, Nielsen KL, Tyson GW, Nielsen PH. (2013). Genome sequences of rare, uncultured bacteria obtained by differential coverage binning of multiple metagenomes. *Nature* **31**: 533–538.

Albers S-V, Jarrell KF. (2015). The archaellum: how Archaea swim. *Front Microbiol* **6**: 23.

Altschul SF, Gish W, Miller W, Myers EW, Lipman DJ. (1990). Basic local alignment search tool. *J Mol Biol* **215**: 403–410.

Bankevich A, Nurk S, Antipov D, Gurevich AA, Dvorkin M, Kulikov AS, *et al.* (2012). SPAdes: a new genome assembly algorithm and its applications to single-cell sequencing. *J Comput Biol* **19**: 455–477.

Bateman A, Coin L, Durbin R, Finn RD, Hollich V, Griffith-Jones S, *et al.* (2004). The Pfam protein families database. *Nucleic Acids Res* **32**: D138–D141.

Bertsch J, Öppinger C, Hess V, Langer JD, Müller V. (2015). Heterotrimeric NADH-oxidizing methylenetetrahydrofolate reductase from the acetogenic bacterium *Acetobacterium woodii*. *J Bacteriol* **197**: 1681–1689.

Boetius A, Ravenschlag K, Schubert CJ, Rickert D, Widdel F, Gieseke A, *et al.* (2000). A marine microbial consortium apparently mediating anaerobic oxidation of methane. *Nature* **407**: 623–626.

Boetius A, Wenzhöfer F. (2013). Seafloor oxygen consumption fuelled by methane from cold seeps. *Nature Geosci* **6**: 725–734.

Boetzer M, Henkel CV, Jansen HJ, Butler D, Pirovano W. (2010). Scaffolding pre-assembled contigs using SSPACE. *Bioinformatics* **27**: 1–2.

Boetzer M, Pirovano W. (2012). Toward almost closed genomes with GapFiller. *Genome Biol* **13**: R56.

Brüggemann H, Falinsky F, Deppenmeier U. (2000). Structure of the $F_{420}H_2$:quinone oxidoreductase of *Archaeoglobus fulgidus*. *Eur J Biochem* **267**: 5810–5814.

Buchenau B, Thauer RK. (2004). Tetrahydrofolate-specific enzymes in *Methanosarcina barkeri* and growth dependence of this methanogenic archaeon on folic acid or p-aminobenzoic acid. *Arch Microbiol* **182**: 313–325.

Dekas AE, Poretsky RS, Orphan VJ. (2009). Deep-sea archaea fix and share nitrogen in methane-consuming microbial consortia. *Science* **326**: 422–426.

Dekas AE, Connon SA, Chadwick GL, Trembath-Reichert E, Orphan VJ. (2015). Activity and interactions of methane seep microorganisms assessed by parallel transcription and FISH-NanoSIMS analyses. *ISME J* **10**: 678–692.

Deppenmeier U, Johann A, Hartsch T, Merkl R, Schmitz RA, Martinez-Arias R, *et al.* (2002). The genome of *Methanosarcina mazei*: evidence for lateral gene transfer between Bacteria and Archaea. *J Mol Microbiol Biotechnol* **4**: 453–461.

Doddema HJ, Vogels GD. (1978). Improved identification of methanogenic bacteria by fluorescence microscopy. *Appl Environ Microbiol* **36**: 752–754.

Eddy SR (1998). Profile hidden Markov models. *Bioinformatics* **14**: 755–763.

Fuchs G. (2011). Alternative pathways of carbon dioxide fixation: insights into the early evolution of life? *Annu Rev Microbiol* **65**: 631–658.

Goenrich M, Thauer RK, Yurimoto H, Kato N. (2005). Formaldehyde activating enzyme (Fae) and hexulose-6-phosphate synthase (Hps) in *Methanosarcina barkeri*: a possible function in ribose-5-phosphate biosynthesis. *Arch Microbiol* **184**: 41–48.

Gurevich A, Saveliev V, Vyahhi N, Tesler G. (2013). QUAST: quality assessment tool for genome assemblies. *Bioinformatics* **29**: 1072–1075.

Haft DH, Selengut JD, White O. (2003). The TIGRFAMs database of protein families. *Nucleic Acids Res*. **31**: 371–373.

Hallam SJ, Putnam N, Preston CM, Detter JC, Rokhsar D, Richardson PM, *et al*. (2004). Reverse methanogenesis: testing the hypothesis with environmental genomics. *Science* **305**: 1457–1462.

Hoehler TM, Alperin MJ, Albert DB, Martens CS. (1994). Field and laboratory studies of methane oxidation in an anoxic marine sediment: evidence for a methanogen-sulfate reducer consortium. *Global Biogeochem Cycles* **8**: 451–463.

Holler T, Widdel F, Knittel K, Amann R, Kellermann MY, Hinrichs K-U, *et al.* (2011). Thermophilic anaerobic oxidation of methane by marine microbial consortia. *ISME J* **5**: 1946–1956.

Kellermann MY, Wegener G, Elvert M, Yukio MY, Lin Y-S, Holler T, *et al*. (2012). Autotrophy as a predominant mode of carbon fixation in anaerobic methane-oxidizing microbial communities. *Proc Natl Acad Sci USA* **109**: 19321–19326.

Kleindienst S, Ramette A, Amann R, Knittel K. (2012). Distribution and *in situ* abundance of sulfate-reducing bacteria in diverse marine hydrocarbon seep sediments. *Environ Microbiol* **14**: 2689–2710.

Knittel K, Boetius A, Lemke A, Eilers H, Lochte K, Pfannkuche O, *et al*. (2003). Activity, distribution, and diversity of sulfate reducers and other bacteria in sediments above gas hydrate (Cascadia Margin, Oregon). *Geomicrobiol J* **20**: 269–294.

Knittel K, Boetius A. (2009). Anaerobic oxidation of methane: progress with an unknown process. *Annu Rev Microbiol **63**:311–334*.

Krüger M, Meyerdierks A, Glöckner FO, Amann R, Widdel F, Kube M, *et al.* (2003). A conspicuous nickel protein in microbial mats that oxidize methane anaerobically. *Nature* **426**: 878–881.

Li B, Ruotti V, Stewart RM, Thomson JA, Dewey CN. (2010). RNA-Seq gene expression estimation with read mapping uncertainty. *Bioinformatics* **26**: 493–500.

Lloyd KG, Alperin MJ, Teske A. (2011). Environmental evidence for net methane production and oxidation in putative ANaerobic MEthanotrophic (ANME) archaea. *Environ Microbiol* **13**: 2548–2564.

Maden BEH. (2000). Tetrahydrofolate and tetrahydromethanopterin compared: functionally distinct carriers in C_1 metabolism. *Biochem J* **350**: 609–629.

McGlynn SE, Chadwick GL, Kempes CP, Orphan VJ. (2015). Single cell activity reveals direct electron transfer in methanotrophic consortia. *Nature* **526**: 531–535.

Merkel AY, Huber JA, Chernyh NA, Bonch-Osmolovskaya EA, Lebedinsky AV. (2013). Detection of putatively thermophilic anaerobic methanotrophs in diffusive hydrothermal vent fluids. *Appl Environ Microbiol* **79**: 915–923.

Meyerdierks A, Kube M, Lombardot T, Knittel K, Bauer M, Glöckner FO, *et al.* (2005). Insights into the genomes of archaea mediating the anaerobic oxidation of methane. *Environ Microbiol* **7**: 1937–1951.

Meyerdierks A, Kube M, Kostadinov I, Teeling H, Glöckner FO, Reinhardt R, *et al.* (2010). Metagenome and mRNA expression analyses of anaerobic methanotrophic archaea of the ANME-1 group. *Environ Microbiol* **12**: 422–439.

Michaelis W, Seifert R, Nauhaus K, Treude T, Thiel V, Blumenberg M, *et al.* (2002). Microbial reefs in the Black Sea fueled by anaerobic oxidation of methane. *Science* **297**: 1013–1015.

Milucka J, Ferdelman TG, Polerecky L, Franzke D, Wegener G, Schmid M, *et al.* (2012). Zero-valent sulphur is a key intermediate in marine methane oxidation. *Nature* **491**: 541–546.

Mock J, Wang S, Huang H, Kahnt J, Thauer RK. (2014). Evidence for a hexaheteromeric methylenetetrahydrofolate reductase in *Moorella thermoacetica*. *J Bacteriol* **196**: 3303–3314.

Moran JJ, Beal EJ, Vrentas JM, Orphan VJ, Freeman KH, House CH. (2008). Methyl sulfides as intermediates in the anaerobic oxidation of methane. *Environ Microbiol* **10**: 162–173.

Nauhaus K, Treude T, Boetius A, Krüger M. (2005). Environmental regulation of the anaerobic oxidation of methane: a comparison of ANME-I and ANME-II communities. *Environ Microbiol* **7**: 98–106.

Niemann H, Lösekann T, de Beer D, Elvert M, Nadalig T, Knittel K, *et al.* (2006). Novel microbial communities of the Haakon Mosby mud volcano and their role as a methane sink. *Nature* **443**: 854–858.

Orphan VJ, Hinrichs K-U, Ussler W III, Paull CK, Taylor LT, Sylva SP, *et al.* (2001a). Comparative analysis of methane-oxidizing archaea and sulfate-reducing bacteria in anoxic marine sediments. *Appl Environ Microbiol* **67**: 1922–1934.

Orphan VJ, House CH, Hinrichs K-U, McKeegan KD, DeLong EF. (2001b). Methane-consuming archaea revealed by directly coupled isotopic and phylogenetic analysis. *Science* **293**: 484–487.

Parks DH, Imelfort M, Skennerton CT, Hugenholtz P, Tyson GW. (2015). CheckM: assessing the quality of microbial genomes recoverd from isolates, single cells, and metagenomes. *Genome Res* **25**: 1043–1055.

Pernthaler A, Amann R. (2004). Simultaneous fluorescence *in situ* hybridization of mRNA and rRNA in environmental bacteria. *Appl Environ Microbiol* **70**: 5426–5433.

Probst AJ, Weinmaier T, Raymann K, Perras A, Emerson JB, Rattei T, *et al.* (2014). Biology of a widespread uncultivated archaeon that contributes to carbon fixation in the subsurface. *Nat Commun* **5**: 1–13.

Reitner J, Peckmann J, Blumenberg M, Michaelis W, Reimer A, Thiel V. (2005). Concretionary methane-seep carbonates and associated microbial communities in Black Sea sediments. *Palaeogeogr Palaeoclimatol Palaeoecol* **227**: 18–30.

Ruff SE, Biddle JF, Teske AP, Knittel K, Boetius A, Ramette A. (2015). Global dispersion and local diversification of the methane seep microbiome. *Proc Natl Acad Sci USA* **112**: 4015–4020.

Seemann T. (2014). Prokka: rapid prokaryotic genome annotation. *Bioinformatics* **30**: 2068–2069.

Shima S, Warkentin E, Grabarse W, Sordel M, Wicke M, Thauer RK, *et al.* (2000). Structure of coenzyme F_{420} dependent methylenetetrahydromethanopterin reductase from two methanogenic archaea. *J Mol Biol* **300**: 935–950.

Spang A, Saw JH, Jørgensen SL, Zaremba-Niedzwiedzka K, Martijn J, Lind AE, *et al.* (2015). Complex archaea that bridge the gap between prokaryotes and eukaryotes. *Nature* **521**: 173–179.

Stokke R, Roalkvam I, Lanzen A, Haflidason H, Steen IH. (2012). Integrated metagenomic and metaproteomic analyses of an ANME-1-dominated community in marine cold seep sediments. *Environ Microbiol* **14**: 1333–1346.

Strous M, Kraft B, Bisdorf R, Tegetmeyer HE. (2012). The binning of metagenomic contigs for microbial physiology of mixed cultures. *Front Microbiol* **3**: 410.

Thauer RK. (1998). Biochemistry of methanogenesis: a tribute to Marjory Stephenson. *Microbiology* **144**: 2377–2406.

Thauer RK, Shima S. (2008). Methane as fuel for anaerobic microorganisms. *Ann N Y Acad Sci* **1125**: 158–170.

Thauer RK, Kaster A-K, Seedorf H, Buckel W, Hedderich R. (2008). Methanogenic archaea: ecologically relevant differences in energy conservation. *Nat Rev Microbiol* **6**: 579–591.

Wang F-P, Zhang Y, Chen Y, He Y, Qi J, Hinrichs K-U, *et al.* (2014). Methanotrophic archaea possessing diverging methane-oxidizing and electron-transporting pathways. *ISME J* **8**: 1069–1078.

Wegener G, Niemann H, Elvert M, Hinrichs K-U, Boetius A. (2008). Assimilation of methane and inorganic carbon by microbial communities mediating the anaerobic oxidation of methane. *Environ Microbiol* **10**: 2287–2298.

Wegener G, Krukenberg V, Riedel D, Tegetmeyer HE, Boetius A. (2015). Intercellular wiring enables electron transfer between methanotrophic archaea and bacteria. *Nature* **526**: 587–590.

Wegener G, Krukenberg V, Ruff ES, Kellermann MY, Knittel K. (submitted 2015). Metabolic capabilities of microorganisms involved in and associated with the anaerobic oxidation of methane. *Front Microbiol*.

Welander PV, Metcalf WW. (2008). Mutagenesis of the C1 oxidation pathway in *Methanosarcina barkeri*: new insights into the Mtr/Mer bypass pathway. *J Bacteriol* **190**: 1928–1936.

Widdel F, Bak F. (1992). Gram-negative mesophilic sulfate-reducing bacteria. In: *The Prokaryotes*. Balows A, Trüper HG, Dworkin M, Harder W, Schleifer K-H (eds). New York: Springer, pp 3352–3378.

Wu M, Scott AJ. (2012). Phylogenomic analysis of bacterial and archaeal sequences with AMPHORA2. *Bioinformatics* **28**: 1033–1034.

Yarza P, Yilmaz P, Pruesse E, Glöckner FO, Ludwig W, Schleifer KH, *et al.* (2014). Uniting the classification of cultured and uncultured bacteria and archaea using 16S rRNA gene sequences. *Nat Rev Microbiol* **12**: 635–645.

Yu NY, Wagner JR, Laird MR, Melli G, Rey S, Lo R, *et al.* (2010). PSORTb 3.0: improved protein subcellular localization prediction with refined localization subcategories and predictive capabilities for all prokaryotes. *Bioinformatics* **26**: 1608–1615.

Zhou J, Bruns MA, Tiedje JM. (1996). DNA recovery from soils of diverse composition. *Appl Environ Microbiol* **62**: 316–322.

Figures and tables

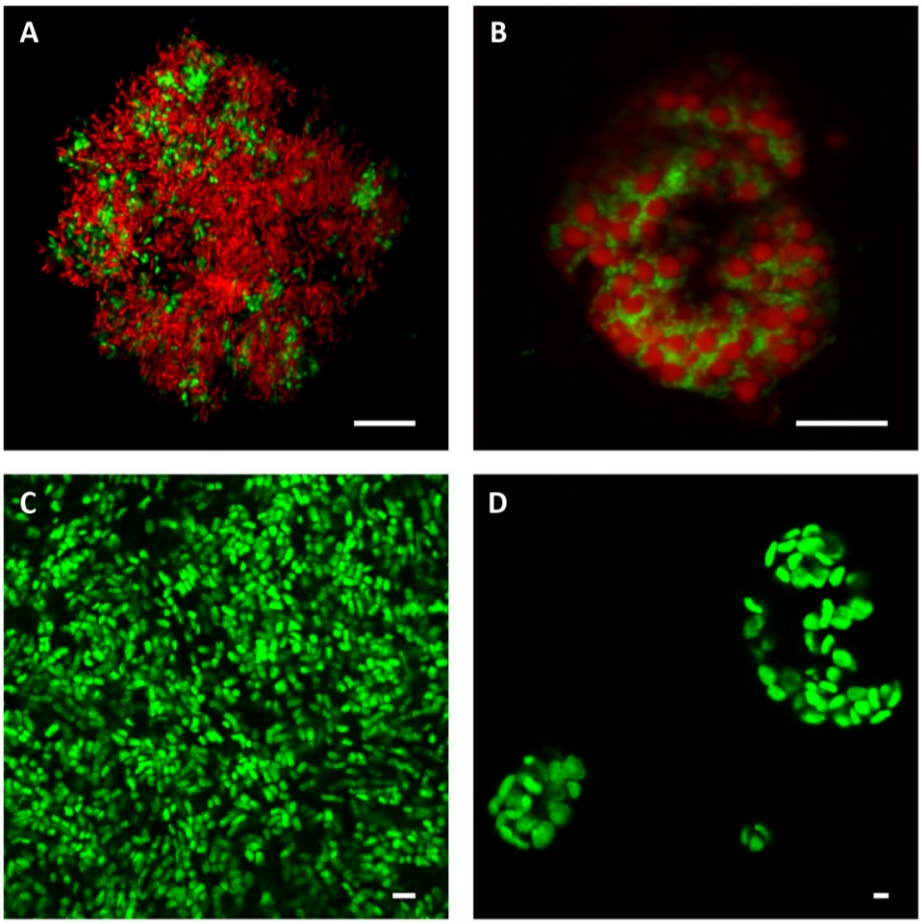

Figure 1 Visualization of the AOM consortia enriched at 60 and 37°C. (**A,B**) Micrograph of CARD-FISH stained cells of (**A**) a thermophilic consortium with ANME-1 cells (red) and HotSeep-1 cells (green), and (**B**) a mesophilic consortium with ANME-1 cells (red) and Seep-SRB-2 cells (green); scale bar: 10 µm. (**C,D**) Autofluorescence of the methanogenic cofactor F_{420} in ANME-1 in (**C**) a section of a thermophilic AOM consortium and (**D**) three mesophilic AOM consortia; scale bar: 2 µm.

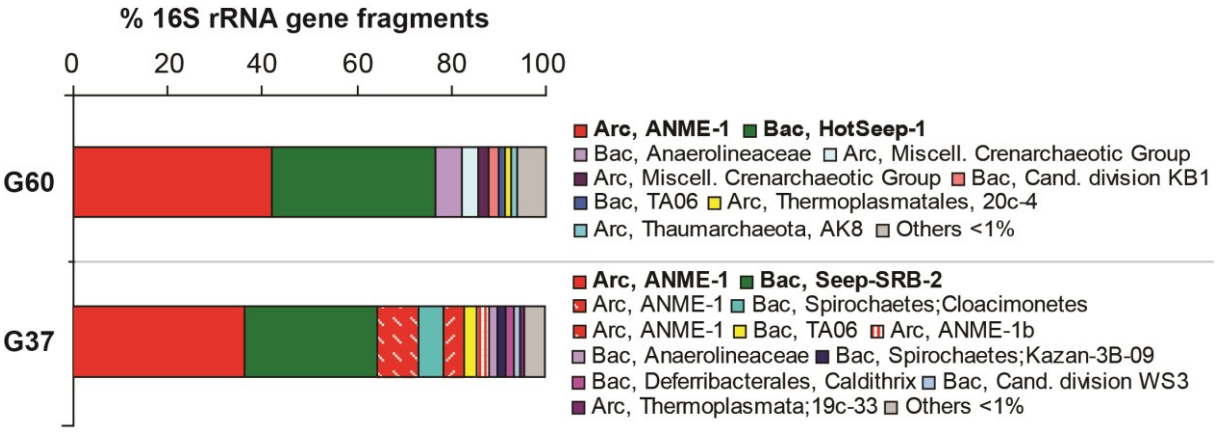

Figure 2 Diversity and relative abundance of 16S rRNA gene fragments recovered from the metagenomic dataset of the meso- and thermophilic AOM enrichments. G60: Thermophilic AOM enrichment dominated by ANME-1 (40%) and HotSeep-1 (35%) related sequences. G37: Mesophilic AOM enrichment dominated by ANME-1 (35%) and Seep-SRB-2 (30%) related sequences.

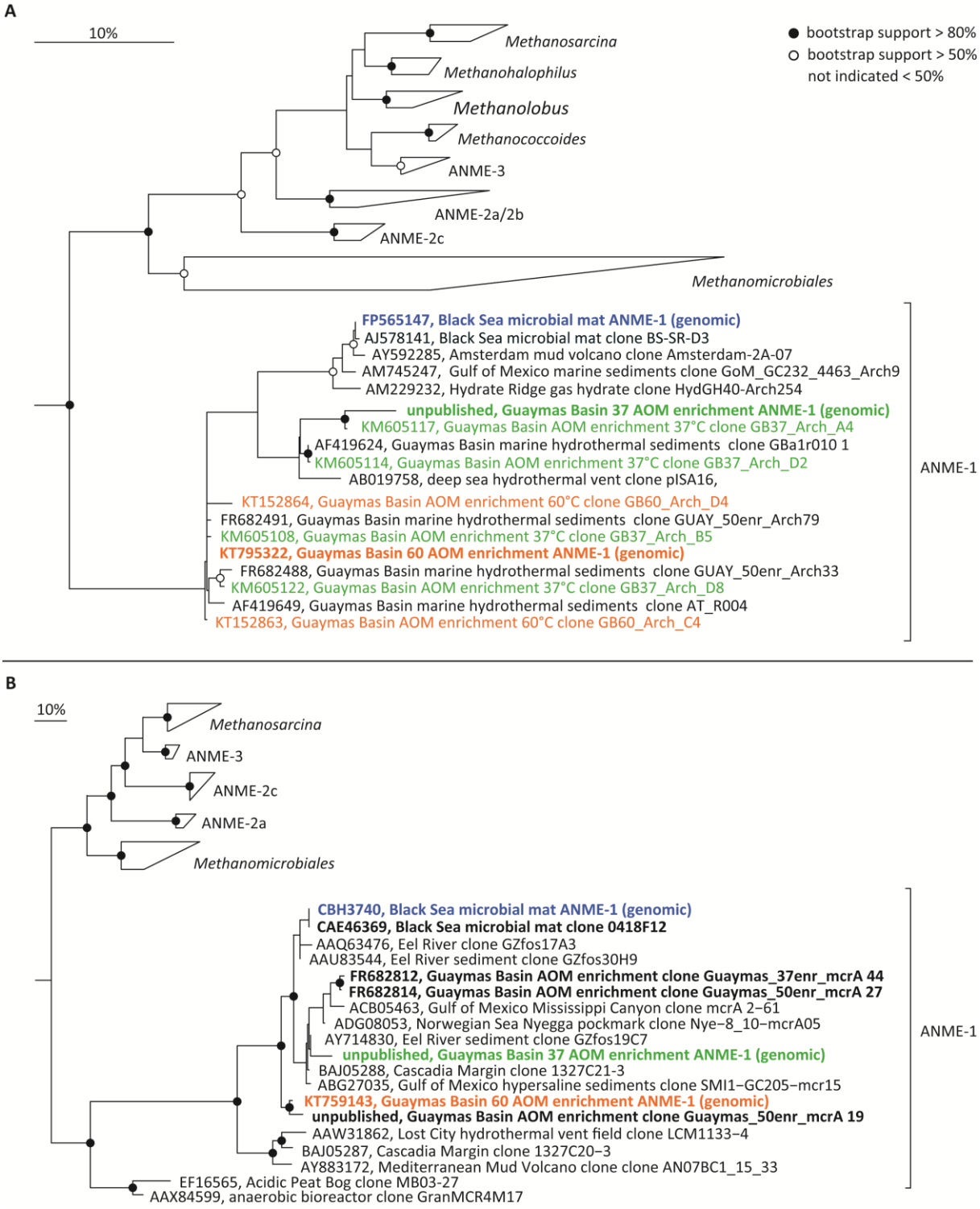

Figure 3 Phylogenetic relatedness of the here studied ANME-1. (**A**) 16S rRNA gene based phylogenetic tree calculated by the maximum likelihood method (RAxML) employing a 50% base frequency filter and 100 bootstrap replicates. The three genomic 16S rRNA gene sequences affiliate in three cluster and share <94% sequence similarity. (**B**) Phylogenetic tree based on the McrA, the key enzyme of the methanogenesis pathway. The tree was calculated from the amino acid sequence alignment of McrA with the maximum likelihood method (RAxML) employing a 50% base frequency filter and 100 bootstrap replicates. The three genomic *mcrA* sequences affiliate in three distinct clusters and share 80% similarity. Genomic sequences are shown in bold. Color code: red, Guaymas Basin 60°C AOM enrichment (G60); green, Guaymas Basin 37°C AOM enrichment (G37); blue, Black Sea microbial mat. Sequences with the same color originate from the same enrichment.

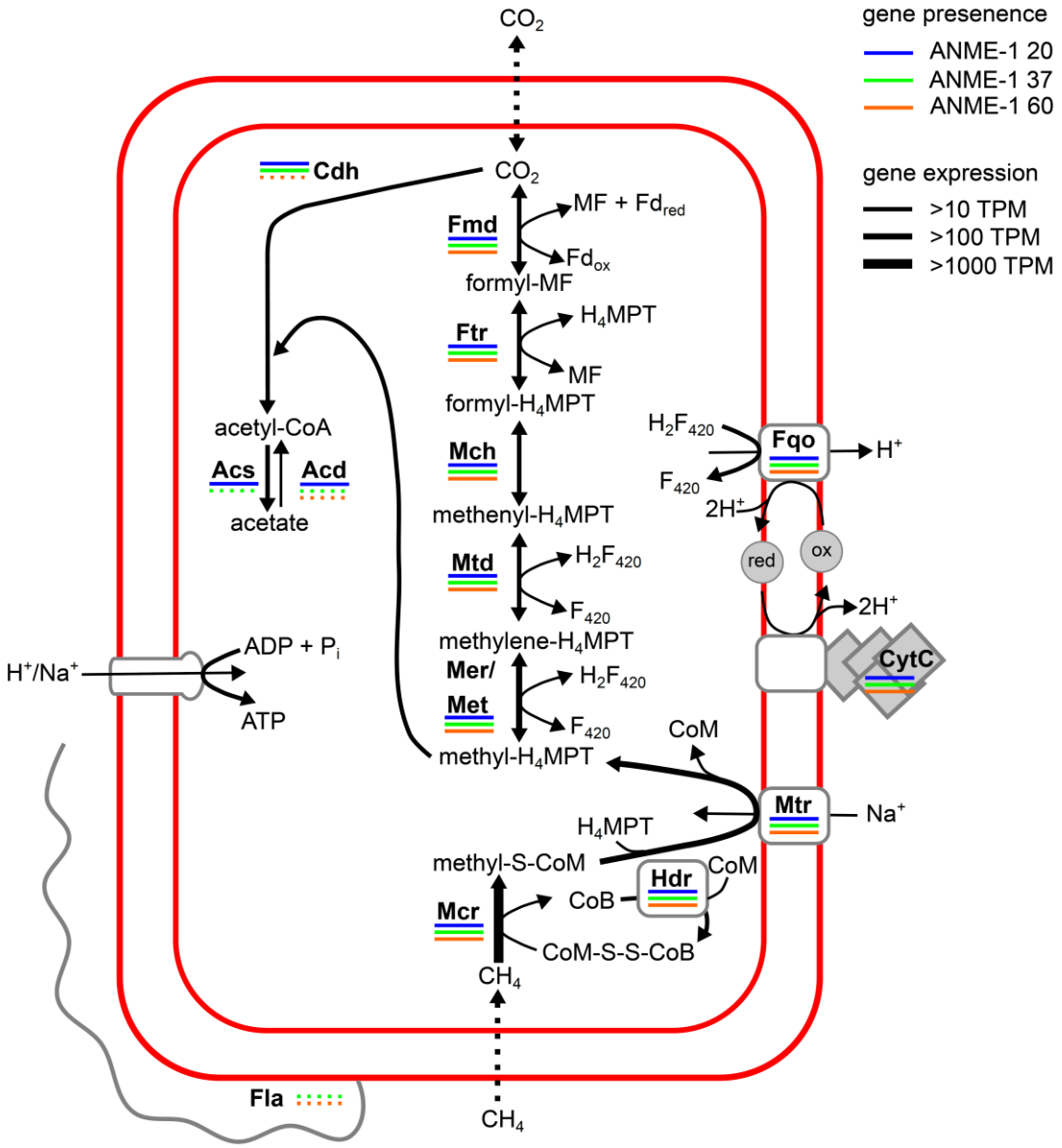

Figure 4 Reconstruction of the central metabolism in ANME-1 from draft genomes of mesophilic, thermophilic and psychrophilic ANME-1 (see Tab. S2, S3, S4). Expression refers to average expression in meso- and thermophilic ANME-1. Color code indicates the presence of the gene in the different ANME-1 draft genomes. Dotted line, not all subunits present. Gene expression expressed as transcripts per million (TPM).

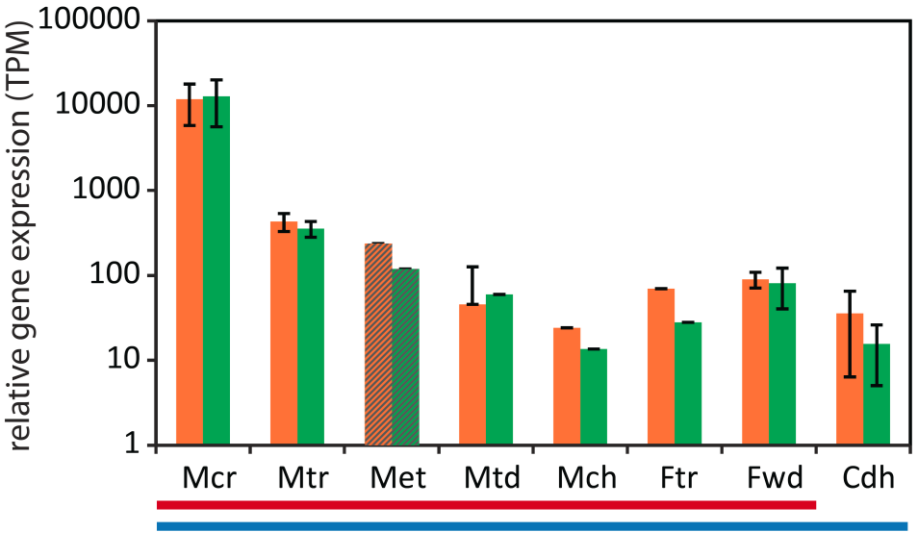

Figure 5 Relative expression of genes attributed to C1 metabolism in ANME-1. Relative gene expression in transcripts per million (TPM) of the genes encoding enzymes of reverse methanogenesis (indicated by red line) and autotrophic CO_2 fixation (indicated by blue line) in mesophilic (green bars) and thermophilic (orange bars) ANME-1. Pattern indicates proposed putative involvement of enzyme in C1 metabolism in ANME-1. Met is proposed to replace Mer, which is absent in ANME-1 draft genomes. Autotrophic CO_2 fixation in ANME-1 is proposed to proceed via the reductive acetyl CoA pathway employing the enzymes of the methanogenesis pathway and additionally the carbon monoxide dehydrogenase/acetyl CoA synthase complex. Bar height indicates average gene expression of multi subunit complexes. If a complex or subunit was present more than once only the one with highest expression is considered here. For Mcr subunits A, B, G were included. Error bar indicates standard deviation of expression between subunits of one complex.

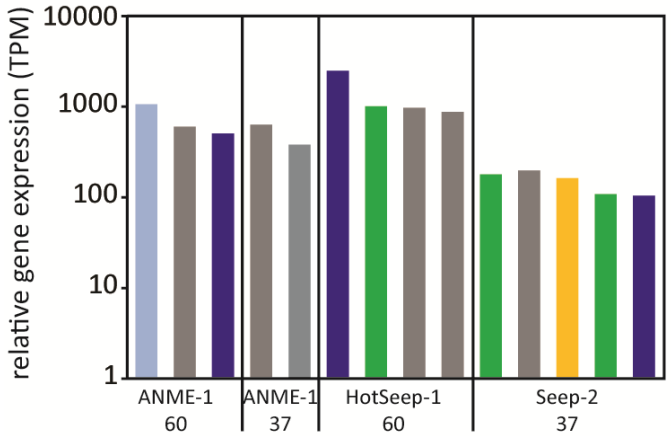

Figure 6 Relative expression of c-type cytochromes in ANME-1 and their bacterial partner. Relative gene expression in transcripts per million (TPM) of cytochromes detected in thermophilic ANME-1, mesophilic ANME-1, HotSeep-1 and Seep-SRB-2 with expression >100 TPM. Color indicates predicted subcellular localization (prediction by PSORTb). Color code: dark blue, extracellular; light blue, putatively extracellular; green, periplasmic; yellow, cytoplasmic; grey, unknown.

Table 1 Overview of the general genome properties and the estimated genome completeness of different ANME-1 draft genomes available.

	ANME-1 60	**ANME-1 37**	**ANME-1 20**
Sample characteristics			
sample source	Guymas Basin enrichment	Guymas Basin enrichment	Black Sea microbial mat
growth temperature (°C)	60°C	37°C	~20°C
dominant AOM organisms	ANME-1/ HotSeep-1	ANME-1/ Seep-SRB-2	ANME-1/ Seep-SRB-1
Genome properties			
assembly size (Mb)	**1.59**	**1.51**	***2.95***
scaffolds	36	4	*13 sc + 17 fs*
% GC	46	52	*43*
ORFs	1635	1493	3618 (*3578*)
rRNAs	3	3	4
tRNAs	41	38	46 (*42*)
Genome completeness			
% tRNAs (20 tRNAs)	**95**	**95**	**88**
tRNAs missing	1 (Tyr)	1 (Tyr)	3 (Tyr, His, Trp)
% SCG (104 *Archaea*-specific genes)	**90**	**91**	**86**
SCGs	98	98	113
SCGs missing	8	8	13
SCGs replicated 2x	2		20
SCGs replicated 3x		1	1
% SCG (189 *Euryarchaeota*-specific genes)	**89**	**92**	**85**
SCGs	171	174	129
SCGs missing	16	11	22
SCGs replicated 2x	2	3	34
SCGs replicated 3x	0	1	4
% contamination	2	4	23
% strain heterogeneity	0	67	78

sc=supercontig; fs=fosmid; values in italic were taken from Meyerdierks *et al*., 2010.

Supplementary information

Supplementary tables

Table S1 Distribution of *Archaea*-specific single copy genes in ANME-1.

Taxon level	ANME-1 60	ANME-1 37	ANME-1 20
Euryarchaeota	86	84	101
Methanosarcinales	37	37	52
Methanomicrobiales	14	18	16
Archaeoglobales	18	9	10
Methanocellales	7	12	15
Methanopyrales	4	3	3
Methanococcales	3	0	1
Methanobacteriales	1	3	0
Halobacteriales	0	1	1
Thermoplasmatales	0	0	2
Thermoccales	0	0	1
Crenarchaeota	1	2	3
Thermoproteales	1	2	1
Desulfurococales	0	0	2
Thaumarchaeota	1	2	0
Nanoarchaeota	0	1	0
Nanoarchaeum	0	1	0
unassigned	10	9	9
unassigned	13	12	9

Table S2 Genes related to C1 metabolism in ANME-1 and their expression in transcripts per million (TPM). Note that no further normalization was applied to compare the data from different organisms.

protein	gene	ANME-1 G60 Locus (gb60anme1_)	ANME-1 G60 TPM	ANME-1 G37 Locus (gb37anme1_)	ANME-1 G37 TPM
reverse methanogenesis					
Methyl coenzyme M reductase subunit A	*mcrA*	00724	12571	00584	10615
Methyl coenzyme M reductase subunit B	*mcrB*	00726	10163	00582	10341
Methyl coenzyme M reductase subunit C	*mcrC*	00399, 01205	64, 80	01061, 00670	42, 18
Methyl coenzyme M reductase subunit D	*mrcD*				
Methyl coenzyme M reductase subunit G	*mcrG*	00725	12838	00583	17605
Tetrahydromethanopterin S-methyltransferase subunit A and F	*mtrAF*	00676, 00984	387, 163	00938	312
Tetrahydromethanopterin S-methyltransferase subunit A or F	*mtrA or mtrF*	00677, 00985	417, 303	00937	329
Tetrahydromethanopterin S-methyltransferase subunit B	*mtrB*	00675, 00983	509, 278	00939	424
Tetrahydromethanopterin S-methyltransferase subunit C	*mtrC*	00674, 00982	328, 221	00616	226
Tetrahydromethanopterin S-methyltransferase subunit D	*mtrD*	00673, 00981	327, 276	00617	390
Tetrahydromethanopterin S-methyltransferase subunit E	*mtrE*	00672, 00980	425, 395	00618	407
Tetrahydromethanopterin S-methyltransferase subunit F	*mtrF*				
Tetrahydromethanopterin S-methyltransferase subunit G	*mtrG*	00678, 00986	399, 415	00936	450
Tetrahydromethanopterin S-methyltransferase subunit H	*mtrH*	00679, 00987	352, 644	00935	306
Coenzyme F420-dependent N5N10-methylene tetrahydromethanopterinreductase	*mer*				
Methylenetetrahydromethanoterin dehydrogenase	*mtd*	00532	45	01147	60
Methenyltetrahydromethanopterincyclohydrolase	*mch*	00374	24	00850	14
Formylmethanofurantetrahydromethanopterin N-formyltransferase	*ftr*	00945, 00328	4, 70	01393, 01391, 00447	28, 12, 2
Formylmethanofuran dehydrogenase subunit A	*fmdA*	00330	94	00160	70
Formylmethanofuran dehydrogenase subunit B	*fmdB*	00331	112	00159, 01286	55, 3
Formylmethanofuran dehydrogenase subunit C	*fmdC*	00329, 00358	67, 0	00161	142
Formylmethanofuran dehydrogenase subunit D	*fmdD*	00332	86	00158	58
putatively involved rev methanogenesis in ANME-1					
methylenetetrahydrofolate reductase subunit F	*metF*	00651, 00653	292, 6	01494	119
methylenetetrahydrofolate reductase subunit V	*metV*	00652	178	01495	118
bifunctional enzyme fae/hps	*fae/hps*	01143, 01118	19, 2	01216, 00127	22, 19
alcohol dehydrogenase	*adh*			00625	3
C1 fixation					
Acetyl-CoA decarbonylase/synthase complex subunit A	*cdhA*	00244	32	0125	24.785
Acetyl-CoA decarbonylase/synthase complex subunit B	*cdhB*	00898	79	00193, 01254	10, 9
Acetyl-CoA decarbonylase/synthase complex subunit C	*cdhC*	00143	18	00908	6.856
Acetyl-CoA decarbonylase/synthase complex subunit D	*cdhD*	00221	14	01249	7.1034
Acetyl-CoA decarbonylase/synthase complex subunit E	*cdhE*			00126	29.03

Table S3 List of selected genes discussed in the main text and their expression value in transcripts per million (TPM). Note that no further normalization was applied to compare the data from different organisms.

protein	gene	ANME-1 G60		ANME-1 G37	
		Locus (gb60anme1_)	TPM	Locus (gb37anme1_)	TPM
nitrogen metabolism					
putative nitrogenase iron protein	*nifH*	00498	2	00426	24
putative nitrogenase-related protein	*nifD*	01602	7	00736	8
nitrogenase cofactor biosynthesis protein	*nifB/Y/X*	01107, 01108	19, 41	00861, 00872	27, 35
nitrogenase cofactor biosynthesis protein	*nifB*			00975	29
glutamate dehydrogenase	*gdhA*	01191	9	00989	32
glutamine synthetase	*glnA*	01194	4	00988	5
putative branched amino acid ABC transporter	*livG*	01342, 00504	15, 4		
putative branched amino acid ABC transporter	*livF*	01343	2		
putative branched amino acid ABC transporter	*livM*	01344, 00505	0, 3		
putative branched amino acid ABC transporter	*livH*	01345, 00506	4, 0		
putative branched amino acid ABC transporter	*livJ/K*	01346	123		
ABC transporter nitrate/sulfonate	*tauB/ntrCD*	00405, 01231	12, 2	01379	4
ABC transporter nitrate/sulfonate	*tauC/ntrB*	00404, 01232	5, 22	01380	8
ABC transporter nitrate/sulfonate	*tauA/ntrA*	00406, 01233	72, 48	01381	20
sulfur metabolism					
sulfate transporter		00384	3	01375	2
adenylylsulfate kinase	*cysC*	00656	7	00679	3
sulfite reductase, assimilatory		00158	10	00976	77
putative sulfur relay protein	*dsrE/F/H*	00642	79	01013, 01529	5, 5
heterodisulfide reductases					
heterodisulfide reductase subunit A	*hdrA*	00537	4	00263, 00734,	1, 2, 112
heterodisulfide reductase subunit B	*hdrB*	00284, 00487	179, 10	00181, 00877	173, 128
heterodisulfide reductase subunit C	*hdrC*	00283, 00689	266, 1	00182, 00347,	144, 1,
heterodisulfide reductase subunit B/C	*hdrB/C*	01238	2		
F420H2:quinone oxidoreductase					
F420H2:quinone oxidoreductase, subunit A	*fqoA*	01254	11	00645	7
F420H2:quinone oxidoreductase, subunit BCD	*fqoBCD*	01255	39	00644	31
F420H2:quinone oxidoreductase, subunit H	*fqoH*	01256	17	00643	27
F420H2:quinone oxidoreductase, subunit L	*fqoL*	01252	19	00647	12
F420H2:quinone oxidoreductase, subunit M	*fqoM*	01251	19	00648	8
F420H2:quinone oxidoreductase, subunit K	*fqoK*	01250	50	00649	24
F420H2:quinone oxidoreductase, subunit J	*fqoJ*	01249	16	00650	7
F420H2:quinone oxidoreductase, subunit N	*fqoN*	01253	9	00646	11
F420H2:quinone oxidoreductase, subunit F	*fqoF*	00238	75	00641	33

Table S3 continued.

NADH oxidoreductase					
NADH oxidoreductase, subunit E	*nuoE*			00621	28
NADH oxidoreductase, subunit F	*nuoF*			00620	25
NADH oxidoreductase, subunit L	*nuoL*	01535	2	00993	5
NADH oxidoreductase, subunit M	*nuoM*	01331, 01333, 01336, 01536	23, 24, 10, 19	00992, 01117, 01119	35, 9, 2
V type ATP synthase					
V-type ATP synthase, subunit A				00252, 01097	7, 10
V-type ATP synthase, subunit B				01411	18
V-type ATP synthase, subunit C		00467	49	01374	60
V-type ATP synthase, subunit D		00195	19	01217	28
V-type ATP synthase, subunit E		00514	13	00519	33
V-type ATP synthase, subunit F		00515	7	00520	29
V-type ATP synthase, subunit H		00513	37	00518	12
V-type ATP synthase, subunit I		00616	6	01354	21
cation transporter					
cation antiporter, subunit B	*mnhB*	01180, 01181, 01182	19, 13, 5	00826, 00827, 00828	29, 12, 4
cation antiporter, subunit C	*mnhC*	01179	9	00829	15
cation antiporter, subunit E	*mnhE*	01183	15	00825	14
cation antiporter, subunit F	*mnhF*	01185	25	00822	8
cation antiporter, subunit G	*mnhG*	01184	18	00824	8
cytochrome C biogenesis					
cytochrome C assembly protein	*ccdA*	01539	1		
putative cytochrome C assembly protein	*ccmA*			00234	4
cytochrome C assembly protein	*ccmB*			00233	4
cytochrome C assembly protein	*ccmC*	00137	4	00355	8
cytochrome C assembly protein	*ccmE*	00139	33	00357	10
cytochrome C assembly protein	*ccmF*	01543	3	01243	4
archaellum					
flagellin	*flaB*	00805, 00806	148, 188		
putative flagellin	*flaB*	00808	1	00521, 01022, 01312, 01313	24, 405, 6, 367
putative flagellar protein	*flaF*	00809	0		
peptidase A24	*flaK*	00906	8	00830	3
flagellar assembly protein	*flaJ*	01290	2		
flagellar accessory protein	*flaH*	01292	2		
archaeallum biosynthesis ATPase	*virB*	01291, 01309	1, 4	00482, 00483	2, 9
putative flagellar assembly protein	*flaJ*	01310, 01311	1, 2	00481	2
flagellar motor protein	*motA*	00081, 00085, 00702, 00939	0, 0, 7, 1		
acetate metabolism					
acetyl CoA ligase	*acs*			1236	11
acetyl CoA synthetase	*acdA*	243, 439	13, 3	124	1

Table S4 Overview of c-type cytochromes detected in different ANME-1. Depicted is the number of hemes as determined by the detected CXXCH motifs, the cytochrome type as according to the best scoring pfamA protein domain model, the predicted subcellular localization according to PSORTb and the expression in transcripts per million (TPM) if available. Note that no further normalization was applied to compare data from different organisms. Data for ANME-1 Guaymas Basin 60 was taken from Wegener *et al*., 2015.

locus	heme number (based on CXXCH motifs)	cytochrome type (according to pfamA domain prediction)	predicted subcellular localization (PSORTb)	relative gene expression data (TPM)
ANME-1 Guaymas Basin 60				
gb60anme1_00109	**4**	**Cytochrome_C7**	**Extracellular**	**506**
gb60anme1_00110	6	Cytochrome_C7	Unknown	19
gb60anme1_00111	9	Cytochrome_C7	Unknown (C or E)	7
gb60anme1_00125	**4**	**Cytochrome_C7**	**Unknown**	**603**
gb60anme1_00239	**8**	**Cytochrom_c3_2**	**Unknown (CM, CW or E)**	**1063**
gb60anme1_01545	5	Cytochrom_c3_2	Cytoplasmic	13
gb60anme1_01542	5	Cytochrom_NNT	Cytoplasmic	73
ANME-1 Guaymas Basin 37				
gb37anme1_00055	5	Cytochrome_C7	Unknown (CM, CW or E)	3
gb37anme1_00335	**4**	**Cytochrome_C7**	**Unknown**	**381**
gb37anme1_01241	5	Cytochrome_C7	Unknown (CM, CW or E)	5
gb37anme1_01244	5	Cytochrom_NNT	Cytoplasmic	86
gb37anme1_00054	9	Cytochrom_NNT	Cytoplasmic	3
gb37anme1_00057	**4**	**Cytochrome_C554**	**Unknown**	**631**
ANME-1 Black Sea				
gnl|3269|SC05_0217	9	Cytochrome_C7	Unknown (CM, CW or E)	
gnl|3286|SC05_0234	5	Cytochrome_C7	Unknown	
gnl|3287|SC05_0235	4	Cytochrome_C7	Unknown	
gnl|3289|SC05_0237	3	Cytochrome_C7	Cytoplasmic	
gnl|3291|SC05_0239	4	Cytochrome_C7	Unknown (CM, CW or E)	
gnl|3282|SC05_0230	8	Cytochrom_c3_2	Cytoplasmic	
gnl|3293|SC05_0241	5	Cytochrom_c3_2	Unknown	
gnl|3296|SC05_0244	5	Cytochrom_NNT	Cytoplasmic	
gnl|2472|SC15_0126	5	Cytochrom_NNT	Cytoplasmic	
gnl|2474|SC15_0128	5	Cytochrome_C554	Unknown (CM, CW or E)	

Table S5 Overview of c-type cytochromes detected in different AOM parner bacteria. Depicted is the number of hemes as determined by the detected CXXCH motifs, the cytochrome type as according to the best scoring pfamA protein domain model, the predicted subcellular localization according to PSORTb and the expression in transcripts per million (TPM). Note that no further normalization was applied to compare data from different organisms. Data for HotSeep-1 was taken from Wegener *et al*., 2015.

locus	heme number (based on CXXCH motifs)	cytochrome type (according to pfamA domain prediction)	predicted subcellular localization (PSORTb)	relative gene expression data (TPM)
HotSeep-1 Guaymas Basin 60				
gnl|2130|HS1_002128	5	Cytochrome_C7	CytoplasmicMembrane	95
gnl|2000|HS1_001998	7	Cytochrome_C7	Unknown	0
gnl|1995|HS1_001993	12	Cytochrom_c3_2	Periplasmic	74
gnl|1996|HS1_001994	12	Cytochrom_c3_2	Unknown (CM, P or E)	86
gnl|1635|HS1_001633	5	Cytochrome_C554	Unknown (CM, P or E)	3
gnl|1799|HS1_001797	4	Cytochrome_C554	Cytoplasmic	0
gnl|1881|HS1_001879	4	Cytochrome_C554	Periplasmic	24
gnl|662|HS1_000660	7	Cytochrome_C554	Unknown (CM, P or E)	0
gnl|2102|HS1_002100	**5**	**Cytochrome_C554**	**Unknown**	**881**
gnl|783|HS1_000781	4	Cytochrome_C554	Cytoplasmic	0
gnl|1098|HS1_001096	4	Cytochrome_C554	Cytoplasmic	7
gnl|1188|HS1_001186	**4**	**Cytochrom_CIII**	**Periplasmic**	**1011**
gnl|1576|HS1_001574	4	Cytochrom_CIII	Periplasmic	3
gnl|161|HS1_000160	**4**	**Cytochrom_CIII**	**Periplasmic**	**179**
gnl|1638|HS1_001636	8	Multi-haem_cyto	Unknown (C or P)	7
gnl|1992|HS1_001990	10	Paired_CXXCH_1	Cytoplasmic	95
gnl|1997|HS1_001995	7	Paired_CXXCH_1	Unknown	9
gnl|2007|HS1_002005	26	Paired_CXXCH_1	Cytoplasmic	7
gnl|1621|HS1_001619	**7**	**Paired_CXXCH_1**	**Unknown**	**974**
gnl|2008|HS1_002006	16	Paired_CXXCH_1	Unknown (CM, P or E)	11
gnl|2101|HS1_002099	**6**	**Paired_CXXCH_1**	**Extracellular**	**2485**
Seep-SRB-2 Guaymas Basin 37				
gb37seep2_00199	9	Cytochrome_C7	Cytoplasmic	82
gb37seep2_01305	9	Cytochrome_C7	Cytoplasmic	3
gb37seep2_02236	9	Cytochrome_C7	Cytoplasmic	2
gb37seep2_02651	12	Cytochrome_C7	Periplasmic	67
gb37seep2_02652	12	Cytochrom_c3_2	Unknown	42
gb37seep2_02650	12	Cytochrom_c3_2	Cytoplasmic	18
gb37seep2_01369	2	Cytochrom_NNT	Unknown	1
gb37seep2_01373	2	Cytochrom_NNT	Unknown	0
gb37seep2_02208	7	Cytochrome_C554	Cytoplasmic	1
gb37seep2_01609	5	Cytochrome_C554	Unknown (CM, P or E)	6
gb37seep2_01615	5	Cytochrome_C554	Periplasmic	6
gb37seep2_01787	4	Cytochrome_C554	Unknown	1
gb37seep2_02404	7	Cytochrome_C554	Cytoplasmic	1
gb37seep2_02452	4	Cytochrome_C554	Periplasmic	3
gb37seep2_02705	3	Cytochrome_C554	Periplasmic	9
gb37seep2_00200	4	Cytochrome_C554	Unknown	1
gb37seep2_00167	**5**	**Cytochrome_C554**	**Cytoplasmic**	**163**
gb37seep2_01096	4	Cytochrome_C554	Unknown (C or P)	1
gb37seep2_01822	**4**	**Cytochrom_CIII**	**Periplasmic**	**108**
gb37seep2_00371	3	Cytochrom_CIII	Periplasmic	55
gb37seep2_01378	8	Multi-haem_cyto	Periplasmic	14
gb37seep2_02644	16	Paired_CXXCH_1	Unknown (CM, P or E)	8
gb37seep2_02645	26	Paired_CXXCH_1	Periplasmic	7
gb37seep2_02648	7	Paired_CXXCH_1	Extracellular	10
gb37seep2_02649	6	Paired_CXXCH_1	Unknown (P or E)	18
gb37seep2_02005	6	Paired_CXXCH_1	Extracellular	1
gb37seep2_02638	**5**	**Paired_CXXCH_1**	**Unknown**	**197**
gb37seep2_02430	6	Paired_CXXCH_1	Extracellular	1
gb37seep2_02637	**4**	**Paired_CXXCH_1**	**Extracellular**	**105**

Chapter V

Metabolic capabilities of microorganisms involved in and associated with the anaerobic oxidation of methane

Gunter Wegener[1,2*], Viola Krukenberg[1], S. Emil Ruff[1#], Matthias Y. Kellermann[2] and Katrin Knittel[1]

[1]Max Planck Institute for Marine Microbiology, Celsiusstraße 1, 28359 Bremen

[2]MARUM, Center for Marine Environmental Sciences, Leobener Str., 29359 Bremen

Submitted to Frontiers in Microbiology;
Special issue: Living on gas – microbial degradation of gaseous alkanes, from mud to genes

[*]Correspondence: Dr. Gunter Wegener, Max Planck Institute for Marine Microbiology, Celsiusstraße 1, Bremen, D28203, Germany; gwegener@mpi-bremen.de

[#]Present address: University of Calgary, 2500 University Drive NW, Calgary, Alberta T2N 1N4, Canada

Keywords: Anaerobic oxidation of methane, archaea, syntrophy, methanogenesis, disproportionation, physiology

Abstract

In marine sediments the anaerobic oxidation of methane with sulfate as electron acceptor (AOM) is responsible for the removal of a major part of the greenhouse gas methane. AOM is performed by consortia of anaerobic methane-oxidizing archaea (ANME) and their specific partner bacteria. The physiology of these organisms is poorly understood, which is due to their slow growth with doubling times in the order of months and the phylogenetic diversity in natural and *in vitro* AOM enrichments. Here we study sediment-free long-term AOM enrichments that were cultivated from seep sediments sampled off the Italian Island Elba (20°C; hereon called E20) and from hot vents of the Guaymas Basin, Gulf of California, cultivated at 37°C (G37) or at 50°C (G50). These enrichments were dominated by consortia of ANME-2 archaea and Seep-SRB-2 partner bacteria (E20) or by ANME-1, forming consortia with Seep-SRB-2 bacteria (G37) or with bacteria of the HotSeep-1 cluster (G50). We investigate lipid membrane compositions as possible factors for the different temperature affinities of the different ANME strains and show autotrophy as characteristic feature for both ANME clades and their partner bacteria. Although in the absence of additional substrates methane formation was not observed, methanogenesis from methylated substrates (methanol and methylamine) could be quickly stimulated in the E20 and G37 enrichments. Responsible for methanogenesis are archaea from the genus *Methanohalophilus* and *Methanococcoides*, which are minor community members during AOM (1 to 7‰ of archaeal 16S rRNA gene amplicons), and which likely feed on methylated substrates produced in side reactions of AOM. In the same two cultures also sulfur disproportionation could be quickly stimulated by addition of zero-valent colloidal sulfur. The isolated partner bacteria are likewise minor community members (1 to 9‰ of bacterial 16S rRNA gene amplicons), whereas the dominant partner bacteria (Seep-SRB-1a, Seep-SRB-2 or HotSeep-1) did not grow on elemental sulfur. Our results support a functioning of AOM as syntrophic interaction of obligate methanotrophic archaea that transfer non-molecular reducing equivalents (i.e. via direct interspecies electron transfer) to obligate sulfate-reducing partner bacteria. Additional catabolic processes in these enrichments but also in sulfate methane interfaces are likely performed by minor community members.

Introduction

In the anoxic marine subsurface large amounts of the potential greenhouse gas methane are formed by microbial and thermal degradation of organic matter. Hence methane is highly abundant in the marine subsurface (Reeburgh, 2007). The efflux of methane from sediments into the water column is however limited, which is mostly due to the effective barrier of methanotrophic microorganisms. The quantitatively most important sink is the coupling of methane oxidation to the reduction of sulfate (AOM) according to the net reaction (Eq. 1)

$$CH_4 + SO_4^{2-} \rightarrow HCO_3^- + HS^- + H_2O \quad (1)$$

with an energy yield of only −34 kJ per mol substrate turnover at standard conditions (Knittel and Boetius, 2009). AOM is performed in dual species microbial consortia of anaerobic methane-oxidizing archaea (ANME), which are closely related to known methanogens, and partner bacteria affiliated to canonical sulfate reducers of the *Desulfosarcina*/*Desulfococcus* clade (Hinrichs *et al.*, 1999; Boetius *et al.*, 2000; Orphan *et al.*, 2001; Knittel *et al.*, 2005) or of the HotSeep-1 group (Krukenberg *et al.,* submitted). Currently three major clades of ANME archaea are known. ANME-2 is the most prominent methanotrophic clade at marine cold gas seeps (Orphan *et al.*, 2002; Mills *et al.*, 2003; Wegener *et al.*, 2008b; Knittel and Boetius, 2009). The temperature at those sites is usually between 4 and 14°C (Knittel and Boetius, 2009). ANME-3 often occurs at mud volcanoes (i.e. Haakon Mosby mud volcano; Niemann *et al*., 2006; *in situ* temperature −1.5°C) and the Eastern Mediterranean seepages (14°C; Omoregie *et al*., 2008). To our knowledge so far ANME-3 does not proliferate *in vitro.* The third phylogenetic group ANME-1 has been originally described at cold seeps (Hinrichs *et al*., 1999), but it is particular abundant in diffusive sulfate methane interfaces (Thomsen *et al*., 2001; Lanoil *et al*., 2005; Harrison *et al*., 2009; Aquilina *et al*., 2010) and in microbial mats and chimney structures at methane seeps in the Black Sea (Michaelis *et al*., 2002; *in situ* temperature of 10°C). In hydrothermally heated sediments such as in the Guaymas Basin (AOM activity up to 70°C) ANME-1 perform thermophilic methane oxidation (Teske *et al*., 2002; Holler *et al*., 2011b; Dowell *et al*., this issue). All ANME clades form dense consortia with deltaproteobacterial partners, which belong either to Seep-SRB-1a from the *Desulfosarcina/Desulfococcus* subcluster (Schreiber *et al*., 2010), Seep-SRB-2 from the *Desulfbacterales* subcluster (Kleindienst *et al*., 2012) or *Desulfobulbus* (mostly ANME-3; Niemann *et al*., 2006). The partner of thermophilic ANME-1 is *Candidatus* Desulfofervidus auxilii (prior known as HotSeep-1; Holler *et al*., 2011b; Wegener *et al*., 2015; Krukenberg *et al*., submitted). Different naturally enriched AOM communities proliferated *in vitro*

(Nauhaus *et al*., 2002; Krüger *et al*., 2005; Holler *et al*., 2009), however cultivation at low temperatures (≤20°C) repeatedly selected for ANME-2, although several source sediments were dominated by other clades (ANME-1 from the Black Sea or ANME-3 at Haakon Mosby mud volcano; Holler *et al*., 2009; own data). The principles underlying this selective growth of ANME-2 *in vitro* have so far not been resolved. Only cultivation at elevated temperatures sustained ANME-1 (Holler *et al*., 2011b).

The potential of ANME to perform methanogenesis has been repeatedly suggested. This hypothesis based on experiments with natural enrichments (Bertram *et al*., 2013), on thermodynamic constrains (Alperin and Hoehler, 2009) and on the phylogenetic proximities and genomic similarities of ANME and known methanogens (Lloyd *et al*., 2011). Furthermore, using radiotracer co-occurrence of AOM and methane formation has been repeatedly measured (Treude *et al*., 2007; Orcutt *et al*., 2008) and ANME-1 archaea have been found to be abundant in potentially methanogenic sedimentary horizons (Lloyd *et al*., 2011). However, tracer transfer from product (DIC) into the reactant pool (methane) might also be explained as inherent process of AOM as suggested by Holler and colleagues (2011a).

The certainly least understood feature of AOM is how archaea and bacteria interact in the characteristic dual-species consortia. The activation and complete oxidation of methane via a reversal of the well-described methanogenesis pathway can be confidently assigned to the ANME archaea (Hallam *et al*., 2004; Meyerdierks *et al*., 2010; Thauer, 2011; Stokke *et al*., 2012; Wang *et al*., 2014). The fate of the released electrons including the localization of sulfate reduction is instead so far controversial. Based on their phylogenetic classification as *Deltaproteobacteria* (Knittel *et al*., 2003; Schreiber *et al*., 2010; Kleindienst *et al*., 2012) and the presence of genes and enzymes of sulfate reduction (Milucka *et al*., 2013; Wegener *et al*., 2015; Krukenberg *et al*., submitted), all different partner bacteria are likely involved in the sulfur cycle. However, it is still unclear if the partner bacteria disproportionate elemental sulfur-derived from incomplete sulfate reduction in ANME-2 (Milucka *et al*., 2012), or if ANME transfer reducing equivalents released during AOM via cytochromes (McGlynn *et al*., 2015) or additionally via nanowires (Wegener *et al*., 2015) to their partner bacteria, which in this case would be sulfate reducers.

Here we retrieved three sediment-free AOM enrichments derived from methane-percolated coastal sands off the Mediterranean Island Elba (Italy; enriched at 20°C; E20) as well as a mesophilic enrichment (37°C; G37) and a thermophilic enrichment culture (50°C; G50) from the Guaymas Basin. We describe community compositions and membrane lipid patterns of these enrichments and performed physiological experiments to test metabolic capabilities

attributed to AOM community members including chemoautotrophy, methanogenesis and sulfur disproportionation. Findings were evaluated in further AOM enrichments obtained from different seep sites.

Material and methods

Production of AOM enrichments and maintenance

Source material for the E20 enrichment were clastic sediments sampled by scuba diving in 2010 from the coastal hydrocarbon seeps off the Mediterranean Island Elba (*in situ* water temperature 12 to 27°C and 12 m water depth, further described in Ruff *et al.*, this issue). By shaking and collecting the supernatant we concentrated slowly settling microbial biomass from rapidly sinking mineral particles (sand). The concentrated biomass (<1% of the sediment weight) resembled 60% of the microbial methane-dependent sulfate reduction rate of the sediment. The G37 and G50 enrichments derived from the methane-rich hydrothermally heated sediments in the Guaymas Basin, Gulf of California, sampled during RV ATLANTIS cruise AT15-56 with the submersible ALVIN in 2009. After determination of applicable cultivation temperatures in a temperature gradient block (Holler *et al*., 2011b), sediments from distinct temperature horizons have been enriched at the determined temperature optima of AOM in a mixed sediment (37°C, 50°C, 60°C). All enrichments were incubated with marine sulfate reducer medium (Widdel and Bak, 1992) and supplied with methane and sulfate as sole potential redox couple for at least three years. Medium was exchanged when sulfide concentrations exceeded 15 mM and biomass was diluted (1:2 or 1:4) when sulfide production exceeded approx. 0.2 mmol l^{-1} day^{-1}. Community structures in the 50°C and 60°C enrichment were highly similar, thus experiments presented here were performed at 50°C. The additional sample "GF" (here only studied for microbial diversity and sulfur disproportionation), derived from the methane seeps in the vicinity of the Gullfaks oil field in the North Sea and was sampled during RV ALKOR cruise 267 in October 2005 (Wegener *et al*., 2008b). Sediment-free AOM enrichments from this site were produced by incubation under AOM conditions at room temperature and subsequent dilution as described above. Further, methanotrophic enrichment cultures from the Mediterranean (NAUTNIL expedition with RV L Atalante in 2003), from Hydrate Ridge (RV SONNE expedition SO148 in 2000), the Black Sea (RV POSEIDON expedition POS 148 in 2004) and Gulf of Mexico RC

SONNE expedition SO 174), which were only screened for their microbial diversity, were retrieved and cultivated as described (see Supplementary Tab. 1).

Cultivation of methanogens from AOM enrichments

To determine potential methanogenesis activity in the AOM enrichments E20, G37 and G50, triplicate sulfate-free culture aliquots of 10 ml (1:10 dilution) were incubated in 20 ml Hungate tubes with alternative substrates (hydrogen (0.1 MPa), carbon monoxide (0.05 MPa), formate, acetate, methylamine and methanol (all 20 mM)) for 30 days at their distinct temperature. The development of methane in the headspace was measured using gas chromatography coupled to flame ionization detection (Focus GC, Thermo equipped with a Poropak column; Analytical columns). In this time interval, methane formation was only observed for methylamine and methanol (for both, E20 and G37), but substrates were already fully turned over after 10 days. For these substrates experiments were repeated with more frequent sampling intervals (Fig. 4 A). Furthermore, for the substrates methanol and methylamine triplicate dilution-to-extinction series with factor 10 dilutions were prepared (down to 10^8). Methane formation was repeatedly measured and the highest active dilutions ($1:10^5$) were further diluted (1:1000). From freeze-thawed pellets of aliquots of these cultures we identified the enriched microbes by direct 16S rRNA gene amplification using the primer pair Arch20F (Massana *et al*., 1997) and Arc1492R (Teske *et al*., 2002) and sequencing (PCR and sequencing as described below for AOM enrichments).

Cultivation of sulfate reducers from the AOM enrichments

To determine potential methane-independent sulfate reduction in the AOM enrichments, triplicate culture aliquots of 10 ml were incubated with possible alternative substrates (hydrogen (0.1 MPa), carbon monoxide (0.05 MPa), methyl sulfide (0.05 MPa) formate, acetate, methylamine and methanol (all 20 mM)) for 30 days at their distinct temperature. The development of sulfide was measured by a copper sulfate assay and spectroscopic analyses (Cord-Ruwisch, 1985). Dilution-to-extinction series (down to 10^8 dilution) were set up from active AOM enrichments (G37, G50) with hydrogen as only used alternative electron source, and incubated at their respective temperature for 2 months. After a subsequent second dilution step (1:100) of the highest sulfide-producing dilutions, enriched microbes were identified by 16S rRNA gene amplification (primer pair GM3/GM4; Muyzer *et al*., 1995) from freeze-thawed pellets of culture aliquots and direct sequencing (PCR and sequencing as described below for AOM enrichments).

Experiments on alternative sulfur sources in the AOM enrichment

To identify the spectrum of sulfur sources used by the microbial communities in the E20, G37 and G50 AOM enrichments, sulfate-free culture aliquots were incubated with the alternative sulfur sources sulfite (5 mM), thiosulfate (20 mM), and with sulfate (20 mM) as control. Furthermore we incubated with colloidal (zero-valent) sulfur (ca. 50 mM) that was prepared according to Steudel and colleagues (1988), and dissolved in anaerobic deionized water (approx. 0.5 mol S^0 per liter). Triplicate incubations with and without methane (0.2 MPa CH_4:CO_2 (90:10)) were performed for each substrate. We measured sulfide production calorimetrically using the copper sulfate assay (Cord-Ruwisch, 1985). Dilution-to-extinction series (as described above) were performed for alternative substrates which showed substantial sulfide production (only in zero-valent sulfur enrichment). The highest active dilutions were further diluted (1:100) and enriched microbes were identified by 16S rRNA gene amplification (primer pair GM3/GM4; Muyzer *et al*., 1995) from freeze-thawed pellets of culture aliquots and direct sequencing (PCR and sequencing conditions as described below for AOM enrichments).

To study the underlying principle of zero-valent sulfur disproportionation, we tested the stoichiometry of sulfur disproportionation by simultaneously measuring sulfate (by ion chromatography; 761 Compact ion chromatograph (Metrohm) with a Metrosep A SUPP 5 column) and sulfide production (copper sulfate assay; Cord-Ruwisch, 1985) in the AOM enrichments and in the zero-valent sulfur enrichments.

Extraction and analysis of archaeal intact polar lipids from the AOM enrichment

Cell pellets from 30 ml AOM enrichment cultures were spiked with an internal standard (phosphatidylcholine $C_{21:0}/_{21:0}$) and 3 g of combusted sand and extracted using a modified Bligh and Dyer protocol (Sturt *et al*., 2004). The obtained TLEs were stored at −20°C until analyses. IPLs were analyzed by high-performance liquid chromatography electrospray ionization mass spectrometry (HPLC-ESI-MS). Separation of IPLs was achieved on a Dionex Ultimate 3000 UHPLC equipped with a Waters Acquity UPLC BEH amide column (150 x 2.1 mm, 1.8 µm particle size). Chromatographic conditions included constant flow rate of 0.4 ml/min with eluent A (75% acetonitrile; 25% dichloromethane; 0.01% formic acid; 0.01% ammonium hydroxide solution (NH_3 aq.)) and eluent B (50% methanol 50% Milli-Q water; 0.4% formic acid; 0.4% NH_{3aq} as previously published (Wörmer *et al*., 2013)). Under a constant flow, the HPLC routine applied: 99% A and 1% B for 2.5 min, increasing to 5% B at 4 min, followed by a linear gradient to 25% B at 22.5 min and then to 40% B at 26.5 min.

Thereafter a 1 min washing step with 40% B followed and afterwards reset to the initial conditions for 8 min to achieve column re-equilibration. Compound detection was conducted on a maXis Ultra-High Resolution qToF-MS (Bruker, Bremen, Germany). IPLs were measured in positive ionization mode scanning a mass-to-charge (m/z) range of 150–2,000, with automated data-dependent MS/MS fragmentation of base peak ions. Compound identification was achieved by monitoring exact masses of possible parent ions (present mainly as H^+ and NH_4^+ adducts) in combination with characteristic fragmentation patterns (Sturt *et al*., 2004; Yoshinaga *et al*., 2011). The reported relative distribution of microbial lipids is based on the peak areas of the respective molecular ions without differentiating for potential differences in response factors; results should therefore be considered as semi-quantitative.

Determination of microbial carbon sources and growth efficiencies in the AOM enrichments

To determine the role of methane and bicarbonate as carbon sources in the AOM enrichment and their assimilation rate in relation to AOM, we incubated triplicate culture aliquots of E20, G37 and G50 (4 ml) in 5 ml Hungate tubes with ^{14}C-bicarbonate (380 kBq; equilibrated with 0.2 MPa CH_4:CO_2 or N_2:CO_2 (90:10)) or with ^{14}C-methane (14 kBq; equilibrated with 0.2 MPa CH_4:CO_2 (90:10)). After 5 days of incubation cell material was transferred to membrane filters (GSWP, 0.2 µm pore size). To remove non-fixed inorganic carbon we washed the filters with saline water (0.5 M NaCl). Potential residual inorganic carbon was removed by exposing the dried filters to a HCl atmosphere for 24 hours. Total radioactivity was determined from liquid incubation aliquots (0.1 ml) and incorporated radioactivity was determined from the particulate organic carbon fraction (POC) collected on filters by liquid scintillation counting (scintillation mixture; Filtercount or Permafluor; Perkin Elmer, Waltham, MA, USA; scintillation counter; 2900TR LSA; Packard, Waltham, MA, USA). Counts for ^{14}C-compound in POC were corrected for background values. To determine carbon fixation efficiencies (CFE) values were normalized to the added amount of radiotracer and the rate of sulfate reduction

$$\text{CFE (\%)} = [^{14}\text{C-POC}_i \text{ (kBq)} / {}^{14}\text{C-total}_i \text{ (kBq)} \times \text{conc}_{CS} \text{ (mmol)} \times 100] / \text{SRR (mmol)} \quad (2)$$

where ^{14}C-POC defines the concentration of radiotracer in the particulate organic carbon (biomass) and ^{14}C-total defines the concentrations of added radiotracer ($^{14}CH_4$ or ^{14}C-inorganic carbon) in an experiment '*i*', and conc_{CS} is the concentration of the carbon

source (either methane or inorganic carbon) and the respective sulfate reduction rate (SRR) in replicate vials determined as described below.

Radiotracer measurement of inorganic carbon fluxes in the AOM enrichments

To track the carbon fluxes between methane and inorganic carbon in AOM enrichments E20, G37 and G50, replicate culture aliquots (4 ml) were incubated in 5 ml Hungate tubes equilibrated with 0.2 MPa CH_4:CO_2 (90:10). After 5 days of pre-incubation the vials were completely filled with methane-saturated medium and carrier-free ^{14}C-bicarbonate (~66 kBq per sample) or ^{35}S-sulfate (100 kBq per sample) was injected into 5 replicates, respectively according to protocols described by Holler and colleagues (2011a). Concurrently controls inactivated by formaldehyde addition were performed to estimate impurities or abiotic reactions. Samples were incubated for 2 days and reactions were stopped by transferring samples into sodium hydroxide solution (0.5 N) or zinc-acetate solution (20% w/v), respectively for ^{14}C and ^{35}S labeling. The ^{14}C-bicarbonate and the $^{35}SO_4$ samples were processed as described before (Kallmeyer *et al*., 2004; Holler *et al*., 2011a). The turnover rates of bicarbonate were inferred by calculating the portion of radiotracer transferred into the methane pool multiplied by the concentration of DIC and divided by the total tracer content in the experiment. Sulfate reduction rates were calculated as described below.

Sequencing of 16S rRNA gene libraries of AOM enrichments

DNA from AOM enrichments was extracted as described before (Zhou *et al*., 1996). The protocol encompassed three cycles of freezing and thawing, chemical lysis in a high-salt extraction buffer (1.5 M NaCl) by heating of the suspension in the presence of sodium dodecyl sulfate and hexadecyltrimethyl-ammonium bromide, and treatment with proteinase K, followed by chloroform:isoamylalcohol extraction (24:1) and isopropanol based nucleic acid precipitation. To analyze the phylogeny of the dominant members of the enrichment and to obtain representative full length 16S rRNA gene sequences, the bacterial and archaeal 16S rRNA genes were amplified from the extracted DNA using the primer pair GM3/GM4 (Muyzer *et al*., 1995) and Arch20F (Massana *et al*., 1997)/Arc1492R (Teske *et al*., 2002), respectively. PCR reaction mixtures were prepared as previously described (Holler *et al*., 2011b) and subjected to the following cycle conditions: 95°C for 5 min; 26 cycles, each 95°C for 1 min, 46°C (GM3/GM4) or 58°C (Arch20F/Arc1492R) for 1.5 min, and 72°C for 3 min; and a final step at 72°C for 10 min. The amplicons of three replicate PCR reactions were pooled. Following gel electrophoresis bands were extracted from an agarose gel and purified

using the QIAquick PCR Purification Kit (Qiagen, Hilden, Germany) according to the manufacturer's recommendations. Purified amplicons were ligated into the pGEM-T Easy vector (Promega, Madison, WI, USA) and transformed into *Escherichia coli* (One Shot Top10 cells; Invitrogen, Carlsbad, CA, USA) following the manufacturer's recommendations. Taq cycle sequencing was performed using ABI BigDye Terminator chemistry and an ABI377 sequencer (Applied Biosystems, Foster City, CA, USA).

Sequencing of 16S rRNA genes retrieved from AOM enrichments

To obtain an overview about the diversity of rare microbial phyla we performed massive parallel tag sequencing of ten long-term AOM enrichment cultures. In addition to the four enrichments presented in detail (E20, GB37, GB50 and GF) we also investigated six enrichment cultures that were inoculated with samples from Amon mud volcano, a Black Sea microbial reef, Black Sea sediments, Caldera mud volcano, the Gulf of Mexico and Hydrate Ridge. The latter six enrichment cultures were used for comparison, but are not focus of this study. From DNA that was extracted as described above, we amplified 16S rRNA genes using the primer pairs GM3/907RM (Muyzer *et al*., 1995; Muyzer *et al*., 1998) for bacteria and Arch20F/Arch958RV (Massana *et al*., 1997; Pires *et al*., 2012) for archaea. The amplicon libraries were prepared, and the V3-V5 region of these amplicons was sequenced on a 454 Genome Sequencer GS FLX+ (Roche, Basel, Switzerland) at the Max Planck Genome Centre (Cologne, Germany). The raw read data was processed based on a standard operating procedure (Schloss *et al*., 2011) using Mothur (release 1.33, 02/2014; Schloss *et al*., 2009). Reads were denoised based on PyroNoise (Quince *et al*., 2009), trimmed, preclustered (Huse *et al*., 2010) and chimeras removed (Edgar *et al*., 2011). After quality filtering we had a total of 122,363 archaeal and 102,762 bacterial reads forming 13,935 unique archaeal and 17,237 unique bacterial sequences with an average length of 488 and 435 nucleotides, respectively. The alignment and taxonomic classification of the sequences was based on the SILVA small subunit reference database (release 119, 07/2014; Quast *et al*., 2013). Operational taxonomic units were clustered at 98% 16S rRNA gene V3-V5 sequence identity using average neighbor clustering. The datasets were subsampled to account for unequal sampling effort prior to community analyses and multivariate statistics.

Comparison of 16S rRNA tags and 16S rRNA gene libraries

To investigate whether the same organisms are present in gene libraries as well as tag datasets we compared the results of the two methods. We made a sequence database of the 16S rRNA

gene tags using blast (Boratyn *et al*., 2013) and then searched this database with target 16S rRNA gene sequences from the enrichments. The headers of the resulting output were matched with an $OTU_{0.02}$ list created by mothur (Schloss *et al*., 2011) to find the sequences that were present in both datasets. We only used sequences that matched the whole length of the sequence and had an E value of basically 0.

Phylogenetic analysis of retrieved 16S rRNA gene sequences

Retrieved partial 16S rRNA gene sequences (from AOM enrichments and alternative substrate enrichments) were aligned with the SILVA Incremental Aligner (SINA) (Pruesse *et al*., 2007) and classified based on the SILVA small subunit database (release 115; Quast *et al*., 2013). Phylogenetic analysis was performed with representative, nearly full length (>1200 bp) sequences (from AOM enrichments, and from methanogenic, sulfate-reducing and sulfur-disproportionating enrichments (see above)) using the ARB software package (Ludwig *et al*., 2004). Maximum likelihood based trees were calculated by RAxML (Stamatakis, 2006) with GTRCAT as nucleotide substitution model including 235 bacterial and 148 archaeal nearly full length sequences (>1200 bp). A base frequency filter was employed to consider only alignment regions which are at least 50% conserved. 100 bootstrap replicates were used to estimate branch support.

Nucleotide sequence accession numbers

The 16S rRNA gene sequences were archived in the NCBI public nucleotide sequence databases under the accession numbers KT899714, KT899739-KT899743 (bacteria) and KT899737, KT899738 and KM605124 (archaea). Pyrosequencing raw reads were deposited in the sequence read archive under Bioproject PRJNA299125 with accession numbers SAMN04194115 to SAMN04194124.

Catalyzed reporter deposition fluorescence *in situ* hybridization (CARD-FISH)

For CARD-FISH culture aliquots were fixed in 2% formaldehyde for 2 h at room temperature, washed with 1× phosphate buffered saline (PBS; 8,2 g l^{-1} NaCl, 0.2 g l^{-1} KCl, 1,8g $Na_2HPO_4 \times 2H_2O$, 0.24g KH_2PO_4, adjusted to pH 7.4) and stored in 1× PBS:ethanol (1:1) at −20°C. Fixed cells were treated with mild sonication (Sonoplus HD70, Bandelin, Berlin Germany) for 30 sec at 10W and filtered onto GTTP filter (0.2 µm pore size). CARD-FISH was performed as described previously (Pernthaler *et al*., 2002). For cell wall permeabilization, filters were sequentially incubated in lysozyme solution (10 mg ml^{-1}

lysozyme, lyophilized powder (SigmaAldrich) in 0.1 M Tris–HCl, 0.05 M EDTA, pH 8) for 30 min at 37°C, proteinase K solution (15 to 150 µg l^{-1} proteinase K (Merck) in 0.1 M Tris–HCl, 0.05 M EDTA, 0.5 M NaCl, pH 8) for 2 min at room temperature and optionally in sodium dodecyl sulfate solution (0.5%) for 10 min at room temperature. Endogenous peroxidases were inactivated by incubating the filters in 0.15% H_2O_2 in methanol (30 min, room temperature). Oligonucleotide probes were synthesized by Biomers (Ulm, Germany) and applied with formamide concentrations in the hybridization buffer according to literature values. For dual CARD-FISH, peroxidases of the first hybridization were inactivated by 0.3% H_2O_2 in methanol (30 min, room temperature). Catalyzed reporter deposition was combined with the fluorochromes Alexa Fluor 488 and Alexa Fluor 594 (Thermo Fisher Scientific). Filters were stained with DAPI (4,6-diamidino-2-phenylindole). Micrographs were obtained by confocal laser scanning microscopy (LSM 780; Zeiss, Oberkochen, Germany).

Results and discussion

Cultivation, microbial diversity and archaeal intact polar lipids in the studied enrichment cultures

The original sediment samples from Guaymas Basin and the Elba seeps showed already high methane-dependent sulfide production when incubating them at AOM conditions (about 0.15 µmol g_{dw}^{-1}; gram dry weight; E20; Ruff *et al.,* this issue to 0.5 and 1.25 µmol g_{dw}^{-1} in Guaymas Basin (G37 and G50; Holler *et al*., 2011b). In E20, cells were separated from the sandy matrix (see Material and Methods). All samples were further enriched for AOM by cultivation in anoxic marine sulfate-reducer medium equilibrated with 0.225 MPa methane and 0.025 MPa carbon dioxide headspace. Cultivation was performed at the respective temperature optima of 20°C (E20) and 37°C and 50°C (G37/G50). From the development of sulfide production rates and dilution frequencies we estimated doubling times of 69 days (G37) and 55 days (G50) (Supplementary Fig. 1 A, B). Due to repeated subsampling for experiments similar required long-term incubations are yet not available for E20, but we expect doubling times in the range of other cold-adapted enrichments (2 to 7 month; Girguis *et al*., 2005; Nauhaus *et al*., 2005). The studied meso- and thermophilic cultures from Guaymas Basin grew faster than the before studied cold-adapted deep sea AOM enrichments (i.e. 7 month in Hydrate Ridge enrichments; Nauhaus *et al*., 2007). Hence, after repeated dilution and cultivation a sediment-free state (<100 mg background sediment per liter culture)

was reached after 1.5 to 2 years in the Guaymas Basin cultures. Cultures are maintained at sulfide production rates of 100 to 250 µmol $l_{inoculum}^{-1}$ d^{-1}. The microbial compositions of the three enrichments were analyzed by sequencing archaeal and bacterial 16S rRNA genes (Fig. 1 A, B, Tab. 1, Supplementary Fig. 2). In E20 the most sequence-abundant archaeal group was ANME-2 (all three subgroups ANME-2a, ANME-2b, ANME-2c), which according to fluorescence *in situ* hybridization (FISH) were associated with Seep-SRB-2 partner bacteria (Fig. 1 C). G37 mainly consisted of dual-species consortia of ANME-1 and Seep-SRB-2 partner bacteria (Fig. 1 D). The dominance of ANME-1 and Seep-SRB-2 is typical for moderately heated surface sediments of the Guaymas Basin seeps (Dowell *et al*., this issue). As shown for 60°C thermophilic AOM enrichments before also the 50°C enrichment was dominated by ANME-1 and their partner bacteria *Ca*. Desulfofervidus auxilii (Wegener *et al*., 2015; Fig. 1 E).

Our results of the E20 enrichment and also prior *in vitro* cultivation at low-temperatures (≤20°C; i.e. Hydrate Ridge, Mediterranean seeps such as Amon mud volcano, Black Sea; Holler *et al*., 2009) showed that low-temperature enrichments of mixed communities always led to ANME-2-dominated enrichments (Supplementary Fig. 2), whereas ANME-1 is usually not sustained *in vitro*. In contrast, cultivation at elevated temperatures (≥37°C) led to ANME-1-dominated enrichments, even from sites that harbored mixed communities (Tab. 1, c.f.; Holler *et al*., 2011b; Kellermann *et al*., 2012). The different temperature optima and growth ranges of ANME-1 and ANME-2 might be due to their cell membrane structure. The ANME-2 in the E20 enrichments assemble their membranes from double layers of diether lipids (intact archaeols) such as hydroxylated (PG)phosphatidylglycerol archaeol (Fig. 1 G, Tab. 2). ANME-1 are instead able to condense diethers to tetraether lipids (Kellermann *et al*., submitted). Hence in the G37 enrichment culture an about 1:1 mixture of diether and tetraether lipids (i.e. glyceroldialkylglyceroltetraether GDGTs) was detected, whereas the high-temperature enrichments (G50 and also G60; the latter only shown in Tab. 2) contained between 80 to 94% tetraether lipids. The formation of GDGT might allow higher temperature optima (Kellermann *et al*., 2012) or better resistance in starvation periods (Schouten *et al*., 2003; Rossel *et al*., 2008). Additionally, next to temperature adaption, tetraether lipids will tighten the cells, which could help ANME-1 to outlast starvation phases. This observation might also explain the predominance of ANME-1 in most deep sulfate-methane interfaces or in inner parts of microbial chimneys where they have to survive under often minimal substrate concentration. The adaption to harsh conditions or limited substrate availability may, on the

other hand, also explain their inability to compete with ANME-2 during cultivation at low temperatures and high substrate availability.

Origin of biomass carbon in AOM-performing microbial enrichments

To interpret natural biomass stable isotope signals and to perform stable isotope studies the dominant biomass carbon sources of the active organisms need to be identified. For AOM methane and inorganic carbon have been suggested as carbon sources (Hinrichs *et al*., 1999; Blumenberg *et al*., 2005; Wegener *et al*., 2008a; Kellermann *et al*., 2012). Here we studied inorganic carbon and methane assimilation into AOM communities using a radiotracer assay with respective labeled carbon sources and tracked the assimilation into the bulk sample. In all three cultures mainly inorganic carbon was assimilated, whereas only 3 to 15% of the biomass carbon derived from methane (Fig. 2). In the absence of methane as energy source, assimilation of inorganic carbon dropped to about 1/10 of the values measured during AOM conditions. This shows that the microbial activity and carbon fixation in the studied cultures strongly depended on the presence of methane and the process of AOM, respectively. During the oxidation of 1 mol methane only 10 to 40 mM of carbon (mostly of inorganic origin) were incorporated. The rates of inorganic carbon assimilation measured here were in the upper range of growth/carbon fixation reported in earlier studies (Nauhaus *et al*., 2007; Wegener *et al*., 2008a). However, in those studies extremely slow-growing AOM enrichments were investigated with doubling times of approx. seven months, e.g. for enrichments from Hydrate Ridge.

The predominant use of inorganic carbon as carbon source for assimilation is in line with earlier observations stating “chemoorganoautotrophy” for mesophilic ANME-1 (Kellermann *et al*., 2012). This growth mode seems to be consistent in cold-adapted and thermophilic methane-oxidizing enrichments. The minor amounts of methane carbon incorporation observed here and in earlier studies (Wegener *et al*., 2008a) should also be interpreted as assimilation of methane-derived inorganic carbon. The assimilation of methane-derived CO_2 and further isotope fractionation might also explain the extremely low carbon isotope values. Carbon fixation in ANME proceeds most likely via the acetyl CoA pathway (Koga and Mori, 2005; Meyerdierks *et al*., 2010), which causes the highest ^{13}C-discrimination (Preuß *et al*., 1989). It is furthermore consistent with the observation of lowest ^{13}C-lipid values in highly active AOM sites, where pore water inorganic carbon derives mostly from methane, thus is also strongly depleted in ^{13}C. In less active AOM sites rather moderate ^{13}C-signatures of archaeal lipids are observed (Elvert *et al*., 2005).

Methanogenesis in the AOM cultures

Using radiotracer isotope assays (i.e. $^{14}CO_2$) transfer of inorganic carbon into the methane pool has been shown for many different AOM systems. This phenomenon has been repeatedly interpreted as capacity of ANME to thrive as methanogens. However, alternatively this tracer transfer was related to enzymatic back reactions. Also our cultures showed substantial tracer transfer from DIC into the methane pool amounting to 5 to 10% of the methane-dependent sulfate reduction rate (Fig. 3). This tracer transfer is independent of a net formation of methane, as in none of the three cultures methane formation was observed without addition of further methanogenic substrates. Hence, in agreement with earlier hypothesis (Holler *et al*., 2011a) the observed tracer flux should be seen as intrinsic back reaction during the oxidation of methane in ANME, which proceeds on the same pathways as methanogenesis (Hallam *et al*., 2004), but is not an energy conserving net reaction.

We furthermore aimed to induce methanogenesis in the AOM enrichments with typical substrates for methanogens. Therefore, we incubated 1:10 diluted AOM enrichments in sulfate-free medium with different methanogenic substrates and screened those enrichments for methane formation. Hydrogen, acetate and carbon monoxide addition did not cause methane formation in any of the three studied enrichments (Tab. 3), also after extended incubation times of several months (data not shown). However, in the E20 and the G37 cultures methylated substrates (methanol, methylamine) were largely converted to methane within 18 days of incubation (Fig. 4 A, B). In contrast, the G50 AOM enrichment culture did not show methanogenic activity even after prolonged incubation of 60 days with these two substrates.

Using the dilution-to-extinction approach with methylamine or methanol we yielded pure cultures of methanogenic archaea from the E20 and G37 enrichments. Sequencing of the 16S rRNA gene amplified from the enrichments identified all methylamine cultures as relatives of *Methanococcoides* spp., whereas organisms in methanol cultures were identified as relatives of *Methanohalophilus* spp.. As methylotrophs, both methanogenic cultures grow on methanol and methylamine. Generally, methylotrophic methanogens can grow rapidly, and are hence relatively easy to cultivate (Sowers and Ferry, 1983; Kendall and Boone, 2006). We also retrieved those groups in archaeal 16S rRNA gene tag datasets of the enrichments (Tab. 4). Both groups contributed between 1 to 3‰ of all archaeal sequences retrieved from the E20 and G37 enrichments. Furthermore, we screened the additional low temperature (4 to 20°C) methanotrophic enrichment cultures (Supplementary Tab. 1) for methanogens. All those enrichments contain few but also up to 10‰ sequences that align with

Methanococcoides or *Methanohalophilus*. In contrast, in the G50 only a single read aligned to *Methanococcoides*. ANME archaea, however, were not enriched in any of the methanogenic enrichments which clearly indicates that ANME cannot thrive as methanogens.

Minor populations of methanogens also regularly appear in sulfate methane interfaces (Wegener *et al*., 2008b; Ruff *et al*., 2015), where they likely also thrive on methylated substrates. These substrates (i.e. methanol, methylamines and methyl sulfides) are not competitively used by other anaerobic microorganisms with potential higher energy yields including sulfate reducers (King, 1984; Kiene *et al*., 1986; Lovley and Klug, 1986). Yet, the source of methylated substrates in those environments and in the studied laboratory enrichments is unclear. We hypothesize that active ANME may leak methylated compounds, as was shown for aerobic methanotrophs (Xin *et al*., 2004). For instance, in ANME-1 the reversal of methanogenesis lacks the methylenetetrahydromethanopterin reductase (Mer) enzyme which might be bypassed by enzymes that lead to the formation of methanol or methylamine as intermediates (Meyerdierks *et al*., 2010). Furthermore, the strong reversibility of the enzymes involved in AOM, particular of the methyl-CoM reductase, might cause trace formation of methylated compounds (Holler *et al*., 2011a). These compounds might be sufficient to sustain the low numbers of methanogens observed in our enrichments and in sulfate methane interfaces. An experimental detection of these compounds is however challenging as they are efficiently consumed by the methanogenic side communities. In G50 methanogens could not be stimulated. The considerably higher maintenance energy at elevated temperatures (Tijhuis *et al*., 1993) might be the reason for the lack of methanogens and stimulation of methanogenesis here. Our results allow an alternative explanation for the observed stimulation of methane and lipid production in Black Sea mats by methylated compounds as demonstrated by Bertram and coworkers (2013). This production is unlikely caused by ANME archaea, but should be rather interpreted as growth of specific methanogenic side communities.

Hydrogenotrophic sulfate reduction and sulfur disproportionation in the AOM enrichments

We tested the capabilities of the three enrichments to metabolize sulfate with alternative energy sources. As shown before *Ca.* D. auxilii, the sulfate-reducing bacterium in thermophilic AOM, instantly reacts on hydrogen with elevated sulfide production and growth uncoupled from ANME-1 (Wegener *et al*., 2015; Krukenberg *et al*., submitted). However, besides G50, also the G37 culture showed sulfide production on hydrogen as substrate. Rates

quickly exceeded those of parallel incubations on methane. Following this observation we cultivated the sulfate reducers from the sediment-free AOM enrichment using the dilution-to-extinction approach. The retrieved cultures were characterized by direct 16S rRNA gene sequencing. The 16S rRNA gene sequence obtained from one of the cultures affiliated to the larger cluster of Seep-SRB-2 bacteria, but was clearly not identical (only 93% sequence similarity which is below the proposed threshold of 94.5% for a genus; Yarza *et al*., 2014) with the Seep-SRB-2 partner bacterium found in this mesophilic and in the cold-adapted AOM culture (Fig. 5). In another hydrogenotrophic culture a bacterium related to *Desulfatitalea tepidiphila* was obtained. The mesophilic *D. tepidiphila* was described to grow as autotroph by hydrogen-dependent sulfate reduction or alternatively by using thiosulfate as electron acceptor and various organic carbon sources as electron donor (Higashioka *et al*., 2013). Hydrogenotrophic sulfate reduction could not be stimulated in the E20 culture, which likewise is dominated by Seep-SRB-2 partner bacteria. Hence it is unlikely that the meso- or psychrophilic AOM partner bacteria can thrive on hydrogen, therewith confirming earlier results which excluded hydrogen as intermediate in low-temperature AOM or as (alternative) substrate of their partner bacteria (Nauhaus *et al*., 2002).

To investigate the response of the AOM cultures to additions of zero-valent sulfur and therewith test the observations made by Milucka and colleagues (2012) we supplied aliquots of the three cultures with freshly prepared colloidal sulfur solution and tracked the development of the chemical endmembers of disproportionation, sulfide and sulfate. As described before (Wegener *et al*., 2015) sulfur disproportionation was absent in the thermophilic AOM culture (Fig 5 C). In contrast, E20 and G37 responded to elemental sulfur addition with rapid sulfide and sulfate production tightly following the 3:1 stoichiometry characteristic for the disproportionation of elemental sulfur (Fig. 5 D, E). Disproportionation stopped when sulfide concentrations reached approx. 3 mM (E20) or 7 mM (G37). A 7:1 stoichiometry between sulfide and sulfate production, as described for another Mediterranean enrichment (Isis mud volcano; cultivated at 20°C and dominated by ANME-2; Milucka *et al*., 2012) has not been observed in any of our enrichments.

Using a dilution-to-extinction approach with colloidal sulfur as only available electron donor we repeatedly isolated specific single strains of sulfur-disproportionating bacteria from the two natural enrichments. Interestingly in the dilution series from G37 we repeatedly isolated a single strain (hereon called GB-DISP1) that is basically identical to the one isolated on hydrogen (Fig. 5 F). GB-DISP1 is a rare member in the 37°C AOM enrichment, accounting for about 9‰ of the bacterial 16S rRNA gene sequences. The at AOM conditions

dominant bacterium Seep-SRB-2 however, did not respond to additions of elemental sulfur, hence pointing towards a neutral role of elemental (zero-valent) sulfur in mesophilic AOM proceeding in the G37 enrichment. Growth experiments with the enriched GB-DISP1 showed that it can grow as sulfate-reducing hydrogenotroph (with activity doubling time of 3 days), it can couple sulfur reduction to hydrogen oxidation (activity doubling time 1 day) or it grows as sulfur-disproportionating bacterium (with activity doubling times of about 1 day). Using hydrogen as electron donor GB-DISP1 thrives at sulfide concentrations of up to 20 mM. Instead via sulfur disproportionation GB-DISP1 grows well to sulfide concentrations of up to 5 mM. Above this value sulfide production slows down and sulfide levels off at around 7 mM. At these sulfide concentrations the energy yield of sulfur disproportionation at 37°C is reduced to approx. −10 kJ mol^{-1} elemental sulfur turnover (Finster, 2008), which is about the minimum free energy yield (ΔG_{min}) to sustain microbial metabolism (Hoehler, 2004).

The E20 dilution-to-extinction series with elemental sulfur yielded several replicates of a single bacterium, hereon called Elba-DISP1, with high identity to the uncultivated deltaproteobacterial cluster MSBL7 (Pachiadaki *et al*., 2014) and the isolated disproportionating bacterium *Desulfurivibrio alkaliphilus* (Sorokin *et al*., 2008). *D. alkaliphilus* was described as halophilic chemoautotrophic sulfate reducer, capable to thrive by sulfur disproportionation even without supplying a sulfide sink (Poser *et al*., 2013). According to our substrate tests Elba-DISP1 thrives exclusively by sulfur disproportionation. Unlike described for *D. alkaliphilus,* we did not succeed to grow Elba-DISP1 as hydrogenotrophic sulfate or elemental sulfur reducer. Furthermore, we searched for sulfur disproportionation in the cold seep AOM enrichment culture 'GF' retrieved from the Gullfaks oil field (Norwegian North Sea). Indeed also this culture showed a relatively fast response to elemental sulfur addition. The disproportionating microorganism enriched from the GF cultures was *Desulfocapsa sulfoexigens* (>99% 16S rRNA gene identity), one of the first described sulfur-disproportionating microorganism (Finster *et al*., 1998). In contrast to many other sulfide-disproportionating enrichments we were able to proliferate the enriched sulfur-disproportionating cultures without the addition of iron as sulfide sink as also shown for halophiles by Poser and colleagues (2013). However, due to the limitation by sulfide developments and expected low growth yields the cell densities remained low in our cultures. We searched for the disproportionating bacteria in the other AOM enrichments that were grown on methane for 5 to 15 years in laboratory. The genus *Desulfocapsa* was found in 5 of 10 enrichments, whereas Elba-DISP1 was only found in the Black Sea enrichment with more than 0.5‰ of the sequences (Supplementary Fig. 2). Bacteria related to GB-DISP1 were not

found in other enrichments than in the GB37 enrichments. Hence, we conclude that disproportionating bacteria are a general impurity of AOM enrichment cultures.

Sulfur-disproportionating bacteria such as *Desulfocapsa* sp. have been furthermore repeatedly identified in reduced ecosystems and in particular at cold seeps (Lloyd *et al*., 2006; Sylvan *et al*., 2012; Ruff *et al*., 2015). A direct connection of these groups to AOM is meanwhile unlikely, as they appear in rather low numbers compared to the known partner bacteria. In the environment they might thrive on elemental sulfur produced by sulfide-oxidizing bacteria or chemical oxidation of sulfide or being involved in the cryptic sulfur cycle rather below the sulfate methane interfaces (Holmkvist *et al*., 2011). Proliferation of disproportionating bacteria in *in vitro* AOM enrichments might be at first surprising. However, the cultivation medium will provide at least trace amounts of elemental sulfur that is produced when sodium sulfide is used as reducing agent. Furthermore, also any leak of oxygen during cultivation will lead to formation of zero-valent sulfur. Activity directly after medium exchange (medium is prepared with about 0.5 mM sulfide) is likely sufficient for the responsible sulfur-disproportionating bacteria to survive later inactivity at increased sulfide concentrations (regular medium change at approx. 12 to 15 mM sulfide). These short periods of activity are likely sufficient to thrive in the infrequently diluted AOM enrichments. At higher temperatures increased demands of maintenance energy may not have allowed survival of disproportionating bacteria in the G50 culture. Likewise ANME on methanotrophic substrates, the abundant partner bacteria, namely Seep-SRB-1, Seep-SRB-2 and HotSeep-1, did not respond to the addition of elemental sulfur. Our results strongly discourage the interpretation of zero-valent sulfur as intermediate exchanged in AOM in at least all here studied AOM enrichment cultures, which are dominated by ANME-1 or ANME-2. In reverse, the results support direct interspecies electron transfer as suggested for thermophilic AOM and psychrophilic AOM (McGlynn *et al*., 2015; Wegener *et al*., 2015) as most likely mechanism for the syntrophy of these ANME and their partner bacteria.

Conclusions

Here we described physiological characteristics of AOM communities at different temperatures from the Elba cold seeps and the Guaymas Basin hydrothermal vent area. We identified inorganic carbon as the dominant carbon source of AOM communities in all three tested AOM cultures, and hence provide additional evidence that all studied ANME and their partner bacteria are autotrophs. Further stable isotope probing experiments should consider

this finding, when considering selection of labeled carbon sources. We found no indications for a capability of ANME to reverse their metabolism towards net methanogenesis. In contrast, we showed the presence of specific known methanogens (*Methanococcoides* spp., *Methanohalophilus* spp.) in all studied low and medium temperature AOM enrichments. Those methanogens can be enriched and isolated using methylated compounds. Under natural and AOM enrichment conditions these organisms might benefit from trace losses of methylated compounds in the enzymatic machinery of AOM-active ANME archaea. Furthermore we were able to enrich sulfur-disproportionating bacteria from different AOM enrichments. None of the sulfur-disproportionating isolates was identical to the abundant AOM partner bacteria (Seep-SRB-1, Seep-SRB-2 or HotSeep-1). A lack of disproportionation in the partner bacteria also questions the production of sulfur intermediates by ANME-2, including their proposed capability of incomplete sulfate reduction (i.e. to disulfide; Milucka *et al*., 2012). Those results are in line with the lack of sulfur disproportionation in the thermophilic Guaymas Basin AOM enrichment (G50), where the partner bacterium has been recently identified as hydrogenotrophic sulfate reducer capable to directly retrieve electrons via nanowires from the ANME (Wegener *et al*., 2015). Although the low temperature enrichments were incapable of growing on hydrogen within consortia they may thrive by similar mechanisms as described for their high-temperature analog.

This study narrows down the metabolic capabilities of the AOM core community, the ANME and their syntrophic partner bacteria. ANME thrive as obligate methane-oxidizing, but autotrophic organisms, which however depend on specific partner bacteria that are obligate autotrophic sulfate-reducers. Of the partner bacteria only HotSeep-1 could be independently isolated from the ANME using hydrogen as molecular electron donor. To conclude, our results are in line with direct interspecies electron transfer as general mechanism between ANME and the partner bacteria. Other metabolic processes observed in AOM cultures and natural enrichments, such as methanogenesis and sulfur disproportionation, are performed by specialized minor community members thriving on potentially AOM derived methylated substrates or purely chemically produced zero-valent sulfur species.

Acknowledgements

Acknowledgements: We thank Susanne Menger and Ramona Appels for culture maintenance. Mirja Meiners, Martina Alisch and Nadine Broda for technical support, the Hinrichs Lab Bremen for analytical support and Marcos Y. Yoshinaga for assisting in identification of lipid mass spectra and Srijak Bhatnagar for support with sequence analyses. Furthermore we thank the scientific party and crew members of the research expeditions and Miriam Weber from the Hydra Institute for supplying the culture material (see Supplementary Tab. 1). We furthermore thank Thomas Holler and Christian Deusner for assistance with the early AOM enrichments and Katie Harding, Oliver Jäckle, and Veronika Will who contributed with experimental data obtained in lab rotations (International Max Planck research school Marine Microbiology MARMIC). *Funding:* We would like to thank the Max Planck Society, the German Research Foundation DFG (funding for G.W., V.K. and S.E.R. via Leibniz Grant to Antje Boetius) and the DFG Excellence cluster MARUM (G.W.) for financial support of this project.

References

Alperin MJ, Hoehler TM. (2009). Anaerobic methane oxidation by archaea/sulfate-reducing bacteria aggregates: 1. Thermodynamic and physical constraints. *Am J Sci* **309**: 869–957.

Aquilina A, Knab NJ, Knittel K, Kaur G, Geissler A, Kelly SP, *et al*. (2010). Biomarker indicators for anaerobic oxidizers of methane in brackish-marine sediments with diffusive methane fluxes. *Org Geochem* **41**: 414–426.

Bertram S, Blumenberg M, Michaelis W, Siegert M, Krüger M, Seifert R. (2013). Methanogenic capabilities of ANME-archaea deduced from ^{13}C-labelling approaches. *Environ Microbiol* **15**: 2384–2393.

Blumenberg M, Seifert R, Nauhaus K, Pape T, Michaelis W. (2005). *In vitro* study of lipid biosynthesis in an anaerobically methane-oxidizing microbial mat. *Appl Environ Microbiol* **71**: 4345–4351.

Boetius A, Ravenschlag K, Schubert CJ, Rickert D, Widdel F, Gieseke A, *et al*. (2000). A marine microbial consortium apparently mediating anaerobic oxidation of methane. *Nature* **407**: 623–626.

Boratyn GM, Camacho C, Cooper PS, Coulouris G, Fong A, Ma N, *et al*. (2013). BLAST: a more efficient report with usability improvements. *Nucleic Acids Res* **41**: W29–W33.

Cord-Ruwisch R. (1985). A quick method for the determination of dissolved and precipitated sulfides in cultures of sulfate-reducing bacteria. *J Microbiol Meth* **4**: 33–36.

Dowell F, Cardman Z, Dasarathy S, Kellermann M, Lipp JS, Ruff SE, *et al*. (submitted 2015). Microbial communities in methane- and short chain alkane-rich hydrothermal sediments of Guaymas Basin. *Front Microbiol.*

Edgar RC, Haas BJ, Clemente JC, Quince C, Knight R. (2011). UCHIME improves sensitivity and speed of chimera detection. *Bioinformatics* **27**: 2194–2200.

Elvert M, Hopmans EC, Treude T, Boetius A, Suess E. (2005). Spatial variations of methanotrophic consortia at cold methane seeps: implications from a high-resolution molecular and isotopic approach. *Geobiology* **3**: 195–209.

Finster K, Liesack W, Thamdrup B. (1998). Elemental sulfur and thiosulfate disproportionation by *Desulfocapsa sulfoexigens* sp. nov., a new anaerobic bacterium isolated from marine surface sediment. *Appl Environ Microbiol* **64**: 119–125.

Finster K. (2008). Microbiological disproportionation of inorganic sulfur compounds. *J Sulfur Chem* **29**: 281–292.

Girguis PR, Cozen AE, DeLong EF. (2005). Growth and population dynamics of anaerobic methane-oxidizing archaea and sulfate-reducing bacteria in a continuous-flow bioreactor. *Appl Environ Microbiol* **71**: 3725–3733.

Hallam SJ, Putnam N, Preston CM, Detter JC, Rokhsar D, Richardson PM, *et al*. (2004). Reverse methanogenesis: testing the hypothesis with environmental genomics. *Science* **305**: 1457–1462.

Harrison BK, Zhang H, Berelson W, Orphan VJ. (2009). Variations in archaeal and bacterial diversity associated with the sulfate-methane transition zone in continental margin sediments (Santa Barbara Basin, California). *Appl Environ Microbiol* **75**: 1487–1499.

Hinrichs K-U, Hayes JM, Sylva SP, Brewer PG, DeLong EF. (1999). Methane-consuming archaebacteria in marine sediments. *Nature* **398**: 802–805.

Hoehler TM. (2004). Biological energy requirements as quantitative boundary conditions for life in the subsurface. *Geobiology* **2**: 205–215.

Holler T, Wegener G, Knittel K, Boetius A, Brunner B, Kuypers MMM, *et al*. (2009). Substantial $^{13}C/^{12}C$ and D/H fractionation during anaerobic oxidation of methane by marine consortia enriched *in vitro*. *Environ Microbiol Rep* **1**: 370–376.

Holler T, Wegener G, Niemann H, Deusner C, Ferdelman TG, Boetius A, *et al*. (2011a). Carbon and sulfur back flux during anaerobic microbial oxidation of methane and coupled sulfate reduction. *Proc Natl Acad Sci USA* **108**: E1484–E1490.

Holler T, Widdel F, Knittel K, Amann R, Kellermann MY, Hinrichs K-U, *et al*. (2011b). Thermophilic anaerobic oxidation of methane by marine microbial consortia. *ISME J* **5**: 1946–1956.

Holmkvist L, Ferdelman TG, Jørgensen BB. (2011). A cryptic sulfur cycle driven by iron in the methane zone of marine sediment (Aarhus Bay, Denmark). *Geochim Cosmochim Acta* **75**: 3581–3599.

Huse SM, Welch DM, Morrison HG, Sogin ML. (2010). Ironing out the wrinkles in the rare biosphere through improved OTU clustering. *Environ Microbiol* **12**: 1889–1898.

Kallmeyer J, Ferdelman TG, Weber A, Fossing H, Jørgensen BB. (2004). A cold chromium distillation procedure for radiolabeled sulfide applied to sulfate reduction measurements. *Limnol Oceanogr Methods* **2**: 171–180.

Kellermann MY, Wegener G, Elvert M, Yoshinaga MY, Lin Y-S, Holler T, *et al*. (2012). Autotrophy as a predominant mode of carbon fixation in anaerobic methane-oxidizing microbial communities. *Proc Natl Acad Sci USA* **109**: 19321–19326.

Kellermann MY, Yoshinaga MY, Wegener G, Krukenberg V, Hinrichs K-U. (submitted 2015). Tracing the production and fate of individual archaeal intact polar lipids using stable isotope probing. *Org Geochem*.

Kendall MM, Boone DR. (2006). The order Methanosarcinales. In: *The Prokaryotes*. Dworkin M, Falkow S, Rosenberg E, Schleifer K-H, Stackebrandt E (eds). New York; Springer, pp 244-256.

Kiene RP, Oremland RS, Catena A, Miller LG, Capone DG. (1986). Metabolism of reduced methylated sulfur compounds in anaerobic sediments and by a pure culture of an estuarine methanogen. *Appl Environ Microbiol* **52**: 1037–1045.

King GM. (1984). Utilization of hydrogen, acetate, and "noncompetitive" substrates by methanogenic bacteria in marine sediments. *Geomicrobiol J* **3**: 275–306.

Kleindienst S, Ramette A, Amann R, Knittel K. (2012). Distribution and *in situ* abundance of sulfate-reducing bacteria in diverse marine hydrocarbon seep sediments. *Environ Microbiol* **14**: 2689–2710.

Knittel K, Boetius A, Lemke A, Eilers H, Lochte K, Pfannkuche O, *et al*. (2003). Activity, distribution, and diversity of sulfate reducers and other bacteria in sediments above gas hydrate (Cascadia margin, Oregon). *Geomicrobiol J* **20**: 269–294.

Knittel K, Lösekann T, Boetius A, Kort R, Amann R. (2005). Diversity and distribution of methanotrophic archaea at cold seeps. *Appl Environ Microbiol* **71**: 467–479.

Knittel K, Boetius A. (2009). Anaerobic oxidation of methane: progress with an unknown process. *Annu Rev Microbiol* **63**: 311–334.

Koga Y, Morii H. (2005). Recent advances in structural research on ether lipids from *Archaea* including comparative and physiological aspects. *Biosci Biotechnol Biochem* **69**: 2019–2034.

Krüger M, Treude T, Wolters H, Nauhaus K, Boetius A. (2005). Microbial methane turnover in different marine habitats. *Palaeogeogr Palaeoclimatol Palaeoecol* **227**: 6–17.

Krukenberg V, Harding K, Richter M, Glöckner FO, Harald Gruber-Vodicka, Adam B, *et al*. (submitted 2015). *Candidatus* Desulfofervidus auxilii, a hydrogenotrophic sulfate-

reducing bacterium involved in the thermophilic anaerobic oxidation of methane. *Environ Microbiol.*

Lanoil BD, La Duc MT, Wright M, Kastner M, Nealson KH, Bartlett D. (2005). Archaeal diversity in ODP legacy borehole 892b and associated seawater and sediments of the Cascadia Margin. *FEMS Microbiol Ecol* **54**: 167–177.

Lloyd KG, Lapham L, Teske A. (2006). An anaerobic methane-oxidizing community of ANME-1b archaea in hypersaline Gulf of Mexico sediments. *Appl Environ Microbiol* **72**: 7218–7230.

Lloyd KG, Alperin MJ, Teske A. (2011). Environmental evidence for net methane production and oxidation in putative ANaerobic MEthanotrophic (ANME) archaea. *Environ Microbiol* **13**: 2548–2564.

Lovley DR, Klug MJ. (1986). Model for the distribution of sulfate reduction and methanogenesis in freshwater sediments. *Geochim Cosmochim Acta* **50**: 11–18.

Ludwig W, Strunk O, Westram R, Richter L, Meier H, Yadhukumar, *et al.* (2004). ARB: a software environment for sequence data. *Nucleic Acids Res* **32**: 1363–1371.

Manz W, Eisenbrecher M, Neu TR, Szewzyk U. (1998). Abundance and spatial organization of Gram-negative sulfate-reducing bacteria in activated sludge investigated by *in situ* probing with specific 16S rRNA targeted oligonucleotides. *FEMS Microbiol Ecol* **25**: 43–61.

Massana R, Murray AE, Preston CM, DeLong EF. (1997). Vertical distribution and phylogenetic characterization of marine planktonic *Archaea* in the Santa Barbara Channel. *Appl Environ Microbiol* **63**: 50–56.

McGlynn SE, Chadwick GL, Kempes CP, Orphan VJ. (2015). Single cell activity reveals direct electron transfer in methanotrophic consortia. *Nature* **526**: 531–535.

Meyerdierks A, Kube M, Kostadinov I, Teeling H, Glöckner FO, Reinhardt R, *et al*. (2010). Metagenome and mRNA expression analyses of anaerobic methanotrophic archaea of the ANME-1 group. *Environ Microbiol* **12**: 422–439.

Michaelis W, Seifert R, Nauhaus K, Treude T, Thiel V, Blumenberg M, *et al.* (2002). Microbial reefs in the Black Sea fueled by anaerobic oxidation of methane. *Science* **297**: 1013–1015.

Mills HJ, Hodges C, Wilson K, MacDonald IR, Sobecky PA. (2003). Microbial diversity in sediments associated with surface-breaching gas hydrate mounds in the Gulf of Mexico. *FEMS Microbiol Ecol* **46**: 39–52.

Milucka J, Ferdelman TG, Polerecky L, Franzke D, Wegener G, Schmid M, *et al*. (2012). Zero-valent sulphur is a key intermediate in marine methane oxidation. *Nature* **491**: 541–546.

Milucka J, Widdel F, Shima S. (2013). Immunological detection of enzymes for sulfate reduction in anaerobic methane-oxidizing consortia. *Environ Microbiol* **15**: 1561–1571.

Muyzer G, Teske A, Wirsen CO, Jannasch HW. (1995). Phylogenetic relationships of *Thiomicrospira* species and their identification in deep-sea hydrothermal vent samples by denaturing gradient gel electrophoresis of 16S rDNA fragments. *Arch Microbiol* **164**: 165–172.

Muyzer G, Brinkhoff T, Nübel U, Santegoeds C, Schäfer H, Wawer C. (1998). Denaturing gradient gel electrophoresis (DGGE) in microbial ecology. In: *Molecular Microbial Ecology Manual*. Kowalchuk GA, de Bruijn FJ, Head IM, Akkermans AD, van Elsas JD (eds). Netherlands: Springer, pp 2645–2671.

Nauhaus K, Boetius A, Krüger M, Widdel F. (2002). *In vitro* demonstration of anaerobic oxidation of methane coupled to sulphate reduction in sediments from a marine gas hydrate area. *Environ Microbiol* **4**: 296–305.

Nauhaus K, Treude T, Boetius A, Krüger M. (2005). Environmental regulation of the anaerobic oxidation of methane: a comparison of ANME-I and ANME-II communities. *Environ Microbiol* **7**: 98–106.

Nauhaus K, Albrecht M, Elvert M, Boetius A, Widdel F. (2007). *In vitro* cell growth of marine archaeal-bacterial consortia during anaerobic oxidation of methane with sulfate. *Environ Microbiol* **9**: 187–196.

Niemann H, Lösekann T, de Beer D, Elvert M, Nadalig T, Knittel K, *et al.* (2006). Novel microbial communities of the Haakon Mosby mud volcano and their role as a methane sink. *Nature* **443**: 854–858.

Omoregie EO, Mastalerz V, de Lange G, Straub KL, Kappler A, Røy H, *et al*. (2008). Biogeochemistry and community composition of iron- and sulfur-precipitating microbial mats at the Chefren mud volcano (Nile Deep Sea Fan, Eastern Mediterranean). *Appl Environ Microbiol* **74**: 3198–3215.

Orcutt B, Samarkin V, Boetius A, Joye S. (2008). On the relationship between methane production and oxidation by anaerobic methanotrophic communities from cold seeps of the Gulf of Mexico. *Environ Microbiol* **10**: 1108–1117.

Orphan VJ, House CH, Hinrichs K-U, McKeegan KD, DeLong EF. (2001). Methane-consuming archaea revealed by directly coupled isotopic and phylogenetic analysis. *Science* **293**: 484–487.

Orphan VJ, House CH, Hinrichs K-U, McKeegan KD, DeLong EF. (2002). Multiple archaeal groups mediate methane oxidation in anoxic cold seep sediments. *Proc Natl Acad Sci USA* **99**: 7663–7668.

Pachiadaki MG, Yakimov MM, LaCono V, Leadbetter E, Edgcomb V. (2014). Unveiling microbial activities along the halocline of Thetis, a deep-sea hypersaline anoxic basin. *ISME J* **8**: 2478–2489.

Pernthaler A, Pernthaler J, Amann R. (2002). Fluorescence *in situ* hybridization and catalyzed reporter deposition for the identification of marine bacteria. *Appl Environ Microbiol* **68**: 3094–3101.

Pires AC, Cleary DF, Almeida A, Cunha A, Dealtry S, Mendonca-Hagler LC, *et al*. (2012). Denaturing gradient gel electrophoresis and barcoded pyrosequencing reveal unprecedented archaeal diversity in mangrove sediment and rhizosphere samples. *Appl Environ Microbiol* **78**: 5520–5528.

Poser A, Lohmayer R, Vogt C, Knoeller K, Planer-Friedrich B, Sorokin D, *et al*. (2013). Disproportionation of elemental sulfur by haloalkaliphilic bacteria from soda lakes. *Extremophiles* **17**: 1003–1012.

Preuß A, Schauder R, Fuchs G. (1989). Carbon isotope fractionation by autotrophic bacteria with three different CO_2 fixation pathways. *Z Naturforsch B* **44**: 397–402.

Pruesse E, Quast C, Knittel K, Fuchs BM, Ludwig W, Peplies J, *et al*. (2007). SILVA: a comprehensive online resource for quality checked and aligned ribosomal RNA sequence data compatible with ARB. *Nucleic Acids Res* **35**: 7188–7196.

Quast C, Pruesse E, Yilmaz P, Gerken J, Schweer T, Yarza P, *et al*. (2013). The SILVA ribosomal RNA gene database project: improved data processing and web-based tools. *Nucleic Acids Res* **41**: D590–596.

Quince C, Lanzén A, Curtis TP, Davenport RJ, Hall N, Head IM, *et al*. (2009). Accurate determination of microbial diversity from 454 pyrosequencing data. *Nature Methods* **6**: 639–641.

Reeburgh WS. (2007). Oceanic methane biogeochemistry. *Chem Rev* **107**: 486–513.

Rossel PE, Lipp JS, Fredricks HF, Arnds J, Boetius A, Elvert M, *et al*. (2008). Intact polar lipids of anaerobic methanotrophic archaea and associated bacteria. *Org Geochem* **39**: 992–999.

Ruff SE, Biddle JF, Teske AP, Knittel K, Boetius A, Ramette A. (2015). Global dispersion and local diversification of the methane seep microbiome. *Proc Natl Acad Sci USA* **112**: 4015–4020.

Ruff SE, Kuhfuss H, Wegener G, Lott C, Ramette A, Wiedling J, *et al*. (submitted 2015). Methane seep in shallow-water permeable sediment harbors high diversity of anaerobic methanotrophic communities, Elba, Italy. *Front Microbiol*.

Schloss PD, Westcott SL, Ryabin T, Hall JR, Hartmann M, Hollister EB, *et al.* (2009). Introducing mothur: open-source, platform-independent, community-supported software for describing and comparing microbial communities. *Appl Environ Microbiol* **75**: 7537–7541.

Schloss PD, Gevers D, Westcott SL. (2011). Reducing the effects of PCR amplification and sequencing artifacts on 16S rRNA-based studies. *PloS One* **6**: e27310.

Schouten S, Wakeham SG, Hopmans EC, Damsté JSS. (2003). Biogeochemical evidence that thermophilic archaea mediate the anaerobic oxidation of methane. *Appl Environ Microbiol* **69**: 1680–1686.

Schreiber L, Holler T, Knittel K, Meyerdierks A, Amann R. (2010). Identification of the dominant sulfate-reducing bacterial partner of anaerobic methanotrophs of the ANME-2 clade. *Environ Microbiol* **12**: 2327–2340.

Sorokin DY, Tourova TP, Mussmann M, Muyzer G. (2008). *Dethiobacter alkaliphilus* gen. nov. sp. nov., and *Desulfurivibrio alkaliphilus* gen. nov. sp. nov.: two novel representatives of reductive sulfur cycle from soda lakes. *Extremophiles* **12**: 431–439.

Sowers KR, Ferry JG. (1983). Isolation and characterization of a methylotrophic marine methanogen, *Methanococcoides methylutens* gen. nov., sp. nov.. *Appl Environ Microbiol* **45**: 684–690.

Stamatakis A. (2006). RAxML-VI-HPC: maximum likelihood-based phylogenetic analyses with thousands of taxa and mixed models. *Bioinformatics* **22**: 2688–2690.

Steudel R, Göbel T, Holdt G. (1988). The molecular composition of hydrophilic sulfur sols prepared by decomposition of thiosulfate. *Z Naturforsch B* **43**: 203–218.

Stokke R, Roalkvam I, Lanzen A, Haflidason H, Steen IH. (2012). Integrated metagenomic and metaproteomic analyses of an ANME-1-dominated community in marine cold seep sediments. *Environ Microbiol* **14**: 1333–1346.

Sturt HF, Summons RE, Smith K, Elvert M, Hinrichs K-U. (2004). Intact polar membrane lipids in prokaryotes and sediments deciphered by high-performance liquid chromatography/electrospray ionization multistage mass spectrometry - new biomarkers for biogeochemistry and microbial ecology. *Rapid Commun Mass Spectrom* **18**: 617–628.

Sylvan JB, Toner BM, Edwards KJ. (2012). Life and death of deep-sea vents: bacterial diversity and ecosystem succession on inactive hydrothermal sulfides. *mBio* **3**: e00279–00211.

Teske A, Hinrichs K-U, Edgcomb V, de Vera Gomez A, Kysela D, Sylva SP, *et al*. (2002). Microbial diversity of hydrothermal sediments in the Guaymas Basin: evidence for anaerobic methanotrophic communities. *Appl Environ Microbiol* **68**: 1994–2007.

Thauer RK. (2011). Anaerobic oxidation of methane with sulfate: on the reversibility of the reactions that are catalyzed by enzymes also involved in methanogenesis from CO_2. *Curr Opin Microbiol* **14**: 292–299.

Thomsen TR, Finster K, Ramsing NB. (2001). Biogeochemical and molecular signatures of anaerobic methane oxidation in a marine sediment. *Appl Environ Microbiol* **67**: 1646–1656.

Tijhuis L, Van Loosdrecht MC, Heijnen JJ. (1993). A thermodynamically based correlation for maintenance gibbs energy requirements in aerobic and anaerobic chemotrophic growth. *Biotechnol Bioeng* **42**: 509–519.

Treude T, Knittel K, Blumenberg M, Seifert R, Boetius A. (2005). Subsurface microbial methanotrophic mats in the Black Sea. *Appl Environ Microbiol* **71**: 6375–6378.

Treude T, Orphan V, Knittel K, Gieseke A, House CH, Boetius A. (2007). Consumption of methane and CO_2 by methanotrophic microbial mats from gas seeps of the anoxic Black Sea. *Appl Environ Microbiol* **73**: 2271–2283.

Wang F-P, Zhang Y, Chen Y, He Y, Qi J, Hinrichs K-U, *et al*. (2014). Methanotrophic archaea possessing diverging methane-oxidizing and electron-transporting pathways. *ISME J* **8**: 1069–1078.

Wegener G, Niemann H, Elvert M, Hinrichs K-U, Boetius A. (2008a). Assimilation of methane and inorganic carbon by microbial communities mediating the anaerobic oxidation of methane. *Environ Microbiol* **10**: 2287–2298.

Wegener G, Shovitri M, Knittel K, Niemann H, Hovland M, Boetius A. (2008b). Biogeochemical processes and microbial diversity of the Gullfaks and Tommeliten methane seeps (Northern North Sea). *Biogeosciences* **5**: 1127–1144.

Wegener G, Krukenberg V, Riedel D, Tegetmeyer HE, Boetius A. (2015). Intercellular wiring enables electron transfer between methanotrophic archaea and bacteria. *Nature* **526**: 587–590.

Widdel F, Bak F. (1992). Gram-negative mesophilic sulfate-reducing bacteria. In: *The Prokaryotes*. Balows A, Trüper HG, Dworkin M, Harder W, Schleifer K-H (eds). New York: Springer, pp 3352–3378.

Wörmer L, Lipp JS, Schröder JM, Hinrichs K-U. (2013). Application of two new LC–ESI–MS methods for improved detection of intact polar lipids (IPLs) in environmental samples. *Org Geochem* **59**: 10–21.

Xin J-Y, Cui J-R, Niu J-Z, Hua S-F, Xia C-G, Li S-B, *et al*. (2004). Production of methanol from methane by methanotrophic bacteria. *Biocatal Biotransfor* **22**: 225–229.

Yarza P, Yilmaz P, Pruesse E, Glöckner FO, Ludwig W, Schleifer K-H, *et al*. (2014). Uniting the classification of cultured and uncultured bacteria and archaea using 16S rRNA gene sequences. *Nat Rev Microbiol* **12**: 635–645.

Yoshinaga MY, Kellermann MY, Rossel PE, Schubotz F, Lipp JS, Hinrichs K-U. (2011). Systematic fragmentation patterns of archaeal intact polar lipids by high-performance liquid chromatography/electrospray ionization ion-trap mass spectrometry. *Rapid Commun Mass Spectrom* **25**: 3563–3574.

Zhou J, Bruns MA, Tiedje JM. (1996). DNA recovery from soils of diverse composition. *Appl Environ Microbiol* **62**: 316–322.

Figures and tables

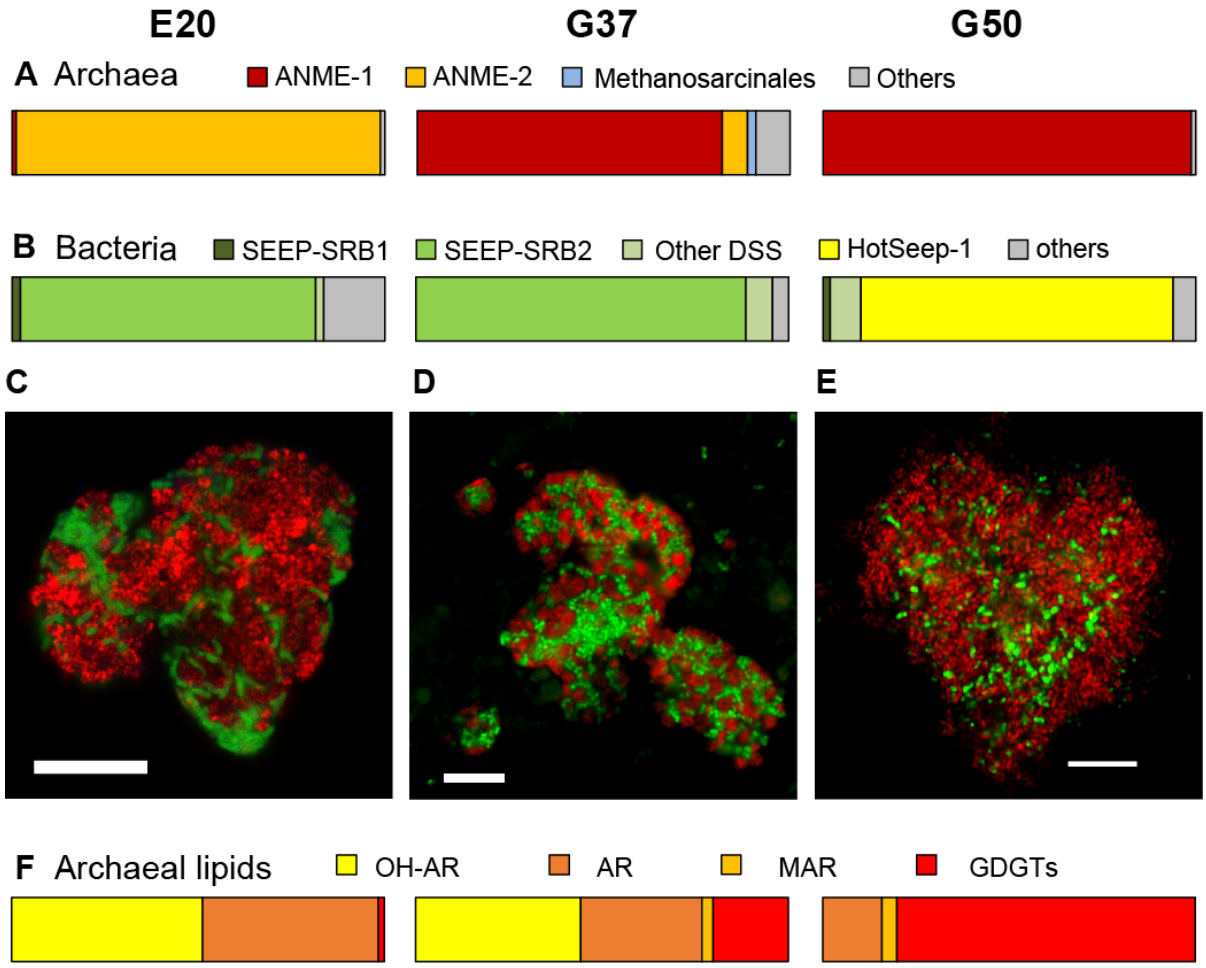

Figure 1 Comparison of community composition, typical microbial aggregates and archaeal lipids of the three AOM enrichment cultures (**A,B**) Comparison of normalized archaeal and bacterial clone numbers retrieved from the enrichment (for clone number see Tab. 1; short, badly aligning sequences were not considered here). (**C-E**) Fluorescence *in situ* hybridization of dual-species aggregates in the enrichment (E20: red=ANME-2-538 (Treude *et al*., 2005), green=DSS658 (Manz *et al.,* 1998); G37: red=ANME-1-350 (Boetius *et al.,* 2000), green=DSS658; G50: red=ANME-1-350, green=HotSeep-1-590 (Holler *et al.,* 2011b)), bars scale 10 µm. (**F**) Major archaeal membrane intact polar lipid types defined by hydrophobic core group: OH=hydroxyarchaeol, AR=archaeol, MAR=macrocyclic archaeol, GDGT=Glycerol dialkyl glycerol tetraether. At higher temperatures ANME-1 archaea tend to produce predominantly GDGTs, likely a temperature adaption (for details and 60°C example see Tab. 2).

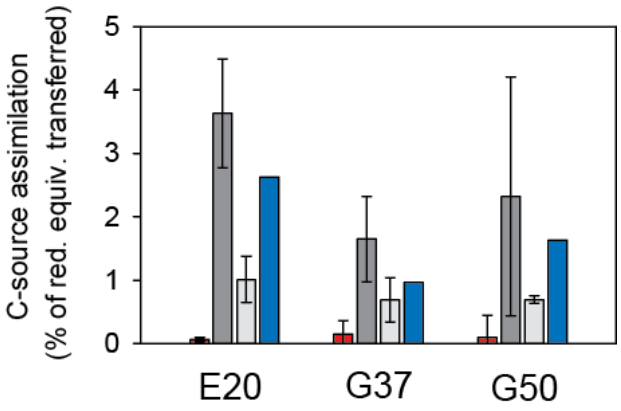

Figure 2 Assimilation of carbon sources in relation to reducing equivalent transfer assuming an average oxidation state of organic carbon of 0 (red=methane assimilation; dark grey=DIC assimilation in presence of methane; light grey=DIC assimilation in absence of methane; blue=derived methane-dependent DIC assimilation; error bars=standard deviation; n=3 per treatment). In all cultures assimilation of inorganic carbon strongly exceeds methane carbon assimilation, suggesting that the latter is likely methane-derived DIC assimilation.

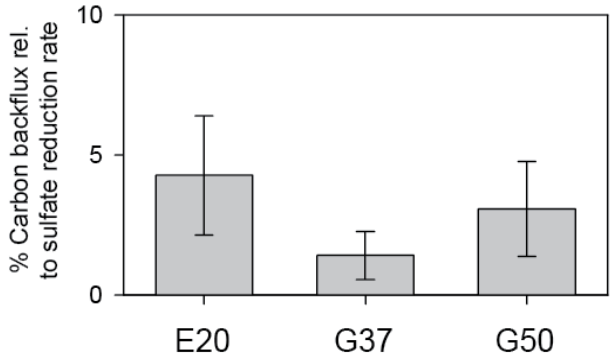

Figure 3 Production of ^{14}C-methane from ^{14}C-bicarbonate relative to AOM rates (here determined by production of ^{35}S-sulfide from ^{35}S-sulfate) in the three studied AOM enrichments incubated at AOM conditions at their respective temperature optima (error bars=standard deviation; n=5 per treatment).

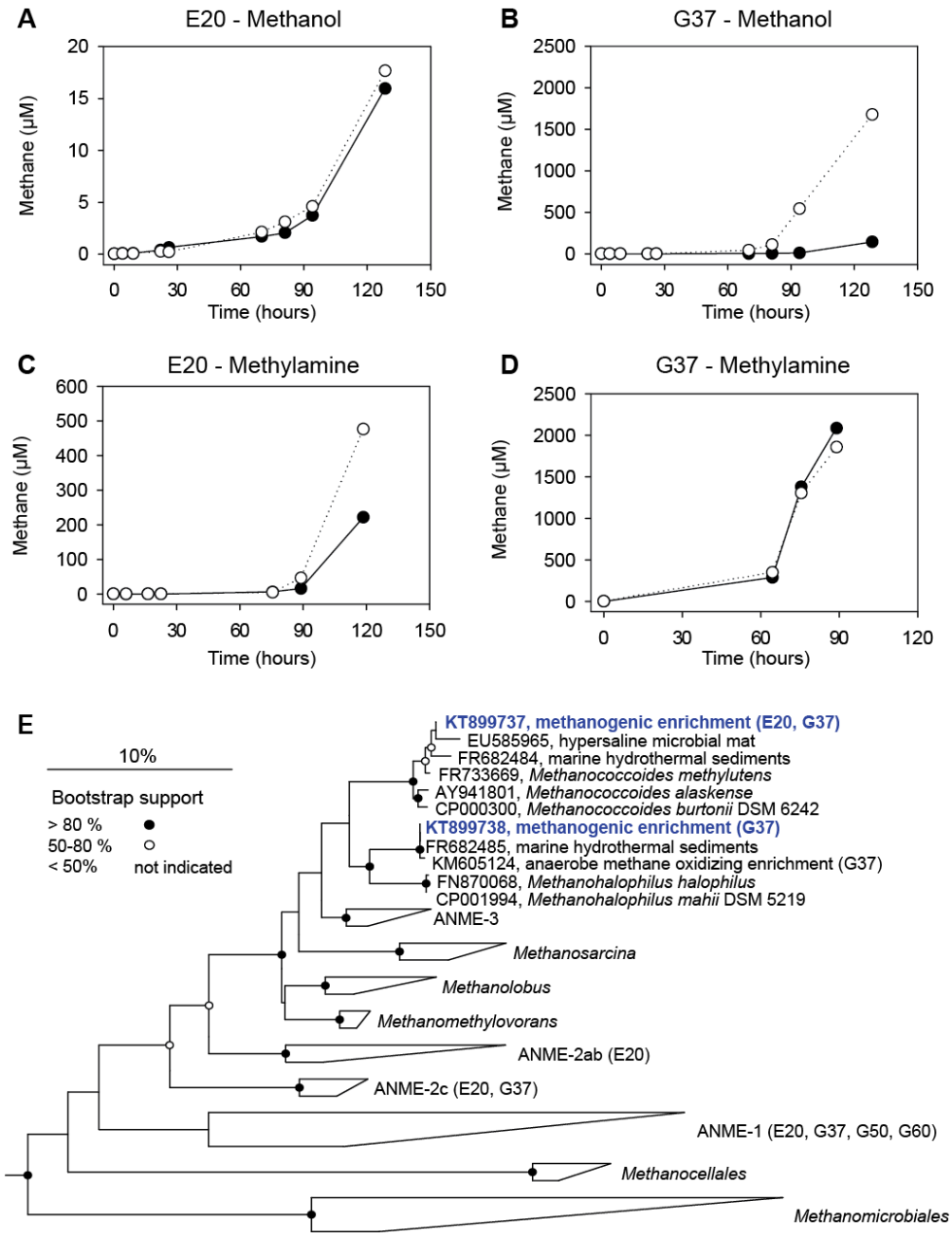

Figure 4 Methanogenesis and methanogenic archaea in AOM cultures. (**A-D**) Methane production in 1:10 dilutions of the E20 and G37 AOM enrichments after addition of methanol or methylamine (10 mM) to the enrichments. Filled and open circles indicate replicate incubations. (**E**) Phylogenetic affiliation of methanogens isolated in dilution-to-extinction approaches with methanol and methylamine.

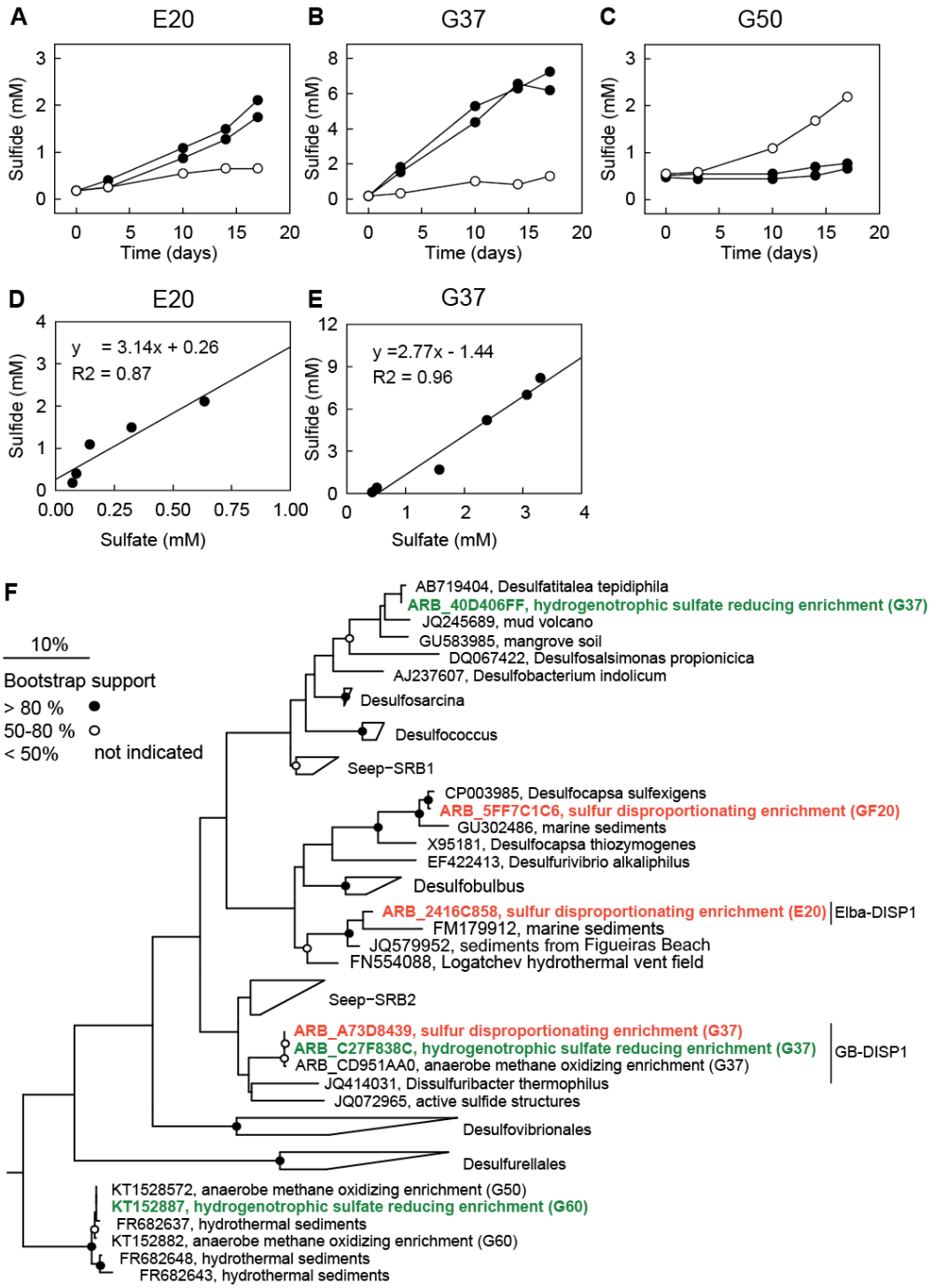

Figure 5 Sulfur disproportionation in AOM enrichment cultures. (**A-C**) Comparison of development of sulfide concentrations in the three AOM enrichments at AOM conditions (methane (2.25 atm) plus sulfate (20 mM; open circles)) and during addition of colloidal sulfur (20 mM; filled circles) within 18 days. (**D-E**) Comparison of sulfide and sulfate production in zero-valent sulfur amendments of E20 and G37; disproportionation has not been observed in G50. The observed approximate 3:1 stoichiometry between sulfide and sulfate production is characteristic for disproportionation of elemental (zero-valent) sulfur. (**F**) Phylogenetic affiliation of sulfur-disproportionating bacteria within the *Deltaproteobacteria* based on full length 16S rRNA gene sequences retrieved from high dilutions of AOM-active cultures supplied with elemental sulfur.

Table 1 Analyzed clones from 16S rRNA gene libraries established from sediment-free anaerobic methane-oxidizing enrichment cultures from Elba and the Guaymas Basin. Percent of total sequences is indicated for AOM organisms in parenthesis.

	enrichment				
Phylogenetic Group	**E20**	**G37**	**G50**	**G60**	**G50 & 60**
Archaea					
Euryarchaeota					
Methanomicrobia					
ANME-1					
ANME-1a		**71 (83%)**	**85 (99%)**	**70 (88%)**	**155 (93%)**
ANME-1b	1 (1%)				
Methanosarcinales					
ANME-2					
ANME-2a-2b	9 (11%)				
ANME-2b	23 (30%)				
ANME-2c	**46 (58%)**	6 (7%)			
Others		3		1	1
Thermoplasmata		6	1	6	7
Thermococci				1	1
Thaumarchaeota				1	1
Crenarchaeota				1	1
Total sequences analyzed	**79**	**86**	**86**	**80**	**166**
Bacteria					
Proteobacteria					
Deltaproteobacteria					
HotSeep-1			**41 (48%)**	**48 (74%)**	**89 (59%)**
Seep-SRB-1	7 (9%)		1 (1%)		1 (1%)
Seep-SRB-2	**35 (46%)**	**60 (88%)**			
Others	2	5	4		4
Betaproteobacteria				1	1
Bacteroidetes	6				
Spirochaetes	3				
Chloroflexi	1				
Planctomycetes	5				
Firmicutes	3				
Candidate division OP-3			37	3	40
Candidate division OP-8	1			6	6
Candidate division JS1		2			
Others	13	1	3	7	10
Total sequences analyzed	**76**	**68**	**86**	**65**	**151**

Table 2 Relative composition of archaeal lipids in the three studied enrichments, and for comparison, of lipids in G60.

	ANME-2		ANME-1	
Diethers	**E20**	**G37**	**G50**	**G60**
1Gly-AR	9			
1Gly-OH-AR	31			
2Gly-AR	18	7	9	3
GNG-AR	3			
PG-AR	12	25	6	2
PG-OH-AR	19	1	0	0
Pent-PG-AR	2			
PE-AR	2			
PE-OH-AR	1	44	0	0
PE-MAR		3	4	2
PI-AR	0			
PI-OH-AR	1			
Tetraethers				
PG-GDGT-PG		0	0	0
PG-GDGT		5	0	0
1Gly-GDGT	1	0	1	5
2Gly-GDGT	1	14	79	88
Summary				
OH-AR	51	44	0	0
AR	47	32	16	5
MAR	0	3	4	2
Tetraether	2	20	80	94

Abbreviations: Headgroups Gly = glycosyl, PG = phosphatidylglycerol, PE = phosphatidylethanolamine, PI = phosphatidylinositol, PE = phosphatidylethanolamine. Core lipid: AR = archaeol, MAR = Macrocyclic archaeol, GDGT = glyceroldibiphytanylglyceroltetraether

Table 3 Stimulation of methanogenesis and sulfate reduction in enrichments from Elba (E20) and Guaymas Basin (G37 and G50) using different substrates (methanogenesis w/o sulfate).

	E20	G37	G50
Substrate		**Methanogenesis**	
AOM control	+	+	+
No-substrate control	0	0	0
Hydrogen	0	0	0
Formate	0	0	0
Acetate	0	0	0
Methanol	+++	+++	0
Methylamine	+++	+++	0
		Sulfate reduction	
AOM control	+	+	+
No-substrate control	0	0	0
Hydrogen	0	++	+++++
Carbon monoxide	0	0	0
Methyl sulfide	0	0	0
Methanol	0	0	0
Acetate	0	0	0
Formate	0	0	0
Propionate	0	0	0

'+' expected rate measured; '++' instant rates low, but rates exceed AOM after longer time, '+++' instant rate low, but rapidly higher than AOM, '+++++' rate instantly 3 times higher than during AOM

Table 4 Methanogenic and sulfur-disproportionating minor community members.

OTU0.02*	E20	G37	G50	Gullfaks	Organism**	Sequences from isolates
A-Otu00017	2.8	1.3	0.1	4.3	*Methanococcoides*	KT899737
A-Otu00024	2.9	1.8	−	7.0	*Methanohalophilus*	KT899738
B-Otu00016	−	−	−	1.0	*Desulfocapsa*	KT899741
BOtu00114	8.6	−	−	−	Elba-DISP1	KT899742
BOtu00373	−	2.2	−	−	GB-DISP1	KT899739; KT899740

*based on 454 pyrosequencing of the 16S rRNA V3-V5 region; **Presented organisms had a taxonomy quality score of 100; Numbers report detected sequences as parts of 1000 (‰).

Supplementary information

Supplementary data description

Here we provide additional phylogenetic analyses of the four AOM enrichment cultures described in the main text and of six other methanotrophic enrichment cultures. All cultivations were performed with anaerobic seawater medium and methane and sulfate as provided electron donor and acceptor source.

Supplementary Table 1 provides an overview on the sample origin and cultivation conditions. Supplementary Table 2 depicts the relative abundance of specific methanogenic and methanotrophic archaea and known AOM partner bacteria and clades of known sulfur-disproportionating bacteria. Supplementary Fig. 2 provides an overview on the distribution of microbial taxa in the different AOM enrichment cultures.

Our results show that long-term, sediment-free AOM enrichments are dominted by typical AOM organisms (ANME clades and their partner bacteria). However these enrichments still harbor a large diversity of different archaea (i.e. *Thermoplasmatales* or MBGD) and bacteria (i.e. *Anaerolinaceae*, *Cladithrix* or relatives of the Candidate divisions JS1, OD1 and OP11). The function of these organisms is so far unknown, however they are most likely heterotrophs feeding on exudates of AOM (Supplementary Fig. 2). Nearly all studied cultures contain sequences of methylotrophic methanogens and disproportionating bacteria. These organisms are usually rare and not identical with ANME and their partner bacteria (Supplementary Tab. 2), however when supplying their specific substrates these groups can grow rapidly.

Supplementary figures and tables

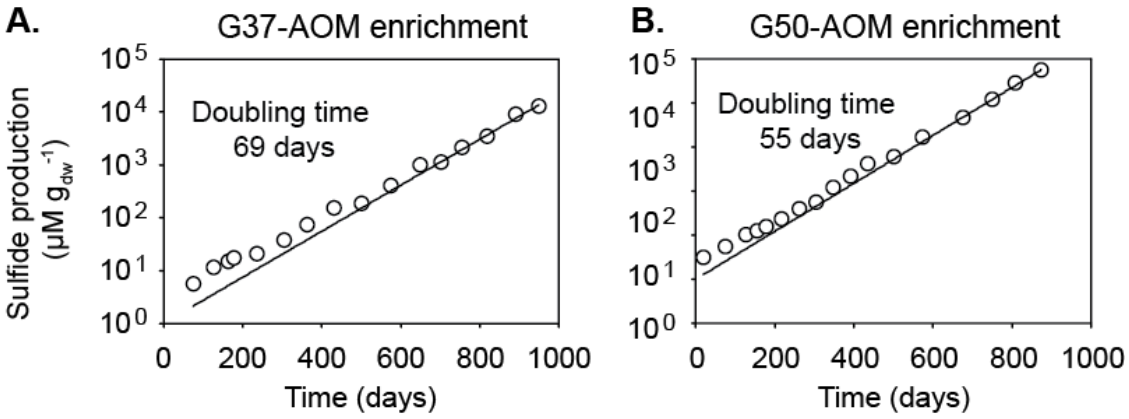

Supplementary Figure 1 Development of sulfide production in the studied mesophilic G37 (**A**) and thermophilic G50 (**B**) AOM enrichment culture normalized to calculated dry weights. The slope of the regression line (calculated by least square fitting) was used to determine activity doubling times $T_d=\ln 2/\ln(\Delta SP/\Delta t)$.

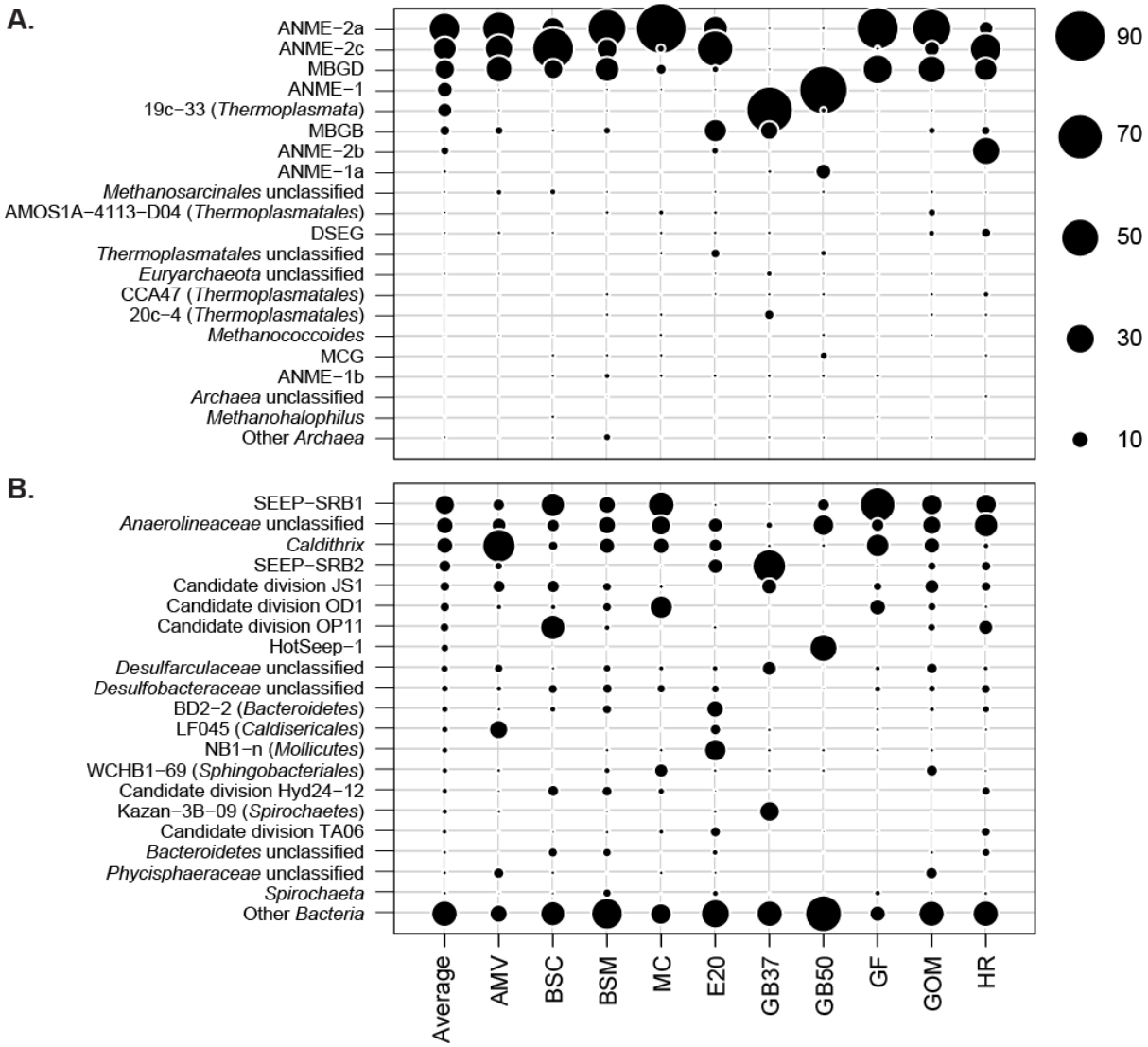

Supplementary Figure 2 Relative sequence abundances of archaea (**A**) and bacteria (**B**) in ten long-term enrichment cultures under strict AOM conditions based on 16S rRNA gene tags of the variable region V3-V5. Bubble sizes depict relative sequence abundances in %. AMV: Amon mud volcano, BSC: Black Sea seep, BSM: Black Sea microbial reef, MC: Menez Caldera seep, E20: Elba seep (20°C), GB37: Guaymas Basin seep (37°C), GB50: Guaymas Basin seep (50°C), GF: Gullfaks seep, GOM: Gulf of Mexico seep, HR: Hydrate Ridge seep. Next to ANME and their partner bacteria, AOM enrichment cultures cultivated on methane and sulfate for many years still contain a large number of other microorganisms with yet unknown function.

Supplementary Table 1 Origin, sampling depth and sampling year of different AOM enrichment cultures. *Temperature (Temp.) describes the *in vitro* incubation temperature.

Sample	Acro-nym	Location	Water depth	Site	Samp-ling	Temp. (°C)*	Sampling campaign
Guaymas50	G50	27.01 N 111.41 W	1999m	Hydrothermal Vent	2009	50	RV Atlantis exp. AT15-45 with submarine Alvin; Chief Scientist A. Teske
Guaymas37	G37	27.01 N 111.41 W	1999m	Hydrothermal Vent	2009	37	
Elba Seep	E20	42.74 N 010.12 E	12m	Cold Seep	2010	20	Hydra Diving Station; PI Miriam Weber
Gullfaks Seep	GF	61.17 N 002.24 E	150m	Cold Seep	2005	20	RV Alkor Cruise 267; Chief Scientist A. Boetius
Amon MV	AMV	31.73 N 032.37 E	1250m	Mud Volcano	2003	20	NAUTINIL exp. RV L Atalante; CS J.-P. Foucher
Black Sea mat	BSM	44.74 N 031.97 E	300m	Microbial Chimney	2004	12	RV POSEIDON exp. 317/3 with submersible JAGO; Chief Scientist. B.B. Jørgensen (METROL)
Black Sea culture	BSC	44.74 N 031.97 E	300m	Microbial Chimney	2004	4	
Menes Caldera	MC	32.11 N 028.16 E	3018m	Cold Seep	2003	20	NAUTINIL exp. RV L Atalante; Jean-Paul Foucher
Hydrate Ridge	HR	44.55 N 125.25 W	780m	Cold Seep	2000	12	RV SONNE Exp. SO-148; CS E.Suess, P. Linke
Gulf of Mexico	GoM	27.74 N 091.31 W	504m	Cold Seep	2003	20	RV Sonne exp. 174; CS G. Bohrmann OTEGA

Supplementary Table 2 Relative abundance of methantrophic and methanogenic archaeal clades, known AOM partner bacteria and disproportionating bacteria in 10 studied AOM enrichment cultures. Values normalized to parts of 1000 (‰).

Organism	E20	G37	G50	GF	AMV	BSC	BSM	MC	GoM	HR
Archaea										
ANME-2a/2b	217	8	10	616	390	177	517	878	528	76
ANME-2c	457	6	7	11	276	601	152	23	87	343
ANME-1	7	15*	805	7	6	5	7	7	5	5
ANME-1a	2	12	87	1	2	2	2	2	2	2
Methanococcoides	3	2	0	5	5	5	2	10	6	2
Methanohalophilus	3	2	0	8	1	0	1	2	3	0
Bacteria										
SEEP-SRB-1a	9	6	58	435	56	205	109	245	158	161
SEEP-SRB-2	83*	383	3	7	25	4	1	4	30	35
HotSeep-1	1	2	270	2	1	1	2	2	2	3
Desulfocapsa	0	0	0	1	22	0	0	1	69	6
Elba-DISP1	10	0	0	0	0	1	0	0	0	0
GB-DISP1	0	2	0	0	0	0	0	0	0	0

* likely underestimated sequence abundance; 0 = <0.5‰ of all sequences.

Chapter VI

Discussion and perspectives

In this Chapter the central findings of the thesis are shortly summarized and discussed in the context of the original thesis hypotheses. The insight obtained into the thermophilic ANME-1/HotSeep-1 consortium including its physiology and genomic profile is discussed in the context of AOM in general and the current knowledge in this field. This Chapter ends by addressing perspectives for future work and by highlighting general concluding remarks to this thesis.

6.1. Physiology and interspecies interaction in thermophilic AOM

Since the discovery of ANME archaea and partner bacteria as central members of AOM consortia these organisms were thought to interact in a syntrophic manner. Several models aimed to explain the coupling of methane oxidation to sulfate reduction (see Chapter I). Among those hypotheses was direct electron transfer from ANME archaea to bacterial partner (Thauer and Shima, 2008; Summers *et al.*, 2010). This hypothesis was supported in metagenomic studies (Meyerdierks *et al.*, 2010; Wang *et al.*, 2014); however experimental evidence and visual detection of structures that would support the model of direct interspecies interaction were missing.

In the framework of this thesis we investigated the physiology of thermophilic AOM consortia composed of ANME-1 and HotSeep-1 (Chapter II). We combined physiological experiments with differential gene expression analysis and electron microscopy. In these consortia we excluded the exchange of molecular intermediates. Instead we observed a dense network of cell-to-cell connections. We furthermore observed that under AOM conditions, HotSeep-1 expresses *pilA*, a gene encoding the major subunit of pili proteins, while both ANME-1 and HotSeep-1 express c-type cytochromes. Based on these results we formulated a model for the functioning of thermophilic AOM via direct electron transfer through conductive charge transport in nanowires. Our model emanates from a combination of c-type cytochromes and pili, which likely together provide a conductive path for electron transfer in thermophilic AOM (Wegener *et al.*, 2015; Chapter II).

Extracellular electron transfer either to insoluble acceptors or to other microbes has been reported previously (Reguera *et al*., 2005; Gorby *et al*., 2006; Summers *et al*., 2010; Rotaru *et al*., 2014, 2015). Iron-reducers of the *Geobacter* spp. produce nanowire-like structures thought to be made of type IV pili (Reguera *et al*., 2005). Pili are general bacterial features that serve functions such as motility or attachment and it is still not fully clear how pili are involved in electron transfer. Two principle mechanisms by which pili conductance is achieved are debated: (1) Based on the stacked arrangement of aromatic amino acids in the PilA protein pili may have a metallic like self-conductance (Vargas *et al*., 2013; Malvankar *et al*., 2014) or, (2) c-type cytochromes that associate on the pili surface facilitate electron hopping along the pili (Summers *et al.*, 2010; Snider *et al.*, 2012). Cytochromes are suggested to be generally relevant for direct electron transfer by *Geobacter* spp. and to promote the transfer of electrons from the cell membrane onto the pili or from the pili to the electron sink (Metha *et al*., 2005; Estevez-Canales *et al*., 2015). This potentially explains the observed expression of both pili and cytochromes under AOM conditions in thermophilic consortia

(Chapter II). We attributed the intercellular filamentous structures, observed in the thermophilic ANME-1/HotSeep-1 consortia, to the production of pili by the bacterial partner and proposed that they may resemble in function the pili-based nanowires produced by *Geobacter* spp., considering the sequence similarity of both PilA proteins. We did not attempt to localize cytochromes in the thermophilic AOM consortia yet. Future studies should address the localization of cytochromes in the extracellular space and also target the conductive property of the observed nanowire-like structures. We also detected type IV pili genes in the genome of the Seep-SRB-2 partner bacterium (Chapter IV). However, the expression level was low, and we cannot infer a general function of pili in ANME-1-dominated consortia presently.

Simultaneously with our proposal of nanowire and cytochrome mediated electron transfer in ANME-1/HotSeep-1 consortia McGlynn and coworkers (2015) proposed direct electron transfer in ANME-2/DSS consortia. Based on *in situ* staining of c-type cytochromes and genome analysis of ANME they proposed electron transfer mediated by cytochromes (McGlynn *et al.*, 2015). The authors allocated a particularly important role to high molecular weight c-type cytochromes (31 heme), that localize in the S-layer of ANME-2 and would permit conductivity of the intercellular matrix. This type of cytochrome was not found in ANME-1 (McGlynn *et al*., 2015; own data Chapter II and IV). However, all available ANME genomes encode a variety of cytochromes and some of those were also shown to be expressed (Meyerdierks *et al.*, 2010; Wang *et al.*, 2014; Wegener *et al.*, 2015; own data Chapter IV) indicating a central role of cytochromes in the functioning of electron transfer in AOM syntrophy. McGlynn and coworkers (2015) focused on the role of the archaea in electron transfer. Hence the bacterial partner and extracellular structures possibly produced by it were not further considered; however such structures were not apparent in the presented TEM images, suggesting their minor importance in ANME-2 consortia.

The recent findings from ANME-1/HotSeep-1 (Chapter II) and ANME-2/DSS consortia (McGlynn *et al*., 2015) suggest a central role of direct electron transfer for the functioning of AOM. Genome analysis indicates that cytochromes are important for this process in both consortia types. The exact mechanism may be dependent on the combination of partners, their specific genomic and physiologic potential and spatial arrangement of cells. Future in depth research is necessary to verify the concept of direct electron transfer in AOM and to explain the cellular fundamentals to achieve it. Syntrophy based on direct interspecies electron transfer in AOM would extend the spread of this mechanism beyond the known *Geobacter*-

involving microbial syntrophies and therewith hints on a larger relevance in nature than anticipated.

6.2. Physiology and genomic profile of the bacterial partner HotSeep-1

So far four main groups of ANME partner bacteria are described: Seep-SRB-1, Seep-SRB-2, *Desulfobulbus*-relatives and HotSeep-1. Phylogenetically those groups are placed as separate clusters in the *Deltaproteobacteria*, but none contained cultured representatives. Prior to the work included in this thesis HotSeep-1 bacteria referenced a deeply-branching cluster; members of it were known as unique partner bacteria in thermophilic AOM consortia (Holler *et al.*, 2011b), but their actual metabolic capabilities were unknown. In the work presented in Chapter II and III we reported on the physiology and genome of a representative of the HotSeep-1 bacteria that resembles the partner bacterium involved in thermophilic AOM.

The main physiologic characteristic of HotSeep-1, that distinguishes it from all other known partner bacteria, is its ability to grow on molecular hydrogen. Using this electron donor and sulfate as acceptor we achieved growth of HotSeep-1 in the absence of ANME archaea. Partner-independent growth of organisms involved in a syntrophy as reducing equivalent scavenging partner is often promoted by artificially providing the intermediate exchanged. We however have disproven hydrogen as shuttled intermediate in the ANME-1/HotSeep-1 syntrophy (Chapter II). Nevertheless, hydrogen is the compound with a redox chemistry most closely mirroring the one involved in direct electron transfer (i.e. when HotSeep-1 growth in thermophilic AOM consortia). To switch from syntrophic to hydrogenotrophic growth HotSeep-1 relies on a single additional enzyme: a hydrogenase. We attribute the observed 3-day lag phase when HotSeep-1 switched from syntrophic to hydrogenotrophic growth to the need to synthesize hydrogenases. We hypothesize that HotSeep-1 channels electrons derived from periplasmic hydrogen oxidation into the enzyme series of sulfate reduction via the same path as electrons that directly enter the cell, i.e. via a periplasmic pool of cytochrome c. In its natural environment, the Guaymas Basin, HotSeep-1 may encounter hydrogen sporadically and therefore has preserved the ability to metabolize it. In contrast, in environments where cold-adapted AOM consortia occur hydrogen concentrations are minimal (Hoehler *et al*., 1994; Hoehler *et al*., 1996), and presence of a hydrogenase system is likely not of selective advantage. Concordantly those bacterial partner from cold-adapted AOM consortia do not respond to hydrogen as growth substrate (Nauhaus

et al., 2005; own data Chapter V). The ability of HotSeep-1 to grow partner-independent allowed novel lines of experimental analyses of the metabolism involved in AOM.

Considering its physiology, HotSeep-1 is not necessarily limited to thermophilic AOM, but might also engage in other syntrophic processes, which base on interspecies hydrogen or direct electron transfer. Sequences closely related to HotSeep-1 were reported to be abundant in short chain alkane-degrading enrichments (Kniemeyer *et al.*, 2007; Adams *et al.*, 2013). Our physiological tests and genome analyses indicate that HotSeep-1 alone cannot degrade alkanes. Instead it may participate in syntrophic hydrocarbon degradation as scavenger of reduced products. The syntrophic alkane metabolizer remains to be identified and we suggest it may be found in the Candidate Division OP 8, *Firmicutes* or *Archaea*; based on sequence data reported by Adams and colleagues (2013) from hydrocarbon-degrading enrichments.

Based on its physiological properties we proposed to name HotSeep-1 *Candidatus* Desulfofervidus auxilii. A *Candidatus* status remains as we could not obtain a pure culture yet. In addition to its physiological properties, we studied the phylogenetic position of HotSeep-1 (Chapter III). Its deep-branching position has been reported previously (Teske *et al.*, 2002; Holler *et al.*, 2011b). *Candidatus* Desulfofervidus auxilii is, according to our understanding, a member of a new family that is tentatively placed in the *Deltaproteobacteria* but the clear classification remained difficult in the absence of close relatives.

6.3. Metabolic potential of ANME-1

The three described ANME clades 1 to 3 comprise uncultured anaerobic methanotrophs, phylogenetically related to the methanogenic archaea. Physiologic differences between members of the different clades are widely unexplored. We focused here on ANME-1. In a comparative genome analysis of different members of the ANME-1 clade, we investigated the diversity in metabolic potential among members of this large clade and suggest metabolic traits unique to ANME-1 (i.e. not known in ANME-2 or -3 or in methanogens). The compared members are likely to represent distinct genera of anaerobic methanotrophs and differ in growth temperature and associated bacterial partner.

We obtained for a meso- and a thermophilic ANME-1 almost complete draft genomes of only ~1.5 Mb, a size considerably smaller than the previously reported ANME-1 assembly (Meyerdierks *et al.*, 2010). This discrepancy in genome size may reflect limited metabolic versatility of the meso- and thermophilic ANME-1 types or may be explained by the composite nature of the previously reported ANME-1 genome (Meyerdierks *et al*., 2010). We

combined our data with previous genomic and proteomic data of ANME-1 (Meyerdierks *et al.*, 2010; Stokke *et al.*, 2012) and showed that central metabolic features such as enzymes of carbon fixation, methanogenesis and redox complexes are common among ANME-1 while they are also shared with the ANME-2 clade and with methanogens (Wang *et al.*, 2014). Like previous studies, we could not identify a gene encoding the Mer protein (Meyerdierks *et al*., 2010; Stokke *et al*., 2011) but could also not convincingly confirm the Mer bypass in meso- and thermophilic ANME-1. Instead, we confirmed, the first by Stokke and colleagues (2012) proposed, modified reverse methanogenesis pathway: the Mer protein is presumably replaced by MetFV that catalyzes an analogous reaction and usually occurs in non-methanogenic organisms, mainly in bacteria. We showed expression of this protein in meso- and thermophilic ANME-1 to levels similar to other enzymes of the methanogenesis pathway, indicating its involvement in this reaction sequence. The same enzyme was also detected in the other ANME-1 datasets (Meyerdierks *et al.*, 2010; Stokke *et al.*, 2012). A utilization of MetFV contrasts the hypothesis of a bypass (Meyerdierks *et al*., 2010) and would allow direct reversal of the methanogenesis pathway without the production of intermediates. In future, biochemical studies are needed to approve an involvement of the MetFV enzyme in reverse methanogenesis as well as to show its subunit composition (e.g. formation of a complex with HdrABC as previously recognized (Bertsch *et al.*, 2015)).

The tight association with bacterial partner and the absence of any potential alternative growth substrates indicates that ANME-1 is an obligate syntrophic metabolizer. In support of this, we did not find genes for canonical sulfate reduction, hydrogenases or any methanogenic activity (Chapter V) which could support a partner-independent lifestyle of ANME-1. This is in contrast with the proposal of ANME operating as a methanogen (see Chapter IV). Instead ANME-1 and also ANME-2 tend to contain and express c-type cytochromes which may support a syntrophic relationship in which ANME directly donates methane-derived electrons (as outlined above and in Chapter IV and V; Meyerdierks *et al*., 2010; Wang *et al.*, 2014; McGlynn *et al.*, 2015). Supposed this to prove true, ANME would constitute the first archaeon and next to *Geobacter* spp. (Rotaru *et al.*, 2014, 2015) the only other organism presently proposed to participate in direct interspecies electron transfer as donating partner. While *G. metallireducens* was shown to form conductive pili, possibly purposing direct electron transfer, the production of similar conductive structures by ANME remains open. In this respect, we detected an incomplete set of flagella genes in the meso- and thermophilic ANME-1 and observed high expression of flagellins and putative flagellins (Chapter IV). As the archaeal flagellum, the archaellum, structurally and evolutionary resembles a bacterial

type IV pilus (Albers *et al.*, 2015), we consider it as a candidate for an extracellular structure of ANME with potential importance in interspecies interaction.

We provided a first insight into the common metabolic potential of ANME-1 members; however the present dataset of ANME-1 is still very limited with only three genomes representing a large group. Future work should attempt to obtain genomic data from various ANME for broader comparative studies to eventually allow drawing general conclusions concerning the metabolic versatility of ANME and their differences to methanogens.

6.4. Metabolic capabilities of organisms in AOM enrichments

The core archaeal and bacterial members of AOM consortia are phylogenetically classified into few but considerably diverse clades. This indicates potential variability in their metabolic capabilities. Chapter V addressed the microbial composition of different AOM enrichments and compared their metabolic capabilities. The three investigated sediment-free AOM enrichments represent different temperature regimes of growth, 20, 37 or 50/60°C, and were dominated by ANME-2c/Seep-SRB-2, ANME-1/Seep-SRB-2 and ANME-1/HotSeep-1, respectively. We performed physiological experiments targeting previously addressed topics: the nature of carbon assimilation (Wegener *et al.*, 2008; Kellermann *et al.*, 2012), the hypothesis of methanogenic activity in ANME (Lloyd *et al.*, 2011) and sulfur metabolism in the bacterial partners (Milucka *et al.*, 2012).

We showed that the investigated enrichments predominantly assimilated inorganic carbon, which confirms previous findings (Wegener *et al.*, 2008; Kellermann *et al.*, 2012) and describes both partners of the AOM consortium as autotrophs. Carbon assimilation activity required the presence of methane, which shows that methane is the primary energy source on which both partner of the consortium depend and is in line with earlier studies by Wegener and colleagues (2008).

With respect to methanogenic metabolism, we showed that in the tested AOM enrichments, only the addition of methylated compounds promotes methanogenesis, by rapidly enriching an initially small community of methylotrophic methanogens of the genera *Methanococcoides* and *Methanohalophilus*. We however did not observe methylotrophic methanogenesis in the thermophilic enrichments, which we explained by the absence of these non-thermophilic organisms after long-term exposure to high temperatures (50-60°C). Our results clearly contrast earlier reports of ANME-1 operating also as a methanogen (Bertram *et al.*, 2013). We hypothesize that in AOM enrichments and naturally in zones of AOM

activity methylotrophic methanogens may thrive from low amounts of methylated side products of the AOM process.

We further showed initiation of alternative sulfur metabolism in the investigated enrichments. In the enrichments at 37 and 50/60°C supply of hydrogen and sulfate resulted in the enrichment of members of the minor community or of HotSeep-1, respectively. Seep-SRB-2 was not enriched with hydrogen, coinciding with the absence of hydrogen-dependent sulfate reduction in the other Seep-SRB-2-dominated enrichment at 20°C. This is in agreement with previous physiologic studies on cold-adapted AOM consortia (Nauhaus *et al*., 2005), which also showed a lack of hydrogen metabolism in the partner bacteria. The absence of hydrogenotrophic growth in Seep-SRB-2 further suggests that interspecies hydrogen transfer is not relevant in Seep-SRB-2-dominated consortia, and is in line with the absence of hydrogenase genes in ANME-1 and ANME-2 (Wang *et al*., 2014; Chapter IV). In the low temperature (20 and 37°C), but not in the thermophilic enrichments we showed sulfur-disproportionating activity. We cultured two novel sulfur-disproportionating bacteria which we found to be unique with respect to their capability to sustain sulfur disproportionation under sulfide concentrations up to 7 mM, a level were the energy gain is lowered to a minimum of −10 kJ per mol^{-1}. For one of the isolates, which we classified as closest relative of the Seep-SRB-2 cluster (93% sequence similarity), we also showed growth by hydrogenotrophic sulfate reduction. This phylogenetic proximity of Seep-SRB-2 to an organism with the capability of hydrogen metabolism and sulfur disproportionation may indicate that those traits were present in a common ancestor and were lost in Seep-SRB-2 as a result of adaptation to a syntrophic lifestyle with ANME. Based on the absence of sulfur disproportionation by Seep-SRB-2 and HotSeep-1, we suggest that zero-valent sulfur transfer is not important in these consortia types, which is in clear contrast to findings from ANME-2a/DSS consortia (Milucka *et al.*, 2012).

Altogether our results suggest that the organisms constituting the here investigated AOM consortia have limited metabolic versatility: ANME are autotrophic methane oxidizers and bacterial partner are autotrophic sulfate reducers. Their syntrophic lifestyle may not be based on a molecular intermediate such as hydrogen or sulfur and may involve the direct exchange of electrons (outlined above and in Chapter II). Hydrogenotrophic growth is a feature clearly contrasting HotSeep-1 from Seep-SRB-2 and possibly other bacterial partner. The small community of organisms not directly involved in AOM can be activated by alternative substrates also after long-term enrichment under AOM conditions. We have shown that those community members carry out processes such as methanogenesis or alternative sulfur

metabolism; understanding their functioning in AOM enrichments and at sites of AOM activity awaits further attention.

6.5. Perspectives for future research on AOM

This thesis presented novel insights into the metabolic capabilities and genomic profiles of AOM organisms and their interspecies interaction, which have expanded our understanding of AOM as a syntrophic process. At the same time the new perspectives encourage to more in depth analysis. Based on the presented work the following future tasks are formulated.

The understanding of syntrophy in AOM continues to be a major interest of AOM research. AOM consortia are phylogenetically and morphologically diverse and so are likely their mechanisms of interaction. The recently proposed models of direct electron transfer via pili and/or cytochromes were developed from the study of specific types of consortia. Hence our knowledge is still too limited to allow general statements. Therefore, in future different AOM consortia types, i.e. constituting diverse combinations of ANME and partner bacteria, should be systematically analyzed applying a standardized set of methodology such as high resolution TEM imaging, cytochrome redox staining and targeted gene and gene expression analyses. The results from such a comparative approach could help in formulating generalized hypothesis concerning the syntrophy strategies across consortia types or determine factors that influence which syntrophy strategy is used; for instance, is the formation of pili linked the distance of cells.

For thermophilic ANME-1/HotSeep-1 consortia pili are proposed to serve a crucial role in direct electron transfer and pili formation was attributed to HotSeep-1 (Chapter II). To verify that the in TAOM consortia observed structures are bacterial pili the *in situ* detection of PilA is a critical task. This could be facilitated by developing and applying immunogold labeling with an antibody targeting the HotSeep-1 PilA protein on thermophilic AOM consortia thin sections for subsequent visualization by TEM. The identification of the filamentous structures observed as pili would be a major step forward; however, a final proof concerning the conductive nature of the pili would still remain. Conductivity measurements have previously revealed the conductive properties of whole consortia (Summers *et al.*, 2010) and specific pili produced by *Geobacter* spp. (Malvankar *et al.*, 2014). In future similar measurements should be attempted in the thermophilic AOM consortia and specifically target the nanowire-like cell connections. To investigate the role of pili-associated cytochromes in electron transfer, these

cytochromes should be visualized for instance via redox staining or also via immunogold labeling with cytochrome targeting antibodies.

With HotSeep-1 a bacterial partner is now cultivated independently; however, a still lasting aim is the partner-independent cultivation of ANME. With respect to the here described potential of thermophilic ANME-1 to grow by solely expelling electrons, it is tempting to reconsider potentiostat cultivation approaches. In such a set up ANME-1 would utilize a poised electrode as terminal electron acceptor omitting the need for a bacterial partner. Although all previous attempts to grow ANME using an electrode as electron sink were unsuccessful, conditions may have not been optimal or the tested organisms were not capable of direct electron transfer.

The enrichment-based work presented in this thesis has shown that deep insights into the physiology of organisms can be obtained from *in vitro* enrichments. We were able to sustain and grow "unculturable" AOM consortia at high enrichment degree for microbiological investigations as well as metagenomic and metatranscriptomic studies. The MPI Bremen currently holds probably the largest collection of AOM consortia enrichments from a range of habitats. Chapter V provided an overview of the different types of consortia available in those cultures and an estimate of their enrichment degree (based on relative sequence abundance). Metagenome sequencing of those enrichments and targeted assembly of the prominent taxa presents a promising approach to extend the number and diversity of available genomes from AOM organisms for comparative analysis. Together with metatranscriptome sequencing gene expression patterns for selected genes such as *pilA* and cytochromes or *mer* and *met* could be compared across ANME types and partner bacteria. Such a comparative analysis of an extended set of genomes would enable addressing the question of metabolic diversity and uniqueness of ANME and their partner bacteria more explicit. Indeed, it would also be the basis to perform comparative analysis of syntrophic strategies on the gene and genome level to possibly generalize the interspecies interaction concepts developed recently.

6.6. Concluding remarks

The research summarized in this thesis has focused on the physiology and genomic potential of anaerobic methane-oxidizing archaea and their partner bacteria. It has provided the first highly complete genomes of a bacterial partner and two ANME-1 subtypes which will be the basis for future comparative genomic approaches. We confirmed in our studies that ANME-1 is a chemoorganoautotroph that likely employs a modified reverse methanogenesis pathway for methane oxidation. We identified HotSeep-1 as a novel chemolithoautotrophic sulfate reducer that, when not grown in syntrophy with ANME, uses hydrogen as sole electron source. For the syntrophy of ANME-1/HotSeep-1 in thermophilic AOM, we proposed a direct electron exchange via conductive nanowires which likely involve bacterial type IV pili and c-type cytochromes of both partners. This expands on the conceivable archaeal-bacterial interactions in AOM and also extends the principle of direct interspecies electron transfer in the microbial world, which still is largely unexplored. In this respect, the work combined in this thesis has contributed to advance our understanding of the physiology of AOM and its syntrophic nature. Likewise new questions arised and the illustrated new perspectives show that there remain many more pieces to be assembled to resolve the AOM puzzle in all its detail.

Bibliography

Adams CJ, Redmond MC, Valentine DL. (2006). Pure-culture growth of fermentative bacteria, facilitated by H_2 removal: bioenergetics and H_2 production. *Appl Environ Microbiol* **72**: 1079–1085.

Adams MM, Hoarfrost AL, Bose A, Joye SB, Girguis PR. (2013). Anaerobic oxidation of short-chain alkanes in hydrothermal sediments: potential influences on sulfur cycling and microbial diversity. *Front Microbiol* **4**: 110.

Alain K, Holler T, Musat F, Elvert M, Treude T, Krüger M. (2006). Microbiological investigation of methane- and hydrocarbon-discharging mud volcanoes in the Carpathian Mountains, Romania. *Environ Microbiol* **8**: 574–590.

Amann R, Fuchs BM. (2008). Single-cell identification in microbial communities by improved fluorescence *in situ* hybridization techniques. *Nat Rev Microbiol* **6**: 339–348.

Barnes RO, Goldberg ED. (1976). Methane production and consumption in anoxic marine sediments. *Geology* **4**: 297–300.

Basen M. (2009). Biochemie und Physiologie der Sulfatreduktion in der anaeroben Oxidation von Methan. Dissertation. Universität Bremen. Germany.

Beal EJ, House CH, Orphan VJ. (2009). Manganese- and iron-dependent marine methane oxidation. *Science* **325**: 184–187.

Bertram S, Blumenberg M, Michaelis W, Siegert M, Krüger M, Seifert R. (2013). Methanogenic capabilities of ANME-archaea deduced from ^{13}C-labelling approaches. *Environ Microbiol* **15**: 2384-2393.

Bertsch J, Öppinger C, Hess V, Langer JD, Müller V. (2015). Heterotrimeric NADH-oxidizing methylenetetrahydrofolate reductase from the acetogenic bacterium *Acetobacterium woodii*. *J Bacteriol* **197**: 1681–1689.

Biebl H, Pfennig N. (1978). Growth yields of green sulfur bacteria in mixed cultures with sulfur and sulfate reducing bacteria. *Arch Microbiol* **117**: 9–16.

Bleicher K, Winter J. (1994). Formate production and utilization by methanogens and by sewage sludge consortia – interference with the concept of interspecies formate transfer. *Appl Microbiol Biotechnol* **40**: 910–915.

Boetius A, Ravenschlag K, Schubert CJ, Rickert D, Widdel F, Gieseke A, *et al.* (2000). A marine microbial consortium apparently mediating anaerobic oxidation of methane. *Nature* **407**: 623–626.

Boetius A, Knittel K. (2010). Habitats of anaerobic methane oxidizers. In: *Handbook of Hydrocarbon and Lipid Microbiology*. Timmis KN (ed). Berlin/Heidelberg: Springer, pp 2194–2202.

Boetius A, Wenzhöfer F. (2013). Seafloor oxygen consumption fuelled by methane from cold seeps. *Nat Geosci* **6**: 725–734.

Boone DR, Johnson RL, Liu Y. (1989a). Diffusion of the interspecies electron carriers H_2 and formate in methanogenic ecosystems and its implications in the measurement of K_m for H_2 or formate uptake. *Appl Environ Microbiol* **55**:1735–1741.

Boone DR, Johnson RL, Liu Y. (1989b). Microbial ecology of interspecies hydrogen and formate transfer in methanogenic ecosystems. In: *Recent Advances in Microbial Ecology.* Hattori T, Ishida Y, Maruyama Y, Morita RY, Uchida A (eds). Tokyo: Japan Scientific Society Press, pp 450–453.

Bryant MP, Wolin EA, Wolin MJ, Wolfe RS. (1967). *Methanobacillus omelianskii*, a symbiotic association of two species of bacteria. *Arch Mikrobiol* **59**: 20–31.

Buffett B, Archer D. (2004). Global inventory of methane clathrate: sensitivity to changes in the deep ocean. *Earth Planet Sci Lett* **227**: 185–199.

Burggraf S, Jannasch HW, Nicolaus B, Stetter KO. (1990). *Archaeoglobus profundus* sp. nov., represents a new species within the sulfate-reducing archaebacteria. *Syst Appl Microbiol* **13**: 24−28.

Canfield DE. (1993). Organic matter oxidation in marine sediments. In: *Interactions of C, N, P and S in Biogeochemical Cycles and Global Change.* Wollast R, Mackenzie FT, Chou L (eds). Berlin: Springer, pp 333−363.

Canfield DE, Kristensen E, Thamdrup B. (2005). Aquatic geomicrobiology. *Adv Mar Biol* **48**: 1−599.

Chen S, Rotaru A-E, Shrestha PM, Malvankar NS, Liu F, Fan W, *et al.* (2014). Promoting interspecies electron transfer with biochar. *Sci Rep* **4**: 5019.

Cicerone RJ, Oremland RS. (1988). Biogeochemical aspects of atmospheric methane. *Glob Biogeochem Cycles* **2**: 299–327.

Conrad R. (2009). The global methane cycle: recent advances in understanding the microbial processes involved. *Environ Microbiol Rep* **1**: 285–292.

Cord-Ruwisch R, Lovley DR, Schink B. (1998). Growth of *Geobacter sulfurreducens* with acetate in syntrophic cooperation with hydrogen-oxidizing anaerobic partners. *Appl Environ Microbiol* **64**: 2232–2236.

Cui M, Ma A, Qi H, Zhuang X, Zhuang G. (2015). Anaerobic oxidation of methane: an "active" microbial process. *Microbiologyopen* **4**: 1–11.

de Bary A (1879) Die Erscheinung der Symbiose: Vortrag gehalten auf der Versammlung Deutscher Naturforscher und Aerzte zu Cassel. R. J. Trübner, Strassburg.

Diekert G, Wohlfarth G. (1994). Metabolism of homoacetogens. *Antonie van Leeuwenhoek* **66**: 209–221.

Dickens GR. (2003). Rethinking the global carbon cycle with a large, dynamic and microbially mediated gas hydrate capacitor. *Earth Planet Sci Lett* **213**: 169–183.

Doddema HJ, Vogels GD. (1978). Improved identification of methanogenic bacteria by fluorescence microscopy. *Appl Environ Microbiol* **36**: 752–754.

Dong X, Plugge CM, Stams AJM. (1994). Anaerobic degradation of propionate by a mesophilic acetogenic bacterium in coculture and triculture with different methanogens. *Appl Environ Microbiol* **60**: 2834–2838.

Estevez-Canales M, Kuzume A, Borjas Z, Füeg M, Lovley D, Wandlowski T, *et al.* (2015). A severe reduction in the cytochrome C content of *Geobacter sulfurreducens* eliminates its capacity for extracellular electron transfer. *Environ Microbiol* **7**: 219–226.

Ettwig KF, Butler MK, Le Paslier D, Pelletier E, Mangenot S, Kuypers MMM, *et al.* (2010). Nitrite-driven anaerobic methane oxidation by oxygenic bacteria. *Nature* **464**: 543–548.

Gorby YA, Yanina S, McLean JS, Rosso KM, Moyles D, Dohnalkova A, *et al.* (2006). Electrically conductive bacterial nanowires produced by *Shewanella oneidensis* strain MR-1 and other microorganisms. *PNAS* **103**: 11358–11363.

Hallam SJ, Girguis PR, Preston CM, Richardson PM, DeLong EF. (2003). Identification of methyl coenzyme M reductase A (*mcrA*) genes associated with methane-oxidizing archaea. *Appl Environ Microbiol* **69**: 5483–5491.

Hallam SJ, Putnam N, Preston CM, Detter JC, Rokhsar D, Richardson PM, DeLong EF. (2004). Reverse methanogenesis: testing the hypothesis with environmental genomics. *Science* **305**: 1457–1462.

Hanson RS, Hanson TE. (1996). Methanotrophic bacteria. *Microbiol Rev* **60**: 439–471.

Haroon MF, Hu S, Shi Y, Imelfort M, Keller J, Hugenholtz P, *et al.* (2013). Anaerobic oxidation of methane coupled to nitrate reduction in a novel archaeal lineage. *Nature* **500**: 567–570.

Harrison BK, Zhang H, Berelson W, Orphan VJ. (2009). Variations in archaeal and bacterial diversity associated with the sulfate-methane transition zone in continental margin sediments (Santa Barbara Basin, California). *Appl Environ Microbiol* **75**: 1487–1499.

Hedges JI, Keil RG. (1995). Sedimentary organic matter preservation: an assessment and speculative synthesis. *Mar Chem* **49**: 137–139.

Heller C, Hoppert M, Reitner J. (2008). Immunological localization of coenzyme M reductase in anaerobic methane-oxidizing archaea of ANME 1 and ANME 2 type. *Geomicrobiol J* **25**: 149–156.

Henneberger R, Moissl C, Amann T, Rudolph C, Huber R. (2006). New insights into the lifestyle of the cold-loving SM1 euryarchaeon: natural growth as a monospecies biofilm in the subsurface. *Appl Environ Microbiol* **72**: 192–199.

Hinrichs K-U, Hayes JM, Sylva SP, Brewer PG, DeLong EF. (1999). Methane-consuming archaebacteria in marine sediments. *Nature* **398**: 802–805.

Hinrichs K-U, Boetius A. (2002). The anaerobic oxidation of methane: new insights in microbial ecology and biogeochemistry. In: *Ocean Margin Systems*. Wefer G, Billet D, Hebbeln D, Jørgensen BB, Schlüter M, van Weering TCE (eds). Berlin/Heidelberg: Springer, pp 457–477.

Hoehler TM, Alperin MJ, Albert DB, Martens CS. (1994). Field and laboratory studies of methane oxidation in an anoxic marine sediment: evidence for a methanogen-sulfate reducer consortium. *Glob Biogeochem Cycles* **8**: 451–463.

Hoehler TM, Alperin MJ, Albert DB, Martens CS. (1998). Thermodynamic control on hydrogen concentrations in anoxic sediments. *Geochim Cosmochim Acta* **62**: 1745–1756.

Holler T, Wegener G, Knittel K, Boetius A, Brunner B, Kuypers MMM, *et al.* (2009). Substantial $^{13}C/^{12}C$ and D/H fractionation during anaerobic oxidation of methane by marine consortia enriched *in vitro*. *Environ Microbiol Rep* **1**: 370–376.

Holler T, Wegener G, Niemann H, Deusner C, Ferdelman TG, Boetius A, *et al*. (2011a). Carbon and sulfur back flux during anaerobic microbial oxidation of methane and coupled sulfate reduction. *Proc Natl Acad Sci USA* **108**: E1484–E1490.

Holler T, Widdel F, Knittel K, Amann R, Kellermann MY, Hinrichs K-U, *et al.* (2011b). Thermophilic anaerobic oxidation of methane by marine microbial consortia. *ISME J* **5**: 1946–1956.

Horita J, Berndt ME. (1999). Abiogenic methane formation and isotopic fractionation under hydrothermal conditions. *Science* **285**: 1055−1057.

IPCC (2007). Climate change 2007: the physical science basis. Contribution of working group I to the fourth assessment report of the Intergovernmental Panel on Climate Change. Solomon S, Qin D, Manning M, Chen Z, Marquis M, Averyt KB, *et al*. (eds). Cambridge (UK) and New York: Cambridge University Press.

Iversen N, Jørgensen BB. (1985). Anaerobic methane oxidation rates at the sulfate-methane transition in marine sediments from Kattegat and Skagerrak (Denmark). *Limnol Oceanogr* **30**: 944–955.

Jannasch HW, Wirsen CO, Molyneaux SJ, Langworthy TA. (1988). Extremely thermophilic fermentative archaebacteria of the genus *Desulfurococcus* from deep-sea hydrothermal vents. *Appl Environ Microbiol* **54**: 1203−1209.

Jaun B, Thauer RK. (2007). Methyl-coenzyme M reductase and its nickel corphin coenzyme F_{430} in methanogenic archaea. In: *Metal Ions in Life Sciences*. Siegel A, Siegel H, Siegel RKO. Chichester: John Wiley & Sons, Ltd, pp 323−356.

Jørgensen BB, Zawacki LX, Jannasch HW. (1990). Thermophilic bacterial sulfate reduction in deep-sea sediments at the Guaymas Basin hydrothermal vent site (Gulf of California). *Deep-Sea Res* **37**: 695−710.

Kaden J, Galushko AS, Schink B. (2002). Cysteine-mediated electron transfer in syntrophic acetate oxidation by cocultures of *Geobacter sulfurreducens* and *Wolinella succinogenes*. *Arch Microbiol* **178**: 53–58.

Kallmeyer J, Boetius A. (2004). Effects of temperature and pressure on sulfate reduction and anaerobic oxidation of methane in hydrothermal sediments of Guaymas Basin. *Appl Environ Microbiol* **70**: 1231–1233.

Kasten S, Jørgensen BB. (2000). Sulfate reduction in marine sediments. In: *Marine Geochemistry*. Schulz HD, Zabel M (eds). Berlin/Heidelberg: Springer, pp 263–281.

Kellermann MY, Wegener G, Elvert M, Yoshinaga MY, Lin Y-S, Holler T, *et al.* (2012). Autotrophy as a predominant mode of carbon fixation in anaerobic methane-oxidizing microbial communities. *Proc Natl Acad Sci USA* **109**: 19321–19326.

Kleindienst S, Ramette A, Amann R, Knittel K. (2012). Distribution and *in situ* abundance of sulfate-reducing bacteria in diverse marine hydrocarbon seep sediments. *Environ Microbiol* **14**: 2689–2710.

Kniemeyer O, Musat F, Sievert SM, Knittel K, Wilkes H, Blumenberg M, *et al.* (2007). Anaerobic oxidation of short-chain hydrocarbons by marine sulphate-reducing bacteria. *Nature* **449**: 898–901.

Knittel K, Boetius A, Lemke A, Eilers H, Lochte K, Pfannkuche O *et al*. (2003). Activity, distribution, and diversity of sulfate reducers and other bacteria in sediments above gas hydrate (Cascadia Margin, Oregon). *Geomicrobiol J* **20**: 269–294.

Knittel K, Lösekann T, Boetius A, Kort R, Amann R. (2005). Diversity and distribution of methanotrophic archaea at cold seeps. *Appl Environ Microbiol* **71**: 467–479.

Knittel K, Boetius A. (2009). Anaerobic oxidation of methane: progress with an unknown process. *Annu Rev Microbiol* **63**: 311–334.

Knittel K, Boetius A. (2011). Anaerobic oxidation of methane with sulfate. In: *Encyclopedia of Geobiology*. Reitner J, Thiel V (eds). Netherlands: Springer, pp 36–47.

Krüger M, Meyerdierks A, Glöckner FO, Amann R, Widdel F, Kube M, *et al.* (2003). A conspicuous nickel protein in microbial mats that oxidize methane anaerobically. *Nature* **426**: 878–881.

Lelieveld J, Crutzen PJ, Dentener FJ. (1998). Changing concentration, lifetime and climate forcing of atmospheric methane. *Tellus B* **50**: 128–150.

Li B, Ruotti V, Stewart RM, Thomson JA, Dewey CN. (2010). RNA-Seq gene expression estimation with read mapping uncertainty. *Bioinformatics* **26**: 493–500.

Liu F, Rotaru A-E, Shrestha PM, Malvankar NS, Nevin KP, Lovley DR. (2012). Promoting direct interspecies electron transfer with activated carbon. *Energy Environ Sci* **5**: 8982–8989.

Liu F, Rotaru A-E, Shrestha PM, Malvankar NS, Nevin KP, Lovley DR. (2014). Magnetite compensates for the lack of a pilin-associated c-type cytochrome in extracellular electron exchange. *Environ Microbiol* **17**: 648–655.

Lloyd KG, Alperin MJ, Teske A. (2011). Environmental evidence for net methane production and oxidation in putative ANaerobic MEthanotrophic (ANME) archaea. *Environ Microbiol* **13**: 2548–2564.

Lloyd KG, Lapham L, Teske A. (2006). An anaerobic methane-oxidizing community of ANME-1b archaea in hypersaline Gulf of Mexico sediments. *Appl Environ Microbiol* **72**: 7218–7230.

Lovley DR, Coates JD, Blunt-Harris EL, Phillips EJP, Woodward JC. (1996). Humic substances as electron acceptors for microbial respiration. *Nat*ure **382**: 445–448.

Lovley DR, Malvankar NS. (2015). Seeing is believing: novel imaging techniques help clarify microbial nanowire structure and function. *Environ Microbiol* **17**: 2209–2215.

Ludwig W, Strunk O, Westram R, Richter L, Meier H, Yudhukumar, *et al.* (2004). ARB: a software environment for sequence data. *Nucleic Acids Res* **32**: 1363–1371.

Maignien L, Parkes RJ, Cragg B, Niemann H, Knittel K, Coulon S, *et al.* (2013). Anaerobic oxidation of methane in hypersaline cold seep sediments. *FEMS Microbiol Ecol* **83**: 214–231.

Malvankar NS, Yalcin SE, Tuominen MT, Lovley DR. (2014). Visualization of charge propagation along individual pili proteins using ambient electrostatic force microscopy. *Nat Nanotechnol* **9**: 1012–1017.

Martens CS. (1990). Generation of short chain acid anions in hydrothermally altered sediments of the Guaymas Basin, Gulf of California. *Appl Geochem* **5**: 71−76.

Martin BD, Schwab E. (2013). Current usage of symbiosis and associated terminology. *Int J Biol* **5**: 32–45.

McGlynn SE, Chadwick GL, Kempes CP, Orphan VJ. (2015). Single cell activity reveals direct electron transfer in methanotrophic consortia. *Nature* **526**: 531–535.

McInerney MJ, Sieber JR, Gunsalus RP. (2009). Syntrophy in anaerobic global carbon cycles. *Curr Opin Biotechnol* **20**: 623–632.

Mehta T, Coppi M V, Childers SE, Lovley DR. (2005). Outer membrane c-type cytochromes required for Fe(III) and Mn(IV) oxide reduction in *Geobacter sulfurreducens*. *Appl Environ Microbiol* **71**: 8634–8641.

Meulepas RJW, Jagersma CG, Khadem AF, Stams AJM, Lens PNL. (2010). Effect of methanogenic substrates on anaerobic oxidation of methane and sulfate reduction by an anaerobic methanotrophic enrichment. *Appl Microbiol Biotechnol* **87**: 1499–1506.

Meyerdierks A, Kube M, Lombardot T, Knittel K, Bauer M, Glöckner FO, *et al.* (2005) Insights into the genomes of archaea mediating the anaerobic oxidation of methane. *Environ Microbiol* **7**: 1937–1951.

Meyerdierks A, Kube M, Kostadinov I, Teeling H, Glöckner FO, Reinhardt R, *et al.* (2010). Metagenome and mRNA expression analyses of anaerobic methanotrophic archaea of the ANME-1 group. *Environ Microbiol* **12**: 422–439.

Michaelis W, Seifert R, Nauhaus K, Treude T, Thiel V, Blumenberg M, *et al.* (2002). Microbial reefs in the Black Sea fueled by anaerobic oxidation of methane. *Science* **297**: 1013–1015.

Milucka J, Ferdelman TG, Polerecky L, Franzke D, Wegener G, Schmid M, *et al.* (2012). Zero-valent sulphur is a key intermediate in marine methane oxidation. *Nature* **491**: 541–546.

Milucka J, Widdel F, Shima S. (2013). Immunological detection of enzymes for sulfate reduction in anaerobic methane-oxidizing consortia. *Environ Microbiol* **15**: 1561–1571.

Moran JJ, Beal EJ, Vrentas JM, Orphan VJ, Freeman KH, House CH. (2008). Methyl sulfides as intermediates in the anaerobic oxidation of methane. *Environ Microbiol* **10**: 162–173.

Morris BEL, Henneberger R, Huber H, Moissl-Eichinger C. (2013). Microbial syntrophy: interaction for the common good. *FEMS Microbiol Rev* **37**: 384–406.

Müller V. (2008). Bacterial fermentation. In: *Encyclopedia of Life Sciences*. Chichester: John Wiley & Sons, Ltd.

Müller N, Griffin BM, Stingl U, Schink B. (2008). Dominant sugar utilizers in sediment of Lake Constance depend on syntrophic cooperation with methanogenic partner organisms. *Environ Microbiol* **10**: 1501–1511.

Nauhaus K, Boetius A, Krüger M, Widdel F. (2002). *In vitro* demonstration of anaerobic oxidation of methane coupled to sulphate reduction in sediment from a marine gas hydrate area. *Environ Microbiol* **4**: 296–305.

Nauhaus K, Treude T, Boetius A, Krüger M. (2005). Environmental regulation of the anaerobic oxidation of methane: a comparison of ANME-I and ANME-II communities. *Environ Microbiol* **7**: 98–106.

Nauhaus K, Albrecht M, Elvert M, Boetius A, Widdel F. (2007). *In vitro* cell growth of marine archaeal-bacterial consortia during anaerobic oxidation of methane with sulfate. *Environ Microbiol* **9**: 187–196.

Niemann H, Elvert M, Hovland M, Orcutt B, Judd A, Suck I, *et al.* (2005). Methane emission and consumption at a North Sea gas seep (Tommeliten area). *Biogeosciences* **2**: 335–351.

Niemann H, Lösekann T, de Beer D, Elvert M, Nadalig T, Knittel K, *et al.* (2006). Novel microbial communities of the Haakon Mosby mud volcano and their role as a methane sink. *Nature* **443**: 854–858.

Orcutt B, Samarkin V, Boetius A, Joye S. (2008). On the relationship between methane production and oxidation by anaerobic methanotrophic communities from cold seeps of the Gulf of Mexico. *Environ Microbiol* **10**: 1108–1117.

Orphan VJ, Hinrichs K-U, Ussler W III, Paull CK, Taylor LT, Sylva SP, *et al.* (2001a). Comparative analysis of methane-oxidizing archaea and sulfate-reducing bacteria in anoxic marine sediments. *Appl Environ Microbiol* **67**: 1922–1934.

Orphan VJ, House CH, Hinrichs K-U, McKeegan KD, DeLong EF. (2001b). Methane-consuming archaea revealed by directly coupled isotopic and phylogenetic analysis. *Science* **293**: 484–487.

Overmann J. (2006). Symbiosis between non-related bacteria in phototrophic consortia. In: *Progress in Molecular and Subcellular Biology*. Overmann J (ed). Berlin/Heidelberg: Springer, pp 21–37.

Overmann J. (2010). The phototrophic consortium "*Chlorochromatium aggregatum*" - a model for bacterial heterologous multicellularity. In: *Recent Advances in Phototrophic Prokaryotes.* Hallenbeck PC (ed). New York: Springer, pp 15–29.

Pereira IAC, Ramos AR, Grein F, Marques MC, da Silva SM, Venceslau SS. (2011). A comparative genomic analysis of energy metabolism in sulfate reducing bacteria and archaea. *Front Microbiol* **2**: 69.

Pernthaler A, Pernthaler J, Amann R. (2002). Fluorescence *in situ* hybridization and catalyzed reporter deposition for the identification of marine bacteria. *Appl Environ Microbiol* **68**: 3094–3101.

Pernthaler A, Dekas AE, Brown CT, Goffredi SK, Embaye T, Orphan VJ. (2008). Diverse syntrophic partnerships from deep-sea methane vents revealed by direct cell capture and metagenomics. *Proc Natl Acad Sci USA* **105**: 7052–7057.

Platen H, Schink B. (1987). Methanogenic degradation of acetone by an enrichment culture. *Arch Microbiol* **149**: 136–141.

Quast C, Pruesse E, Yilmaz P, Gerken J, Schweer T, Glöckner FO, *et al.* (2013). The SILVA ribosomal RNA gene database project: improved data processing and web-based tools. *Nucleic Acids Res* **41**: D590–D596.

Raghoebarsing AA, Pol A, van de Pas-Schoonen KT, Smolders AJP, Ettwig KF, Rijpstra WIC, *et al.* (2006). A microbial consortium couples anaerobic methane oxidation to denitrification. *Nature* **440**: 918–921.

Reddy CA, Bryant MP, Wolin MJ. (1972). Characteristics of S organism isolated from *Methanobacillus omelianskii*. *J Bacteriol* **109**: 539–545.

Reeburgh WS. (1976). Methane consumption in Cariaco Trench waters and sediments. *Earth Planet Sci Lett* **28**: 337–344.

Reeburgh WS. (1980). Anaerobic methane oxidation: rate depth distribution in Skan Bay sediments. *Earth Planet Sci Lett* **47**: 345–352.

Reeburgh WS. (2007). Oceanic methane biogeochemistry. *Chem Rev* **107**: 486–513.

Regnier P, Dale AW, Arndt S, LaRowe DE, Mogollón J, Van Cappellen P. (2011). Quantitative analysis of anaerobic oxidation of methane (AOM) in marine sediments: a modeling perspective. *Earth-Sci Rev* **106**: 105–130.

Reguera G, McCarthy KD, Mehta T, Nicoll JS, Tuominen MT, Lovley DR. (2005). Extracellular electron transfer via microbial nanowires. *Nature* **435**: 1098–1101.

Reitner J, Peckmann J, Blumenberg M, Michaelis W, Reimer A, Thiel V. (2005a). Concretionary methane-seep carbonates and associated microbial communities in Black Sea sediments. *Palaeogeogr Palaeoclimatol Palaeoecol* **227**: 18–30.

Reitner J, Peckmann J, Reimer A, Schumann G, Thiel V. (2005b). Methane-derived carbonate build-ups and associated microbial communities at cold seeps on the lower Crimean shelf (Black Sea). *Facies* **51**: 66–79.

Rotaru A-E, Shrestha PM, Liu F, Markovaite B, Chen S, Nevin K, *et al*. (2014). Direct interspecies electron transfer between *Geobacter metallireducens* and *Methanosarcina barkeri*. *Appl Environ Microbiol* **80**: 4599–4605.

Rotaru A-E, Woodard TL, Nevin KP, Lovley DR, Clarke T. (2015). Link between capacity for current production and syntrophic growth in *Geobacter* species. *Front Microbiol* **6**: 744.

Sakai S, Imachi H, Sekiguchi Y, Ohashi A, Harada H, Kamagata Y. (2007). Isolation of key methanogens for global methane emission from rice paddy fields: a novel isolate affiliated with the clone cluster Rice Cluster I. *Appl Environ Microbiol* **73**: 4326–4331.

Schink B. (1991). Syntrophism among prokaryotes. In: *The Prokaryotes*. Balows A, Trüper HG, Dworkin M, Schleifer K-H (eds). New York: Springer, pp 276–299.

Schink B. (1997). Energetics of syntrophic cooperation in methanogenic degradation. *Microbiol Mol Biol Rev* **61**: 262–280.

Schink B. (2002). Synergistic interactions in the microbial world. *Antonie van Leeuwenhoek* **81**: 257–261.

Schink B, Stam AJM. (2006). Syntrophism among prokaryotes. In: *The Prokaryotes*. Dworkin M, Falkow S, Rosenberg E, Schleifer K-H, Stackebrandt E (eds). New York: Springer, pp 309–335.

Schoell M. (1988). Multiple origins of methane in the Earth. *Chem Geol* **71**: 1–10.

Scholten JC, Conrad R. (2000). Energetics of syntrophic propionate oxidation in defined batch and chemostat cocultures. *Appl Environ Microbiol* **66**: 2934–2942.

Schouten S, Wakeham SG, Hopmans EC, Damste JSS. (2003). Biogeochemical evidence that thermophilic archaea mediate the anaerobic oxidation of methane. *Appl Environ Microbiol* **69**: 1680−1686.

Schreiber L, Holler T, Knittel K, Meyerdierks A, Amann R. (2010). Identification of the dominant sulfate-reducing bacterial partner of anaerobic methanotrophs of the ANME-2 clade. *Environ Microbiol* **12**: 2327–2340.

Segarra KEA, Schubotz F, Samarkin V, Yoshinaga MY, Hinrichs K-U, Joye SB. (2015). High rates of anaerobic methane oxidation in freshwater wetlands reduce potential atmospheric methane emissions. *Nat Commun* **6**: 7477.

Sieber JR, McInerney MJ, Gunsalus RP. (2012). Genomic insights into syntrophy: the paradigm for anaerobic metabolic cooperation. *Annu Rev Microbiol* **66**: 429–452.

Simoneit BRT, Lonsdale PF. (1982). Hydrothermal petroleum in mineralized mounds at the seabed of Guaymas Basin. *Nature* **295**: 198−202.

Smith JA, Nevin KP, Lovley DR. (2015). Syntrophic growth via quinone-mediated interspecies electron transfer. *Front Microbiol* **6**: 121.

Snider RM, Strycharz-Glaven SM, Tsoi SD, Erickson JS, Tender LM. (2012). Long-range electron transport in *Geobacter sulfurreducens* biofilms is redox gradient-driven. *Proc Natl Acad Sci USA* **109**: 15467–15472.

Sørensen KB, Finster K, Ramsing NB. (2001). Thermodynamic and kinetic requirements in anaerobic methane oxidizing consortia exclude hydrogen, acetate, and methanol as possible electron shuttles. *Microb Ecol* **42**: 1–10.

Spormann AM, Widdel F. (2000). Metabolism of alkylbenzenes, alkanes, and other hydrocarbons in anaerobic bacteria. *Biodegradation* **11**: 85–105.

Stams AJ, Plugge CM. (2009). Electron transfer in syntrophic communities of anaerobic bacteria and archaea. *Nat Rev Microbiol* **7**: 568–577.

Stokke R, Roalkvam I, Lanzen A, Haflidason H, Steen IH. (2012). Integrated metagenomic and metaproteomic analyses of an ANME-1-dominated community in marine cold seep sediments. *Environ Microbiol* **14**: 1333–1346.

Summers ZM, Fogarty HE, Leang C, Franks AE, Malvankar NS, Lovley DR. (2010). Direct exchange of electrons within aggregates of an evolved syntrophic coculture of anaerobic bacteria. *Science* **330**: 1413–1415.

Teske A, Hinrichs K-U, Edgcomb V, de Vera Gomez A, Kysela D, Sylva SP, *et al.* (2002). Microbial diversity of hydrothermal sediments in the Guaymas Basin: evidence for anaerobic methanotrophic communities. *Appl Environ Microbiol* **68**: 1994–2007.

Thauer RK. (1998). Biochemistry of methanogenesis: a tribute to Marjory Stephenson. *Microbiology* **144**: 2377–2406.

Thauer RK, Kaster A-K, Seedorf H, Buckel W, Hedderich R. (2008). Methanogenic archaea: ecologically relevant differences in energy conservation. *Nat Rev Microbiol* **6**: 579–591.

Thauer RK, Shima S. (2008). Methane as fuel for anaerobic microorganisms. *Ann N Y Acad Sci* **1125**: 158–170.

Treude T, Boeutius A, Knittel K, Wallmann K, Jørgensen BB. (2003). Anaerobic oxidation of methane above gas hydrates at the Hydrate Ridge, NE Pacific Ocean. *Mar Ecol Prog Ser* **264**: 1–14.

Treude T, Orphan V, Knittel K, Gieseke A, House CH, Boetius A. (2007). Consumption of methane and CO_2 by methanotrophic microbial mats from gas seeps of the anoxic Black Sea. *Appl Environ Microbiol* **73**: 2271–2283.

Vargas M, Malvankar NS, Tremblay P-L, Leang C, Smith JA, Patel P, *et al*. (2013). Aromatic amino acids required for pili conductivity and long-range extracellular electron transport in *Geobacter sulfurreducens*. *mBio* **4**: e00105–e00113.

Wallmann K, Pinero E, Burwicz E, Haeckel M, Hensen C, Dale A, *et al.* (2012). The global inventory of methane hydrate in marine sediments: a theoretical approach. *Energies* **5**: 2449–2498.

Wang F-P, Zhang Y, Chen Y, He Y, Qi J, Hinrichs K-U, *et al.* (2014). Methanotrophic archaea possessing diverging methane-oxidizing and electron-transporting pathways. *ISME* **8**: 1069–1078.

Wankel SD, Adams MM, Johnston DT, Hansel CM, Joye SB, Girguis PR. (2012). Anaerobic methane oxidation in metalliferous hydrothermal sediments: influence on carbon flux and decoupling from sulfate reduction. *Environ Microbiol* **14**: 2726–2740.

Wegener G, Niemann H, Elvert M, Hinrichs K-U, Boetius A. (2008). Assimilation of methane and inorganic carbon by microbial communities mediating the anaerobic oxidation of methane. *Environ Microbiol* **10**: 2287–2298.

Wegener G, Krukenberg V, Riedel D, Tegetmeyer HE, Boetius A. (2015). Intercellular wiring enables electron transfer between methanotrophic archaea and bacteria. *Nature* **526**: 587–590.

Welhan JA. (1988). Origins of methane in hydrothermal systems. *Chem Geol* **71**: 183−198.

Whiticar MJ, Faber E, Schoell M. (1986). Biogenic methane formation in marine and freshwater environments: CO_2 reduction vs. acetate fermentation - isotope evidence. *Geochim Cosmochim Acta* **50**: 693–709.

Widdel F, Musat F, Knittel K, Galushko A. (2007). Anaerobic degradation of hydrocarbons with sulphate as electron acceptor. In: *Sulphate-Reducing Bacteria: Environmental and Engineered Systems*. Barton LL, Hamilton WA (eds). Cambridge (UK): Cambridge University Press, pp 265–330.

Wu W-M, Hickey RF, Jain MK, Zeikus JG. (1993). Energetics and regulations of formate and hydrogen metabolism by *Methanobacterium formicicum*. *Arch Microbiol* **159**: 57–65.

Yoshinaga MY, Holler T, Goldhammer T, Wegener G, Pohlman JW, Brunner B, *et al.* (2014). Carbon isotope equilibration during sulphate-limited anaerobic oxidation of methane. *Nat Geosci* **7**: 190–194.

Zehnder AJB, Brock TD. (1979). Methane formation and methane oxidation by methanogenic bacteria. *J Bacteriol* **137**: 420–432.

Acknowledgements

I would like to thank everyone who was in some way involved in this PhD project.

Many thanks to Antje Boetius for giving me the opportunity to do my PhD on the fascinating topic of AOM and for support and advice throughout the years.

Thank you Professor Fischer for agreeing to review my thesis and for helpful discussions.

Many thanks to the other members of my defense committee Jens Harder, Gunter Wegener, Rafael Laso Pérez and Tobias Vonnahme.

My greatest thanks to Gunter! Thank you for offering me to work with you on the amazing AOM consortia and for sharing many exciting moments with me! I feel very lucky to have been your student and to have had the chance to learn from you. I am always impressed by your ideas and enthusiasm! Thank you for all the support in the last 5 years and for always being there to answer my questions and to give me advice!

Many thanks to:
Halina Tegetmeyer for excellent support in everything regarding sequencing, thank you for always taking time to answer my questions; Michael Richter and Harald Gruber-Vodicka for teaching me everything concerning genomics and metagenomics, from sequencing technology to assembly and annotation, your advice and help were immensely important to me; Katrin Knittel for always having time for a question and for teaching me much about phylogeny; Pierre Offree for answers and advice to questions about microbial metabolism; Christian Quast and Elmar Prüsse for bioinformatics support and for helping me when I broke something; All the TAs in Habitat and Microbiology, especially Mirja Meiners, Susanne Menger and Nicole Rödiger for great support in microbiological work, radiotracer experiments and for teaching me much about molecular techniques; The IT team, especially Carsten John and Oliver Artmann for being helpful with anything regarding computer issues; Christiane Glöckner for help and support throughout the time of MarMic; Everyone in the Habitat Group for making it a very great group to work in; The MGG group for a friendly atmosphere in the corridor and for giving me an office space.

Special thanks to my lab rotation students, Oliver Jäckle, Katie Harding and Rafael Laso Pérez, for your great work and contributions to my projects.

Special thanks to the many great office mates I had throughout the years. Pier and Emiliano thank you for making the time in our ‘avocado tree’ office so nice and also for all the coffee you have made for me! Pier I am happy to share an office with you for so long and I always appreciate your advice and help very much!

Mar, Gaby, Julia, Juliane and Philipp thank you for your company throughout the years of MarMic and MPI and for the many nice moments outside the MPI. Katy, Josi, Rafa, Christiane and Gerd thank you for the time with you in the Habitat Group and for your support. Felix and Massi thank you for tolerating the many discussions about AOM in your office. Christiane thank you for so much help with statistics and R. Rafa thank you for your amazing help! Gerd thank you for continuous support and for the ‘we are going to make it’.

Many thanks also to my friends and room mates for making the time in Bremen so nice. Daihann, Lilit and Svetlana I am very happy to have met you here. Marthe and Silvia thank you for being my friends for so long.

Finally to my family: Danke für all Eure Unterstützung. Ich hätte mir nicht nicht mehr wünschen können!

Appendix

Erklärung

Hiermit erkläre ich, Viola Krukenberg, dass ich

- die Arbeit selbständig verfasst und geschrieben habe,
- keine anderen als die von mir angegebenen Quellen und Hilfsmittel verwendet habe und
- die den benutzten Werken wörtlich oder inhaltlich entnommenen Stellen als solche kenntlich gemacht habe und
- die 3 vorgelegten Exemplare dieser Arbeit in identischer Ausführung abgegeben habe.

Ort, Datum Unterschrift

Cover:

Fluorescence micrograph of a thermophilic consortium of anaerobic methane-oxidizing archaea (red) and their bacterial partners (green).